USCEE Report 400

Final Report

October 1970

UNIVERSITY OF SOUTHERN CALIFORNIA

INSTABILITIES IN LASER PROPAGATION IN FLUIDS

William G. Wagner

This research was sponsored by the Advanced Research Projects Agency of the Department of Defense and was monitored by the Office of Naval Research under Contract No. 00014-67-A-0269-0006, under ARPA Order No. 306-62, Code No. 421. Contract period: August 1, 1968 to October 31, 1970.

ELECTRONIC SCIENCES LABORATORY

Engineering

USCEE Report 400

Final Report
October 1970

INSTABILITIES IN LASER PROPAGATION IN FLUIDS

William G. Wagner

Electronic Sciences Laboratory
University of Southern California
Los Angeles, California 90007

This research was sponsored by the Advanced Research Projects Agency of the Department of Defense and was monitored by the Office of Naval Research under Contract No. 00014-67-A-0269-0006, under ARPA Order No. 306-62, Code No. 421. Contract period: August 1, 1968 to October 31, 1970.

The work described in this report was performed as part of a continuing investigation on laser interactions with fluids by

Dr. William G. Wagner

Dr. John D. Reichert

Wei-Yeu Chen

The authors wish also to acknowledge very useful conversations with Dr. John H. Marburger.

TABLE OF CONTENTS

INTRODUCTION

The distortions of a laser beam produced by density and thermal variations in a fluid medium have been the subject of many investigations. In general, such studies on the effects of heat deposition from the laser beam upon the propagation of that beam can be classified into two groups, depending upon whether time dependence is considered. Most available experiments are conveniently understood by reference to theoretical studies of the gross effects of thermal deposition and fluid motion, which assume that a steady state will be achieved for the deflection and distortion of the laser beam. On the other hand, several years ago it was shown that one of the solutions for beam propagation was unstable, in the sense that small distortions in the beam would be amplified if the power level was greater than a threshold determined by the thermal conductivity of the fluid. For the most part, those investigations that do assume some time dependence for the beam pattern were concentrated on studies of the growth of small amplitude perturbations from an initially uniform beam.

The work described in this report was motivated by the discovery of instabilities in the system of equations describing electromagnetic wave propagation and fluid dynamics. Initially, it appeared desirable to attempt an exploration of the extended development of the instabilities noted for a uniform beam. The basic equations are discussed in Part I, and in Part II the linearized stability analysis is presented along with an evaluation of the threshold for these growing waves. To follow the growth of the disturbances, computer studies were undertaken. In the course of these studies it became apparent that there was some merit to introducing a new concept to judge the value of an algorithm for computing the solutions of a system of partial

differential equations. This concept was called "utility", and is discussed in Part III, along with several examples of its application to simpler partial differential equations. The advantage of this concept is that it is relatively easy to apply to complicated systems of partial differential equations, whereas the stability concept leads to a very complicated procedure for deciding on the value of a numerical routine. In Part IV are presented the results of a calculation of beam distortion for a very high intensity pulse propagating through air for several kilometers. Analytical arguments are advanced which suggest that the qualitative features of the distortions are correct, which lends credence to the computer output.

Speed and memory size in a computer place certain restrictions on one's ability to investigate phenomena in the laser beam problem. In the attempt to calculate distortions of the type predicted by the linearized instability analysis, cylindrical symmetry was imposed on the problem in order to facilitate the computer calculation. Had this not been necessary, or had some other independent variable been eliminated rather than the angle about the beam axis, much more pronounced evidence of beam and fluid instabilities would likely have been observed for substantially lower powers, powers that may be achievable. Arguments supporting this proposition are contained in Part V.

Part VI of this report contains an analytic discussion of beam bending and thermal blooming for a slab beam propagating through a wind. A formula is derived which provides for the transition between two regimes in which conduction and forced convection, respectively, dominate the dissipation of heat deposited in the medium from the laser beam. This formula appears to be useful for the analysis of several experiments.

PART I

BASIC EQUATIONS

When an intense laser beam propagates through a fluid, many interesting phenomena take place. This laser-fluid system can be described by a macroscopic model which involves Maxwell's equations, the Navier-Stokes equation, an energy conservation equation, and the continuity equation for fluid motion. These equations which describe the behavior of intense electromagnetic beams and the associated sound and thermal fluctuations, are coupled by stimulated Raman scattering, electrostriction, the high frequency Kerr effect, absorption heating, and the density and temperature dependence of the dielectric constant. In this paper, a systematic discussion is presented for an intense laser beam propagating through air, which has a negligible Kerr constant. If the frequencies are outside the Raman scattering range, the instabilities are primarily caused by optical-accoustic coupling of the laser beam and the gases. These effects are of long duration compared to those of self-focusing. As the beam passes through air, the intensity profile induces a nonuniform temperature gradient transverse to the propagating direction of the beam, due to the energy absorption from the beam. This thermal non-equilibrium and electrostriction together cause the generation of a density gradient and hence a sound wave. These density changes react back on the incident beam through changes in the dielectric constant. A detailed mathematical description of the model adopted here will be presented.

Maxwell's equations for the electric field vector $\vec{E}$ in a charge and current free region can be employed to yield the wave equation for the electric field

$$\nabla \times (\nabla \times \vec{E}) = -\frac{1}{c^2}\frac{\partial^2(\varepsilon\vec{E})}{\partial t^2} \qquad (1)$$

where the permittivity, ε, is taken to be

$$\varepsilon = \varepsilon_L + \varepsilon_2 \overline{E^2} \qquad (2)$$

Here and throughout this paper, Heavyside-Lorentz units are used for electrical quantities. These units are sometimes called rationalized gaussian units. The time average in (2) is to be taken over a time large compared with an optical period. Many such time averaged terms will be encountered below and in all cases an average over "several" optical periods is intended. Such average quantities may, of course, still be functions of time, but will vary slowly on the time scale of an optical period.

For an isotropic medium free of charge, the electric displacement vector is parallel to $\vec{E}$ and is divergenceless. Under these conditions one, therefore, has

$$\nabla \cdot (\varepsilon\vec{E}) = 0 \qquad (3)$$

From (3) one obtains

$$\nabla \cdot \vec{E} = -\vec{E} \cdot \nabla (\log \varepsilon).$$

Substituting this expression in (1) produces

$$\nabla^2 \vec{E} + \vec{\nabla}(\vec{E} \cdot \vec{\nabla} \log \varepsilon) = \frac{1}{c^2}\frac{\partial^2(\varepsilon\vec{E})}{\partial t^2} \qquad (4)$$

Since processes involving acoustical and thermal effects are considered here, the change in ε over an optical wavelength is small compared with the changes over a typical acoustical length. Thus the term involving $\nabla\varepsilon$ will be neglected in (4), leaving:

$$c^2\nabla^2\vec{E} \approx \frac{\partial^2}{\partial t^2}(\varepsilon\vec{E}). \qquad (5)$$

When processes involving electronic states of the molecules of the fluid are important, the $\vec{\nabla}\varepsilon$ term must be retained in the wave equation for $\vec{E}$.

The permittivity ε is, in general, a function of the mass density ρ of the fluid and the temperature T. In fluids $\left(\frac{\partial \varepsilon}{\partial T}\right)_\rho$ will be small except for such large temperatures that there is significant population of vibrational modes of the molecules. When anharmonic effects in the vibrational spectrum become important, careful attention must be given to the dependence of ε on T at constant density. For a considerable range of density and temperature, however, $\left(\frac{\partial \varepsilon}{\partial T}\right)_\rho \approx 0$, so that ε can be taken to be a function of ρ only. The dependence of ε on density can be approximated by the formulas resulting from Lorentz-Lorenz local field theory. This approach leads to the formula

$$\rho\left(\frac{\partial \varepsilon}{\partial \rho}\right)_T \approx \frac{(\varepsilon - 1)(\varepsilon + 2)}{3} + \frac{2}{3}(\varepsilon_L - 1)(\varepsilon - \varepsilon_L) \qquad (6)$$

The second term on the RHS of (6) is usually extremely small because $(\varepsilon - \varepsilon_L)$, the nonlinear piece, is small. Furthermore, particularly in gases, $(\varepsilon_L - 1)$ is extremely small. For the situations considered in the present analysis, both these factors are small, so that (6) is conveniently simplified to

$$\rho\left(\frac{\partial \varepsilon}{\partial \rho}\right)_T \approx \frac{(\varepsilon - 1)(\varepsilon + 2)}{3} \; . \qquad (6a)$$

This Clausius-Mossotti relation will be used later in the detailed analysis of the laser-fluid equations.

The equation for the fluid motion, the Navier-Stokes equation, is

$$\rho \frac{Dv_i}{Dt} = \rho g_i + \frac{\partial}{\partial x_j}\sigma_{ij} + \overline{\frac{\partial}{\partial x_j}\sigma'_{ij}} \qquad (7)$$

where $\vec{v}$ is the velocity of a material element of the fluid, $\vec{g}$ is the gravitational acceleration vector, σ_{ij} is the viscosity stress tensor,[1] σ'_{ij} is the interaction stress tensor coupling the electromagnetic field to the fluid.[2]

The time derivative $\frac{D}{Dt}$ is the "material" derivative; i.e., one that follows the motion of a material "particle" of the medium relative to a fixed coordinate system. This derivative can be expressed in the form

$$\frac{D(\ )}{Dt} = \frac{\partial(\ )}{\partial t} + \vec{v} \cdot \nabla (\ ). \qquad (8)$$

The viscosity stress tensor is given, to a first approximation, by the linear terms of an expansion in powers of the viscosity coefficients:

$$\sigma_{ij} = \eta\left(\frac{\partial v_i}{\partial x_j} + \frac{\partial v_j}{\partial x_i}\right) + \eta' \frac{\partial v_k}{\partial x_k} \delta_{ij} \qquad (9)$$

where η is the coefficient of shear viscosity and η' is the compressional viscosity coefficient. Sometimes η and η' are called the "first" and "second" viscosity coefficients and were previously denoted μ and λ, respectively, in the notation used by Stokes. The coefficient η' is occasionally called the dilational viscosity coefficient.

The interaction stress tensor for the electromagnetic field and the fluid will be taken to be

$$\sigma'_{ij} = -P\delta_{ij} - \frac{E^2}{2}\left[\varepsilon - \rho\left(\frac{\partial \varepsilon}{\partial \rho}\right)_T\right] \delta_{ij} + \varepsilon E_i E_j \qquad (10)$$

A derivation of this tensor, valid for static electromagnetic fields is given on page 67 of Reference [2]. In a vacuum, this expression becomes the familiar Maxwell stress tensor

$$\sigma'_{ij} = E_i E_j - \frac{1}{2} E^2 \delta_{ij} .$$

This tensor is not strictly correct for optical fields. Expression (10) results from a derivation with an isothermal constraint. A similar derivation with an adiabatic constraint, actually an isentropic constraint, gives the same result, except that the partial derivative $\left(\frac{\partial \varepsilon}{\partial \rho}\right)_T$ at constant temperature is replaced

by $\left(\frac{\partial \varepsilon}{\partial \rho}\right)_s$, the derivative at constant entropy. The difference in these two constraints is contained in the thermodynamic relation

$$\rho\left(\frac{\partial \varepsilon}{\partial \rho}\right)_s = \rho\left(\frac{\partial \varepsilon}{\partial \rho}\right)_T + T\left(\frac{\partial \varepsilon}{\partial T}\right)_\rho \left[\frac{\frac{1}{\gamma C_p}}{\frac{\beta v_s^2}{} - \beta T}\right] \tag{11}$$

where C_p is the specific heat per unit mass at constant pressure, γ is the ratio of specific heat at constant pressure to that at constant volume, β is thermal expansion coefficient $\frac{1}{V}\left(\frac{\partial V}{\partial T}\right)_p = -\frac{1}{\rho}\left(\frac{\partial \rho}{\partial T}\right)_p$, and v_s is the isentropic velocity of sound, $\sqrt{\left(\frac{\partial P}{\partial \rho}\right)_s}$.

The difference term in (11) is very small for reasons that have already been discussed, $\left(\frac{\partial \varepsilon}{\partial T}\right)_\rho \approx 0$. The term in square brackets is roughly $\frac{1}{2}$. Thus, for the present purposes, it will suffice to use the "isothermal" stress tensor given in (10). Actually, neither constraint is strictly valid, but corrections would be small and would necessitate a detailed examination of fluid boundary layers and the explicit mechanisms of heat deposition in the control volume.

The pressure P occurring in (10) is the thermodynamic pressure. This pressure is not identical with the mean pressure, $P_m \equiv -\frac{1}{3}[\sigma_{ii} + \overline{\sigma'_{ii}}]$, but is, rather, the thermodynamic intensive variable that enters into the equation of state of the fluid:

$$P = P(\rho, T) \tag{12}$$

Combining equations (7), (9), and (10), one obtains

$$\rho \frac{D\vec{v}}{Dt} = \rho\vec{g} - \vec{\nabla}P + \vec{f}_{es} + \vec{f}_{visc} \tag{13}$$

where the electrostrictive force density $\vec{f}_{es}$ is obtained by substituting (10) in (7):

$$\vec{f}_{es} = \left\langle -\frac{1}{2}\vec{\nabla}(\varepsilon E^2) + \vec{\nabla}\left[\frac{E^2}{2}\rho\left(\frac{\partial\varepsilon}{\partial\rho}\right)_T\right] + \varepsilon(E\cdot\nabla)\vec{E}\right\rangle$$

$$= \left\langle -\frac{1}{2}E^2\left[\left(\frac{\partial\varepsilon}{\partial\rho}\right)_T\vec{\nabla}\rho + \left(\frac{\partial\varepsilon}{\partial T}\right)_\rho\vec{\nabla}T\right] - \varepsilon(E\cdot\nabla)\vec{E} + \right.$$

$$\left. + \frac{1}{2}E^2\left(\frac{\partial\varepsilon}{\partial\rho}\right)_T\vec{\nabla}\rho + \rho\vec{\nabla}\left[\frac{E^2}{2}\left(\frac{\partial\varepsilon}{\partial\rho}\right)_T\right] + \varepsilon(E\cdot\nabla)\vec{E}\right\rangle$$

$$= -\frac{1}{2}\overline{\left[E^2\left(\frac{\partial\varepsilon}{\partial T}\right)_\rho\right]}\vec{\nabla}T + \frac{\rho}{2}\vec{\nabla}\overline{\left[E^2\left(\frac{\partial\varepsilon}{\partial\rho}\right)_T\right]}$$

$$= \frac{1}{2}\vec{\nabla}\overline{\left[E^2\rho\left(\frac{\partial\varepsilon}{\partial\rho}\right)_T\right]} - \frac{1}{2}\overline{E^2\vec{\nabla}\varepsilon} \qquad (14)$$

The time averages here are taken over several optical periods and the relation (3), $\nabla\cdot(\varepsilon\vec{E}) = 0$ has been used to get (14).

The viscous force density $\vec{f}_{visc}$, appearing in (13), is obtained by substituting (9) in (7):

$$\vec{f}_{visc} = \eta\nabla^2\vec{v} + (\eta+\eta')\vec{\nabla}(\nabla\cdot v) \qquad (15)$$

where terms involving $\vec{\nabla}\eta$ and $\vec{\nabla}\eta'$ have been dropped. In other words, η and η' have been taken to be constant throughout the fluid. This is a good approximation for gases where η, for example, increases slightly with temperature. Models, based on the Lennard-Jones potential energy function, suggest that $\eta \sim \sqrt{T}$. In liquids, on the other hand, the viscosity decreases rather strongly with increasing temperature, so that gradients of the viscosity coefficients could have some small effect.

Putting (14) and (15) in (13), one can write

$$\rho\frac{D\vec{v}}{Dt} = \rho\vec{g} - \vec{\nabla}p + \frac{1}{2}\vec{\nabla}\overline{\left[E^2\rho\left(\frac{\partial\varepsilon}{\partial\rho}\right)_T\right]} - \frac{1}{2}\overline{E^2\vec{\nabla}\varepsilon}$$

$$+ \eta\nabla^2\vec{v} + (\eta+\eta')\vec{\nabla}(\nabla\cdot v) \qquad (16)$$

The equation of continuity of matter in the fluid is

$$\frac{\partial \rho}{\partial t} + \vec{\nabla} \cdot (\rho \vec{v}) = 0 \tag{17}$$

The general equation for heat transfer in the fluid is

$$\rho T \frac{Ds}{Dt} = \phi_\eta - \nabla \cdot \vec{q} \tag{18a}$$

where s is the entropy per unit mass in the fluid, ϕ_η is the viscous dissipation function, and $\vec{q}$ is the total energy flux vector. The flux $\vec{q}$ can be divided into several parts:

$$\vec{q} = \vec{q}_{cond} + \vec{q}_{rad} + \vec{F} \tag{18b}$$

where $\vec{F}$ is a "material" Poynting vector to be discussed below, and $\vec{q}_{cond}$ and $\vec{q}_{rad}$ are the parts due to conduction and thermal radiation. In particular,

$$\vec{q}_{cond} \equiv - \kappa \vec{\nabla} T \tag{18c}$$

where the thermal conductivity, κ, a function of ρ and T is defined by this relation. The thermal radiation flux, $\vec{q}_{rad}$, can be approximated, for small temperature differences, by Newton's law of cooling:

$$\nabla \cdot \vec{q}_{rad} = \rho C_v q (T - T_o) \tag{18d}$$

where C_v is the heat capacity per unit mass at constant volume, $T - T_o$ is the local temperature excess, and q is a radiation coefficient introduced by Stokes.[2] Because this effect is extremely small in the parameter regime of the present analysis, this thermal radiation term will be dropped.

The viscous dissipation function, ϕ_η, appearing in (18a) is given by

$$\phi_\eta \equiv \sigma_{ij} \frac{\partial v_i}{\partial x_j} \tag{18e}$$

Combining (18a), (18b), (18c), and dropping the term shown in (18d), one obtains

$$\rho T \frac{Ds}{Dt} = \phi_\eta + \vec{\nabla} \cdot (\kappa \vec{\nabla} T) - \vec{\nabla} \cdot \vec{F} \qquad (19)$$

The LHS of (19) can be re-expressed, and the entropy eliminated, by using the thermodynamic relation

$$\rho T \frac{Ds}{Dt} = \rho C_v \frac{DT}{Dt} - \frac{C_v (\gamma - 1)}{\beta} \frac{D\rho}{Dt} \qquad (20)$$

where the thermodynamic parameters entering here have all been defined above. Actually (20) is obtained only if one neglects the dependence of the state of the fluid on the electric field. Strictly speaking, the entropy is a function of ρ, T, and $\vec{E}$. As shown on page 51 of Reference [2], one has the approximate expression

$$s \approx s_o(T,\rho) + \frac{E^2}{2} \left(\frac{\partial \varepsilon}{\partial T}\right)_\rho \qquad (21)$$

Since $\left(\frac{\partial \varepsilon}{\partial T}\right)_\rho$ is small, as discussed above, it is consistent to drop the very small second term in (21) and thus get (20).

Combining (19) and (20), one then gets

$$\rho C_v \frac{DT}{Dt} - \frac{C_v (\gamma - 1)}{\beta} \frac{D\rho}{Dt} = \phi_\eta + \vec{\nabla} \cdot (\kappa \vec{\nabla} T) - \vec{\nabla} \cdot \vec{F} \qquad (22)$$

The term $\vec{\nabla} \cdot \vec{F}$ in this equation is associated with a model for the absorption of electromagnetic energy by the fluid. A linear absorption coefficient, α, for the deposition of electromagnetic energy in the fluid is to be introduced. This coefficient is taken to be independent of the frequency of the electromagnetic radiation, so the model will not be valid for frequencies near the resonance lines of the molecules in the fluid. In this model, the electric field will be damped by a factor $e^{-\frac{\alpha}{2} z}$ where z is the direction of propagation and the energy deposited in the medium is taken to be $\alpha c \sqrt{\varepsilon}\, \overline{E^2} \equiv \alpha P_L$ where P_L is the laser intensity in (ergs/sec)/cm^2. It is this term that the divergence of $\vec{F}$ represents in (22). This "material" Poynting vector $\vec{F}$ is understood to

be the time average

$$\vec{F} = \langle \vec{F}_T - \vec{F}_0 \rangle \tag{23}$$

where $\vec{F}_T \equiv c\vec{E} \times \vec{B}$ is the total Poynting vector, whereas $\vec{F}_0$ is the Poynting vector that would result from the same fields in the absence of absorption. The time average is taken, as usual, over several optical periods.

In order to be consistent in the introduction of this absorption model, certain terms should be added to the wave equation and to the Navier-Stokes equation. Specifically, the term $\alpha c \frac{\partial(\sqrt{\epsilon}\vec{E})}{\partial t}$ should[†] be added to the RHS of (5) and a vector $\vec{C}$ should be added to the RHS of (16). The counter term $\vec{C}$ is given by

$$\vec{C} = \frac{1}{2} \rho \left(\frac{\partial \epsilon}{\partial \rho}\right)_T \frac{\alpha}{c\sqrt{\epsilon}} \vec{F} \tag{24}$$

This is strictly a counter term whose purpose is to remove the α dependence from the Navier-Stokes equation. No physical significance is attached to this term.

Making these modifications and collecting the operative equations for convenience, the following set of nonlinear coupled partial differential equations is obtained for description of the macroscopic representation of the laser-fluid system.

WAVE EQUATION

$$c^2 \nabla^2 \vec{E} = \frac{\partial^2}{\partial t^2} (\epsilon \vec{E}) + \alpha c \frac{\partial}{\partial t} (\sqrt{\epsilon} E) \tag{25a}$$

$$\epsilon = \epsilon_L + \epsilon_2 \overline{E^2} \tag{25b}$$

$$\rho \left(\frac{\partial \epsilon}{\partial \rho}\right)_T \approx \frac{(\epsilon - 1)(\epsilon + 2)}{3} , \left(\frac{\partial \epsilon}{\partial T}\right)_\rho \approx 0 \tag{25c}$$

[†]Instead of adding this term explicitly, the same effect can be obtained by considering the permittivity, ϵ, to be complex and frequency dependent. The present procedure is used to avoid the logical difficulty of putting frequency dependence in the space-time wave equation.

NAVIER-STOKES EQUATION

$$\rho \frac{D\vec{v}}{Dt} = \rho\vec{g} - \vec{\nabla}P + \frac{1}{2}\vec{\nabla}\left[\overline{E^2 \rho\left(\frac{\partial\epsilon}{\partial\rho}\right)_T}\right] - \frac{1}{2}\overline{E^2 \vec{\nabla}\epsilon} +$$

$$+ \eta \nabla^2 \vec{v} + (\eta + \eta')\vec{\nabla}(\vec{\nabla}\cdot\vec{v}) + \vec{C} \qquad (26a)$$

$$\vec{C} = \frac{1}{2}\rho\left(\frac{\partial\epsilon}{\partial\rho}\right)_T \frac{\alpha}{c\sqrt{\epsilon}}\vec{F} \qquad (26b)$$

HEAT TRANSFER EQUATION

$$\rho C_v \frac{DT}{Dt} - \frac{C_v(\gamma - 1)}{\beta}\frac{D\rho}{Dt} = \phi_\eta + \vec{\nabla}\cdot(\kappa\vec{\nabla}T) + \alpha c\sqrt{\epsilon}\,\overline{E^2} \qquad (27a)$$

$$\phi_\eta \equiv \sigma_{ij}\frac{\partial v_i}{\partial x_j} = \left[\eta\left(\frac{\partial v_i}{\partial x_j} + \frac{\partial v_j}{\partial x_i}\right) + \eta'\frac{\partial v_k}{\partial x_k}\delta_{ij}\right]\frac{\partial v_i}{\partial x_j} \qquad (27b)$$

FLUID CONTINUITY EQUATION

$$\frac{\partial\rho}{\partial t} + \nabla\cdot(\rho\vec{v}) = 0 \qquad (28)$$

EQUATION OF STATE

$$P = P(\rho, T) \qquad (29)$$

Due to the complexity of this set of equations, it is not possible to obtain exact solutions analytically. Only the linearized solutions have been discussed.[4,5] In the next section a linearized analysis of this set of equations is presented and, in subsequent sections, the nonlinearities will be considered.

PART II

LINEARIZED ANALYSIS

Linearized analysis is a standard pertubation technique. In this scheme, it is assumed that each of the dependent variables in the problem can be expressed as the sum of its slowly varying zeroth-order component and a small first-order correction.[6] In this way, a set of linear equations for small disturbances is obtained. This approach to the analysis of the laser-fluid system was first investigated by Brueckner and Jorna.[4] In the present approach, two variables are used to describe the perturbed electromagnetic field, one for the component of the field which is vibrating in phase with the primary beam and one for the component out of phase. In this way, the four-photon coupling induced by periodic fluctuations in the dielectric constant can be included. This coupling was not included in the original formulation given by Brueckner and Jorna. The dispersion relation for these linearized equations has been evaluated and is more complicated in structure than that presented by Brueckner and Jorna. For propagation through air, however, the numerical differences are minor. The wave with the largest growth rate, resulting from resonant interactions between scattered electromagnetic waves and the thermal wave, propagates almost perpendicularly to the laser beam. The direction is such that the change in frequency of the scattered electromagnetic wave and the frequency of the thermal wave, which is zero, are approximately the same.

A detailed analysis will now be presented. Separating each quantity into a zeroth-order and a first-order perturbation, one has

$$E \approx E_{(0)} + E_{(1)} \tag{30a}$$

$$\rho \approx \rho_0 + \rho_1 \tag{30b}$$

$$T \approx T_0 + T_1 \tag{30c}$$

$$P \approx P_0 + \rho_1\left(\frac{\partial P}{\partial \rho}\right)_T + T_1\left(\frac{\partial P}{\partial T}\right)_\rho = P_0 + \frac{v_s^2}{\gamma}\rho_1 + \frac{v_s^2}{\gamma}\beta\,\rho_0\,T_1 \tag{30d}$$

$$\begin{aligned}\varepsilon &\approx \left[\varepsilon_{L(0)} + \rho_1\left(\frac{\partial \varepsilon_L}{\partial \rho}\right)_T + T_1\left(\frac{\partial \varepsilon_L}{\partial T}\right)_\rho\right] + \\ &\quad + \left[\varepsilon_{2(0)} + \rho_1\left(\frac{\partial \varepsilon_2}{\partial \rho}\right)_T + T_1\left(\frac{\partial \varepsilon_2}{\partial T}\right)_\rho\right]\left(E_{(0)} + E_{(1)}\right)^2 \\ &\approx \varepsilon_{0e} + \varepsilon_1\end{aligned} \tag{30e}$$

where ρ_0, T_0, P_0, $\varepsilon_{L(0)}$, and $\varepsilon_{2(0)}$ are taken to be constants describing the unperturbed medium, v_s is the isentropic velocity of sound in the unperturbed medium, γ is the ratio of specific heats, β is the coefficient of thermal expansion for the fluid, and the zeroth and first order dielectric constants are given by

$$\varepsilon_{0e} \equiv \varepsilon_{L(0)} + \varepsilon_{2(0)}\,\overline{E_0^2} \tag{30f}$$

$$\begin{aligned}\varepsilon_1 \equiv &\left[\left(\frac{\partial \varepsilon_L}{\partial \rho}\right)_0 + \left(\frac{\partial \varepsilon_2}{\partial \rho}\right)_0 \overline{E_0^2}\right]\rho_1 + \left[\left(\frac{\partial \varepsilon_L}{\partial T}\right)_0 + \left(\frac{\partial \varepsilon_2}{\partial T}\right)_0 \overline{E_0^2}\right]T_1 + \\ &+ 2\,\varepsilon_{2(0)}\,\overline{E_{(0)}\,E_{(1)}}\end{aligned} \tag{30g}$$

The indicated averages are taken over several optical periods and the subscript zero on the partial derivatives indicates that they are to be evaluated at the density and temperature of the unperturbed fluid.

When equations (30) are substituted into (25a) and the zeroth-order and first-order terms are separated, one gets

$$\nabla^2 \vec{E}_{(0)} - \frac{1}{c^2} \frac{\partial^2 \left(\varepsilon_{oe} \vec{E}_{(0)} \right)}{\partial t^2} - \frac{\alpha}{c} \frac{\partial \left(\sqrt{\varepsilon_{oe}} \vec{E}_{(0)} \right)}{\partial t} = 0 \qquad (31a)$$

and

$$\nabla^2 \vec{E}_{(1)} - \frac{1}{c^2} \frac{\partial^2 \left(\varepsilon_{oe} \vec{E}_{(1)} \right)}{\partial t^2} - \frac{\alpha}{c} \frac{\partial \left(\sqrt{\varepsilon_{oe}} \vec{E}_{(1)} \right)}{\partial t} = \frac{1}{c^2} \frac{\partial^2 \left(\varepsilon_1 \vec{E}_{(0)} \right)}{\partial t^2} \qquad (31b)$$

There would have been an additional small term $-\vec{\nabla}[\vec{E}_0 \cdot \vec{\nabla} \log \varepsilon]$ on the RHS of (31b), had equation (4) not been simplified by dropping $\vec{\nabla}\varepsilon$ to get (14). Since α is treated as a first order quantity, a term $\frac{\alpha}{2c\sqrt{\varepsilon_{oe}}} \frac{\partial(\varepsilon_1 E_0)}{\partial t}$ was also dropped from the RHS of (31b)

The primary electromagnetic wave is chosen to be a linearly polarized plane wave propagating in the z-direction:

$$\vec{E}_{(0)} = \frac{1}{2} \hat{e}_y E_0 e^{i(\omega_L t - k_L z)} e^{-\frac{\alpha}{2} z} + \text{c.c.} =$$

$$= \hat{e}_y |E_0| e^{-\frac{\alpha}{2} z} \cos(\omega_L t - k_L z + \delta) \qquad (32a)$$

where c.c. stands for "complex conjugate" and δ is the phase of the complex constant, E_0. With

$$\omega_L \equiv \frac{k_L c}{\sqrt{\varepsilon_{oe}}} , \qquad (32b)$$

equation (32a) gives a solution of (31a), except for negligible terms of order α^2.

The first order correction $\vec{E}_{(1)}$ described by (27b) is taken to be of the form

$$\vec{E}_{(1)} = \frac{1}{2} \hat{e}_y \left[f e^{i(\omega_+ t - \vec{k}_+ \cdot \vec{x} + \delta)} + g e^{-i(\omega_- t - \vec{k}_- \cdot \vec{x} + \delta)} \right] e^{-\frac{\alpha}{2} z} + \text{c.c.} \qquad (33a)$$

where f and g are complex amplitudes, δ is the phase of the primary beam, and

$$\omega_{\pm} \equiv \omega_L \pm \omega \tag{33b}$$

$$\vec{k}_{\pm} \equiv k_L \hat{e}_z \pm \vec{k} \tag{33c}$$

$$k_{\pm}^2 = k_L^2 + k^2 \pm 2 k_3 k_L \tag{33d}$$

It is presumed that

$$\omega << \omega_L \tag{34a}$$

and that

$$|\vec{k}| << k_L \ . \tag{34b}$$

Under this assumption, it follows that $\hat{e}_z \cdot \vec{k}_{\pm}$ is approximately equal to k_L. One can easily check, now that the factor

$$e^{-\frac{\alpha}{2} z}$$

appearing in (33a) is consistent with the term containing α in (31b) to a very good approximation. Thus, $\vec{E}_{(0)}$ and $\vec{E}_{(1)}$ both have the same damping factor

$$e^{-\frac{\alpha}{2} z} \ .$$

Because of the mathematical complexity, it is convenient to express the first order electric field $\vec{E}_{(1)}$ in another form. Equation (33a) is rewritten:

$$\vec{E}_{(1)} = \hat{e}_y \, e^{-\frac{\alpha}{2} z} \left[E_1' \cos(\omega_L t - k_L z + \delta) + E_1'' \sin(\omega_L t - k_L z + \delta)\right] \tag{35}$$

where

$$E_1' \equiv \left(\frac{f+g}{2}\right) e^{i(\omega t - \vec{k} \cdot \vec{x})} + \text{c.c.} =$$

$$= |f + g| \cos(\omega t - \vec{k} \cdot \vec{x} + \delta') \tag{35a}$$

and

$$E_1'' \equiv i \cdot \left(\frac{f-g}{2}\right) e^{i(\omega t - \vec{k} \cdot \vec{x})} + \text{c.c.} =$$

$$= |f - g| \cos(\omega t - \vec{k} \cdot \vec{x} + \delta'') \tag{35b}$$

where δ' is the phase of the complex number $(f+g)$ and δ'' is the phase of $i(f-g)$. Since $\omega << \omega_L$, the amplitudes E_1' and E_1'' are slowly varying functions of time compared with the rapidly varying primary beam.

Using (32a) and (35), the time averages appearing in equations (30f) and (30g) are easily computed and found to be:

$$\overline{E_{(0)}^2} = \frac{1}{2} |E_0|^2 e^{-\alpha z} \tag{36}$$

and

$$\overline{E_{(0)} E_{(1)}} = \frac{1}{2} |E_0| E_1' e^{-\alpha z} = \frac{1}{2} |E_0| |f+g| e^{-\alpha z} \cos(\omega t - \vec{k} \cdot \vec{x} + \delta')$$

$$= \frac{1}{4} |E_0| (f+g) e^{i(\omega t - \vec{k} \cdot \vec{x})} e^{-\alpha z} + c.c. \tag{37}$$

The first order sound and thermal waves are taken to be

$$\begin{pmatrix} \rho_1 \\ T_1 \end{pmatrix} = \frac{1}{2} \begin{pmatrix} \rho' \\ T' \end{pmatrix} e^{i(\omega t - \vec{k} \cdot \vec{x})} + c.c. \tag{38}$$

where ρ' and T' are complex amplitudes. The frequency ω and wave vector $\vec{k}$ appearing in (38) are the same as those shown in (33b) and (33c). These waves at frequency $\pm (\omega_L^{\pm} - \omega_L)$ are often called thermal Rayleigh waves or Brillouin waves.

The particle velocity $\vec{v}$ can be taken to be a first order quantity for the case where the unperturbed medium is stationary. For this reason and because the unperturbed medium is taken to be uniform, so that $\vec{\nabla} \rho_0$ and $\vec{\nabla} T_0$ are zero, there is no difference in first order between $\frac{D(\ )}{Dt}$ and the partial derivative $\frac{\partial(\ )}{\partial t}$. Thus, all of the material derivatives reduce to ordinary partial derivatives and there is no distinction between Eulerian and Lagrangian representations in the first order calculations. The continuity equation (28) becomes

$$\frac{\partial \rho_1}{\partial t} + \rho_0 \nabla \cdot \vec{v} = 0 \tag{39}$$

and the Navier-Stokes equation (26a) becomes

$$\rho_0 \frac{\partial \vec{v}}{\partial t} - [\eta \nabla^2 \vec{v} + (\eta + \eta') \vec{\nabla} (\nabla \cdot \vec{v})] = -\nabla P_1 + \frac{1}{2} \vec{\nabla} \left[\overline{E^2} \frac{(\varepsilon - 1)(\varepsilon + 2)}{3}\right] - \frac{1}{2} \overline{E^2_{(0)}} \vec{\nabla}\varepsilon + \vec{C}$$

$$= - \frac{v_s^2}{\gamma} [\vec{\nabla}\rho_1 + \beta\rho_0 \vec{\nabla} T_1] + \left[\frac{1}{2} \rho \left(\frac{\partial \varepsilon}{\partial \rho}\right)_T \vec{\nabla} \overline{E^2} + \frac{(\varepsilon - 1)}{3} \overline{E^2_{(0)}} \vec{\nabla} \varepsilon\right] + \vec{C} \tag{40}$$

The Clausius-Mossotti relation (25c) and equation (30d) have been used to obtain (40).

Now (39) and (40) can be combined in such a way as to remove $\vec{v}$ from the equations. To accomplish this, (39) is differentiated with respect to time and the divergence of (40) is taken. The quantity $\frac{\partial}{\partial t} \nabla \cdot \vec{v} \equiv \nabla \cdot \frac{\partial \vec{v}}{\partial t}$ is then eliminated between the resulting equations to produce:

$$\frac{\partial^2 \rho_1}{\partial t^2} - \frac{2\eta + \eta'}{\rho_0} \nabla^2 \left(\frac{\partial \rho_1}{\partial t}\right) - \frac{v_s^2}{\gamma} [\nabla^2 \rho_1 + \beta\rho_0 \vec{\nabla} T_1] =$$

$$= - \nabla \cdot \left[\frac{1}{2} \rho \left(\frac{\partial \varepsilon}{\partial \rho}\right)_T \vec{\nabla} \overline{E^2} + \frac{(\varepsilon - 1)}{3} \overline{E^2_{(0)}} \vec{\nabla} \varepsilon + \vec{C}\right]$$

$$= - \frac{\varepsilon - 1}{3} \overline{E^2_{(0)}} \nabla^2 \varepsilon - \frac{(\varepsilon - 1)(\varepsilon + 2)}{3} \nabla^2 \overline{E_{(0)} E_{(1)}} \tag{41}$$

where the Clausius-Mossotti relation has again been used and the extremely small term, $\frac{1}{3} (\varepsilon - 1) \alpha \overline{E^2} \hat{e}_z \cdot \vec{\nabla}\varepsilon$, has been dropped along with other second order terms. The gravity term is also dropped in (41) because it is of no interest in the present considerations. The counter term $\vec{C}$ has performed the task for which it was introduced. The net effect of the term is the instruction that the Laplacian acting on $\overline{E_{(0)} E_{(1)}}$ should not act on the damping factor $e^{-\alpha z}$.

For convenience, the following notation is introduced:

$$u^2 \equiv \frac{v_s^2}{\gamma} \quad , \qquad \text{so that} \tag{42a}$$

u = isothermal speed of sound in the unperturbed medium

$$A \equiv \left(\frac{\partial \varepsilon_1}{\partial \rho}\right)_T + \left(\frac{\partial \varepsilon_2}{\partial \rho}\right)_T \overline{E_{(0)}^2} \approx \frac{1}{\rho_0} \frac{(\varepsilon_{oe} - 1)(\varepsilon_{oe} + 2)}{3} \tag{42b}$$

$$B \equiv \left(\frac{\partial \varepsilon_1}{\partial T}\right)_\rho + \left(\frac{\partial \varepsilon_2}{\partial T}\right)_\rho \overline{E_{(0)}^2} \tag{42c}$$

$$N \equiv \frac{(2\eta + \eta')}{\rho_0} \tag{42d}$$

In this notation, $\nabla^2 \varepsilon$ becomes, to first order,

$$\nabla^2 \varepsilon = \vec{\nabla} \cdot \left[\left(\frac{\partial \varepsilon}{\partial \rho}\right)_T \vec{\nabla} \rho_1 + \left(\frac{\partial \varepsilon}{\partial T}\right)_\rho \vec{\nabla} T_1\right] = A \nabla^2 \rho_1 + B \nabla^2 T_1 \tag{43}$$

and equation (41) becomes

$$\frac{\partial^2 \rho_1}{\partial t^2} - N \nabla^2 \left(\frac{\partial \rho_1}{\partial t}\right) = u^2 [\nabla^2 \rho_1 + \beta \rho_0 \nabla^2 T_1] +$$

$$+ \frac{\varepsilon_{oe} - 1}{3} \left[\overline{E_{(0)}^2} (A \nabla^2 \rho_1 + B \nabla^2 T_1) + (\varepsilon_{oe} + 2) \nabla^2 \overline{E_{(0)} E_{(1)}}\right] \tag{44}$$

To first order, the thermal transfer equation (27a) becomes

$$\rho_0 C_v \frac{\partial T_1}{\partial t} - \frac{C_v(\gamma - 1)}{\beta} \frac{\partial \rho_1}{\partial t} = \kappa \nabla^2 T_1 + \alpha c \sqrt{\varepsilon_{oe}} \left[\overline{E_{(0)}^2} + 2 \overline{E_{(0)} E_{(1)}}\right] . \tag{45}$$

Upon substitution of equations (32a), (35), (36), (37) and (38) into equations (31b), (44), and (45), the Fourier transform of the set of linearized equations is obtained and the corresponding Fourier amplitudes are related by a set of four simultaneous linear equations. Two of these equations result from (31b) because two different frequencies enter into that equation. The constant

term $\alpha c\sqrt{\varepsilon_{oe}}\ \overline{E^2_{(0)}}$ is dropped from (45) because it corresponds to a uniform linear increase in the temperature of the medium which is of no interest in the dispersion relation. The damping factor

$$e^{-\frac{\alpha}{2}z}$$

divides out of (31b), the first order wave equation, but the factor $e^{-\alpha z}$ entering (44) and (45) with the $\overline{E_{(0)}E_{(1)}}$ terms does not divide out. There are two alternatives: One could go back and try to insert a double damping factor

$$\left(e^{-\frac{\alpha}{2}z}\right)^2$$

in (38), but this would be rather artificial. Instead, since α is small, the damping factor is merely replaced by 1 in (44) and (45). Thus the considerations below pertain only to values of z small enough that the decreasing amplitude of the electromagnetic waves does not significantly alter the equations for thermal and sound propagation. The four equations relating f, g, ρ', and T' are:

$$\left[\left(\varepsilon_{oe} + \frac{\varepsilon_{2(0)}}{2}E_o^2\right)\omega_+^2 - c^2k_+^2\right]f + \left[\frac{\varepsilon_{2(0)}}{2}E_o^2\omega_+^2\right]g + \left[\frac{1}{2}AE_o\omega_+^2\right]\rho' + \left[\frac{1}{2}BE_o\omega_+^2\right]T' = 0 \tag{46}$$

$$\left[\frac{\varepsilon_{2(0)}}{2}E_o^2\omega_-^2\right]f + \left[\left(\varepsilon_{oe} + \frac{\varepsilon_{2(0)}}{2}E_o^2\right)\omega_-^2 - c^2k_-^2\right]g + \left[\frac{1}{2}AE_o\omega_-^2\right]\rho' + \left[\frac{1}{2}BE_o\omega_-^2\right]T' = 0 \tag{47}$$

$$\left[\alpha c\sqrt{\varepsilon_{oe}}E_o\right]f + \left[\alpha c\sqrt{\varepsilon_{oe}}E_o\right]g + \left[i\frac{C_v(\gamma-1)}{\beta}\omega\right]\rho' + \left[-\kappa k^2 - i\rho_o C_v\omega\right]T' = 0 \tag{48}$$

$$\left[\frac{(\varepsilon_{oe}-1)(\varepsilon_{oe}+2)}{6} E_o k^2\right] f + \left[\frac{(\varepsilon_{oe}-1)(\varepsilon_{oe}+2)}{6} E_o k^2\right] g +$$

$$+ \left[\omega^2 - iN\omega k^2 - \left(u^2 - \frac{\varepsilon_{oe}-1}{6} AE_o^2 k^2\right)\right] \rho' +$$

$$+ \left[\left(-u^2 \beta\rho_o + \frac{\varepsilon_{oe}-1}{6} BE_o^2\right) k^2\right] T' = 0 \qquad (49)$$

Throughout these equations, E_o has been written in place of $|E_o|$. Since only $|E_o|$ appears, the phase δ does not enter these equations. Therefore, without loss of generality. E_o will be considered to be real and positive. The consistency condition for these four equations is the vanishing of the determinant of the coefficients of f, g, ρ' and T'. Since in (48), and also in (49), f and g have the same coefficient, this 4X4 determinant can be written as the sum of two 3X3 determinants after replacing the first column by the difference of the first and second columns. These two 3X3 determinants may then be added to form a single 3X3 determinant after absorbing the external factors into the top rows. Expanding the resulting 3X3 determinant along its top row and setting the result equal to zero, one obtains the following relation between the frequency and the wave vector $\vec{k}$, the dispersion relation for the system:

$$0 = \left\{\left(i\omega + \frac{\kappa}{\rho_o C_v} k^2\right)\left[\omega^2 - iN\omega k^2 - \left(u^2 - \frac{\varepsilon_{oe}-1}{6} AE_o^2\right)k^2\right] - i(\gamma-1)\left(u^2 - \frac{\varepsilon_{oe}-1}{6}\frac{BE_o^2}{\beta\rho_o}\right)\omega k^2\right\} \cdot$$

$$\cdot\left\{\left(c^2k_+^2 - \varepsilon_{oe}\omega_+^2\right)\left(c^2k_-^2 - \varepsilon_{oe}\omega_-^2\right) - \frac{\varepsilon_{2(0)}E_o^2}{2} \cdot\right.$$

$$\left.\cdot\left[\omega_+^2\left(c^2k_-^2 - \varepsilon_{oe}\omega_-^2\right) + \omega_-^2\left(c^2k_+^2 - \varepsilon_{oe}\omega_+^2\right)\right]\right\}$$

$$+\left\{\begin{array}{l} Ak^2\left[\frac{(\varepsilon_{oe}-1)(\varepsilon_{oe}+2)}{6}\left(i\omega + \frac{\kappa}{\rho_o C_v} k^2\right) - \frac{\alpha c\sqrt{\varepsilon_{oe}}}{C_v}\left(u^2 - \frac{\varepsilon_{oe}-1}{6}\frac{BE_o^2}{\rho_o\beta}\right)\right] + \\ + B\left\{i\frac{(\gamma-1)}{\beta\rho_o} - \frac{(\varepsilon_{oe}-1)(\varepsilon_{oe}+2)}{6}\omega k^2 - \frac{\alpha c\sqrt{\varepsilon_{oe}}}{\rho_o C_v}\left[\omega^2 - iN\omega k^2 - \left(u^2 - \frac{\varepsilon_{oe}-1}{6} AE_o^2\right)k^2\right]\right\} \end{array}\right\} \cdot$$

$$\cdot\frac{E_o^2}{2}\left[\omega_+^2\left(c^2k_-^2 - \varepsilon_{oe}\omega_-^2\right) + \omega_-^2\left(c^2k_+^2 - \varepsilon_{oe}\omega_+^2\right)\right] \qquad (50)$$

In order to put (50) in a slightly more compact form, the following abbreviations are introduced.

$$\kappa' \equiv \frac{\kappa}{\rho_o C_v} \tag{51}$$

$$n_{oe} \equiv \sqrt{\varepsilon_{oe}} = \text{index of refraction of unperturbed medium} \tag{52}$$

$$I_L \equiv \frac{n_{oe}\, cE_o^2}{2} = \text{power in incident laser beam/unit area} \tag{53}$$

$$A' \equiv \frac{\varepsilon_{oe}-1}{6} AE_o^2 \tag{54}$$

$$B' \equiv \frac{\varepsilon_{oe}-1}{6} B \frac{E_o^2}{\rho_o \beta} \tag{55}$$

$$2\omega_L \xi_+ \equiv (c^2k_+^2 - \varepsilon_{oe}\omega_+^2) \tag{56}$$

$$2\omega_L \xi_- \equiv (c^2k_-^2 - \varepsilon_{oe}\omega_-^2) \tag{57}$$

The dispersion relation can now be expressed in the form:

$$\left\{(\omega - i\kappa' k^2)[\omega^2 - iN\omega k^2 - (u^2 - A')k^2] - (\gamma-1)(u^2-B')\omega k^2\right\} \cdot$$

$$\cdot \left[\xi_+\xi_- - \frac{\varepsilon_{2(0)}E_o^2}{2}\left(\frac{\xi_+\omega_-^2 + \xi_-\omega_+^2}{2\omega_L}\right)\right] =$$

$$= -\left\{Ak^2\left[\frac{\rho_o A}{2}(\omega - i\kappa' k^2) + i\frac{\alpha c n_{oe}\beta}{C_v}(u^2 - B')\right] + \right.$$

$$\left. + B\left\{\frac{\gamma-1}{\beta}\frac{A}{2}\omega k^2 + i\frac{\alpha c n_{oe}}{\rho_o C_v}\left[\omega^2 - iN\omega k^2 - (u^2 - A')k^2\right]\right\}\right\} \cdot$$

$$\cdot \frac{E_o^2}{2}\left(\frac{\xi_+\omega_-^2 + \xi_-\omega_+^2}{2\omega_L}\right) \tag{58}$$

For comparison, the dispersion relation obtained by K. A. Brueckner and S. Jorna[4] for frequencies outside the Raman scattering range is:

$$\omega[\omega^2 - v_s^2 k^2 - iN\omega k^2]\,\xi_L + I_L(\nu\omega + i\delta)k^2 = 0 \tag{59}$$

where

$$\xi_L \equiv \left(k^2 - \frac{2\varepsilon_{2(0)}}{n_{oe}^3 c} I_L k_L^2\right) - 4\left(\frac{n_{oe} k_L}{ck}\right)^2 \left(\omega - \frac{c}{n_{oe}} k_z\right)^2 \tag{59a}$$

$$\nu \equiv \frac{\rho_o A^2 k_L^2}{n_{oe}^3 c} \tag{59b}$$

$$\delta \equiv \frac{2A\beta v_s^2 \alpha k_L^2}{n_{oe}^2 C_\rho} \tag{59c}$$

Although equation (58) is considerably more complicated in structure than equation (59), the general features of the two equations are the same. As a first approach to the analysis of (58), one should realize that (53) relates the power in the primary laser beam to E_o^2. Thus, the free modes of the system can be obtained by letting $E_o^2 \to 0$ in (58). With no power in the incident beam, therefore, (58) reduces to

$$\left[\left(\omega - i\frac{\kappa}{\rho_o C_v} k^2\right)(\omega^2 - iN\omega k^2 - u^2 k^2) - (\gamma-1)u^2\omega k^2\right]\cdot$$
$$\cdot\left[c^2(k_L^2 + k^2 + 2k_L k_3) - \varepsilon_{L(0)}\,(\omega_L + \omega)^2\right]\cdot$$
$$\cdot\left[c^2(k_L^2 + k^2 - 2k_L k_3) - \varepsilon_{L(0)}\,(\omega_L - \omega)^2\right] = 0 \tag{60}$$

The first factor in (60) contains a non-propagating thermal wave and two damped sound waves coupled by the term $(\gamma-1)u^2\omega k^2$. The last two factors correspond to the four free modes for scattered, undamped electromagnetic waves:

$$\frac{\omega}{\omega_L} = \sigma \pm \sqrt{1 + \frac{k^2}{k_L^2} + 2\sigma\frac{k_3}{|k_L|}} \qquad \text{where } \sigma = \pm 1 \tag{61}$$

specified by given values of k^2 and k_3. Two of the roots are low frequency ($\omega << \omega_L$), whereas the other two have frequencies of the same order as the laser frequency. It is clear that the roots at the high frequency should be eliminated, because it has been assumed previously, in evaluating time averages, that the perturbed solutions vary much more slowly than the optical waves. Therefore, factors like

$$[c^2k^2 - \varepsilon_{L(0)}\omega_+^2] \tag{62}$$

will be replaced by

$$\varepsilon_{L(0)}[2\omega_L][c_L k_+ - \omega_+] , \tag{63}$$

where

$$c_L \equiv \frac{c}{\sqrt{\varepsilon_{L(0)}}} = \text{velocity of light in the medium} \tag{64}$$

Thus the free modes will include three thermal-sound waves and two electromagnetic waves.

All of the terms in (60) result from the left hand side of (58) because the right hand side is proportional to the power in the primary laser beam. Now, as the power in the laser beam is turned on, the right hand side couples the five free modes described by (60). Additional tiny coupling arises inside the left hand side itself through the A', B', and $\varepsilon_{2(0)}$ terms.

For detailed consideration, the case of a primary laser beam at 10.6 μ propagating through air at approximately 10°C and at standard pressure will be discussed. The numerical values for the parameters appearing in the dispersion relation are:[7]

$\omega_L = 1.773 \times 10^{14}\ \text{sec}^{-1}$, $k_L = 5{,}920\ \text{cm}^{-1}$ $\rho_0 = 1.25 \times 10^{-3}\ \text{gm/cm}^3$

$N = 0.284\ \text{cm}^2/\text{sec}$ $\beta = 3.67 \times 10^{-3}\ \text{deg}^{-1}$

$$C_v = 7.143 \times 10^6 \text{ erg/gm-deg} \qquad \gamma = 1.4$$

$$\kappa' = 0.28 \text{ cm}^2/\text{sec} \qquad \varepsilon_o = 1 + 5.65 \times 10^{-4}$$

$$n_o = 1 + 2.82 \times 10^{-4} \qquad \alpha = (3 \times 10^{-7} \text{ cm}^{-1})\,\alpha_o$$

$$u^2 = 8.39 \times 10^8 \text{ (cm/sec)}^2 \qquad \frac{\alpha n_o c u^2 \beta}{C_v} = (3.831 \times 10^3)\,\alpha_o$$

$$\frac{\alpha n_o e}{\rho_o C_v} = 0.988\,\alpha_o \qquad \frac{\varepsilon_{2(0)} E_o^2}{2} = \left(1.37 \times 10^{-25} \frac{\text{sec}^3}{\text{gm cm}^2}\right) I_L$$

$$A = 0.452 \frac{\text{cm}^3}{\text{gm}} + \left(1.10 \times 10^{-22} \frac{\text{cm sec}^3}{\text{gm}^2}\right) I_L$$

$$\frac{A(\gamma-1)}{2\beta} = 24.7 \frac{\text{cm}^3 \text{ deg}}{\text{gm}} + \left(6.00 \times 10^{-21} \frac{\text{cm sec}^3 \text{ deg}}{\text{gm}^3}\right) I_L$$

$$\varepsilon_{oe} = 1 + 5.65 \times 10^{-4} + \left(1.37 \times 10^{-25} \frac{\text{sec}^3}{\text{gm cm}^2}\right) I_L$$

$$A' = \left(2.84 \times 10^{-15} \frac{\text{cm}^2 \text{ sec}}{\text{gm}}\right) I_L + \left(1.38 \times 10^{-36} \frac{\text{sec}^4}{\text{gm}^2}\right) I_L^2$$

$$B = \frac{\varepsilon_{2(0)} E_o^2}{T_o} = -\left(4.84 \times 10^{-28} \frac{\text{sec}^3}{\text{gm cm}^2 \text{ deg}}\right) I_L$$

$$B' = -\left(0.662 \times 10^{-36} \frac{\text{sec}^4}{\text{gm}}\right) I_L^2$$

In the above list a dimensionless absorption constant α_o of order unity has been introduced and the power I_L is in units of ergs/sec per square centimeter. Now, using these numerical values, one finds that the power dependent terms are very small for power fluxes less than 10 MW/cm^2, except for the term which represents energy absorption. In other places in the dispersion relation, the power dependent terms are connected with the nonlinear index, and will be omitted in the following. (The terms omitted are related to self-focusing in a manner described by Brueckner and Jorna.[4]) This neglect of the nonlinear index and of the weak dependence of the optical coefficients of gases on the temperature for fixed density allows the simplification of the dispersion

relation to:

$$\left\{[\omega - i\kappa' k^2][\omega^2 - iN\omega k^2 - u^2k^2] - (\gamma-1)\, u^2\omega k^2\right\}\cdot$$

$$\cdot[c_L k_+ - \omega_+][c_L k_- - \omega_-] =$$

$$= -\frac{Ak^2\omega_L I_L}{2\varepsilon_L}\left\{[c_L k_+ - \omega_+] + [c_L k_- - \omega_-]\right\}\cdot$$

$$\cdot\left[\frac{\rho_0 A}{2}(\omega - i\kappa' k^2) + i\,\frac{\alpha c n_0 \beta u^2}{C_v}\right] \qquad (65)$$

In addition, for air at reasonable powers, the term $\frac{\rho_0 A}{2}(\omega - i\kappa' k^2)$ on the right hand side is negligible compared to $\frac{\alpha c n_0 \beta u^2}{C_v}$. Introducing the variable

$$\nu \equiv \frac{k_3}{k} \qquad (66)$$

instead of k_3, and defining

$$\tau \equiv \frac{A\omega_L \beta\alpha I_L}{\sqrt{\varepsilon_L}\, C_p}, \qquad (67)$$

which corresponds to the parameter used in Ref. [4], the dispersion relation can be written in the form

$$[(\omega - i\kappa' k^2)(\omega^2 - iN\omega k^2 - u^2k^2) - (\gamma-1)u^2\omega k^2] =$$

$$= \frac{i\tau}{2} v_s^2 k^2\left[\frac{1}{\omega - \frac{i\alpha c_L}{2} - c_L\left(k\nu + \frac{k^2}{2k_L}\right)} - \frac{1}{\omega - \frac{i\alpha c_L}{2} - c_L\left(k\nu - \frac{k^2}{2k_L}\right)}\right] \qquad (68)$$

The problem at this stage is the determination of the maximum growth rate of any Fourier component of a distortion of the plane wave as a function of the absorbed power from the beam. That is, one must solve the dispersion relation for the frequencies as a function of k, ν, I_L, and the characteristic parameters of the medium, and then find the maximum value of (- Im ω) for real ν and k with $|\nu| < 1$. Such a problem cannot be solved analytically without

further approximations. One region of interest would be the high power limit, where the driving term would overwhelm the losses resulting from thermal conduction, viscosity, and the absorption of electromagnetic energy. In that case, all the imaginary terms in equation (68), with the sole exception of the "i" immediately preceding τ, can be dropped, reducing the dispersion relation to the form employed by Brueckner and Jorna in equation (45) of the reference [3].

To proceed analytically, Brueckner and Jorna[4] neglected the second term in the brackets on the right hand side of (68), and assumed that the maximum growth rate would occur somewhere on the curve in the ν, k plane determined by the constraint

$$\mathrm{Re}\left[\omega - c_L\left(k\nu + \frac{k^2}{2k_L}\right)\right] = 0. \tag{69}$$

Along that curve, the maximum growth rate is

$$(-\mathrm{Im}\ \omega)_{max} = \frac{1}{2}\sqrt{\tau}\ (1.08)\ , \tag{70}$$

which corresponds to

$$v_s\ k = \sqrt{\frac{\tau}{2}}\left[\frac{0.97515}{0.56305}\sqrt{\frac{1}{0.93063}}\right] \tag{71}$$

(These results differ from those in reference [4], which are erroneous.) There is no assurance that the actual maximum growth rate does lie along the one-dimensional subset of the ν,k plane assumed in reference [4]. In reference [5], a search was conducted along the line

$$\nu + \frac{k}{2k_L} = 0\ .$$

However, the result for the maximum,

$$\frac{1}{2}\sqrt{\tau}\ \ (1.06), \tag{72}$$

is two percent smaller. No other curve in the ν, k plane has been found which allows an analytical search. Nevertheless, one suspects that these answers are sufficiently close and that further analytical effort is not justified, because of the previous approximations.

An interesting unknown not discussed previously is the power flux required to stimulate these instabilities. This threshold power is clearly a critical function of the losses in the system, which therefore renders it important to treat them carefully. If the second term on the right hand side of equation (68) is dropped, the instability appears to have no threshold, because the conduction loss, which must be overcome, vanishes as $k \to 0$. However, as $k \to C$, the Stokes and anti-Stokes terms on the right hand side of equation (68) tend to cancel each other, and, therefore, there is a threshold power flux for these stimulated thermal Rayleigh scattering instabilities. This threshold was determined by computer to be 312 ergs/sec per square centimeter. (The computer program itself is exhibited in Appendix A of this report.)

The presence of a wind does not alter the growth rates for distortions. This can be easily seen by considering the problem from a frame of reference moving with the fluid. A uniform beam remains a uniform beam in the moving frame, although its direction of propagation is shifted. This shift in direction has no effect upon the stability discussion.

In order to attempt to examine the behavior of the beam in more detail, without being restricted to the linearized equations, a computer solution of the full set of laser-fluid equations was attempted. Certain computational problems were encountered and are discussed in the next section. Then, in Section IV, the results of the computer calculation are discussed.

PART III

STABILITY AND UTILITY ANALYSIS

It is well known that in the solution of partial differential equations two problems arise. The first problem is that the system of difference equations may not be stable against error growth. The second problem is that the solution of the difference equations may not converge to that of the differential equations. Von Neumann[8] proposed a necessary condition for stability for linear partial differential equations of parabolic and hyperbolic types. This condition has been generalized by Kato[9] and others.[10]

In this section, a handy sufficient condition for stability of difference systems associated with parabolic and hyperbolic equations, both linear and non-linear, will be discussed. Consideration will be given to the generation of errors in computer solutions and a new criterion for the utility of numerical integration schemes for complicated systems of equations will be proposed. The new term "utility" is introduced to distinguish the criterion from the better known criterion of "stability". Some simple applications of this criterion will be examined in this chapter, as a

prelude to its use in the more complicated laser-fluid problem.

The concept of "utility" is basically very simple. A differencing scheme is "useful" if the solutions of the difference equations are sufficiently accurate approximations to the solutions of the partial differential equations over the domain of interest. Such an integration technique may not be stable, according to the usual definition of "stability" and, thus, may not be convergent either. This lack of stability and convergence does not cause alarm, because the accuracy can be estimated. The best analogy would be an asymptotic series expansion for a function. Such an expansion may not converge to the function, yet can still be a highly satisfactory description of the function over the domain of interest.

A. The Stability Criteria

The most general form for a multi-level difference scheme is

$$A_q W_{n+q} + A_{q-1} W_{n+q-1} + \cdots\cdots\cdots + A_0 W_n + b_n = 0 \qquad (73)$$

where $A_q, A_{q-1}, \cdots A_0$ are finite-difference operators which are functions of time in general. The time is designated by n and W_n is the dependent variable of the difference equation. The actual solutions, $U_n = U(n\Delta t)$, for the associated system of differential equations will not be the same as W_n because of truncation errors h_n introduced at each step of the calculation.

An equation of the form shown in (73) results from converting any system of partial differential equations into a system of difference equations. The vector W_n is a vector with many components representing the values of each of the dependent variables at each of the spatial mesh points. In addition, some of the components of W_n can be taken to represent temporal derivatives of the dependent variables if the equation is of second or higher order in time.

Assuming that (73), when supplemented by suitable boundary and initial condition has a unique solution, one may write

$$W_{n+g} = B_{g-1} W_{n+g-1} + \cdots\cdots + B_0 W_n + J_n \ , \qquad (74)$$

where

$$B_j = -A_g^{-1} A_j \ , \quad J_j = -A_g^{-1} b_j$$

The solution of the system of differential equations, evaluated at the time $n\Delta t$, will be denoted by U_n, and the value of the solutions of the difference equations generated by the computer by W_n'. The difference between these values will be called the error and will be denoted by e_n. In general $W_n' \neq W_n$ because of round off errors.

If e_n is sufficiently small then it will satisfy a linear system of difference equations.

$$e_{n+g} = C_{g-1} e_{n+g-1} + \cdots\cdots + C_0 e_n + G_n \ . \qquad (75)$$

G_n represents the local errors introduced at each step and is the sum of truncation errors and round off errors. For linear equations, $C_j = B_j$ and C_j will be independent of n if the time does not enter explicitly into the linear equation. However, if the basic system of equations is non-linear, then $C_j(n) \neq B_j(n)$.

The vectors $e_n, e_{n+1}, \cdots\cdots, e_{n+g-1}$ as well as $W_n, W_{n+1} \cdots\cdots, W_{n+g-1}$ can be arranged so that the com-

ponents form new vectors, E_n and W_n, with g times as many components

$$E_n = \begin{pmatrix} e_{n+g-1} \\ e_{n+g-2} \\ \vdots \\ e_n \end{pmatrix} \quad \text{and} \quad W_n = \begin{pmatrix} w_{n+g-1} \\ w_{n+g-2} \\ \vdots \\ w_n \end{pmatrix} \tag{76}$$

Then equations (74) and (75) can be rewritten in the form

$$W_{n+1} = \tilde{B}_n W_n + \tilde{J}_n \,, \tag{77}$$

$$E_{n+1} = \tilde{C}_n E_n + \tilde{G}_n \,, \tag{78}$$

where

$$\tilde{B}_n \equiv \tilde{B}(n,\Delta t) \equiv \begin{bmatrix} B_{g-1}(n) & B_{g-2}(n) & \cdots & B_1(n) & B_0(n) \\ I & 0 & \cdots & 0 & 0 \\ 0 & I & \cdots & 0 & 0 \\ \vdots & \vdots & \ddots & \vdots & \vdots \\ 0 & 0 & \cdots & I & 0 \end{bmatrix} \tag{79}$$

$$\tilde{C}_n \equiv \tilde{C}(n,\Delta t) \equiv \begin{bmatrix} C_{g-1}(n) & C_{g-2}(n) & \cdots & C_1(n) & C_0(n) \\ I & 0 & \cdots & 0 & 0 \\ 0 & I & \cdots & 0 & 0 \\ \vdots & \vdots & \ddots & \vdots & \vdots \\ 0 & 0 & \cdots & I & 0 \end{bmatrix} \tag{80}$$

and

$$\tilde{\delta}_n = \begin{pmatrix} \delta_n \\ 0 \\ \vdots \\ 0 \end{pmatrix} \quad , \quad \tilde{G}_n = \begin{pmatrix} G_n \\ 0 \\ \vdots \\ 0 \end{pmatrix} . \tag{81}$$

The matrices, I, appearing in (79) and (80) are identity operators for the subspaces over which the difference operators B_j and C_j operate.

For homogeneous difference equations with time independent coefficients, the index n on $\tilde{B}_n$ can be dropped and equation (77) becomes

$$W_{n+1} = \tilde{B} W_n \tag{82}$$

where $\tilde{B} = \tilde{B}(\Delta t)$. Kantorowitch[11] defined a system of linear homogeneous difference equations with time independent coefficients to be "stable" if, for specified T, there exists a positive number τ such that $[\tilde{B}(\Delta t)]^n$ is uniformly bounded for all Δt such that $0 < \Delta t < \tau$ and for all integers n such that $0 < n\Delta t < T$.

A straightforward generalization for the case where $\tilde{B}$ is also a function of the time index n would be the following.

Definition: A system of difference equations is called stable if, for specified T, there exists a positive number τ such that the set of operator products $\tilde{B}(n,\Delta t)\tilde{B}(n-1,\Delta t) \cdots \tilde{B}(1,\Delta t)$ is uniformly bounded for all

Δt such that $0 < \Delta t < \tau$ and for all integers n such that $0 < n\Delta t < T$.

In case the spatial coordinates do not enter explicitly, the analysis of the system can be simplified by a Fourier transform technique. In such cases equation (82) will lead to an equation of the form

$$\overline{W}_{n+1}(k) = G(\Delta t, k)\,\overline{W}_n(k) \qquad (83)$$

where $\overline{W}_n(k)$ is the spatial Fourier transform of W_n. The matrix $G(\Delta t, k)$ is called the amplification matrix. An equivalent statement of the Kantorowitch stability criterion is that for specified T, there exists a positive number τ such that the set of operators $G^n(\Delta t, k)$ is uniformly bounded for all values of k and for all Δt such that $0 < \Delta t < \tau$ and for all integers n such that $0 < n\Delta t < T$.

The value of the Kantorowitch stability criterion lies in the proof by P.D. Lax[10,12] that in the limit that Δt tends to zero, all systems which are stable lead to solutions which converge to those of the associated differential equations and vice versa. To proceed it is useful to introduce some standard terms:

(1) The L_p norm of a column vector v, denoted by $|v|_p$ is defined by $|v|_p = \left[\sum_{i=1}^{N} |v_i|^p\right]^{1/p}$.

(2) The maximum norm or the L_∞ norm of a column vector,

V , denoted by $|V|_\infty$ is defined by $|V|_\infty = \max_i |V_i|$.

(3) The induced matrix norm of a matrix $\mathcal{X}$, denoted by $\|\mathcal{X}\|_p$ or $\|\mathcal{X}\|_\infty$ is defined by $\|\mathcal{X}\| = \max_V \frac{|\mathcal{X}V|}{|V|}$.

(4) The radius of a matrix $\mathcal{X}$, denoted by $R(\mathcal{X})$, is defined by $R(\mathcal{X}) \equiv \max_i \left(\sum_j |\mathcal{X}_{ij}| \right) = \|\mathcal{X}\|_\infty$.
The radius of a product of matrices is not greater than the product of the radii of the matrices.

(5) The spectral radius of a matrix $\mathcal{X}$, denoted by $\rho(\mathcal{X})$, is defined by $\rho(\mathcal{X}) = \max_i |\lambda_i|$,
where λ_i $(i = 1, 2, \cdots, m)$ are the eigenvalues of $\mathcal{X}$. Clearly, it is true that $\rho(\mathcal{X}) \le R(\mathcal{X}) = \|\mathcal{X}\|_\infty$.
If $\mathcal{X}$ is a normal matrix (commutes with its hermitoan adjoint), then it can easily be shown that

$$[\rho(\mathcal{X})]^n = R(\mathcal{X}^n) = [R(\mathcal{X})]^n .$$

With the aid of these terms, the Von Neumann necessary condition for stability can be stated in the following way. A necessary condition for stability is that there exists positive numbers τ and D such that the spectral radius $\rho(G)$ of the amplification matrix $G(\Delta t, k)$ satisfies $\rho(G) \le 1 + D\Delta t$ for all k and all Δt such that $0 < \Delta t < \tau$. If $G(\Delta t, k)$ is a normal matrix (commutes with its hermitian conjugate), then the Von Neumann condition is sufficient as well as necessary.

Many sufficient conditions for stability have been proposed.[10;12] The analysis for stability has been generalized to the case in which the coefficients of the differential equations are time dependent by P.D. Lax[10,13] and many others.[10] It was further generalized by W.G. Strang[10,14] and many others[10] to the case in which the fundamental system of equations is non-linear. These extensions will not be detailed here. Instead a handy sufficient condition for stability will be considered.

Theorem: A sufficient condition for stability is that, for specified T, there exist positive numbers τ and D such that

$$\bar{R} \leq 1 + D\Delta t \tag{84}$$

for all Δt such that $0 < \Delta t < \tau$, where

$$\bar{R} = \max_n R(\tilde{B}(n,\Delta t)) \equiv \max_n \| \tilde{B}(n,\Delta t) \|_0 \tag{85}$$

for all positive integers $n < T/\Delta t$. For a linear equation with time independent coefficients,

$$\tilde{R} = R(\tilde{B}) = \| \tilde{B} \|_\infty .$$

Proof: For $\bar{R} \leq 1 + D\Delta t$, it follows that $\bar{R}^n \leq K$ where $K = e^{DT}$. Therefore,

$$\| \tilde{B}(n,\Delta t)\tilde{B}(n-1,\Delta t) \cdots \tilde{B}(1,\Delta t) \|_\infty$$
$$= R(\tilde{B}(n,\Delta t)\tilde{B}(n-1,\Delta t) \cdots \tilde{B}(1,\Delta t))$$

$$\leq R(\tilde{B}(n,\Delta t))\, R(\tilde{B}(n-1,\Delta t)) \cdots R(\tilde{B}(1,\Delta t))$$

$$\leq \text{Max}\left\{\overline{R}^n, 1\right\} \leq K,$$

for all Δt and n such that $0<\Delta t<\tau$ and $0<n\Delta t<T$ so that the maximum norm is uniformly bounded. Since the maximum norm is uniformly bounded, then the matrix product is uniformly bounded. Thus the stability definition given above is satisfied. Q.E.D.

A matrix $\mathcal{K}$ is called a dominant diagonal matrix if the "interior radius", $R_{in}(\mathcal{K}) > 0$, where

$$R_{in}(\mathcal{K}) \equiv \min_i |\mathcal{K}_{ii}| - \max_i \sum_{j\neq i} |\mathcal{K}_{ij}|. \tag{86}$$

Lemma: For a two level implicit scheme $A(n+1)w_{n+1} = w_n$, a sufficient condition for stability for specified T is that there exist positive numbers τ and D such that

$$0 < \frac{1}{\overline{R}_{in}} \leq 1 + D\Delta t , \tag{87}$$

for all Δt such that $0<\Delta t<T$ and for all integers n such that $0<n\Delta t<T$, where

$$\overline{R}_{in} \equiv \min_n R_{in}(A(n)).$$

Proof: Since $R_{in}(A(n)) > 0$ for all n such that $0 < n\Delta t < T$, it is true that $A^{-1}(n) = B(I + E + E^2 + E^3 + \cdots)$ where

$$B = \begin{pmatrix} A_{11}^{-1} & 0 \cdots \\ 0 & A_{22}^{-1} \cdots \\ \vdots & \end{pmatrix}, \qquad E = I - AB; \text{ i.e., } E_{ij} = \begin{cases} 0 & \text{for } i = j \\ -\frac{a_{ij}}{a_{ii}} & \text{for } i \neq j. \end{cases}$$

It follows that

$$R(A^{-1}(n)) \leq R(B)\left[1 + R(E) + (R(E))^2 + (R(E))^3 + \cdots\right] = \frac{R(B)}{1 - R(E)}$$

$$\leq \frac{1}{\left[\max_i |a_{ii}|\right]\left[1 - \max_i \sum_{j \neq i} \left|\frac{a_{ij}}{a_{ii}}\right|\right]} \leq \frac{1}{\min_i |a_{ii}| - \max_i \sum_{j \neq i} |a_{ij}|}$$

$$= \frac{1}{R_{in}(A(n))}.$$

Therefore, since $\left(\frac{1}{R_{in}}\right)^n = (1 + D\Delta t)^n \leq K$ where $K = e^T$ it follows that

$$\|A^{-1}(1)A^{-1}(2)\cdots A^{-1}(n-1)A^{-1}(n)\|_\infty$$

$$\vdots = R(A^{-1}(1)A^{-1}(2)\cdots A^{-1}(n-1)A^{-1}(n))$$

$$\leq R(A^{-1}(1))R(A^{-1}(2))\cdots R(A^{-1}(n-1))R(A^{-1}(n))$$

$$\leq \frac{1}{R_{in}(A(1))} \cdot \frac{1}{R_{in}(A(2))} \cdots \cdots \frac{1}{R_{in}(A(n-1))} \cdot \frac{1}{R_{in}(A(n))}$$

$$\leq \left(\frac{1}{R_{in}}\right)^n \leq K.$$

Thus a uniform bound is obtained and the stability definition is satisfied. Q.E.D.

The above lemma offers a sufficient condition for stability of an implicit difference scheme. It is conceivable, of course, that some stable implicit difference schemes might not satisfy the criterion given in this lemma. More generous sufficient conditions can be given, but none is as easy to apply as this one.

As a practical note, it might be remarked that, for actual computation, one is often interested in using the largest value of Δt consistent with the stability requirements for a given mesh size. This is certainly the situation in the computer solution of the laser-fluid equations attempted in Part IV of this study. In such cases the relation of τ to the spatial mesh size is of great interest. The spatial intervals are often dictated by the scale of the initial configuration. For example, if the dependent variable at $t=0$ is $\sin 2\pi x$ then it is unlikely that values of Δx larger than 0.3 would be useful from the standpoint of convergence requirements. The connection between τ and the spatial mesh size can be illustrated with the diffusion equation

$$\frac{\partial u}{\partial t} = K\frac{\partial^2 u}{\partial x^2} + b\,u \qquad (88)$$

where the term bu is included to allow some exponential growth in the solution. The simplest explicit difference scheme representing (88) is

$$\frac{u_j^{n+1} - u_j^n}{\Delta t} = \frac{K}{(\Delta x)^2}\left[u_{j+1}^n - 2u_j^n + u_{j-1}^n\right] + bu_j^n , \qquad (89)$$

where n is the time index and j is the spatial step index. This difference equation can be put in the form

$$u_j^{n+1} = \left[1 - \frac{2K\Delta t}{(\Delta x)^2} + b\Delta t\right] u_j^n + \frac{K\Delta t}{(\Delta x)^2} u_{j+1}^n + \frac{K\Delta t}{(\Delta x)^2} u_{j-1}^n . \qquad (90)$$

Using, for simplicity, the handy sufficient criterion given by the theorem above, one would use (90) to evaluate $\bar{R}$. Since the time does not enter explicitly, $\bar{R} = R$. It is trivial to compute $\bar{R}$ directly from (90) without writing down the matrix $\tilde{B}$ explicitly. Doing so, one finds

$$\bar{R} = \left|1 - \frac{2K\Delta t}{(\Delta x)^2} + b\Delta t\right| + \left|\frac{K\Delta t}{(\Delta x)^2}\right| + \left|\frac{K\Delta t}{(\Delta x)^2}\right| .$$

Since K , Δt , and (Δx) are all positive, this expression simplifies immediately to

$$\bar{R} = \left|1 - \frac{2K\Delta t}{(\Delta x)^2} + b\Delta t\right| + \frac{2K\Delta t}{(\Delta x)^2} . \qquad (91)$$

The stability condition now enters through the argument necessary to remove the magnitude bars in (91). One must be careful to realize that the D in the stability

theorem: $\bar{R} \leq 1 + D\Delta t$ must not be a function of ΔX. All of stability analysis is couched in a framework in which ΔX is supposed to be allowed to go to zero in some manner. The D of the theorem must not be affected by $\Delta x \to 0$. In other words, one is not allowed to consider $\frac{2K\Delta t}{(\Delta X)^2}$ to be of order Δt as it would be for fixed ΔX. The theorem does not intend ΔX to be fixed. Thus the removal of the magnitude bars in (91) requires further analysis. The term $b\Delta t$ may, of course, be considered to be of order Δt because b is indeed fixed, independent of ΔX. If it is true that

$$\frac{2K\Delta t}{(\Delta X)^2} \leq 1 \tag{92}$$

then (91) becomes

$$\bar{R} = \left[1 - \frac{2K\Delta t}{(\Delta X)^2} + b\Delta t\right] + \frac{2K\Delta t}{(\Delta X)^2} = 1 + b\Delta t \tag{93}$$

and b plays the role of D in the theorem and the scheme is stable. The stability condition is (92), so that

$$\Delta t \leq \frac{(\Delta X)^2}{2K} \equiv \tau. \tag{94}$$

Thus τ has been discovered and related to ΔX. There is one other possibility for removing the magnitude bars in (91). If $\frac{2K\Delta t}{(\Delta X)^2} > 1$, then (91) becomes

$$\bar{R} = \frac{4K\Delta t}{(\Delta X)^2} - 1 - b\Delta t > 1 + O(\Delta t),$$

so that the scheme fails to meet the sufficient condition given in the theorem.

The points to be emphasized in the example above are the following. The quantity D appearing in the stability theorems must not depend on the spatial mesh sizes. The usefulness of the sufficient condition arises through the relation derived connecting τ with the spatial mesh sizes. This relationship typically arises by requiring the part of $\overline{R}$ that is not of order Δt to be less than or equal to one. Furthermore, a term containing spatial mesh sizes in the denominator is <u>not</u> of order Δt. As indicated earlier, there are certainly more generous sufficient conditions available in the literature than the one illustrated here, but none are as quick and easy to apply. Since, however, in computational work one never actually lets Δx and Δt go to zero, it is not clear that analysis based on such limit notions is necessarily the best approach to practical problems. As a matter of fact, peculier paradoxes such as the one discussed on page 230 of Reference[10],arise from such limit notions. In hope of obtaining criteria of greater practical value, the utility viewpoint has been devised and will be presented next.

B. The Utility Criteria

The theorems mentioned above are not practically applicable in general because, by omitting local error, there is no way to estimate the maximum error growth. Also, the increment of space variables $(\Delta x, \Delta y, \Delta z, \cdots)$ and the increment of time variable Δt do not tend to zero in actual computation. Therefore, a new criterion, "utility" is proposed here to avoid some unnecessarily stringent requirements and to limit the maximum error growth at the same time. The notation of the preceeding section will be employed below.

Definition: For given ϵ and T, and for any given initial and boundary conditions, a difference scheme is useful if there exist positive numbers τ_1 and τ_2 such that for any Δt in the interval $\tau_1 \leq \Delta t \leq \tau_2$, the absolute errors are bounded by ϵ, for all integers n such that $0 < n\Delta t < T$, where T is the physical time of interest for a given problem, Δt is the increment in time, n is the time index, and τ_1 and τ_2 are to be determined by the round off and truncation error, respectively.

Theorem: For given ϵ and T, a necessary and sufficient condition for utility is that there exist positive numbers τ_1 and τ_2 such that for any Δt in the interval

$$\tau_1 \le \alpha t \le \tau_2 \quad ,$$

$$\left| \tilde{C}_n \{ \tilde{C}_{n-1} [\tilde{C}_{n-2} (\cdots (\tilde{C}_1 E_1 + \tilde{G}_1) + \cdots) + \tilde{G}_{n-2}] + \tilde{G}_{n-1} \} + \tilde{G}_n \right|_\infty$$

$$\le \epsilon \quad , \tag{95}$$

for all integers n such that $0 < n\alpha t < T$, where

$$\left| \tilde{C}_n \{ \tilde{C}_{n-1} [\cdots] + \tilde{G}_{n-1} \} + \tilde{G}_n \right|_\infty$$

$$= \max_{i} \left| \tilde{C}(n)_{i,j_1} \{ \tilde{C}(n-1)_{j_1,j_2} [\cdots] + \tilde{G}(n)_{j_1} \} + \tilde{G}(n)_i \right| \quad . \tag{96}$$

<u>Proof:</u> From the difference equation for the error, one gets

$$E_1 = \tilde{G}_1$$

$$E_2 = \tilde{C}_1 E_1 + \tilde{G}_1$$

$$E_3 = \tilde{C}_2 E_2 + \tilde{G}_2 = \tilde{C}_2 \{ \tilde{C}_1 E_1 + \tilde{G}_1 \} + \tilde{G}_2$$

$$E_4 = \tilde{C}_3 E_3 + \tilde{G}_3 = \tilde{C}_3 \{ \tilde{C}_2 [\tilde{C}_1 E_1 + \tilde{G}_1] + \tilde{G}_2 \} + \tilde{G}_3$$

$$\cdots\cdots\cdots\cdots$$

$$\cdots\cdots\cdots\cdots$$

$$E_{n+1} = \tilde{C}_n \{ \tilde{C}_{n-1} [\cdots (\tilde{C}_1 E_1 + \tilde{G}_1) \cdots] + \tilde{G}_{n-1} \} + \tilde{G}_n \quad .$$

It is easily seen from the definition of E_n that

$$\max_n \left| e_n \right|_\infty = \max_n \left| E_n \right|_\infty \quad , \tag{97}$$

for all integers n such that $0 < n\alpha t < T$. Therefore, ϵ is the upper bound of the maximum absolute error

for any Δt in the interval $\tau_1 \le \Delta t \le \tau_2$. The maxima shown in (97) exist because only a finite set of values of n are involved for $\tau_1 > 0$. Q.E.D.

For linear equations with constant coefficients, $\tilde{C}$ is independent of n. If one makes the additional assumption that $\tilde{G}$ is also independent of n, then equation (95) becomes

$$\left| (I + \tilde{C} + \tilde{C}^2 + \tilde{C}^3 + \cdots + \tilde{C}^n)\tilde{G} \right|_\infty$$

$$= \left| \frac{\tilde{C}^{n+1} - I}{\tilde{C} - I} \tilde{G} \right|_\infty \le \epsilon . \qquad (98)$$

The local error $\tilde{G}_n$ can be expressed in the form:

$$\tilde{G}_n = P_n + H_n = P_n + h_n \Delta t^{s+1} \qquad (99)$$

where P_n and H_n are the local round off error and truncation error, respectively. For a general difference scheme, one may write $H_n = h_n \Delta t^{s+1}$, where s is determined by the difference scheme.[8]

A handy sufficient condition for utility will now be given. The following notation is introduced for convenience:

$$\bar{R} \equiv \max_n R(\tilde{C}_n) \equiv \max_n \| \tilde{C}_n \|_\infty \qquad (100)$$

$$\bar{G} \equiv \max_n |P_n|_\infty + \max_n |H_n|_\infty \equiv \bar{P} + \bar{h} \Delta t^{s+1} \qquad (101)$$

where the maxima are computed over the finite set of values of n such that $0 < n\Delta t < T$ for specified T, τ_1, and τ_2 such that $\tau_1 \le \Delta t \le \tau_2$. The set of integers n is finite because of the upper bound: $\frac{T}{\tau_1}$.

Theorem: For given ϵ and T, a sufficient condition for utility is that there exist positive numbers τ_1 and τ_2 such that

$$\frac{\bar{R}^{n+1} - 1}{\bar{R} - 1} \left(\bar{P} + \bar{h} \Delta t^{s+1} \right) \le \epsilon \qquad (102)$$

for all Δt such that $\tau_1 \le \Delta t \le \tau_2$ and for all integers n such that $0 < n\Delta t < T$.

Proof: The quantity appearing in line (95) of the preceeding theorem is

$$\left| \tilde{C}_n \left\{ \tilde{C}_{n-1} \left[\tilde{C}_{n-2} \left(\cdots \left(\tilde{C}_1 \tilde{G}_1 + \tilde{G}_1 \right) + \cdots \right) + \tilde{G}_{n-2} \right] + \tilde{G}_{n-1} \right\} + \tilde{G}_n \right|_\infty$$

$$\le \left\| \tilde{C}_n \right\|_\infty \left\{ \left\| \tilde{C}_{n-1} \right\|_\infty \left[\left\| \tilde{C}_{n-2} \right\|_\infty \left(\cdots \left(\quad \right) + \cdots \right) + \left| \tilde{G}_{n-2} \right|_\infty \right] + \left| \tilde{G}_{n-1} \right|_\infty \right\} + \left| \tilde{G}_n \right|_\infty$$

$$\le \bar{R} \left\{ \bar{R} \left[\bar{R} \left(\cdots \left(\bar{R} \bar{G} + \bar{G} \right) + \cdots \right) + \bar{G} \right] + \bar{G} \right\}_{n \text{ times}} + \bar{G}$$

$$= \left[1 + \bar{R} + \bar{R}^2 + \bar{R}^3 + \cdots + \bar{R}^n \right] \bar{G}$$

$$= \frac{\bar{R}^{n+1} - 1}{\bar{R} - 1} \left(\bar{P} + \bar{h} \Delta t^{s+1} \right)$$

Q.E.D.

For $n = \frac{T}{\Delta t}$, the LHS of (102) becomes $\frac{\bar{R}^{\frac{T}{\Delta t}+1} - 1}{\bar{R} - 1}(\bar{P} + \bar{\tau}\Delta t^{s+1})$. If Δt is very large, then the truncation error $\bar{\tau}\,\Delta t^{s+1}$ will become large and the error can surpass the bound. If, on the other hand, Δt is very small, then the round off error from $\bar{P}$ can build to a large value and surpass the error bound ϵ. There may, however, exist a region of Δt, $(\tau_1 \le \Delta t \le \tau_2)$, in which the utility condition is satisfied. Obviously, if $\bar{R} \equiv 1$, then the proof above breaks down in the last line and the criterion can be stated

$$(n+1)(\bar{P} + \bar{\tau}\Delta t^{s+1}) \le \epsilon, \qquad (103)$$

for all n such that $0 < n\Delta t < T$. This criterion would require that the minimum of $\frac{\bar{P}}{\Delta t} + \bar{\tau}\Delta t^{s}$ be less than ϵ/T. The condition, (103) would not be useful unless one actually could estimate $\bar{P}$ and $\bar{\tau}$. This can be done easily only for very simple schemes. There is, however, no necessity to take $\bar{R} = 1$ since, without loss of generality, a larger value can be used in place of $\bar{R}$. Thus (102) may be used in all cases.

A very useful corollary to this theorem can be given, based on the precondition that $\|\hat{C}\|_\infty$ can be written in the form

$$\|\hat{C}_n\|_\infty = 1 + \bar{\sigma}_n \Delta t \quad \text{so that} \quad \bar{R} = 1 + \bar{\sigma}\Delta t \qquad (104)$$

where, unlike the case of stability criteria, δ_n (and hence $\bar{\delta}$) is allowed to depend on the spatial mesh sizes. One should notice that condition (104) for $\bar{R}$ is not the same as the stability criterion (86) for two reasons: $\bar{\delta}$, unlike D, is allowed to depend on the spatial mesh sizes and, furthermore, the $\bar{R}$ in (104) is equal to $\max_n \| \tilde{C}_n \|_\infty$ only for $0 < n < \frac{T}{t_1}$, a finite set of values.

Corollary: If precondition (104) is satisfied, then the sufficient condition (102) becomes

$$\frac{(1+\bar{\delta}\Delta t)^{n+1} - 1}{\bar{\delta}\Delta t} (\bar{P} + \bar{\pi}\Delta t^{n+1}) \leq \epsilon . \qquad (105)$$

The precondition bears further discussion. Certainly, for the difference scheme

$$E_j^{n+1} = 2E_j^n + \frac{\sigma\Delta t}{\Delta x} E_{j-1}^n , \qquad (106)$$

it is true that $\| \tilde{C}_n \|_\infty = 2 + \frac{\sigma\Delta t}{\Delta x}$, so that the precondition (100) is not satisfied. In such a situation, the sufficient condition (105) could not be applied and one would have to use (102). Equation (106) represents an unusual situation, however. For difference equations resulting from differential equations written in a form where only first derivatives with respect to time arise, then one can have the explicit scheme:

$$\frac{E^{n+1}-E^n}{\Delta t} = Q_n E^n \implies E^{n+1} = E^n + \Delta t Q_n E^n, \qquad (107)$$

where Q_n is a matrix operating on the components of E^n. Notice that in this canonical situation an unusual factor like the 2 in (106) does not enter.

It happens that in very many difference schemes, the precondition (104) is automatically satisfied. There are cases, however, for which (104) imposes a real condition. For example, the diffusion equation (88) leads to (91):

$$\| C_n \|_\infty = R = \left| 1 - \frac{2K\Delta t}{(\Delta x)^2} + k\Delta t \right| + \frac{2K\Delta t}{(\Delta x)^2}.$$

Thus $\| C_n \|_\infty$ can be put in the form $1 + \bar{\delta}\Delta t$, as shown in (93) with $\bar{\delta} = k$, only at the price of accepting the condition

$$\frac{2K\Delta t}{(\Delta x)^2} \le 1 \qquad (108)$$

which happens to be the stability condition (92). Thus, in this example, one gets the stability condition as a precondition for the utility condition:

$$\frac{(1+k\Delta t)^{n+1}-1}{k\Delta t}\left(\bar{P} + \bar{h}\Delta t^{s+1}\right) \le \epsilon \qquad (109)$$

and furthermore $\bar{\delta}$ is independent of mesh size in this case. Both (108) and (109) must be satisfied in order

to appeal to the sufficiency condition (105) for utility. Instead, one can, of course, use the simple condition (102) If $\nu = 0$ in (88), then one still gets the stability criterion as a precondition and one can use (103) for the utility criterion as already discussed.

There is a third option available, if one wishes to use neither (102) nor the combination (104)-(105). One can decide to accept a slightly more restrictive condition. For example, from (91) one can write

$$\bar{R} \leq 1 + \left[\frac{4K}{(\Delta x)^2} + \nu\right]\Delta t \equiv 1 + \bar{\delta}_{eff}\Delta t \qquad (110)$$

and use $\bar{\delta}_{eff}$ in (105) to get the rather strong condition for utility

$$\frac{(1+\bar{\delta}_{eff}\Delta t)^{n+1} - 1}{\bar{\delta}_{eff}\Delta t}\left(\bar{P} + \bar{F}\Delta t^{s+1}\right) \leq \epsilon \; . \qquad (111)$$

The Schrödinger equation is similar to the diffusion equation (88), except that the factor, i, multiplies $\frac{\partial}{\partial t}$ on the left hand side of the equation. This innocuous looking factor of i has the crucial effect that no explicit difference scheme for the Schrödinger equation can be stable.[15] This can easily be seen by computing $\bar{R}$. This time there is no stability condition such as (92) and, correspondingly, the precondition (104) is, more or less, automatically

satisfied and (105) gives a utility criterion which, unlike (109), involves the spatial mesh sizes. The Schrödinger equation and other examples will be analyzed in detail at the end of this section to further illustrate the application of the utility criterion.

The practical value of criterion (105) or (111) lies in the fact that large values of n will often be used, say $n \leq N \equiv \frac{T}{\Delta t} \approx 100$. It is then useful to rewrite (105) in the form

$$(1+\bar{\delta}\Delta t)^{n+1} \leq 1 + (\bar{\delta}\Delta t)\frac{\epsilon}{(\bar{P}+\bar{h}\Delta t^{s+1})} \approx (\bar{\delta}\Delta t)\frac{\epsilon}{(\bar{P}+\bar{h}\Delta t^{s+1})}, \quad (112)$$

where it is presumed that the error bound ϵ is generous enough compared to the errors in any single step that the 1 will be insignificant and can be dropped. Taking logarithms, one then obtains the critical condition

$$\log(1+\bar{\delta}\Delta t) \approx \frac{\log(\bar{\delta}\Delta t)}{N+1} + \frac{1}{N+1}\log\left[\frac{\epsilon}{\bar{P}+\bar{h}\Delta t^{s+1}}\right]$$

$$\approx \frac{1}{N}\log\left[\frac{\epsilon}{\bar{P}+\bar{h}\Delta t^{s+1}}\right]. \quad (113)$$

where, again, it is presumed that the error bound is generous enough that a term can be dropped on the RHS. It is also presumed that $N>>1$ so that $N+1 \approx N$. Thus the useful form of (105) under these conditions is

$$\log(1+\bar{\delta}\Delta t) \leq \frac{1}{N}\log\left[\frac{\epsilon}{\bar{P}+\bar{h}\Delta t^{s+1}}\right]. \quad (114)$$

Now attention is called to the fact that it does not matter very much what one uses in (114) for the ratio, $\frac{\epsilon}{\bar{P} + \bar{h}\Delta t^{s+1}}$, because only $\frac{1}{N}$ times the logarithm of this ratio enters. For example, if

$$\frac{\epsilon}{\bar{P} + \bar{h}\Delta t^{s+1}} \approx 100 \qquad \text{and} \qquad N = 100,$$

where N is the number of steps to be used, then

$$\log(1 + \bar{\delta}\Delta t) \leq \frac{\log(100)}{100} = \frac{2.303}{50} = 0.04606.$$

Then, using a table of natural logarithms, one finds:

$$\Delta t \leq \frac{1}{21\bar{\delta}}. \tag{115}$$

If, on the other hand, a considerably more generous bound is used, say,

$$\frac{\epsilon}{\bar{P} + \bar{h}\Delta t^{s+1}} \approx 10^{22} \qquad \text{for} \qquad N = 100,$$

then

$$\log(1 + \bar{\delta}\Delta t) \leq \frac{22(2.303)}{100} = 0.507,$$

so that the condition is

$$\Delta t < \frac{1}{(\frac{1}{2})\bar{\delta}}.$$

Thus changing the error bound, ϵ, by a factor of 10^{20} only relaxes the criterion for Δt by a factor of 14. Thus one might expect to try to use the rough criterion

$$\Delta t < \frac{1}{\gamma_0 \bar{\delta}} \qquad \text{with} \quad \gamma_0 \simeq 10 , \tag{116}$$

for almost any system of equations. If (116) leads to instabilities in the computer solution, then one might increase γ_0 to, say, 40 and try again. If, on the other hand (116) leads to stable solutions, but is too restrictive, then one might decrease γ_0 to, say, 1 and try again to get stable solutions. Following this course, $\bar{P}$ and $\bar{h}$ would have to be estimated only if one wished to know the value of the error bound ϵ corresponding to (116). One must, of course, be able to distinguish between mathematical instabilities and true physical instabilities (such as the $e^{\alpha t}$ in (88))which may arise in the computer output. With some experience one is able to spot earmarks of some of the mathematical instabilities quite easily.[10]

For implicit two level schemes, it is easier to use the slightly different criterion given in the following lemma.

Lemma: For a two level implicit scheme $A^{(n+1)}E_{n+1} = E_n$, a sufficient condition for utility is

$$0 < \frac{\left[\frac{1}{\bar{R}_{in}}\right]^{n+1} - 1}{\left[\frac{1}{\bar{R}_{in}}\right] - 1} (\bar{P} + \bar{h}\Delta t^{s+1}) \leq \epsilon , \tag{117}$$

for all integers n such that $0 < n\Delta t < T$, where

$$R_{in}(A) \equiv \min_i |A_{ii}| - \max_i \sum_{j \neq i} |A_{ij}| \tag{117a}$$

and

$$\bar{R}_{in} \equiv \min_n R_{in}(A(n)). \tag{117b}$$

In some ways the utility criterion is similar to the "practical stability condition" discussed in Reference [10], but the philosophy is drastically different due to the fact that the utility criterion makes no attempt to deal overtly with questions of stability. It should also be mentioned that the utility criterion is easy to apply, even to the complicated set of equations describing the laser-fluid system. The "practical stability criterion" and other common stability criteria are extremely difficult to apply.

Partly the difference in the ease of application of the various tests arises from the fact that stability and bounded error growth (utility) really are slightly different concepts. In large part, however, the differences arise because some of the stability methods are made very complicated in order to weaken the condition on Δt as much as possible. In this regard it is quickly admitted that more complicated utility tests can easily be devised, but such matters will not be

considered here. It is a part of the utility philosophy that utility criteria should be less complicated than the equations one wishes to solve in the first place. In this way it is hoped that the major part of the computer time can be spent solving the equations of interest, rather than trying to unravel stability or utility criteria. Stable or unstable, convergent or divergent, if the computer solution correctly describes the phenomena for which the differential equations were written, then that is utility at its finest.

C. Examples of Utility Analysis

In order to illustrate the application of the utility criterion, several examples will now be given. The criterion will be applied to the Schrödinger equation, the Dirac equation, and a nonlinear partial differential equation similar to the laser self-focusing equation. In each case, three different iteration schemes are considered: a two level explicit difference scheme, a two level implicit difference scheme, and a simple multi-level "Leap-Frog" scheme. The method of finite differences is not necessarily the best means of solving these particular differential equations, nor are the selected difference schemes necessarily the best. These examples are presented chiefly to illustrate the application of utility criteria. For simplicity, it is assumed in these examples that $\epsilon = 10^{-5}$ and $\bar{P} = 10^{-15}$

Certain transformations are introduced in the examples in order to reduce truncation errors. This technique is a standard numerical procedure and is often called the "integral method." The Schrödinger equation, for example, may be put in the form:

$$\frac{\partial}{\partial t}\left[\psi \exp\left(-\frac{1}{i\hbar}\int_0^t V dt'\right)\right]$$

$$= \frac{i\hbar}{2m}(\nabla^2\psi)\exp\left(-\frac{1}{i\hbar}\int_0^t V dt'\right) \qquad (118)$$

Integrating, now, from t_n to t_{n+1}, one obtains:

$$\psi^{n+1}\exp\left(-\frac{1}{i\hbar}\int_0^{t_{n+1}} V dt\right)$$

$$= \psi^n \exp\left(-\frac{1}{i\hbar}\int_0^{t_n} V dt\right) + \frac{i\hbar}{2m}\int_{t_n}^{t_{n+1}} dt\,(\nabla^2\psi)\exp\left(-\frac{1}{i\hbar}\int_0^t V dt'\right) \qquad (119)$$

Taking $\psi = \Psi \exp\left(\frac{1}{i\hbar}\int_0^t V dt'\right)$ and making the approximation that

$$(\nabla^2\psi)\exp\left(-\frac{1}{i\hbar}\int_0^t V dt'\right)$$

$$\approx (\nabla^2\psi^n)\exp\left(-\frac{1}{i\hbar}\int_0^{t_n} V dt'\right),$$

one can proceed to obtain difference equations for the better dependent variable, Ψ^n. The integral method is incorporated into the examples below for the Schrödinger equation.

1. Schroedinger Equation

$$i\hbar\frac{\partial\psi}{\partial t} = H\psi \qquad (120)$$

i.e.

$$i\hbar\frac{\partial\psi}{\partial t} = -\frac{\hbar^2}{2m}\nabla^2\psi + V\psi \qquad (121)$$

Let

$$\psi = \Psi \exp\left(\frac{1}{i\hbar}\int_0^t V dt\right) \qquad (122)$$

so that

$$i\hbar\frac{\partial\Psi}{\partial t} = \exp\left(-\frac{1}{i\hbar}\int_0^t V\,dt\right)\left[-\frac{\hbar^2}{2m}\nabla^2\left(\Psi\exp\left(\frac{1}{i\hbar}\int_0^t V\,dt\right)\right)\right] \qquad (123)$$

(a). Two level explicit difference scheme (forward time differences)

$$\begin{aligned}\Psi_{ijk}^{n+1} = \Psi_{ijk}^{n} + \frac{i\hbar}{2m}\Big\{&\Big[\Psi_{i+1jk}^{n}\exp\left(\frac{1}{i\hbar}\int_0^{t_n}(V_{i+1jk}-V_{ijk})\,dt\right)\\ &+\Psi_{i-1jk}^{n}\exp\left(\frac{1}{i\hbar}\int_0^{t_n}(V_{i-1jk}-V_{ijk})\,dt\right)-2\Psi_{ijk}^{n}\Big]\frac{1}{(\Delta x)^2}\\ &+\Big[\Psi_{ij+1k}^{n}\exp\left(\frac{1}{i\hbar}\int_0^{t_n}(V_{ij+1k}-V_{ijk})\,dt\right)\\ &+\Psi_{ij-1k}^{n}\exp\left(\frac{1}{i\hbar}\int_0^{t_n}(V_{ij-1k}-V_{ijk})\,dt\right)-2\Psi_{ijk}^{n}\Big]\frac{1}{(\Delta y)^2}\\ &+\Big[\Psi_{ijk+1}^{n}\exp\left(\frac{1}{i\hbar}\int_0^{t_n}(V_{ijk+1}-V_{ijk})\,dt\right)\\ &+\Psi_{ijk-1}^{n}\exp\left(\frac{1}{i\hbar}\int_0^{t_n}(V_{ijk-1}-V_{ijk})\,dt\right)-2\Psi_{ijk}^{n}\Big]\frac{1}{(\Delta z)^2}\Big\}\Delta t\end{aligned} \qquad (124)$$

Since this is a linear equation, the error satisfies the relation:

$$\begin{aligned}E_{ijk}^{n+1} = E_{ijk}^{n} + \frac{i\hbar}{2m}\Big\{&\Big[E_{i+1jk}^{n}\exp\left(\frac{1}{i\hbar}\int_0^{t_n}(V_{i+1jk}-V_{ijk})\,dt\right)\\ &+E_{i-1jk}^{n}\exp\left(\frac{1}{i\hbar}\int_0^{t_n}(V_{i-1jk}-V_{ijk})\,dt\right)-2E_{ijk}^{n}\Big]\frac{1}{(\Delta x)^2}\\ &+\Big[E_{ij+1k}^{n}\exp\left(\frac{1}{i\hbar}\int_0^{t_n}(V_{ij+1k}-V_{ijk})\,dt\right)\\ &+E_{ij-1k}^{n}\exp\left(\frac{1}{i\hbar}\int_0^{t_n}(V_{ij-1k}-V_{ijk})\,dt\right)-2E_{ijk}^{n}\Big]\frac{1}{(\Delta y)^2}\end{aligned}$$

$$+\left[E^{n}_{i,j,k+1}\exp\left(\frac{1}{i\hbar}\int_{0}^{t_n}(V_{i,j,k+1}-V_{i,j,k})\,dt\right)\right.$$

$$\left.+E^{n}_{i,j,k-1}\exp\left(\frac{1}{i\hbar}\int_{0}^{t_n}(V_{i,j,k-1}-V_{i,j,k})\,dt\right)-2E^{n}_{i,j,k}\right]\frac{1}{(\Delta z)^2}\Big\}\Delta t$$

$$+P^{n}_{i,j,k}+H^{n}_{i,j,k}\,. \qquad (125)$$

For given ϵ and T, the necessary and sufficient condition for utility, involving matrix multiplication of the $\tilde{C}_n$, can be determined by using a computer. However, the sufficient condition (105) for utility of Δt for fixed $N=100$ where $T=N\Delta t=100\Delta t$ can be obtained very easily as follows:

$$R(\tilde{C})=1+\bar{\delta}\Delta t=\left|1+\frac{-i\hbar}{m}\Delta t\left(\frac{1}{(\Delta x)^2}+\frac{1}{(\Delta y)^2}+\frac{1}{(\Delta z)^2}\right)\right|$$

$$+\left|\frac{i\hbar}{m}\right|\Delta t\left[\frac{1}{(\Delta x)^2}+\frac{1}{(\Delta y)^2}+\frac{1}{(\Delta z)^2}\right]$$

$$\approx 1+\frac{\hbar}{m}\Delta t\left[\frac{1}{(\Delta x)^2}+\frac{1}{(\Delta y)^2}+\frac{1}{(\Delta z)^2}\right]$$

$$\Rightarrow\quad \bar{\delta}=\frac{\hbar}{m}\left[\frac{1}{(\Delta x)^2}+\frac{1}{(\Delta y)^2}+\frac{1}{(\Delta z)^2}\right] \qquad (126)$$

$$|h\Delta t|=|h|\Delta t$$

$$\approx\left\{\frac{1}{2}\left|\frac{\partial^2\Psi}{\partial t^2}\right|+\frac{\hbar}{12m\Delta t}\left[\left|\frac{\partial^4\Psi}{\partial x^4}\right|(\Delta x)^2+\left|\frac{\partial^4\Psi}{\partial y^4}\right|(\Delta y)^2+\left|\frac{\partial^4\Psi}{\partial z^4}\right|(\Delta z)^2\right]\right\}\Delta t\,, \qquad (127)$$

so that $S=0$.

If the initial condition of Ψ and the potential V are smooth functions of x,y,z, for a reasonable time interval

T of physical interest, then the local truncation error may be assumed to be about the same order as that of the round off error. The sufficient condition for utility is simply

$$\Delta t \leq \frac{m}{4\hbar\left[\frac{1}{(\Delta x)^2}+\frac{1}{(\Delta y)^2}+\frac{1}{(\Delta z)^2}\right]} . \tag{128}$$

Actually, there is an upper limit for T depending on the smoothness of V as well as on the boundary and on the initial condition of Ψ .

(2). Two level implicit difference scheme (backward time differences)

From (123)

$$\begin{aligned}
&\Psi_{ijk}^{n+1} - \frac{i\hbar}{2m}\Big\{\Big[\Psi_{i+1jk}^{n+1}\exp\Big(\frac{1}{i\hbar}\int_0^{t_{n+1}}(V_{i+1jk}-V_{ijk})dt\Big)\\
&+\Psi_{i-1jk}^{n+1}\exp\Big(\frac{1}{i\hbar}\int_0^{t_{n+1}}(V_{i-1jk}-V_{ijk})dt\Big)-2\Psi_{ijk}^{n+1}\Big]\frac{1}{(\Delta x)^2}\\
&+\Big[\Psi_{ij+1k}^{n+1}\exp\Big(\frac{1}{i\hbar}\int_0^{t_{n+1}}(V_{ij+1k}-V_{ijk})dt\Big)\\
&+\Psi_{ij-1k}^{n+1}\exp\Big(\frac{1}{i\hbar}\int_0^{t_{n+1}}(V_{ij-1k}-V_{ijk})dt\Big)-2\Psi_{ijk}^{n+1}\Big]\frac{1}{(\Delta y)^2}\\
&+\Big[\Psi_{ijk+1}^{n+1}\exp\Big(\frac{1}{i\hbar}\int_0^{t_{n+1}}(V_{ijk+1}-V_{ijk})dt\Big)\\
&+\Psi_{ijk-1}^{n+1}\exp\Big(\frac{1}{i\hbar}\int_0^{t_{n+1}}(V_{ijk-1}-V_{ijk})dt\Big)-2\Psi_{ijk}^{n+1}\Big]\frac{1}{(\Delta z)^2}\Big\}\Delta t\\
&=\Psi_{ijk}^{n}
\end{aligned} \tag{129}$$

The error satisfies the equation

$$E^{n+1}_{ijk} - \frac{i\hbar}{2m}\Big\{\Big[E^{n+1}_{i+1jk}\exp\Big(\frac{1}{i\hbar}\int_0^{t_{n+1}}(V_{i+1jk}-V_{ijk})\,dt\Big) + E^{n+1}_{i-1jk}\exp\Big(\frac{1}{i\hbar}\int_0^{t_{n+1}}(V_{i-1jk}-V_{ijk})\,dt\Big) - 2E^{n+1}_{ijk}\Big]\frac{1}{(\Delta x)^2} + \Big[E^{n+1}_{ij+1k}\exp\Big(\frac{1}{i\hbar}\int_0^{t_{n+1}}(V_{ij+1k}-V_{ijk})\,dt\Big) + E^{n+1}_{ij-1k}\exp\Big(\frac{1}{i\hbar}\int_0^{t_{n+1}}(V_{ij-1k}-V_{ijk})\,dt\Big) - 2E^{n+1}_{ijk}\Big]\frac{1}{(\Delta y)^2} + E^{n+1}_{ijk+1}\exp\Big(\frac{1}{i\hbar}\int_0^{t_{n+1}}(V_{ijk+1}-V_{ijk})\,dt\Big) + E^{n+1}_{ijk-1}\exp\Big(\frac{1}{i\hbar}\int_0^{t_{n+1}}(V_{ijk-1}-V_{ijk})\,dt\Big) - 2E^{n+1}_{ijk}\Big]\frac{1}{(\Delta z)^2}\Big\}\Delta t$$
$$= E^{n}_{ijk} + P^{n}_{ijk} + \alpha^{n}_{ijk}. \qquad (130)$$

To apply (117), one computes:

$$R_{in}(A) = \Big|1 + \frac{i\hbar}{m}\Delta t\Big(\frac{1}{(\Delta x)^2}+\frac{1}{(\Delta y)^2}+\frac{1}{(\Delta z)^2}\Big)\Big| - \Big|\frac{-i\hbar}{m}\Big|\Delta t\Big(\frac{1}{(\Delta x)^2}+\frac{1}{(\Delta y)^2}+\frac{1}{(\Delta z)^2}\Big)$$
$$\approx 1 - \frac{\hbar}{m}\Delta t\Big(\frac{1}{(\Delta x)^2}+\frac{1}{(\Delta y)^2}+\frac{1}{(\Delta z)^2}\Big). \qquad (131)$$

For $N = \frac{T}{\Delta t} = 100$, the sufficient condition for utility is

$$\Delta t \le \frac{m}{5\hbar\Big(\frac{1}{(\Delta x)^2}+\frac{1}{(\Delta y)^2}+\frac{1}{(\Delta z)^2}\Big)}. \qquad (132)$$

(3). A simple multilevel difference scheme (Leap-Frog Scheme)

$$\Psi_{ijk}^{n+1} = \Psi_{ijk}^{n-1} + \frac{i\hbar}{m}\Big\{\Big[\Psi_{i+1jk}^{n}\exp\Big(\frac{1}{i\hbar}\int_0^{t_n}(V_{i+1jk}-V_{ijk})dt\Big)$$

$$+\Psi_{i-1jk}^{n}\exp\Big(\frac{1}{i\hbar}\int_0^{t_n}(V_{i-1jk}-V_{ijk})dt\Big)-2\Psi_{ijk}^{n}\Big]\frac{1}{(\Delta x)^2}$$

$$+\Big[\Psi_{ij+1k}^{n}\exp\Big(\frac{1}{i\hbar}\int_0^{t_n}(V_{ij+1k}-V_{ijk})dt\Big)$$

$$+\Psi_{ij-1k}^{n}\exp\Big(\frac{1}{i\hbar}\int_0^{t_n}(V_{ij-1k}-V_{ijk})dt\Big)-2\Psi_{ijk}^{n}\Big]\frac{1}{(\Delta y)^2}$$

$$+\Big[\Psi_{ijk+1}^{n}\exp\Big(\frac{1}{i\hbar}\int_0^{t_n}(V_{ijk+1}-V_{ijk})dt\Big)$$

$$+\Psi_{ijk-1}^{n}\exp\Big(\frac{1}{i\hbar}\int_0^{t_n}(V_{ijk-1}-V_{ijk})dt\Big)-2\Psi_{ijk}^{n}\Big]\frac{1}{(\Delta z)^2}\Big\}\Delta t. \tag{133}$$

Since $\beta=2$ for three levels, $\tilde{C}$ has a very simple form namely

$$\tilde{C} = \begin{pmatrix} C_1 & I \\ I & 0 \end{pmatrix}. \tag{134}$$

Therefore,

$$R(\tilde{C}) = 1+\delta\Delta t = |1| + \Big|\frac{-2i\hbar}{m}\Delta t\Big(\frac{1}{(\Delta x)^2}+\frac{1}{(\Delta y)^2}+\frac{1}{(\Delta z)^2}\Big)\Big|$$
$$+\Big|\frac{2i\hbar}{m}\Big|\Delta t\Big(\frac{1}{(\Delta x)^2}+\frac{1}{(\Delta y)^2}+\frac{1}{(\Delta z)^2}\Big)$$
$$\approx 1+\frac{4\hbar}{m}\Delta t\Big(\frac{1}{(\Delta x)^2}+\frac{1}{(\Delta y)^2}+\frac{1}{(\Delta z)^2}\Big). \tag{135}$$

Again, for $N=\frac{T}{\Delta t}=100$, the sufficient condition for utility is

$$\Delta t \le \frac{m}{16\hbar\Big(\frac{1}{(\Delta x)^2}+\frac{1}{(\Delta y)^2}+\frac{1}{(\Delta z)^2}\Big)}. \tag{136}$$

2. Dirac Equation

$$(\not{p} - \frac{e}{c}\not{A} - mc)\psi = 0. \tag{137}$$

For the explicit representation

$$\gamma^i = \begin{bmatrix} 0 & \sigma^i \\ -\sigma^i & 0 \end{bmatrix} \qquad i = 1,2,3 \tag{138a}$$

$$\gamma^0 = \begin{bmatrix} 1 & 0 \\ 0 & -1 \end{bmatrix}, \tag{138b}$$

where

$$\sigma^1 = \begin{pmatrix} 0 & 1 \\ 1 & 0 \end{pmatrix}, \quad \sigma^2 = \begin{pmatrix} 0 & -i \\ i & 0 \end{pmatrix}, \quad \sigma^3 = \begin{pmatrix} 1 & 0 \\ 0 & -1 \end{pmatrix},$$

the equation has the form

$$\begin{bmatrix} \left[\frac{imc}{\hbar} + \left(\frac{\partial}{\partial x^0} + \frac{ie}{\hbar c}A^0\right)\right] & 0 & \left(\frac{\partial}{\partial x^3} + \frac{ie}{\hbar c}A^3\right) & \left[\left(\frac{\partial}{\partial x^1} + \frac{ie}{\hbar c}A^1\right) - i\left(\frac{\partial}{\partial x^2} + \frac{ie}{\hbar c}A^2\right)\right] \\ 0 & \left[\frac{imc}{\hbar} + \left(\frac{\partial}{\partial x^0} + \frac{ie}{\hbar c}A^0\right)\right] & \left[\left(\frac{\partial}{\partial x^1} + \frac{ie}{\hbar c}A^1\right) + i\left(\frac{\partial}{\partial x^2} + \frac{ie}{\hbar c}A^2\right)\right] & -\left(\frac{\partial}{\partial x^3} + \frac{ie}{\hbar c}A^3\right) \\ -\left(\frac{\partial}{\partial x^3} + \frac{ie}{\hbar c}A^3\right) & \left[-\left(\frac{\partial}{\partial x^1} + \frac{ie}{\hbar c}A^1\right) + i\left(\frac{\partial}{\partial x^2} + \frac{ie}{\hbar c}A^2\right)\right] & \left[\frac{imc}{\hbar} - \left(\frac{\partial}{\partial x^0} + \frac{ie}{\hbar c}A^0\right)\right] & 0 \\ \left[-\left(\frac{\partial}{\partial x^1} + \frac{ie}{\hbar c}A^1\right) - i\left(\frac{\partial}{\partial x^2} + \frac{ie}{\hbar c}A^2\right)\right] & \left(\frac{\partial}{\partial x^3} + \frac{ie}{\hbar c}A^3\right) & 0 & \left[\frac{imc}{\hbar} - \left(\frac{\partial}{\partial x^0} + \frac{ie}{\hbar c}A^0\right)\right] \end{bmatrix} \begin{bmatrix} \psi_1 \\ \psi_2 \\ \psi_3 \\ \psi_4 \end{bmatrix}$$

$$= 0. \tag{139}$$

Let

$$\psi_1 = \bar{\psi}_1 \exp\left(-\frac{imc}{\hbar} x^0\right) \quad , \quad \psi_2 = \bar{\psi}_2 \exp\left(-\frac{imc}{\hbar} x^0\right)$$

$$\psi_3 = \bar{\psi}_3 \exp\left(+\frac{imc}{\hbar} x^0\right) \quad , \quad \psi_4 = \bar{\psi}_4 \exp\left(+\frac{imc}{\hbar} x^0\right) .$$

Then

$$\frac{\partial \bar{\psi}_1}{\partial x^0} + \frac{ie}{\hbar c} A^0 \bar{\psi}_1 + \exp\left(\frac{2imcx^0}{\hbar}\right)\left[\left\{\frac{\partial}{\partial x^3} + \frac{ie}{\hbar c} A^3\right) \bar{\psi}_3 + \left[\left(\frac{\partial}{\partial x^1} + \frac{ie}{\hbar c} A^1\right) - i\left(\frac{\partial}{\partial x^2} + \frac{ie}{\hbar c} A^2\right)\right] \bar{\psi}_4 \right\} = 0 \qquad (140a)$$

$$\frac{\partial \bar{\psi}_2}{\partial x^0} + \frac{ie}{\hbar c} A^0 \bar{\psi}_2 + \exp\left(\frac{2imcx^0}{\hbar}\right)\left\{\left[\left(\frac{\partial}{\partial x^1} + \frac{ie}{\hbar c} A^1\right) + i\left(\frac{\partial}{\partial x^2} + \frac{ie}{\hbar c} A^2\right)\right] \bar{\psi}_3 - \left(\frac{\partial}{\partial x^3} + \frac{ie}{\hbar c} A^3\right) \bar{\psi}_4 \right\} = 0 \qquad (140b)$$

$$\frac{\partial \bar{\psi}_3}{\partial x^0} + \frac{ie}{\hbar c} A^0 \bar{\psi}_3 + \exp\left(-\frac{2imcx^0}{\hbar}\right)\left\{\left(\frac{\partial}{\partial x^3} + \frac{ie}{\hbar c} A^3\right) \bar{\psi}_1 + \left[\left(\frac{\partial}{\partial x^1} + \frac{ie}{\hbar c} A^1\right) - i\left(\frac{\partial}{\partial x^2} + \frac{ie}{\hbar c} A^2\right)\right] \bar{\psi}_2 \right\} = 0 \qquad (140c)$$

$$\frac{\partial \bar{\psi}_4}{\partial x^0} + \frac{ie}{\hbar c} A^0 \bar{\psi}_4 + \exp\left(-\frac{2imcx^0}{\hbar}\right)\left\{\left[\left(\frac{\partial}{\partial x^1} + \frac{ie}{\hbar c} A^1\right) + i\left(\frac{\partial}{\partial x^2} + \frac{ie}{\hbar c} A^2\right)\right] \bar{\psi}_1 - \left(\frac{\partial}{\partial x^3} + \frac{ie}{\hbar c} A^3\right) \bar{\psi}_2 \right\} = 0 . \qquad (140d)$$

(a). Two level explicit difference scheme (forward time differences)

$$\bar{\psi}^{n+1}_{1(i,j,k)} = \bar{\psi}^{n}_{1(i,j,k)} - \frac{ie}{\hbar c} A^0 \bar{\psi}^{n}_{1(i,j,k)} \Delta x^0 - \exp\left(\frac{2imcx^{0(n)}}{\hbar}\right)$$

$$\cdot \left[\left(\frac{\bar{\psi}^{n}_{3(i,j,k+1)} - \bar{\psi}^{n}_{3(i,j,k-1)}}{2\Delta x^3} + \frac{ie}{\hbar c} A^3 \bar{\psi}^{n}_{3(i,j,k)}\right)\right.$$

$$+\left(\frac{\bar{\psi}^{n}_{4(i+1,j,k)} - \bar{\psi}^{n}_{4(i-1,j,k)}}{2\Delta x^1} + \frac{ie}{\hbar c} A^1 \bar{\psi}^{n}_{4(i,j,k)}\right)$$

$$\left. -i\left(\frac{\bar{\psi}^{n}_{4(i,j+1,k)} - \bar{\psi}^{n}_{4(i,j-1,k)}}{2\Delta x^2} + \frac{ie}{\hbar c} A^2 \bar{\psi}^{n}_{4(i,j,k)}\right)\right] \Delta x^0 \qquad (141a)$$

$$\bar{\Psi}^{n+1}_{2(i,j,k)} = \bar{\Psi}^{n}_{2(i,j,k)} - \frac{ie}{\hbar c} A^{0} \bar{\Psi}^{n}_{2(i,j,k)} \Delta X^{0} - \exp\left(\frac{2imc X^{0}(n)}{\hbar}\right) \cdot$$

$$\cdot \left[\left(\frac{\bar{\Psi}^{n}_{3(i+1,j,k)} - \bar{\Psi}^{n}_{3(i-1,j,k)}}{2\Delta X^{1}} + \frac{ie}{\hbar c} A^{1} \bar{\Psi}^{n}_{3(i,j,k)} \right) \right.$$

$$+ i \left(\frac{\bar{\Psi}^{n}_{3(i,j+1,k)} - \bar{\Psi}^{n}_{3(i,j-1,k)}}{2\Delta X^{2}} + \frac{ie}{\hbar c} A^{2} \bar{\Psi}^{n}_{3(i,j,k)} \right)$$

$$\left. - \left(\frac{\bar{\Psi}^{n}_{4(i,j,k+1)} - \bar{\Psi}^{n}_{4(i,j,k-1)}}{2\Delta X^{3}} + \frac{ie}{\hbar c} A^{3} \bar{\Psi}^{n}_{4(i,j,k)} \right) \right] \Delta X^{0} \qquad (141b)$$

$$\bar{\Psi}^{n+1}_{3(i,j,k)} = \bar{\Psi}^{n}_{3(i,j,k)} - \frac{ie}{\hbar c} A^{0} \bar{\Psi}^{n}_{3(i,j,k)} \Delta X^{0} - \exp\left(\frac{-2imc X^{0}(n)}{\hbar}\right) \cdot$$

$$\cdot \left[\left(\frac{\bar{\Psi}^{n}_{1(i,j,k+1)} - \bar{\Psi}^{n}_{1(i,j,k-1)}}{2\Delta X^{3}} + \frac{ie}{\hbar c} A^{3} \bar{\Psi}^{n}_{1(i,j,k)} \right) \right.$$

$$+ \left(\frac{\bar{\Psi}^{n}_{2(i+1,j,k)} - \bar{\Psi}^{n}_{2(i-1,j,k)}}{2\Delta X^{1}} + \frac{ie}{\hbar c} A^{1} \bar{\Psi}^{n}_{2(i,j,k)} \right)$$

$$\left. - i \left(\frac{\bar{\Psi}^{n}_{2(i,j+1,k)} - \bar{\Psi}^{n}_{2(i,j-1,k)}}{2\Delta X^{2}} + \frac{ie}{\hbar c} A^{2} \bar{\Psi}^{n}_{2(i,j,k)} \right) \right] \Delta X^{0} \qquad (141c)$$

$$\bar{\Psi}^{n+1}_{4(i,j,k)} = \bar{\Psi}^{n}_{4(i,j,k)} - \frac{ie}{\hbar c} A^{0} \bar{\Psi}^{n}_{4(i,j,k)} \Delta X^{0} - \exp\left(\frac{-2imc X^{0}(n)}{\hbar}\right)$$

$$\cdot \left[\left(\frac{\bar{\Psi}^{n}_{1(i+1,j,k)} - \bar{\Psi}^{n}_{1(i-1,j,k)}}{2\Delta X^{1}} + \frac{ie}{\hbar c} A^{1} \bar{\Psi}^{n}_{1(i,j,k)} \right) \right.$$

$$+ i \left(\frac{\bar{\Psi}^{n}_{1(i,j+1,k)} - \bar{\Psi}^{n}_{1(i,j-1,k)}}{2\Delta X^{2}} + \frac{ie}{\hbar c} A^{2} \bar{\Psi}^{n}_{1(i,j,k)} \right)$$

$$\left. - \left(\frac{\bar{\Psi}^{n}_{2(i,j,k+1)} - \bar{\Psi}^{n}_{2(i,j,k-1)}}{2\Delta X^{3}} + \frac{ie}{\hbar c} A^{3} \bar{\Psi}^{n}_{2(i,j,k)} \right) \right] \Delta X^{0} . \qquad (141d)$$

Following the same procedure as for the Schroedinger equation, one can show that for $N=\frac{X^0}{\Delta X^0}=100$, the sufficient condition (111) for utility is

$$\Delta X^0 \leq \frac{1}{4\left[\frac{e}{\hbar c}\sum_{\ell=0}^{3}|A^\ell| + \left(\frac{1}{\Delta X^1}+\frac{1}{\Delta X^2}+\frac{1}{\Delta X^3}\right)\right]} . \qquad (142)$$

Naturally, there is an upper limit for X^0 as there was for the Schrödinger equation.

(b). Two level implicit difference scheme (backward time differences)

$$\bar{\Psi}^{n+1}_{1(i,j,k)} + \frac{ie}{\hbar c}A^0\bar{\Psi}^{n+1}_{1(i,j,k)}\Delta X^0 + exp\left(\frac{2imcX^0(n+1)}{\hbar}\right)\cdot$$

$$\cdot\left[\left(\frac{\Psi^{n+1}_{3(i,j,k+1)}-\Psi^{n+1}_{3(i,j,k-1)}}{2\Delta X^3}+\frac{ie}{\hbar c}A^3\Psi^{n+1}_{3(i,j,k)}\right)\right.$$

$$+\left(\frac{\Psi^{n+1}_{4(i+1,j,k)}-\Psi^{n+1}_{4(i-1,j,k)}}{2\Delta X^1}+\frac{ie}{\hbar c}A^1\bar{\Psi}^{n+1}_{4(i,j,k)}\right)$$

$$\left.-i\left(\frac{\Psi^{n+1}_{4(i,j+1,k)}-\Psi^{n+1}_{4(i,j-1,k)}}{2\Delta X^2}+\frac{ie}{\hbar c}A^2\Psi^{n+1}_{4(i,j,k)}\right)\right]\Delta X^0 = \Psi^{n}_{1(i,j,k)} \qquad (143a)$$

$$\bar{\Psi}^{n+1}_{2(i,j,k)} + \frac{ie}{\hbar c}A^0\Psi^{n+1}_{2(i,j,k)}\Delta X^0 + exp\left(\frac{2imcX^0(n+1)}{\hbar}\right)\cdot$$

$$\cdot\left[\left(\frac{\bar{\Psi}^{n+1}_{3(i+1,j,k)}-\Psi^{n+1}_{3(i-1,j,k)}}{2\Delta X^1}+\frac{ie}{\hbar c}A^1\bar{\Psi}^{n+1}_{3(i,j,k)}\right)\right.$$

$$+i\left(\frac{\Psi^{n+1}_{3(i,j+1,k)}-\Psi^{n+1}_{3(i,j-1,k)}}{2\Delta X^2}+\frac{ie}{\hbar c}A^2\bar{\Psi}^{n+1}_{3(i,j,k)}\right)$$

$$\left.-\left(\frac{\bar{\Psi}^{n+1}_{4(i,j,k+1)}-\Psi^{n+1}_{4(i,j,k-1)}}{2\Delta X^3}-\frac{ie}{\hbar c}A^3(\Psi^{n+1}_{4(i,j,k)})\right)\right]\Delta X^0 = \bar{\Psi}^{n}_{2(i,j,k)} \qquad (143b)$$

$$\Psi^{n+1}_{3(i,j,k)} + \frac{ie}{\hbar c} A^0 \Psi^{n+1}_{3(i,j,k)} \Delta x^0 + \exp\left(\frac{-2imc x^0(n+1)}{\hbar}\right) \cdot$$

$$\cdot \left[\left(\frac{\Psi^{n+1}_{1(i,j,k+1)} - \Psi^{n+1}_{1(i,j,k-1)}}{2\Delta x^3} + \frac{ie}{\hbar c} A^3 \Psi^{n+1}_{1(i,j,k)} \right) \right.$$

$$+ \left(\frac{\Psi^{n+1}_{2(i+1,j,k)} - \Psi^{n+1}_{2(i-1,j,k)}}{2\Delta x^1} + \frac{ie}{\hbar c} A^1 \Psi^{n+1}_{2(i,j,k)} \right)$$

$$\left. - i \left(\frac{\Psi^{n+1}_{3(i,j+1,k)} - \Psi^{n+1}_{3(i,j-1,k)}}{2\Delta x^2} + \frac{ie}{\hbar c} A^2 \Psi^{n+1}_{3(i,j,k)} \right) \right] \Delta x^0 = \Psi^{n}_{3(i,j,k)} \qquad (143c)$$

$$\Psi^{n+1}_{4(i,j,k)} + \frac{ie}{\hbar c} A^0 \Psi^{n+1}_{4(i,j,k)} \Delta x^0 + \exp\left(\frac{-2imc x^0(n+1)}{\hbar}\right) \cdot$$

$$\cdot \left[\left(\frac{\Psi^{n+1}_{1(i+1,j,k)} - \Psi^{n+1}_{1(i-1,j,k)}}{2\Delta x^1} + \frac{ie}{\hbar c} A^1 \Psi^{n+1}_{1(i,j,k)} \right) \right.$$

$$+ i \left(\frac{\Psi^{n+1}_{1(i,j+1,k)} - \Psi^{n}_{1(i,j-1,k)}}{2\Delta x^2} + \frac{ie}{\hbar c} A^2 \Psi^{n+1}_{1(i,j,k)} \right)$$

$$\left. - \left(\frac{\Psi^{n+1}_{2(i,j,k+1)} - \Psi^{n+1}_{2(i,j,k-1)}}{2\Delta x^3} + \frac{ie}{\hbar c} A^3 \Psi^{n+1}_{2(i,j,k)} \right) \right] \Delta x^0 = \Psi^{n}_{4(i,j,k)}. \qquad (143d)$$

Following the same procedure as for the Schrodinger equation, one gets

$$\frac{1}{R_{in}(A)} \leq \frac{1}{1 - \left[\frac{e}{\hbar c} \sum_{l=1}^{3} |A^l| + \frac{1}{\Delta x^1} + \frac{1}{\Delta x^2} + \frac{1}{\Delta x^3} \right] \Delta x^0} \qquad (144)$$

Therefore, the sufficient condition for utility with $N = \frac{x^0}{\Delta x^0} = 100$ is

$$\Delta x^0 \leq \frac{1}{5 \left[\frac{e}{\hbar c} \sum_{l=1}^{3} |A^l| + \left(\frac{1}{\Delta x^1} + \frac{1}{\Delta x^2} + \frac{1}{\Delta x^3} \right) \right]}. \qquad (145)$$

(c). A simple multilevel difference scheme (Leap-Frog scheme)

$$\Psi^{n+1}_{1(i,j,k)} = \Psi^{n-1}_{1(i,j,k)} - \frac{2ie}{\hbar c}A^0\Psi^{n}_{1(i,j,k)}\Delta x^0 - \exp\left(\frac{2imcx^0(n)}{\hbar}\right)\cdot$$
$$\cdot\left[\left(\frac{\Psi^{n}_{3(i,j,k+1)} - \Psi^{n}_{3(i,j,k-1)}}{2\Delta x^3} + \frac{ie}{\hbar c}A^3\Psi^{n}_{3(i,j,k)}\right)\right.$$
$$+\left(\frac{\Psi^{n}_{4(i+1,j,k)} - \Psi^{n}_{4(i-1,j,k)}}{2\Delta x^1} + \frac{ie}{\hbar c}A^1\Psi^{n}_{4(i,j,k)}\right)$$
$$\left.-i\left(\frac{\Psi^{n}_{4(i,j+1,k)} - \Psi^{n}_{4(i,j-1,k)}}{2\Delta x^2} + \frac{ie}{\hbar c}A^2\Psi^{n}_{4(i,j,k)}\right)\right]2\Delta x^0 \qquad (146a)$$

$$\Psi^{n+1}_{2(i,j,k)} = \Psi^{n-1}_{2(i,j,k)} - \frac{2ie}{\hbar c}A^0\Psi^{n}_{2(i,j,k)}\Delta x^0 - \exp\left(\frac{2imcx^0(n)}{\hbar}\right)\cdot$$
$$\cdot\left[\left(\frac{\Psi^{n}_{3(i+1,j,k)} - \Psi^{n}_{3(i-1,j,k)}}{2\Delta x^1} + \frac{ie}{\hbar c}A^1\Psi^{n}_{3(i,j,k)}\right)\right.$$
$$+i\left(\frac{\Psi^{n}_{3(i,j+1,k)} - \Psi^{n}_{3(i,j-1,k)}}{2\Delta x^2} + \frac{ie}{\hbar c}A^2\Psi^{n}_{3(i,j,k)}\right)$$
$$\left.-\left(\frac{\Psi^{n}_{4(i,j,k+1)} - \Psi^{n}_{4(i,j,k-1)}}{2\Delta x^3} + \frac{ie}{\hbar c}A^3\Psi^{n}_{4(i,j,k)}\right)\right]2\Delta x^0 \qquad (146b)$$

$$\Psi^{n+1}_{3(i,j,k)} = \Psi^{n-1}_{3(i,j,k)} - \frac{2ie}{\hbar c}A^0\Psi^{n}_{3(i,j,k)}\Delta x^0 - \exp\left(\frac{-2imcx^0(n)}{\hbar}\right)\cdot$$
$$\cdot\left[\left(\frac{\Psi^{n}_{1(i,j,k+1)} - \Psi^{n}_{1(i,j,k-1)}}{2\Delta x^3} + \frac{ie}{\hbar c}A^3\Psi^{n}_{1(i,j,k)}\right)\right.$$
$$+\left(\frac{\Psi^{n}_{2(i+1,j,k)} - \Psi^{n}_{2(i-1,j,k)}}{2\Delta x^1} + \frac{ie}{\hbar c}A^1\Psi^{n}_{2(i,j,k)}\right)$$
$$\left.-i\left(\frac{\Psi^{n}_{2(i,j+1,k)} - \Psi^{n}_{2(i,j-1,k)}}{2\Delta x^2} + \frac{ie}{\hbar c}A^2\Psi^{n}_{2(i,j,k)}\right)\right]2\Delta x^0 \qquad (146c)$$

$$\Psi^{n+1}_{4(i,j,k)} = \Psi^{n-1}_{4(i,j,k)} - \frac{2ie}{\hbar c}A^0\Psi^{n}_{4(i,j,k)}\Delta x^0 - \exp\left(\frac{-2imcx^0(n)}{\hbar}\right)\cdot$$
$$\cdot\left[\left(\frac{\Psi^{n}_{1(i+1,j,k)} - \Psi^{n}_{1(i-1,j,k)}}{2\Delta x^1} + \frac{ie}{\hbar c}A^1\Psi^{n}_{1(i,j,k)}\right)\right.$$
$$+i\left(\frac{\Psi^{n}_{1(i,j+1,k)} - \Psi^{n}_{1(i,j-1,k)}}{2\Delta x^2} + \frac{ie}{\hbar c}A^2\Psi^{n}_{1(i,j,k)}\right)$$
$$\left.-\left(\frac{\Psi^{n}_{2(i,j,k+1)} - \Psi^{n}_{2(i,j,k-1)}}{2\Delta x^3} + \frac{ie}{\hbar c}A^3\Psi^{n}_{2(i,j,k)}\right)\right]2\Delta x^0 . \qquad (146d)$$

Then

$$\bar{R} = 1 + 2\left[\frac{e}{\hbar c}\sum_{l=0}^{3}|A^l| + \left(\frac{1}{\Delta x^1} + \frac{1}{\Delta x^2} + \frac{1}{\Delta x^3}\right)\right]\Delta x^0 \qquad (147)$$
$$= 1 + \zeta\,\Delta x^0$$

so that the sufficient condition for utility with $N = \frac{x^0}{\Delta x^0} = 100$ is

$$\Delta x^0 \leq \frac{1}{\zeta\left[\frac{e}{\hbar c}\sum_{l=0}^{3}|A^l| + \left(\frac{1}{\Delta x^1} + \frac{1}{\Delta x^2} + \frac{1}{\Delta x^3}\right)\right]}. \qquad (148)$$

3. Non-Linear Self-Focusing Equation

$$i\frac{\partial A}{\partial t} + i\frac{\partial A}{\partial z} + \frac{\partial^2 A}{\partial r^2} + \frac{1}{r}\frac{\partial A}{\partial r} + |A|^2 A = 0 \qquad (149)$$

Let $A = A_1 + iA_2$, so that

$$\frac{\partial A_1}{\partial t} + \frac{\partial A_1}{\partial z} + \frac{\partial^2 A_2}{\partial r^2} + \frac{1}{r}\frac{\partial A_2}{\partial r} + (A_1^2 + A_2^2)A_2 = 0 \qquad (150a)$$

$$\frac{\partial A_2}{\partial t} + \frac{\partial A_2}{\partial z} - \frac{\partial^2 A_1}{\partial r^2} - \frac{1}{r}\frac{\partial A_1}{\partial r} - (A_1^2 + A_2^2)A_1 = 0 \qquad (150b)$$

(a). Two level explicit scheme (forward time differences)

$$A^{n+1}_{1(i,j)} = A^n_{1(i,j)} - \left\{\frac{A^n_{1(i,j+1)} - A^n_{1(i,j-1)}}{2\Delta z}\right.$$
$$+ \frac{A^n_{2(i+1,j)} + A^n_{2(i-1,j)} - 2A^n_{2(i,j)}}{(\Delta r)^2} + \frac{1}{i\Delta r}\cdot\left(\frac{A^n_{2(i+1,j)} - A^n_{2(i-1,j)}}{2\Delta r}\right)$$
$$\left. + \left[(A^n_{1(i,j)})^2 + (A^n_{2(i,j)})^2\right]A^n_{2(i,j)}\right\}\Delta t \qquad (151a)$$

$$A^{n+1}_{2(i,j)} = A^n_{2(i,j)} + \left\{-\frac{A^n_{2(i,j+1)} - A^n_{2(i,j-1)}}{2\Delta z}\right.$$
$$+ \frac{A^n_{1(i+1,j)} + A^n_{1(i-1,j)} - 2A^n_{1(i,j)}}{(\Delta r)^2} + \frac{1}{i\Delta r}\cdot\left(\frac{A^n_{1(i+1,j)} - A^n_{1(i-1,j)}}{2\Delta r}\right)$$
$$\left. + \left[(A^n_{1(i,j)})^2 + (A^n_{2(i,j)})^2\right]A^n_{1(i,j)}\right\}\Delta t \qquad (151b)$$

The error satisfies the approximate relation:

$$E^{n+1}_{1(i,j)} = E^{n}_{1(i,j)} - \Big\{ \frac{E^{n}_{1(i,j+1)} - E^{n}_{1(i,j-1)}}{2\Delta z} + \frac{E^{n}_{2(i+1,j)} + E^{n}_{2(i-1,j)} - 2E^{n}_{2(i,j)}}{(\Delta r)^2}$$

$$+ \frac{1}{i\Delta r} \cdot \left(\frac{E^{n}_{2(i+1,j)} - E^{n}_{2(i-1,j)}}{2\Delta r} \right) + \left[(A^{n}_{1(i,j)})^2 + 3 (A^{n}_{2(i,j)})^2 \right] E^{n}_{2(i,j)}$$

$$+ 2A^{n}_{1(i,j)} A^{n}_{2(i,j)} E^{n}_{1(i,j)} \Big\} \Delta t + P^{n}_{1(i,j)} + H^{n}_{1(i,j)} \qquad (152a)$$

$$E^{n+1}_{2(i,j)} = E^{n}_{2(i,j)} + \Big\{ - \frac{E^{n}_{2(i,j+1)} - E^{n}_{2(i,j-1)}}{2\Delta z} + \frac{E^{n}_{1(i+1,j)} + E^{n}_{1(i-1,j)} - 2E^{n}_{1(i,j)}}{(\Delta r)^2}$$

$$+ \frac{1}{i\Delta r} \cdot \left(\frac{E^{n}_{1(i+1,j)} - E^{n}_{1(i-1,j)}}{2\Delta r} \right) + \left[(A^{n}_{2(i,j)})^2 + 3 (A^{n}_{1(i,j)})^2 \right] E^{n}_{1(i,j)}$$

$$+ 2A^{n}_{1(i,j)} A^{n}_{2(i,j)} E^{n}_{2(i,j)} \Big\} \Delta t + P^{n}_{2(i,j)} + H^{n}_{2(i,j)} . \qquad (152b)$$

This yields

$$\bar{R} \le |1 + 2j_1 \Delta t| + \frac{9}{2} \frac{\Delta t}{(\Delta r)^2} + \frac{\Delta t}{\Delta z} + 2j_2 \Delta t$$

$$\le 1 + \left[\frac{1}{\Delta z} + \frac{9}{2(\Delta r)^2} + 2(j_1 + j_2) \right] \Delta t = 1 + \bar{\delta} \Delta t , \qquad (153)$$

where

$$j_1 = \max_{i,j,n} \left| A^n_{1(i,j)} A^n_{2(i,j)} \right| , \quad j_2 = \frac{1}{2} \max_{i,j,n} \left[(A^n_{1(i,j)})^2 + 3(A^n_{2(i,j)})^2, (A^n_{2(i,j)})^2 + 3(A^n_{1(i,j)})^2 \right].$$

For $N = \frac{T}{\Delta t} = 100$, the sufficient condition is

$$\Delta t \leq \frac{1}{4\left[\frac{1}{\Delta z} + \frac{9}{2(\Delta r)^2} + 2(j_1 + j_2)\right]} . \tag{154}$$

for all $n = 1, 2, \cdots, N$.

(b). Two level implicit scheme (backward time differences)

$$A^{n+1}_{1(i,j)} + \left\{ \frac{A^{n+1}_{1(i,j+1)} - A^{n+1}_{1(i,j-1)}}{2\Delta z} + \frac{A^{n+1}_{2(i+1,j)} + A^{n+1}_{2(i-1,j)} - 2A^{n+1}_{(i,j)}}{(\Delta r)^2} \right.$$
$$\left. + \frac{i}{i\Delta r} \cdot \left(\frac{A^{n+1}_{1(i+1,j)} - A^{n+1}_{2(i-1,j)}}{2\Delta r} \right) + \left[A^{n+1}_{1(i,j)})^2 + (A^{n+1}_{2(i,j)})^2 \right] A^{n+1}_{2(i,j)} \right\} \Delta t$$

$$= A^n_{1(i,j)} \tag{155a}$$

$$A^{n+1}_{2(i,j)} + \left\{ \frac{A^{n+1}_{2(i,j+1)} - A^{n+1}_{2(i,j-1)}}{2\Delta z} - \frac{A^{n+1}_{1(i+1,j)} + A^{n+1}_{1(i-1,j)} - 2A^{n+1}_{1(i,j)}}{(\Delta r)^2} \right.$$
$$\left. - \frac{1}{i\Delta r} \cdot \left(\frac{A^{n+1}_{1(i+1,j)} - A^{n+1}_{1(i-1,j)}}{2\Delta r} \right) + \left[(A^{n+1}_{1(i,j)})^2 + (A^{n+1}_{2(i,j)})^2 \right] A^{n+1}_{1(i,j)} \right\} \Delta t$$

$$= A^n_{2(i,j)} . \tag{155b}$$

Following the same procedure as in the first two examples,

$$\overline{R}_{in} = |1 + 2j_1 \Delta t| - \left(\frac{9}{2} \frac{1}{(\Delta r)^2} + \frac{1}{\Delta z} + 2j_2\right) \Delta t$$
$$\geq 1 - \left[\frac{1}{\Delta z} + \frac{9}{2(\Delta r)^2} + 2(j_1 + j_2) \right] \Delta t . \tag{156}$$

For $N = \frac{T}{\Delta t} = 100$, the sufficient condition is

$$\Delta t \leq \frac{1}{5\left[\frac{1}{\Delta z} + \frac{9}{2(\Delta r)^2} + 2(j_1 + j_2)\right]} . \qquad (157)$$

(c). A simple multilevel difference scheme (Leap-Frog scheme)

$$A^{n+1}_{1(ij)} = A^{n-1}_{1(ij)} - 2\left\{ \frac{A^n_{1(i,j+1)} - A^n_{1(i,j-1)}}{2\Delta z} + \frac{A^n_{2(i+1,j)} + A^n_{2(i-1,j)} - 2A^n_{2(ij)}}{(\Delta r)^2} + \frac{1}{i\Delta r}\cdot\left(\frac{A^n_{2(i+1,j)} - A^n_{2(i-1,j)}}{2\Delta r}\right) + \left[(A^n_{1(ij)})^2 + (A^n_{2(ij)})^2\right] A^n_{2(ij)} \right\} \Delta t \qquad (158a)$$

$$A^{n+1}_{2(ij)} = A^{n-1}_{2(ij)} + 2\left\{ - \frac{A^n_{2(i,j+1)} - A^n_{2(i,j-1)}}{2\Delta z} + \frac{A^n_{1(i+1,j)} + A^n_{1(i-1,j)} - 2A^n_{1(ij)}}{(\Delta r)^2} + \frac{1}{i\Delta r}\cdot\left(\frac{A^n_{1(i+1,j)} - A^n_{1(i-1,j)}}{2\Delta r}\right) + \left[(A^n_{1(ij)})^2 + (A^n_{2(ij)})^2\right] A^n_{1(ij)} \right\} \Delta t . \qquad (158b)$$

This yields

$$\bar{R} \leq 1 + 2\left[\frac{1}{\Delta z} + \frac{9}{2(\Delta r)^2} + 2(j_1 + j_2)\right]\Delta t = 1 + \bar{\delta}\Delta t . \qquad (159)$$

Therefore, the sufficient condition for utility of Δt with $N = \frac{T}{\Delta t} = 100$ is

$$\Delta t \leq \frac{1}{8\left[\frac{1}{\Delta z} + \frac{9}{2(\Delta r)^2} + 2(j_1 + j_2)\right]} , \qquad (160)$$

for all $n = 1, 2, \cdots, N$.

Another example, the laser-fluid system of equations considered in this study, will be given in the next

section. It is similar to, but actually simpler than, the self-focusing example just considered.

PART IV

COMPUTER SOLUTION OF THE LASER-FLUID EQUATIONS

In this section a computer solution of the full set of laser-fluid equations is presented. The two major difficulties in using numerical techniques to solve differential equations by computer are error growth and excessive computation time. In order to control the error growth, the utility criterion discussed in the preceding section has been used. Furthermore, highly accurate seven-point difference quotient representations of the differential operators were employed to reduce truncation error. A procedure for obtaining such representations is given in Appendix II. In order to handle the economic problem of large computation time, a certain amount of efficiency is introduced by minimizing the amount of core storage required of the computer. This was accomplished in part by using overlaying techniques to store several pieces of information at the same site in the computer. Thus information is stored only as long as it is needed and then is replaced with current material. The computation time was also minimized by making use of a nonuniform grid. The seven-point difference relations allowed a relatively large grid size without undue truncation error and the nonuniform grid permitted a greater grid density in the region of special interest. Thus an accurate solution could be obtained with a minimum of computation.

The laser-fluid equations were solved in the near field region of a laser pulse, initially gaussian in both r and z, propagating through air at 1 atm of pressure and at 10°C. A cylindrical geometry was used and cylindrical symmetry (no dependence on the angle ϕ) was preserved at the price of dropping the gravity term in the Navier-Stokes equation. Having cylindrical symmetry amounts to a considerable simplification in the problem, so that the inclusion

of the free convection effects due to gravity was not attempted in this analysis. The problem described above amounts to a mixed initial-boundary problem. The initial configurations of the laser beam and the fluid are specified subject to certain boundary conditions at $r = 0$ which must be satisfied at all times. Furthermore, the boundary condition at $z = 0$ is time-dependent, because the tail of the gaussian must be fed into the spatial region. For the numerical solution, a spatial mesh of grid points or stations is used to represent the rz-plane. At a given instant in time, the values of the various dependent variables are obtained at all of the stations. The difference equations are then employed with these values of the dependent variables to advance a step in time. This procedure is repeated over and over until the desired time interval has been traversed. An explicit difference scheme was used in this calculation, because such schemes are simplest to handle.

The laser-fluid equations are given in equations (25a)-(29) in Part I. As mentioned above, the gravity term was dropped. Also, the thermal conductivity, κ, was taken to be constant because its derivatives are very small. The equation of state was taken to be the ideal gas law. The numerical values used for the various parameters are the same as those given for the linearized analysis in Part II, because the same temperature and pressure were used for the undisturbed medium. The laser frequency ω and the dimensionless absorption constant α_0 were chosen to be 1.773×10^{14} sec^{-1} and 10, respectively. The wave equation, (25a), for linearly polarized light in an absorptive medium is taken to be

$$c^2\nabla^2 E = \frac{\partial^2}{\partial t^2}(\epsilon E) + \alpha c \frac{\partial}{\partial t}(\sqrt{\epsilon}\, E). \qquad (161)$$

This equation is an approximate equation describing an electric field which is polarized linearly. Strictly speaking, of course, Maxwell's equations do not

allow cylindrically symmetric, linearly polarized beam.

The solution of (161) is taken to be in the form

$$E = \frac{1}{2}(E_1 + iE_2)\, e^{i(\omega_L t - k_L z)}\, e^{-\frac{\alpha}{2}z} + \text{c.c.} \quad , \tag{162}$$

where E_1 and E_2 are slowly varying functions of $\vec{\ }$ and t and the laser frequency and wave number are related by

$$\epsilon_{oe}\omega_L^2 = c^2 k_L \quad , \tag{162a}$$

where ϵ_{oe} is defined in (30f). Substituting (162) into (161) and dropping the second derivatives of E_1 and E_2 with respect to time, one can put the wave equation in the form

$$\begin{aligned}
\frac{\partial E_1}{\partial t} = &- \frac{c^2 k_L}{\omega_L \epsilon}\frac{\partial E_1}{\partial z} + \frac{c^2}{2\omega_L \epsilon}\left[\nabla^2 E_2 + \alpha \frac{\partial E_2}{\partial z}\left(\sqrt{\frac{\epsilon_o}{\epsilon}} - 1\right) + \frac{\alpha^2}{4} E_2\right] \\
&+ \frac{\alpha c}{2\omega_L \epsilon}\left[\omega_L\,(\sqrt{\epsilon_o} - \sqrt{\epsilon})\, E_1 - \frac{1}{2\sqrt{\epsilon}}\frac{d\epsilon}{d\rho}\frac{\partial \rho}{\partial t} E_2\right] + \\
&+ \frac{\omega_L}{2\epsilon}(\epsilon - \epsilon_o) E_2 - \frac{1}{\epsilon}\frac{d\epsilon}{d\rho}\frac{\partial \rho}{\partial t} E_1 + \\
&- \frac{1}{2\omega_L \epsilon}\left[\frac{d^2\epsilon}{d\rho^2}\left(\frac{\partial \rho}{\partial t}\right)^2 E_2 - \frac{c^2 k_L}{\omega_L \epsilon}\left(2\frac{d\epsilon}{d\rho}\left(\frac{\partial \rho}{\partial t}\right)\frac{\partial E_2}{\partial z} - \frac{c^2 k_L}{\omega_L}\frac{\partial^2 E_2}{\partial z^2}\right)\right]
\end{aligned} \tag{163}$$

$$\begin{aligned}
\frac{\partial E_2}{\partial t} = &- \frac{c^2 k_L}{\omega_L \epsilon}\frac{\partial E_2}{\partial z} - \frac{c^2}{2\omega_L \epsilon}\left[\nabla^2 E_1 + \alpha \frac{\partial E_1}{\partial z}\left(\sqrt{\frac{\epsilon_o}{\epsilon}} - 1\right) + \frac{\alpha^2}{4} E_1\right] + \\
&+ \frac{\alpha c}{2\omega_L \epsilon}\left[\omega_L\,(\sqrt{\epsilon_o} - \sqrt{\epsilon})\, E_2 + \frac{1}{2\sqrt{\epsilon}}\frac{d\epsilon}{d\rho}\frac{\partial \rho}{\partial t} E_1\right] + \\
&- \frac{\omega_L}{2\epsilon}(\epsilon - \epsilon_o) E_1 - \frac{1}{\epsilon}\frac{d\epsilon}{d\rho}\frac{\partial \rho}{\partial t} E_2 + \\
&+ \frac{1}{2\omega_L \epsilon}\left[\frac{d^2\epsilon}{d\rho^2}\left(\frac{\partial \rho}{\partial t}\right)^2 E_1 - \frac{c^2 k_L}{\omega_L \epsilon}\left(2\frac{d\epsilon}{d\rho}\frac{\partial \rho}{\partial t}\frac{\partial E_1}{\partial z} - \frac{c^2 k_L}{\omega_L}\frac{\partial^2 E_1}{\partial z^2}\right)\right]
\end{aligned} \tag{164}$$

Introducing, now, cylindrical coordinates and using cylindrical symmetry and the other simplifications mentioned above, one obtains the laser-fluid equations in the following form:

$$\frac{\partial \rho}{\partial t} = - v_r \frac{\partial \rho}{\partial r} - v_z \frac{\partial \rho}{\partial z} - \rho\left(\frac{\partial v_r}{\partial r} + \frac{v_r}{r} + \frac{\partial v_z}{\partial z}\right) \tag{165}$$

$$\begin{aligned}\frac{\partial T}{\partial t} = \frac{1}{\rho}\Bigg\{\frac{1}{C_v}\Bigg[\kappa\left(\frac{\partial^2 T}{\partial r^2} + \frac{1}{r}\frac{\partial T}{\partial r} + \frac{\partial^2 T}{\partial z^2}\right) + \frac{\alpha c}{2}\sqrt{\epsilon}\ (E_1^2 + E_2^2)\, e^{-\alpha z} \\ + \eta\left[2\left(\frac{\partial v_r}{\partial r}\right)^2 + \frac{2}{r^2} v_r^2 + 2\left(\frac{\partial v_z}{\partial z}\right)^2 + 2\frac{\partial v_z}{\partial r}\frac{\partial v_r}{\partial z} + \left(\frac{\partial v_z}{\partial r}\right)^2 + \left(\frac{\partial v_r}{\partial z}\right)^2\right] \\ + \eta'\left(\frac{\partial v_r}{\partial r} + \frac{v_r}{r} + \frac{\partial v_z}{\partial z}\right)^2\Bigg] + T(\gamma-1)\left(\frac{\partial \rho}{\partial t} + v_r\frac{\partial \rho}{\partial r} + v_z\frac{\partial \rho}{\partial z}\right)\Bigg\} \\ - \left\{v_r\frac{\partial T}{\partial r} + v_z\frac{\partial T}{\partial z}\right\}\end{aligned} \tag{166}$$

$$\begin{aligned}\frac{\partial v_r}{\partial t} = - \left(v_r\frac{\partial v_r}{\partial r} + v_z\frac{\partial v_r}{\partial z} + \frac{R}{M}\frac{\partial T}{\partial r}\right) \\ + \frac{1}{2}\left[\epsilon'\left(E_1\frac{\partial E_1}{\partial r} + E_2\frac{\partial E_2}{\partial r}\right) + \frac{1}{2}(E_1^2 + E_2^2)\,\epsilon''\frac{\partial \rho}{\partial r}\right] e^{-\alpha z} \\ + \frac{1}{\rho}\Bigg[(\eta + \eta')\frac{\partial}{\partial r}\left(\frac{\partial v_r}{\partial r} + \frac{v_r}{r} + \frac{\partial v_z}{\partial z}\right) \\ + \eta\left(\frac{\partial^2 v_r}{\partial r^2} + \frac{1}{r}\frac{\partial v_r}{\partial r} - \frac{v_r}{r^2} + \frac{\partial^2 v_r}{\partial z^2}\right) - \frac{R}{M} T \frac{\partial \rho}{\partial r}\Bigg]\end{aligned} \tag{167}$$

$$v_\theta = 0 \tag{168}$$

$$\frac{\partial v_z}{\partial t} = -\left(v_r \frac{\partial v_z}{\partial r} + v_z \frac{\partial v_z}{\partial z} + \frac{R}{M}\frac{\partial T}{\partial z}\right)$$
$$+ \frac{1}{2}\left[\varepsilon'\left(E_1 \frac{\partial E_1}{\partial z} + E_2 \frac{\partial E_2}{\partial z}\right) - \frac{1}{2}\alpha(E_1^2+E_2^2)\,\varepsilon' + \frac{1}{2}(E_1^2 + E_2^2)\,\varepsilon''\frac{\partial \rho}{\partial z}\right] e^{-\alpha z}$$
$$+ \frac{1}{\rho}\left[(\eta + \eta')\frac{\partial}{\partial z}\left(\frac{\partial v_r}{\partial r} + \frac{v_r}{r} + \frac{\partial v_z}{\partial z}\right)\right.$$
$$\left. + \eta\left(\frac{\partial^2 v_z}{\partial r^2} + \frac{1}{r}\frac{\partial v_z}{\partial r} + \frac{\partial^2 v_z}{\partial z^2}\right) - \frac{R}{M} T \frac{\partial \rho}{\partial z}\right] \tag{169}$$

$$\frac{\partial E_1}{\partial t} = \frac{c^2}{2\omega_L \varepsilon}\left[-2 k_L \frac{\partial E_1}{\partial z} + \frac{\partial^2 E_2}{\partial r^2} + \frac{1}{r}\frac{\partial E_2}{\partial r} + \frac{\partial^2 E_2}{\partial z^2} + \alpha \frac{\varepsilon_o - \varepsilon}{\sqrt{\varepsilon}\,(\sqrt{\varepsilon_o} + \sqrt{\varepsilon})}\frac{\partial E_2}{\partial z} + \frac{\alpha^2}{4} E_2\right]$$
$$+ \frac{\alpha c}{2\varepsilon}\left[\frac{\varepsilon_o - \varepsilon}{\sqrt{\varepsilon_o} + \sqrt{\varepsilon}} E_1 - \frac{1}{2\omega_L \sqrt{\varepsilon}}\varepsilon' \frac{\partial \rho}{\partial t} E_2\right] + \frac{\omega_L}{2\varepsilon}(\varepsilon - \varepsilon_o) E_2 - \frac{1}{\varepsilon}\varepsilon' \frac{\partial \rho}{\partial t} E_1$$
$$- \frac{1}{2\omega_L \varepsilon}\left[\varepsilon''\left(\frac{\partial \rho}{\partial t}\right)^2 E_2 - \frac{c^2 k_L}{\omega_L \varepsilon}\left(2\varepsilon' \frac{\partial \rho}{\partial t}\frac{\partial E_2}{\partial z} - \frac{c^2 k_L}{\omega_L}\frac{\partial^2 E_2}{\partial z^2}\right)\right] \tag{170}$$

$$\frac{\partial E_2}{\partial t} = -\frac{c^2}{2\omega_L \varepsilon}\left[2 k_L \frac{\partial E_2}{\partial z} + \frac{\partial^2 E_1}{\partial r^2} + \frac{1}{r}\frac{\partial E_1}{\partial r} + \frac{\partial^2 E_1}{\partial z^2} + \alpha \frac{\varepsilon_o - \varepsilon}{\sqrt{\varepsilon}\,(\sqrt{\varepsilon_o} + \sqrt{\varepsilon})}\frac{\partial E_1}{\partial z} + \frac{\alpha^2}{4} E_1\right]$$
$$+ \frac{\alpha c}{2\varepsilon}\left[\frac{\varepsilon_o - \varepsilon}{\sqrt{\varepsilon_o} + \sqrt{\varepsilon}} E_2 + \frac{1}{2\omega_L \sqrt{\varepsilon}}\varepsilon' \frac{\partial \rho}{\partial t} E_1\right] - \frac{\omega_L}{2\varepsilon}(\varepsilon - \varepsilon_o) E_1 - \frac{1}{\varepsilon}\varepsilon' \frac{\partial \rho}{\partial t} E_2$$
$$+ \frac{1}{2\omega_L \varepsilon}\left[\varepsilon''\left(\frac{\partial \rho}{\partial t}\right)^2 E_1 - \frac{c^2 k_L}{\omega_L \varepsilon}\left(2\varepsilon' \frac{\partial \rho}{\partial t}\frac{\partial E_1}{\partial z} - \frac{c^2 k_L}{\omega_L}\frac{\partial^2 E_1}{\partial z^2}\right)\right] \tag{171}$$

where the notations

$$\varepsilon' \equiv \frac{d\varepsilon}{d\rho} \qquad \text{and} \qquad \varepsilon'' \equiv \frac{d^2\varepsilon}{d^2\rho} \tag{172a}$$

have been employed and

$$\varepsilon = \varepsilon_L + \frac{1}{2}\,\varepsilon_2\,(E_1^2 + E_2^2) \tag{172b}$$

The easiest way to obtain a variable grid size is to introduce a transformation to a new independent variable. Thus, in order to have more grid points in the region of special interest, small r, the nonlinear transformation

$$\frac{r}{r_o} \equiv \frac{x}{1 - x} \tag{173}$$

can be employed. The scale value, r_o, can be chosen later according to the dictates of convenience. After this transformation, equations (165) - (171) become, for $x \neq 0$:

$$\frac{\partial \rho}{\partial t} = -\left\{\rho\left[\frac{(1-x)^2}{r_o}\frac{\partial v_r}{\partial x} + \frac{1-x}{r_o x}\,v_r + \frac{\partial v_z}{\partial z}\right] + \frac{(1-x)^2}{r_o}\,v_r\,\frac{\partial \rho}{\partial x} + v_z\,\frac{\partial \rho}{\partial z}\right\} \tag{174}$$

$$\frac{\partial T}{\partial t} = \frac{1}{\rho}\left\{\frac{\kappa}{C_v}\left[\frac{(1-x)^4}{r_o^2}\frac{\partial^2 T}{\partial x^2} + \frac{(1-x)^3}{r_o^2}\left(\frac{1-2x}{x}\right)\frac{\partial T}{\partial x} + \frac{\partial^2 T}{\partial z^2}\right]\right.$$

$$+ \frac{2\eta+\eta'}{C_v}\left[\frac{(1-x)^4}{r_o^2}\left(\frac{\partial v_r}{\partial x}\right)^2 \frac{(1-x)^2}{r_o^2 x^2}\,v_r^2 + \left(\frac{\partial v_z}{\partial z}\right)^2\right]$$

$$+ \frac{\eta}{C_v}\left[\frac{2(1-x)}{r_o}\frac{\partial v_z}{\partial x}\frac{\partial v_r}{\partial z} + \frac{(1-x)^4}{r_o^2}\left(\frac{\partial v_z}{\partial x}\right)^2 + \left(\frac{\partial v_r}{\partial z}\right)^2\right]$$

$$\left. + \frac{2\eta'}{C_v}\left[\frac{(1-x)^3}{r_o^2 x}\,v_r\,\frac{\partial v_r}{\partial x} + \frac{1-x}{r_o x}\,v_r\,\frac{\partial v_z}{\partial z} +\right.\right.$$

$$+\frac{(1-x)^2}{r_o}\frac{\partial v_r}{\partial x}\frac{\partial v_z}{\partial z}\Bigg]+T(\gamma-1)\left[\frac{\partial \rho}{\partial t}+\frac{(1-x)^2}{r_o}v_r\frac{\partial \rho}{\partial x}+v_z\frac{\partial \rho}{\partial z}\right]$$

$$+\frac{\alpha c}{2c_v}\sqrt{\epsilon}\,(E_1^2+E_2^2)\,e^{-\alpha z}\Bigg\}$$

$$-\left\{\frac{(1-x)^2}{r_o}v_r\frac{\partial T}{\partial x}+v_z\frac{\partial T}{\partial z}\right\} \qquad (175)$$

$$\frac{\partial v_r}{\partial t}=\frac{1}{\rho}\Bigg\{\eta\frac{\partial^2 v_r}{\partial z^2}+\frac{(1-x)^2}{r_o}\left[(\eta+\eta')\frac{\partial^2 v_z}{\partial z\partial x}-\frac{R}{M}T\frac{\partial \rho}{\partial x}\right]$$

$$+(2\eta+\eta')\left[\frac{(1-x)^4}{r_o^2}\frac{\partial^2 v_r}{\partial x^2}+\frac{(1-x)^3}{r_o^2 x}(1-2x)\frac{\partial v_r}{\partial x}-\frac{(1-x)^2}{r_o^2 x^2}v_r\right]\Bigg\}$$

$$+\frac{(1-x)^2}{r_o}\Bigg\{\frac{1}{2}\left[\epsilon'\left(E_1\frac{\partial E_1}{\partial x}+E_2\frac{\partial E_2}{\partial x}\right)+\frac{\epsilon''}{2}(E_1^2+E_2^2)\frac{\partial \rho}{\partial x}\right]e^{-\alpha z}$$

$$-\left(\frac{R}{M}\frac{\partial T}{\partial x}+v_r\frac{\partial v_r}{\partial x}\right)\Bigg\}-v_z\frac{\partial v_r}{\partial z} \qquad (176)$$

$$\frac{\partial v_z}{\partial t}=\frac{1}{\rho}\Bigg\{-\frac{R}{M}T\frac{\partial \rho}{\partial z}+(\eta+\eta')\left(\frac{(1-x)^2}{r_o}\frac{\partial^2 v_r}{\partial x\partial z}+\frac{1-x}{r_o x}\frac{\partial v_r}{\partial z}+\frac{\partial^2 v_z}{\partial z^2}\right)$$

$$+\eta\left(\frac{(1-x)^4}{r_o^2}\frac{\partial^2 v_z}{\partial x^2}+\frac{(1-x)^3}{r_o^2 x}(1-2x)\frac{\partial v_z}{\partial x}+\frac{\partial^2 v_z}{\partial z^2}\right)\Bigg\}$$

$$-\left\{\frac{R}{M}\frac{\partial T}{\partial z}+\frac{(1-x)^2}{r_o}v_r\frac{\partial v_z}{\partial x}+v_z\frac{\partial v_z}{\partial x}\right\}$$

$$+\frac{1}{2}\left[\epsilon'\left(E_1\frac{\partial E_1}{\partial z}+E_2\frac{\partial E_2}{\partial z}\right)+\frac{1}{2}(E_1^2+E_2^2)\left(-\alpha\epsilon'+\epsilon''\frac{\partial \rho}{\partial z}\right)\right]e^{-\alpha z} \qquad (177)$$

$$\frac{\partial E_1}{\partial t} = \frac{1}{\varepsilon}\left\{\frac{c^2}{2\omega_L}\left[\frac{(1-x)^4}{r_o^2}\frac{\partial^2 E_2}{\partial x^2} + \frac{(1-x)^3}{r_o^2 x}(1-2x)\frac{\partial E_2}{\partial x} + \frac{\partial^2 E_2}{\partial z^2}\right.\right.$$

$$\left. - 2k_L\frac{\partial E_1}{\partial z} + \alpha\frac{\varepsilon_o-\varepsilon}{\sqrt{\varepsilon}\,(\sqrt{\varepsilon_o}+\sqrt{\varepsilon})}\frac{\partial E_2}{\partial z} + \frac{\alpha^2}{4}E_2\right]$$

$$- \left[\frac{1}{2\omega_L}\varepsilon''\left(\frac{\partial \rho}{\partial t}\right)^2 + \frac{\omega_L}{2}(\varepsilon_o-\varepsilon)\right]E_2 + \frac{c^2 k_L}{2\omega_L^2\varepsilon}\left[2\varepsilon'\frac{\partial \rho}{\partial t}\frac{\partial E_2}{\partial z} - \frac{c^2 k_L}{\omega_L}\frac{\partial^2 E_2}{\partial z^2}\right]$$

$$\left. + \frac{c}{2}\left[\alpha\frac{\varepsilon_o-\varepsilon}{\sqrt{\varepsilon_o}+\sqrt{\varepsilon}}E_1 - \frac{\alpha}{2\omega_L\sqrt{\varepsilon}}\varepsilon'\frac{\partial \rho}{\partial t}E_2\right] - \varepsilon'\frac{\partial \rho}{\partial t}E_1\right\} \qquad (178)$$

$$\frac{\partial E_2}{\partial t} = \frac{1}{\varepsilon}\left\{-\frac{c^2}{2\omega_L}\left[\frac{(1-x)^4}{r_o^2}\frac{\partial^2 E_1}{\partial x^2} + \frac{(1-x)^3}{r_o^2 x}(1-2x)\frac{\partial E_1}{\partial x} + \frac{\partial^2 E_1}{\partial z^2} + 2k_L\frac{\partial E_2}{\partial z}\right.\right.$$

$$\left. + \alpha\frac{\varepsilon_o-\varepsilon}{\sqrt{\varepsilon}\,(\sqrt{\varepsilon_o}+\sqrt{\varepsilon})}\frac{\partial E_1}{\partial z} + \frac{\alpha^2}{4}E_1\right] + \left[\frac{1}{2\omega_L}\varepsilon''\left(\frac{\partial \rho}{\partial t}\right)^2 + \frac{\omega_L}{2}(\varepsilon_o-\varepsilon)\right]E_1$$

$$- \frac{c^2 k_L}{2\omega_L^2\varepsilon}\left[2\varepsilon'\frac{\partial \rho}{\partial t}\frac{\partial E_1}{\partial z} - \frac{c^2 k_L}{\omega_L}\frac{\partial^2 E_1}{\partial z^2}\right]$$

$$\left. + \frac{c}{2}\left[\alpha\frac{\varepsilon_o-\varepsilon}{\sqrt{\varepsilon_o}+\sqrt{\varepsilon}}E_1 - \frac{\alpha}{2\omega_L\sqrt{\varepsilon}}\varepsilon'\frac{\partial \rho}{\partial t}E_1\right] - \varepsilon'\frac{\partial \rho}{\partial t}E_2\right\} \qquad (179)$$

Because of the symmetry of the problem and the regularity of the differential equations, the following boundary conditions must be satisfied at x = 0:

$$\frac{\partial E_1}{\partial x} = \frac{\partial E_2}{\partial x} = \frac{\partial T}{\partial x} = \frac{\partial \rho}{\partial x} = \frac{\partial v_z}{\partial x} = \frac{\partial v_r}{\partial z} = \frac{\partial^2 v_r}{\partial z^2} = v_r = 0$$

and (180)

$$\frac{\partial^2 v_r}{\partial x^2} = 2\frac{\partial v_r}{\partial x}$$

Equations (174)-(179) are not useful at x = 0 because indeterminate ratios such as v_r/x appear in these equations. Applying equations (180) and using L'Hopital's rule to evaluate the indeterminate ratios, one obtains the following equations for use at x = 0:

$$\frac{\partial \rho}{\partial t} = -\left\{\rho\left(\frac{2}{r_o}\frac{\partial v_r}{\partial x} + \frac{\partial v_z}{\partial z}\right) + v_z\frac{\partial \rho}{\partial z}\right\} \tag{181}$$

$$\frac{\partial T}{\partial t} = \frac{1}{\rho}\left\{\frac{\kappa}{C_v}\left(\frac{2}{r_o^2}\frac{\partial^2 T}{\partial x^2} + \frac{\partial^2 T}{\partial z^2}\right) + \frac{2\eta+\eta'}{C_v}\left[\frac{2}{r_o^2}\left(\frac{\partial v_r}{\partial x}\right)^2 + \left(\frac{\partial v_z}{\partial z}\right)^2\right]\right.$$
$$+ \frac{2\eta'}{C_v}\left[\frac{1}{r_o^2}\left(\frac{\partial v_r}{\partial x}\right)^2 + \frac{2}{r_o}\frac{\partial v_r}{\partial x}\frac{\partial v_z}{\partial z}\right] + T(\gamma-1)\left(\frac{\partial \rho}{\partial t} + v_z\frac{\partial \rho}{\partial z}\right)$$
$$\left. + \frac{\alpha c}{2C_v}\sqrt{\varepsilon}\,(E_1^2 + E_2^2)\,e^{-\alpha z}\right\} - v_z\frac{\partial T}{\partial z} \tag{182}$$

$$\frac{\partial v_r}{\partial t} = 0 \tag{183}$$

$$\frac{\partial v_z}{\partial t} = \frac{1}{\rho}\left\{-\frac{R}{M}T\frac{\partial \rho}{\partial z} + (2\eta+\eta')\frac{\partial^2 v_z}{\partial z^2} + \frac{2\eta}{r_o^2}\frac{\partial^2 v_z}{\partial x^2}\right\}$$
$$- \left\{\frac{R}{M}\frac{\partial T}{\partial z} + v_z\frac{\partial v_z}{\partial t}\right\} + \frac{1}{2}\left[\varepsilon'\left(E_1\frac{\partial E_1}{\partial z} + E_2\frac{\partial E_2}{\partial z}\right)\right.$$
$$\left. + \frac{1}{2}(E_1^2 + E_2^2)\left(-\alpha\varepsilon' + \varepsilon''\frac{\partial \rho}{\partial z}\right)\right] \tag{184}$$

$$\frac{\partial E_1}{\partial t} = \frac{1}{\varepsilon}\left\{\frac{c^2}{2\omega_L}\left[\frac{2}{r_o^2}\frac{\partial^2 E_2}{\partial x^2} + \frac{\partial^2 E_2}{\partial z^2} - 2k_L\frac{\partial E_1}{\partial z} + \alpha\frac{\varepsilon_o-\varepsilon}{\sqrt{\varepsilon}\,(\sqrt{\varepsilon_o}+\sqrt{\varepsilon})}\frac{\partial E_2}{\partial z}\right.\right.$$
$$\left.\left. + \frac{\alpha^2}{4}E_2\right] - \left[\frac{1}{2\omega_L}\varepsilon''\left(\frac{\partial \rho}{\partial t}\right)^2 + \frac{\omega_L}{2}(\varepsilon_o-\varepsilon)\right]E_2 +$$

$$+\frac{c^2k_L}{2\omega_L^2\varepsilon}\left[2\varepsilon'\frac{\partial\rho}{\partial t}\frac{\partial E_2}{\partial z}-\frac{c^2k_L}{\omega_L}\frac{\partial^2E_2}{\partial z^2}\right]+$$

$$+\frac{c}{2}\left[\alpha\frac{\varepsilon_o-\varepsilon_1}{\sqrt{\varepsilon_o}+\sqrt{\varepsilon}}E_1-\frac{\alpha}{2\omega_L\sqrt{\varepsilon}}\varepsilon'\frac{\partial\rho}{\partial t}E_2\right]-\varepsilon'\frac{\partial\rho}{\partial t}E_1\Bigg\} \qquad (185)$$

$$\frac{\partial E_2}{\partial t}=\frac{1}{\varepsilon}\Bigg\{-\frac{c^2}{2\omega_L}\left[\frac{2}{r_o^2}\frac{\partial^2E_1}{\partial x^2}+\frac{\partial^2E_1}{\partial z^2}+2k_L\frac{\partial E_2}{\partial z}+\alpha\frac{\varepsilon_o-\varepsilon}{\sqrt{\varepsilon}\,(\sqrt{\varepsilon_o}-\sqrt{\varepsilon})}\frac{\partial E_1}{\partial z}\right.$$

$$\left.+\frac{\alpha^2}{4}E_1\right]+\left[\frac{1}{2\omega_L}\varepsilon''\left(\frac{\partial\rho}{\partial t}\right)^2+\frac{\omega_L}{2}(\varepsilon_o-\varepsilon)\right]E_1$$

$$-\frac{c^2k_L}{2\omega_L^2\varepsilon}\left[2\varepsilon'\frac{\partial\rho}{\partial t}\frac{\partial E_1}{\partial z}-\frac{c^2k_L}{\omega_L}\frac{\partial^2E_1}{\partial z^2}\right]$$

$$+\frac{c}{2}\left[\alpha\frac{\varepsilon_o-\varepsilon}{\sqrt{\varepsilon_o}+\sqrt{\varepsilon}}E_2-\frac{\alpha}{2\omega_L\sqrt{\varepsilon}}\varepsilon'\frac{\partial\rho}{\partial t}E_1\right]-\varepsilon'\frac{\partial\rho}{\partial t}E_2\Bigg\} \qquad (186)$$

Equations (174)-(186) are the basic equations to be used for the solution of laser-fluid problems in the near field region when cylindrical symmetry pertains. These equations must, of course, be converted to difference equations before the computer solution can be attempted. The difference equations will not be presented here, because they are included in the computer program shown in Appendix C. The interested reader will be able to locate the difference equations in the program listing. As indicated earlier, seven-point difference quotients were used to represent the differential operators appearing in (174)-(186). These difference quotients and a method for deriving them are shown in Appendix B. These expressions will be used in the consideration of the utility criterion for the laser-fluid system of equations.

Once equations (174)-(186) have been obtained, it is vital that the utility criterion or some other criterion be applied to determine useful time step sizes and corresponding grid spacings. In spite of the complexity of these equations, the utility criterion is extremely easy to obtain. This is one of the attractive features of the utility approach. To illustrate the ease of application of the handy sufficiency tests for utility described in Part III, the derivation of the utility criterion for the laser-fluid system will now be given. In the interest of brevity and to emphasize the simplicity of the derivation, it will be presumed that the reader is well acquainted with the discussion of the utility method given in Part III and with the examples presented there.

An examination of equations (174)-(186) reveals that it is sufficient to consider either (178) or (179) and ignore all the other equations. These two equations dominate the utility criterion and either (178) or (179) can be used, because either choice produces the same condition. Choosing, then, to deal with (178) and keeping only the most important terms, one can obtain a utility criterion from the equation

$$\frac{\partial E_1}{\partial t} \approx \frac{c^2}{2\omega_L \varepsilon} \left[\frac{(1-x)^4}{r_o^2} \frac{\partial^2 E_2}{\partial x^2} + \frac{(1-x)^3}{r_o^2 x} (1-2x) \frac{\partial E_2}{\partial x} + \frac{\partial^2 E_2}{\partial z^2} - 2k_L \frac{\partial E_1}{\partial z} - \frac{c^2 k_L^2}{\omega_L^2 \varepsilon} \frac{\partial^2 E}{\partial z^2} \right] \tag{187}$$

Using the fact that $c^2 k_L^2 = \varepsilon_{oe} \omega_L^2$ and putting $\varepsilon \approx \varepsilon_{oe} \approx 1$ one can simplify (187) to produce

$$\frac{\partial E_1}{\partial t} \approx \frac{c}{2k_L} \left[\frac{(1-x)^4}{r_o^2} \frac{\partial^2 E_2}{\partial x^2} + \frac{(1-x)^3 (1-2x)}{r_o^2 x} \frac{\partial E_2}{\partial x} - 2k_L \frac{\partial E_1}{\partial z} \right] \tag{188}$$

The corresponding seven-point explicit difference equation is

$$E_{1,jk}^{n+1} \approx E_{1,jk}^{n} + \frac{c\Delta t}{2k_L}\left\{ \frac{(1-x)^3}{r_o^2}\left[\left(\frac{\partial^2}{\partial x^2}\right)_{7,4} + \frac{(1-2x)}{x}\left(\frac{\partial}{\partial x}\right)_{7,4}\right] E_{2,jk}^{n} \right.$$

$$\left. - 2k_L \left(\frac{\partial}{\partial z}\right)_{7,4} E_{1,jk}^{n}\right\} \qquad (189)$$

where the difference operators $\left(\frac{\partial^2}{\partial x^2}\right)_{7,4}$ and $\left(\frac{\partial}{\partial x}\right)_{7,4}$ are shown in equations (B12) and (B12') of Appendix B, respectively. The superscript n is the time index and j and k are, respectively, the x and z indices for the spatial grid points. Thus,

$$x = j\Delta x \qquad \text{and} \qquad z = k\Delta z$$

The various coefficients are maximized for the choices

$$(1 - x) \to 1 \qquad \text{and} \qquad \frac{1 - 2x}{x} \to \frac{1}{\Delta x}$$

where, in the denominator, $x = j\Delta x \to \Delta x$ because (189) does not apply at $j = 0$. [Equation (189) was taken from (178), whereas (185) is the appropriate equation at $x = 0$.] After making these replacements, one obtains

$$E_{1,jk}^{n+1} \approx E_{1,jk}^{n} + \frac{c\Delta t}{2k_L}\left\{\frac{1}{r_o^2(\Delta x)^2}\left[\Delta_j^2 + \Delta_j\right] E_{2,jk}^{n} - \frac{2k_L}{\Delta z}\Delta_k E_{1,jk}^{n}\right\}, \qquad (190)$$

where

$$\Delta_j^2 \equiv (\Delta x)^2\left(\frac{\partial^2}{\partial x^2}\right)_{7,4} \quad \text{operating on subscript j}$$

$$\Delta_j \equiv (\Delta x)\left(\frac{\partial}{\partial x}\right)_{7,4} \quad \text{operating on subscript j}$$

$$\Delta_k \equiv (\Delta z)\left(\frac{\partial}{\partial z}\right)_{7,4} \quad \text{operating on subscript k.}$$

One finds that the precondition (104) is already satisfied because no diagonal term arises from Δ_k when the seven-point scheme $\left(\frac{\partial}{\partial z}\right)_{7,4}$ is used. Thus condition (105) can be used. Using equations (B12) and (B12'), $\overline{R}$ is trivially computed from (190) and one obtains

$$\overline{R} = 1 + \overline{\delta}\Delta t,$$

where

$$\overline{\delta} = \frac{c}{2k_L r_o^2 (\Delta x)^2}\left[\left(\frac{3}{2}+\frac{3}{4}\right) + \left(\frac{3}{2}-\frac{3}{4}\right) + \frac{6}{20} + \left(\frac{1}{60}+\frac{1}{90}\right)\right.$$

$$\left. + \left(\frac{1}{60}-\frac{1}{90}\right) + \frac{49}{18}\right] + \frac{c}{\Delta z}\left[\frac{3}{4}+\frac{3}{4}+\frac{6}{20}+\frac{1}{30}\right]$$

$$\approx c\left[\frac{3}{k_L r_o^2 (\Delta x)^2} + \frac{2}{\Delta z}\right], \qquad (191)$$

then, using (116) with $q_o = 4$, one obtains the utility condition

$$\frac{1}{c\Delta t} \geq \left[\frac{12}{k_L r_o^2 (\Delta x)^2} + \frac{8}{\Delta z}\right]. \qquad (192)$$

This is such a strong constraint that one immediately wonders if, perhaps, more generous sufficiency theorems for utility should not be sought. The utility philosophy suggests a more practical approach: Try the condition and then try to violate it and compare the results. This was done for the problem discussed in this report and no escape from (192) was possible. In fact, if the criterion was violated by a factor of order 5 in Δt, then classic instability phenomena were observed in the computer output. Thus, by a stroke of bad luck, it appears that (192) must be obeyed.

In order to emphasize the implications of (192) for the study of the propagation of laser pulses, a description of the accessible parameter regime

will now be given. As a starting point for this discussion, the parameter values used in the actual calculation will be listed. The electric field at t = 0 was taken to be of the form

$$E_1 = F\, e^{-4\left(\frac{r}{r_o}\right)^2} e^{-4\left(\frac{z-z_{po}}{z_o}\right)^2} \qquad (193)$$

$$E_2 = 0 \ ,$$

where

$r_o \equiv$ full $\frac{1}{e}$-width of $E_1(r, z = z_p, t = 0)$

$\equiv \sqrt{2} \cdot$ [full $\frac{1}{e}$-width of I_L at $z = z_p$, $t = 0$]

$I_L \equiv$ [on-axis intensity (in ergs/cm^2 sec) at $r = 0$, $z = z_{po}$, $t = 0$, time averaged over several optical periods]

$\equiv \frac{1}{2} \sqrt{\varepsilon_{oe}}\, c\, F^2$

$z_o =$ full $\frac{1}{e}$-width of $E_1(r = 0, z, t = 0)$

$z_{po} =$ location of the peak at $t = 0$ (194)

$$F^2 = \frac{2I_L}{\sqrt{\varepsilon_{oe}}\, c} \equiv \frac{16\, P_L}{\sqrt{\varepsilon_{oe}}\, c\, r_o^2} \equiv \frac{64\, U}{\Pi \sqrt{2\Pi}\, \varepsilon_{oe}\, r_o^2\, z_o}$$

= peak value of the electric field, squared

P_L = total power (in ergs/sec) of the pulse at $z = z_p$, $t = 0$, time averaged over several optical periods

U = total energy in the pulse at $t = 0$, time averaged over several optical periods.

The values taken for these quantities were

$$r_o = 200 \text{ cm}$$

$$z_o = 9 \times 10^5 \text{ cm} = 9 \text{ km}$$

$$z_{po} = 13.5 \times 10^5 \text{ cm} = 13 \text{ km}$$

$$F = 4.7 \times 10^3 \ [\text{erg/cm}^3]^{1/2} \tag{195}$$

$$I_L = 3.3 \times 10^{17} \ [\text{ergs/(cm}^2 \text{ sec}]$$

$$P_L = 5.2 \times 10^{21} \text{ ergs/sec}$$

$$U - 9.8 \times 10^{16} \text{ ergs}$$

and the air was taken to be initially in its unperturbed state at 1 atm pressure and at 10°C.

The spatial grid was composed of 80 x 16 - 1280 mesh points. The z-axis was evenly divided into 80 steps of size $\Delta z = 0.45 \times 10^5$ cm = 0.45 km beginning at z = 0 and extending to $z = 35.6 \times 10^5$ cm = 35.6 km. Thus the peak of E_1 was initially located at the 30^{th} mesh point on the z-axis and its $\frac{1}{e}$-width extended from the 20^{th} to the 40^{th} mesh point. The radial variable x has the range $0 \leq x \leq 1$ and this range was evenly divided into 22 steps of size $\Delta x = \frac{1}{22}$, but only the 16 sites closest to the z-axis were used. The more distant sites correspond to radial distances greater than 5 beam half-widths. The first step away from the z-axis corresponds to the radial distance $\Delta r = \frac{200 \text{ cm}}{21} = 9.5 \text{ cm} \approx \frac{1}{10}$ (radial half-width). The time step size was taken to be $\Delta t = 10^{-7}$ sec and 100 steps were made so that the time interval $0 \leq t \leq 10^{-5}$ sec was traversed.

Taking these grid sizes and time steps and substituting into the utility condition (192), one gets

$$\frac{1}{c\,t} = \frac{1}{3000} \geq \frac{1}{40800} + \frac{1}{5630} = \left[\frac{12}{k_L r_o^2 (\Delta x)^2} + \frac{8}{\Delta z}\right] \qquad (196)$$

Thus, for the chosen step size, Δz, the value used for Δt would violate the condition, were it to be doubled. Of course, the condition (192) is only approximate, but, as mentioned above, good solutions could not be obtained for $\Delta t \sim 10^{-6}$ for Δz. Clearly the value $\frac{1}{22}$ used for Δx does not saturate the Δx piece of (196) and one could probably use Δx as small as $\frac{1}{60}$. Such a small step size for Δx would, however, require three times as much spatial mesh points and would exceed the storage capacity of the computer which was used.

The desire is to use as large a value of Δt as one can. In this regard, the Δx piece of (196) is generous and would permit $\Delta t \sim 10^{-6}$. The Δz step size would have to be increased to $\Delta z \sim 5$ km to allow this, however. Such a large step size would be larger than the 4.5 km half-width of the pulse selected, so that no details of deformation of the pulse could be observed.

If the beam is made narrower in radial extent, the Fresnel length decreases and diffraction effects become important. The Fresnel length is 310 km for $r_o = 200$ cm, so that one would become involved with far field effects if the beam radius were decreased by more than a factor of 5. Making the pulse longer in the z-direction expands the time scale over which interesting effects may be studied. If, on the other hand, the pulse is shortened in the z-direction, then one must shift to smaller values of Δz in order to be able to follow details of the development of the pulse. Shifting to smaller Δz requires, because of (196), that one use smaller values of Δt. The net effect is that no profit is derived from using shorter pulses, because they can be followed only for correspondingly shorter times.

One aspect of the parameter regime has not yet been discussed: the range of power for the beam. Since the power, P_L, does not appear in the utility criterion, its role must be determined by experimentation with the computer program. Very small powers are not interesting because there is very little interaction with the fluid. In order to see instabilities and nonlinear effects during short times, one would wish to consider beams with large power densities. The extremely large values shown in (195) produce interesting effects, in a time interval of 10^{-5} seconds. Such beams can not be followed for more than about 100 time steps, however, because the various dependent variables begin to develop large curvatures and vary on a scale smaller than the mesh sizes. Thus if one wishes to follow the development for a longer period of time, the mesh sizes must be decreased and eventually the time step will have to be smaller, and then many more time steps will be required. In this regard, one must keep in mind that if the mesh size is decreased, while the initial pulse size is not decreased, then more mesh points will be required and the storage capacity of the computer also becomes a limiting factor. The final remaining option is to increase the power in the beam even more. The net effect is that the large curvatures develop faster and the development can be followed only for shorter periods of time.

One final remark about numerical solution of the laser-fluid equations will be made before discussing the results of the computer calculation. Strong growth, instabilities and nonlinear effects, can often not be followed because of the mesh sizes employed. If these strong oscillations or secular growths are generated by tiny rapidly changing terms; that is, if the instabilities arise due to ripple effects which become strongly enhanced, then a crude mesh size can smooth these effects out and, thereby, prohibit the occurrence of the strongly growing phenomena by removing their source. Very strong

instabilities were found in Part II for the linearized laser-fluid equations. The strongest of these instabilities are generated by very short wavelength ripple. The mesh size employed in the present calculation will begin to wash out ripple about an order of magnitude larger in wavelength than the ripple which is most strongly amplified in the linearized analysis. Thus, one must bear in mind that some physical sources of pulse distortion will be excised by the mesh selected.

Accepting the many restrictions noted above, we have examined the propagation of a 200 cm by 9 km pulse with 10^{17} ergs for 10^{-5} seconds. The pulse moves three kilometers during this time and it is possible to observe the onset of the laser-fluid interaction in some detail.

The results of the calculation are presented in Figures [1] - [17]. The electric field is conveniently considered in terms of the quantity

$$|E| \equiv [E_1^2 + E_2^2]^{1/2}, \tag{197}$$

where E_1 and E_2 are the slowly varying electric field amplitudes defined in (162). The instantaneous electric field is thus given by

$$E = |E| \cos [\omega_L t - k_L z + \delta_E] \tag{198}$$

where the phase δ_E is given by

$$\delta_E = \mathrm{Tan}^{-1} (E_2/E_1)$$

As shown in (193), at $t = 0$, E_2 is taken to be zero and, consequently, δ_E is zero initially. Thus

$$|E| = E_1 \quad \text{at} \quad t = 0 \tag{199}$$

and E_1 is described by equations (193)-(195) initially. This initial pulse shape is exhibited in Figure [1a] and in Figure [3].

In Figure [1] the z-profile of the pulse is shown at the initial time, at 10^{-5} second, and at two intermediate times. For $t \neq 0$, the pulses are not absolutely symmetric about their peaks. In order to exhibit this asymmetry, the curves are plotted as a function of $|z - z_c|$, where z_c is the center of the pulse. This device allows direct comparison of the leading and trailing edges of the pulses. The center, z_c, is defined to be the point equidistant from the leading and trailing edges at $|E| = 1 \left(\frac{erg}{cm^3}\right)^{1/2}$. These values are:

$$\begin{array}{llll} t = 0 & t = 6 \times 10^{-6} \text{ sec} & t = 8 \times 10^{-6} \text{ sec} & t = 10^{-5} \text{ sec} \\ z_c = 30 & z_c \approx 34 & z_c \approx 35.3 & z_c \approx 36.6 \end{array} \tag{200}$$

where for convenience, distances along the z-axis will be given in units of the grid size: $\Delta z = 0.45 \times 10^5$ cm = 0.45 km. One notices, therefore, from (200) that this pulse center propagates at the velocity $v_c \approx 2.97 \times 10^{10}$ cm/sec, the velocity of light. The pulse peaks, however, are observed to drift backward with respect to z_c:

$$\begin{array}{llll} t = 0 & t = 6 \times 10^{-6} \text{ sec} & t = 8 \times 10^{-6} \text{ sec} & t = 10^{-5} \text{ sec} \\ z_p \approx 30 & z_p \approx 34 & z_p \approx 35.2 & z_p \approx 35.3 \end{array} \tag{201}$$

so that after 10^{-5} seconds, the peak has lost about two thirds of a kilometer with respect to z_c. Note that the exponential damping factor shown in (162) is not included in the quantity $|E|$ appearing in the graphs. For air, this factor is larger than 0.95, even at $t = 10^{-5}$ sec. Other than this effect, very little energy is lost from the beam due to heating of the fluid, so the distortion effects shown in Figure [1] are rather minor and are noticeable only near the peak of the pulse. Extra detail of this peak distortion is shown in Figure [2]. For purposes of this display, the leading edges have been placed

together so that the curves intersect at $|E| = 10^3 \left(\frac{erg}{cm^3}\right)^{1/2}$ and the corresponding abscissa has been labeled 42.5, the location of this point at t = 0. The retrograde peak motion and the corresponding loss of fore and aft symmetry in the vicinity of the peak are plainly seen.

The radial beam profile is exhibited in Figures [3] and [4]. The radial slice shown at each value of the time is taken through the position of the maximum, z_p, in the z-profile. In Figure [3] the entire beam profile is shown for the initial and final times only. Comparison of the curves reveals a small on-axis increase extending out to the beam halfwidth (half of the full $\frac{1}{e}$-width) at $\frac{r_o}{2} = 100$ cm. The effect amounts to a 47% increase in the on-axis intensity. Details and intermediate states are given in Figure [4].

Although the radial peak is on axis in the slice through the peak in the z-profile, this is not the case for slices taken behind z_p. For example, at $t = 10^{-5}$ sec, the principal peak is at $z_p \approx 35.3$. As one moves away from this peak toward the trailing edge, the radial peak moves off axis giving a maximal effect near z = 31. The principal peak of the pulse is, however, always on axis. The radial profile at z = 31 is shown in Figure [5]. This is clearly only a small detail at $t = 10^{-5}$ sec. The position of this off-axis secondary peak is also located in Figure [9] and marked with tiny squares.

In order to follow the development of the phase of the electric field, the quantity $|E_1|$ is plotted in Figures [6], [7], and [8] for $t \neq 0$. Of course, at t = 0, $|E_1| = |E|$ and the phase, δ_E, is zero. In these three figures, the graph of $|E|$ is marked with dotted lines for comparison. The corresponding value of $|E_2|$ can be deduced from these figures, using (197). These figures show far more dramatic effects than the curves discussed above. At $t = 6 \times 10^{-6}$ sec, the phase is still nearly zero and E_1 is positive everywhere.

At $t = 8 \times 10^{-6}$ sec, however, E_1 has changed sign over a three kilometer region extending from slightly in front of the peak of $|E|$ toward the trailing edge of the beam. This is clear-cut evidence of the onset of laser-fluid interaction in the trailing edge of the beam. It is clear that the front of the pulse and the distant tail are, as yet, unaffected by this interaction. It is interesting that the unperturbed part of the leading edge does not reach as far back as the principal peak. Thus, the peak already feels the effects of the interaction to some degree and comparison of (200) and (201) reveals that the peak will now begin to lose ground with respect to the center of the pulse. This effect has already been noted in the graphs of $|E|$.

Since there are now places where $|E_1|$ is zero, it is clear that the phase goes to $\frac{\pi}{2}$ at these sites. The amplitude E_2 responds strongly at those places where $E_1 = 0$, fulfilling the obligation to conserve power. One notices that the graph of $|E|$ remains very smooth, giving no indication that the phase is varying rapidly. Figure [8] shows the later development of the region in which E_1 changed sign. The region in which $E_1 < 0$ is now seven kilometers long, nearly as big as the $\frac{1}{e}$ width of $|E|$. This region has advanced now to a point well in advance of the principal peak and extends back far into the tail. It appears that this node is propagating forward at nearly four times the speed of light. Furthermore, there has been another sign reversal of E_1 slightly behind the peak. It is this kind of oscillatory behavior in E_1, with large variations on the scale of the chosen mesh size, that brings a halt to further observation of the beam development by this method.

On the rz-plane shown in Figure [9], the constant phase curve, $E_1 = 0$, is shown in detail at $t = 10^{-5}$ sec. Also marked, with small open circles, is

the on-axis extent of the similar curve at $t = 8 \times 10^{-6}$ sec, encountered in Figure [7]. Also indicated on the same figure is the locus of off-axis maxima in the z-profile of the pulse, both at $t = 0$ and $t = 10^{-5}$ sec. At $t = 0$, the pulse is described by (193) and clearly the off-axis maxima in z are all positioned at $z_{po} = 30$. As the pulse propagates, however, the peak moves slower than the velocity of light, as previously noted. The off-axis portions of the pulse, however, have much smaller intensity and, consequently, interact very little with the fluid. These portions of the pulse will suffer no delay, and move steadily ahead of the principal peak. One notices that at two thirds of the radial halfwidth of the beam, the delay disappears almost completely. As mentioned above, the small squares locate the secondary peaks present at $t = 10^{-5}$ sec.

The phase front information presented in Figures [6]-[9] is an interesting feature of the results of the computer solution. Since $|E_1|$ turns out to be a rapidly varying function of time, it is of interest to attempt to understand the mechanism responsible for the behavior of E_1. In order to understand this behavior, one must realize that the phase depends on the state of the fluid. The state of the fluid given by the computer calculation is shown in Figures [10]-[16]. Before these figures are discussed, however, it is convenient to examine certain analytic estimates for the fluid variables. Such estimates will allow insight into the behavior of E_1, and, later, will facilitate the discussion of the computer results for the fluid variables.

In order to describe the behavior of E_1, it is useful to write the electric field in the form

$$E = \mathcal{E}_0(r, z-ct)\, e^{i(\omega_L t - \frac{\sqrt{\varepsilon}\omega_L}{c} z)} + \text{c.c.} \qquad (202)$$

where

$$\mathcal{E}_0 \equiv \frac{F}{2} e^{-4(\frac{r}{r_0})^2} e^{-4(\frac{z-ct}{z_0})^2} \tag{202a}$$

and

$$\sqrt{\epsilon} \simeq 1 + \frac{\epsilon_0 - 1}{2\rho_0} \rho_1 \tag{202b}$$

where F is a slowly varying amplitude, ρ_1 is the local density excess, $(\rho-\rho_0)$, and z_{po} has been put equal to zero for the present considerations. Combining equations (202)-(202b), the electric field can be put in the form shown in (162) with

$$E_1 = \left[F \cos\left(k_L z \frac{\epsilon_0 - 1}{2\rho_0} \rho_1\right)\right] e^{-4(\frac{r}{r_0})^2} e^{-4(\frac{z-ct}{z_0})^2}$$

$$E_2 = \left[-F \sin\left(k_L z \frac{\epsilon_0 - 1}{2\rho_0} \rho_1\right)\right] e^{-4(\frac{r}{r_0})^2} e^{-4(\frac{z-ct}{z_0})^2} \tag{203}$$

These expressions agree with (193) at t = 0 and offer a way to estimate the behavior of E_1 at subsequent times. On the basis of (203) the nodes of E_1 might be expected to be determined by

$$\cos\left(k_L z \frac{\epsilon_0 - 1}{2\rho_0} \rho_1\right) = 0 \tag{204}$$

Actually, this expression should be modified slightly if one wishes to attempt to get quantitative agreement with the computer solution. It is clear that (203) requires E_2 to vanish at z = 0 at all times. This is not the same boundary condition which was used in the computer solution. Actually one should use

$$E_1 \sim \cos\psi$$

with (205)

$$\psi \approx k_L \int_{z-ct}^{z} \left[\frac{\varepsilon_o - 1}{2\rho_o}\rho_1\right]_{z',\,t'} dz' \,.$$

The integrand in (205) should be evaluated at z' and t', where

$$c(t' - t) = z' - z.$$

Although (205) will be used in the future to analytically describe a laser beam quantitatively, for the present (204) may be employed to gain insight into the behavior of E_1.

It is clear from (203) and (205) that the mechanism responsible for the behavior of E_1 is easily exhibited. To actually follow the behavior of E_1, however, it is clearly necessary to determine the state of the fluid. In particular, the density excess, ρ_1, must be obtained as a function of time and position. In order to analytically describe the fluid for the time interval and parameter ranges of the computer solution, the laser-fluid equations may be simplified to

$$\rho_o \frac{\partial T_1}{\partial t} \approx \frac{\gamma - 1}{\beta}\frac{\partial \rho_1}{\partial t} + \frac{\alpha c}{C_v}\overline{E^2} \tag{206}$$

and

$$\frac{\partial^2 \rho_1}{\partial t^2} \approx u^2 \beta \rho_o \nabla^2 T_1 \tag{207}$$

where T_1 is the local temperature excess, $T-T_o$. One must recall that the intensity, $c\overline{E^2}$, appearing in (206) is a function of time and position. Integrating (206) from zero to t and combining the resulting equation with (207) to eliminate T_1, one can obtain

$$\frac{\partial^2 \rho_1}{\partial t^2} \approx v_s^2 \frac{\beta \alpha I_L}{c C_p} \left(\frac{32 z_o}{r_o^2}\right) e^{-8\left(\frac{r}{r_o}\right)^2} \left(\frac{8r^2}{r_o^2} - 1\right) \int_{z-ct}^{z} e^{-8\left(\frac{\nu}{z_o}\right)^2} \frac{d\nu}{z_o} \qquad (208)$$

It is straightforward to integrate this expression and, although the details will not be given here, it is clear that ρ_1 will have the form

$$\rho_1 \approx \left[\left(\frac{8r^2}{r_o^2} - 1\right) e^{-\frac{8r^2}{r_o^2}}\right] F(z,t) \qquad (209)$$

so that $\rho < \rho_o$ on axis and there is an off-axis maximum in the density. In other words, there will be a pile-up of the fluid at a distance $r \approx \frac{r_o}{2}$ from the axis.

The temperature distribution can easily be obtained by integrating (206) from zero to t:

$$T_1 \approx \frac{z_o \alpha P_L}{c \rho_o C_v} e^{-8\frac{r^2}{r_o^2}} \int_{z-ct}^{z} e^{-8\left(\frac{\nu}{z_o}\right)^2} \frac{d\nu}{z_o} \qquad (210)$$

A negligible term involving ρ_1 can be evaluated using (209) and has been dropped to get (210).

Combining (210) with (204) the behavior of E_1 can be visualized and studies analytically. Closed contours such as those shown in Figure [9] are predicted and other qualitative features are correct. A detailed comparison of this analytical procedure and the computer result is in progress and it is now clear that striking quantitative agreement is obtained. This success is of great interest because the analytic procedure, unlike the present computer

solution, is not limited to 10^{-5} seconds.

The computer result for the state of the fluid at $t = 10^{-5}$ sec will now be considered. For this discussion, it is useful to keep several characteristic distances in mind. Since the state of the fluid is governed by the intensity profile

$$I_L(r,z,t) \equiv \frac{1}{2} \sqrt{\epsilon_{oe}}\, c\, |E|^2 , \tag{211}$$

rather than by $|E|$ directly, the following initial parameters are relevant. The full $\frac{1}{e}$-width of the z-profile

$$\text{of} \quad P_L = \frac{z_o}{\sqrt{2}} = 14.1 \quad \text{in units of } \Delta z \equiv 0.45 \text{ km} \tag{212}$$

$$\text{At} \quad z = z_p^2 \pm \frac{z_o}{4} = z_p \pm 5, \quad \frac{\partial^2 I_L}{\partial z^2} = 0 \quad \text{so that} \quad \frac{\partial I_L}{\partial z} \tag{213}$$

has extrema separated by 10 units. The full $\frac{1}{e}$-width of the radial profile

$$\text{of} \quad I_L = \frac{r_o}{\sqrt{2}} = 0.707\, r_o = 141 \text{ cm} \tag{214}$$

$$\text{At} \quad r = \frac{r_o}{4} = 50 \text{ cm}, \quad \frac{\partial^2 I_L}{\partial r^2} = 0 , \tag{215}$$

so that $\frac{I_L}{\partial r}$ has a maximum. The maxima on opposite sides of the axis are separated by 100 cm.

The local temperature excess, $T - T_o$, where $T_o = 10°C$ is shown in Figure [10] as a function of z at $t = 10^{-5}$ sec. This curve is in complete quantitative agreement with the analytical result shown in (210). The hottest place in the beam lies on the axis at $z \approx 33.3$. Since the intensity peak is at $z_p \approx 35.3$, it is clear that the thermal peak is lagging behind the intensity peak. Since $z_c \approx 36.6$ at this time, it is clear that the thermal peak is

almost exactly midway between the initial and final pulse centers. Thus one finds, as expected, that the thermal peak propagates at velocity $\frac{c}{2}$ for small times. This and other properties of the thermal profile are readily understood on the basis of the following considerations. The temperature responds to the heat deposited in the medium, so that from (210):

$$T(z) - T_o \approx \int_{z-(z_p-z_{po})}^{z} \left[\frac{\alpha}{\rho_o C_v} I_L\ (r,z',t = 0)\ \frac{dz'}{c}\right]. \tag{216}$$

Due to the symmetry of I_L and the fact that it is gaussian, it follows from (216) that T(z) should reach a maximum midway between z_{po} and z_p for small times. Furthermore, the graph of $T(z) - T_o$ should be symmetric about its maximum. Both of these features are evident in Figure [10]. Since the peak moves much less than its halfwidth in 10^{-5} seconds, the integrand in (216) is essentially constant. Evaluating $I_L(r,z',0)$ at the midpoint of the interval, one gets

$$T(z) - T_o \approx \frac{z_p - z_{po}}{c} \cdot \frac{\alpha}{\rho_o C_v}\ I_L(r,z - \frac{z_p - z_{po}}{2},\ t = 0) \tag{217}$$

From (217) one concludes that the width of the thermal distribution should equal the width of the intensity distribution. Indeed, one sees in Figure [10] that the temperature distribution has width 14.1, which is to be compared with (212).

The corresponding radial temperature distribution at z = 33, the position of the maximum at $t = 10^{-5}$ sec, is given in Figure [11]. This curve, also, is in complete quantitative agreement with the analytical result shown in (210). The temperature has reached a maximum of more than 1000°K on axis and the full width of the distribution is found to be $0.67\ r_o = 134$ cm, 5%

narrower than the initial radial intensity width. One might have expected the temperature distribution to be broader than the intensity profile because the large radial velocity of the fluid should carry some of the deposited energy away. In fact, this effect may possibly be observed in the following way. One might compare the temperature distribution not to the original gaussian intensity profile, but rather to the $\frac{1}{e}$ width of the radial intensity profile at $t = 10^{-5}$ sec. This final intensity profile has a width of 128 cm or 5% less than the temperature width. The average of the two intensity widths is 134.5 cm, almost exactly the observed temperature width. This average may be the best measure, because the thermal peak is midway between the initial and final intensity peaks.

The z-component, v_z, of the fluid velocity is shown in Figure [12] as a function of z. A double log plot is used which omits values of v_z between 10^{-3} cm/sec and -10^{-3} cm/sec. This kind of plot allows negative values of v_z to be plotted below the "axis". The zero of the velocity distribution occurs around z = 32.2, so the "center of velocity" lags slightly behind the thermal maximum. From (169) one might expect to find

$$v_z \sim \frac{\partial T}{\partial z} \sim \frac{\partial I_L}{\partial z} \tag{218}$$

so that the peaks in Figure [12] would be separated by 10 units according to (213). Indeed, the peaks are found to be separated by 10.2 units. Furthermore, since the temperature curve is symmetric about its maximum, (218) would suggest that v_z should be antisymmetric about its zero. This effect is certainly observed in Figure [12]. The velocity distribution is delayed with respect to the temperature distribution, but this symmetry property is unaffected.

At the same value of z, corresponding to the center of velocity of the z component, the radial component, v_r, is plotted in Figure [13]. This value of z corresponds also the the largest radial velocities, so that z = 32 might also be termed the site of greatest kinetic energy in the fluid. The radial velocity maximum is forty-six hundred times larger than the maximum axial velocity. This effect arises because of the great disparity in the intensity widths in the two directions. As a matter of fact

$$\frac{(v_r)\ \max}{(v_z)\ \max} = 4625 \qquad \text{and} \qquad \frac{z_o}{r_o} = \frac{9 \times 10^5}{200} = 4500.$$

The curve of v_r is forced to go to zero, as r goes to zero, by the boundary conditions shown in (180). One notices, however, that the peak is located at the distance 0.25 r_o from the axis, exactly the location of the maximum of $\frac{\partial I_L}{\partial r}$ shown in (215). Thus one finds

$$v_r \sim \frac{\partial I_L}{\partial r} \sim \frac{\partial T}{\partial r} \tag{219}$$

as would be expected from (177)

Bringing up the rear in the sequence of effects is the density minimum at $z \approx 31.5$. The density decrement $-(\rho-\rho_o)$ is shown in Figure [14]. Using (207), one might expect

$$\frac{\partial^2 \rho}{\partial t^2} \sim \frac{\partial^2 T}{\partial r^2}, \tag{220}$$

so that ρ and T will have the same z dependence.† There should, however, be a double time delay, since two time integrations are indicated in (220). The

†One gets the same conclusion by analyzing the function F(z,t) shown in (209) in a manner analogous to the reasoning employed to obtain (217).

width of the density decrement is found to be 14.5, about 3% wider than the thermal and intensity widths. The maximum fractional decrement $\frac{\rho_o - \rho}{\rho_o} \approx 4 \times 10^{-5}$.

The radial density distribution is exhibited in Figure [15] at z = 32, the location of the density minimum in the z-profile. Again, a double log plot is given so that both positive and negative density excesses can be conveniently represented. This time a density pile-up is observed because the fluid has been blown away from the axis so fast that a compression wave is generated. The zero in the graph is at 0.36 r_o, right at the halfwidths of the thermal and intensity distributions. Thus inside the thermal halfwidth the density is depressed; outside the fluid has piled up. The radial density profile shown in Figure [15] is in excellent agreement with that predicted in (209). For example, the zero observed at $\frac{r}{r_o} \approx 0.36$ is predicted to occur at

$$\frac{r}{r_o} = \frac{1}{\sqrt{8}} = 0.354 \ .$$

Similarly, the location of the peak observed at $\frac{r}{r_o} \approx 0.51$ is predicted to occur at

$$\frac{r}{r_o} = \frac{1}{2}.$$

Similarly, the ratio of peak height to valley depth is also correctly predicted. As a matter of fact, when one takes the trouble to evaluate the function F(z,t) appearing in (209), he finds precise agreement between (209) and Figure [15]. Thus, both (209) and (210) are in complete quantitative agreement with the result of the computer calculation.

Figures [16] and [17] exhibit the parade of effects, illustrating graphically the various delays, pulse shapes, and widths. Physically the

delays make sense. First the beam blasts through, heating the fluid as it passes. As explained above, the temperature maximum moves at $\frac{c}{2}$ and, thus, behind the laser peak. As this temperature wave passes along, the fluid picks up kinetic energy and the flow velocities increase. The center of this effect trails the heat wave, allowing time for the fluid to respond. Then, as the fluid begins to flow away from the propagating center of velocity, density deficits are left in the wake and corresponding radial compression waves set out from the beam axis.

To summarize the results briefly, in portions of the pulse where the intensity is small there is very little interaction with the fluid and these portions move without appreciable distortion. The peak of the pulse, however, interacts fairly strongly with the fluid and the peak is delayed relative to the center of the pulse. A parade of effects ensues; the center and edges of the pulse are followed by the peak, which, in turn, is followed consecutively by the thermal wave, the center of velocity, and the density waves. The front edge of the pulse propagates without appreciable distortion, but strong phase oscillations are set up near the peak and rapidly overtake the undistorted front section indicating that soon the entire beam will be distorted to some degree. The strongest instabilities, predicted in the linearized analysis of Part II did not appear because they are generated by ripple with wavelength an order of magnitude smaller than the mesh size used.

There is very little hope of obtaining computer solutions of the laser-fluid equations except in the tightly limited regime reported here, unless a different calculational procedure can be devised. Since, however, it appears that a certain amount of analytical headway has been made, there is reason to believe that, with appropriate combination of analytical and computer methods,

the beam can be followed for considerably longer periods of time. Effort is currently being directed toward this objective.

PART V

BEAM FED TURBULENCE

Many experiments have been reported for which theories assuming steady state beam profiles, after initial transients die out, provide rather good explanations of the principal features. However, that is probably true only because these experiments are conducted at relatively low power fluxes. Theoretically, one expects a time-dependent state of the system because of the instabilities discussed earlier. Such instabilities are not observed in practice because they cannot develop within the distances allowed for the propagation of beams. However, alternate considerations for a beam of finite cross section suggest that the beam may drive the fluid into a time-dependent, or turbulent, state at powers which are not completely unreasonable.

It may be impossible to prove analytically that such a turbulent state develops, because the investigation of hydrodynamic stability is very difficult even for the simplest flows. However, an argument can be made from dimensional considerations, an approach that promises to be very useful. Namely, for the problem of a beam of radius a and power flux I passing through air, it is possible to estimate a parameter W, which plays the role of an effective Reynolds number for our problem. It will be shown that the parameter W takes on values of the order of 30,000 for a beam with intensity I = 1 kilowatt/ cm^2 of radius 1 meter. Since it is known that flows with Reynolds numbers substantially lower than 30,000 are turbulent, the flows for the laser-heated atmospheric path should also be expected to show significant time dependence.

Consider the equations of motion for the air, and the equation governing heat transfer, which take the following form if it is assumed that the air can

be assumed incompressible. (That amounts to dropping terms of order u^2/v_s^2, where u is a typical flow speed, and v_s is the speed of sound. For the problems under consideration, u^2/v_s^2 will be less than 10^{-5}, and the incompressible fluid approximation will be quite good.)

$$\rho\,(\vec{v}\cdot\nabla)\,\vec{v} = -\nabla P - \beta T_1 \rho \vec{g} + \frac{\rho}{\rho_o}\,\eta\,\nabla^2\vec{v} + \frac{\rho}{\rho_o}\,(\eta+\eta')\,\nabla(\nabla\cdot v)$$

$$\rho\,(\nabla\cdot\vec{v}) = -(\vec{v}\cdot\nabla)\,\rho = \beta\rho\,(\vec{v}\cdot\nabla)\,T_1 \qquad (221)$$

$$\rho\,C_p\,(\vec{v}\cdot\nabla)\,T_1 = \alpha I + \nabla\cdot(\kappa\nabla T_1) + \frac{\rho}{\rho_o}\,[\eta\,(v_{i,j}+v_{j,i})^2 + \eta'\,(\nabla\cdot\vec{v})^2]$$

Assuming the Reynolds number is high, the inertial terms will dominate the viscous terms in the Navier-Stokes equation. Thus, there must be a balance between the inertial terms and the bouyancy forces, which implies that $\rho u^2/a \sim \rho\beta T_1 g$, where ρ is the density of air, β is the coefficient of thermal expansion, T_1 is a typical value for the temperature rise, and g is the acceleration due to gravity. The pressure variation will be of order ρu^2. In the heat transfer equation, the convection term will dominate the conduction term, and the beam heating will overwhelm the viscous dissipation, so that there must be a balance between heat deposition from the beam, and convective heat transfer, which implies that $\rho C_p\, u T_1/a \sim \alpha I$. Combining these two relations we find that $u^3 \sim \alpha\beta a^2 I g/\rho C_p$. With that expression for u, we then define a parameter W, which is expected to indicate regimes where steady flow and where time-dependent flow may be anticipated. W is an estimate of the relative importance of inertial terms to viscous terms in controlling the flow:

$$W = \frac{au\rho_o}{\eta} = a\,\frac{\rho_o}{\eta}\,(\alpha\beta a^2 I g/\rho C_p)^{1/3} \qquad (222)$$

For a beam with $I = 10^{10}$ ergs/cm$^2\cdot$sec, $a = 100$ cm, $T_o = 273°K$ and $\alpha = 3 \times 10^{-6}$ cm^{-1}, $W = 30{,}000$.

For many experiments described in the literature, the values of W are much smaller, and thus one would not expect any turbulent fluid flow to be observed. For example, in the original experiment of Gordon, Leite, Moore, Porto, and Whinnery[16] the parameter W takes on a value about 10^{-3}, and in the more recent experiments of Smith and Gebhardt,[17] W is of order 10.

The parameter W introduced here is different from the Grasshof number, which is referred to in some discussions of the convective flows set up by the absorption of energy from a laser beam.[18] In fact, the conceptual basis for using the Grasshof number in a discussion attempting to explain the transition between smooth flow and time-dependent flow seems less relevant because the Grasshof number appears to be more sensible when the thermal bouyant forces are balanced by viscous forces. In the present discussions, the thermal bouyant forces are balanced by inertial effects.

We are planning experiments to determine the critical value of W, W_{cr}, which determines the onset of turbulent convective flows for the geometry appropriate to laser beam transmission. It is also our aim to attempt a theoretical evaluation of this critical value. At the present time we can only speculate that W_{cr} may be between 10^3 and 10^4.[19] The theoretical approach appears fairly difficult because the question of the stability of flows even without heat sources has only been answered theoretically for very simple geometries.[20-21] The question of stability for fluids which are heated or cooled appears to have been treated mainly for cases in which the fluid would be motionless, and has not been explored for a problem like the present one.[21-22] The first part of that problem would be to determine a steady-state flow pattern for a fluid with a distributed heat source within a right circular cylinder with its axis aligned at some angle to the vertical. For

the case of a horizontal cylinder of infinitely small radius, the flow pattern has been calculated by Yih.[23-24]

Unfortunately, however, that solution is not of great value for the present problem because the size of the cylinder radius is a critical parameter. Nevertheless, it is expected that Yih's solution will assist in obtaining the asymptotic form of the steady-state flow at large distances from the laser beam cylinder. Once that time-independent flow pattern has been determined, the linearization of the hydrodynamic equations for perturbations from the flow pattern will lead to an eigenvalue problem, which eventually will yield a critical value for W. Ostrach[25] suggests that the eigenvalue problem can be bypassed as the stability of fully developed natural convection flows can be found by using the appropriate velocity profile in the classical theory of hydrodynamic stability. This assertion rests upon his analysis of the stability of free convection above a flat heated plate, where instability first appears for a Reynolds number of 283.

Above the threshold for beam induced turbulence, governed by W_{cr}, general arguments[26] lead to a size for the smallest eddies, $a(W_{cr}/W)^{3/4}$. For a 1-meter beam, if W_{cr} should be about 10^3, then the eddies might have sizes as small as 7 cm for a power flux of 1 kW/cm^2. The associated density fluctuation would then be expected to result in considerably increased scattering of the beam.

The arguments presented here show that there are substantially more important sources of instability in the laser-fluid system than those discussed in earlier linearized analyses. It is felt that these fluid instabilities will be enhanced by their interaction with the scattering of the laser beam, because of the general result that instabilities in fluids result if the heating of

the fluid is greater in those regions where the density of the fluid is greater.[27]

At the present time we can only outline the general nature of the effects to be expected above a critical power level. Much additional work clearly needs to be done, both of an experimental and theoretical nature.

BLANK PAGE

PART VI

LASER RADIATION IN A MOVING MEDIUM

In order to consider the effects of forced fluid flow on a laser beam, the equations for the laser-fluid system will be analyzed for a two-dimensional steady state situation. For simplicity, consider a uniform slab-shaped laser beam of width, a, in the y-direction, of infinite extent in the x-direction, and propagating in the z-direction. If there is a transverse motion of the medium in the y-direction, due to wind or to convection above a heated surface, an asymmetric distribution of temperature and density will be generated in the beam region. This asymmetry leads to a curving of the laser beam toward the source of the fluid motion as shown in Figure [18].

This self-curving or "wind prism" effect can be explained by the following simple physical argument. Consider the case of fast flow, where flow transit time through the beam cross section is much less than thermal conduction times. [The flow is not presumed, however, to move at speeds comparable to the sound velocity in the medium.] As the fluid passes the beam cross section, it is heated and becomes less dense, so that the density at $y = a$ is less than at $y = 0$. Thus, the index of refraction at $y = a$ is less than at $y = 0$, so that the beam is effectively moving through a prism and will bend toward the negative y-direction. As this wind velocity decreases to zero, the wind prism goes away, to be replaced by an effective convex thermal lens. In the absence of wind, thermal conduction will lead to a temperature distribution symmetric about $y = \frac{a}{2}$. The hottest place will be in the center of the slab and the density distribution will have a minimum there. Thus, the index of refraction has a minimum at $y = \frac{a}{2}$ and the beam is effectively moving through a defocusing lens. The beam will, therefore, tend to spread out or "bloom" as indicated in Figure [19].

Akhmanov, et al.,[18] and other groups[16,17,28-31] have predicted and observed the phenomena of thermal blooming and self-curving in the presence of a wind. These two effects will be considered simultaneously here for the simple slab geometry and a formula for the development of the beam profile will be given which included both types of behavior. The slab geometry will overemphasize the self-curving effect slightly, compared to a cylindrical beam, but qualitative features and order of magnitude will be correct. The results of the present model will be compared with a cylindrical beam experiment at the end of this section and reasonable agreement will be demonstrated. In fact, this comparison will serve to illustrate the importance of thermal conduction in the description of a "blooming wind prism."

In order to relate the two effects and to make quantitative estimates of the curvature of the beam, equations (25a) - (29) for the laser-fluid system will be specialized to this case. A cartesian geometry is used with the fluid variables T and ρ being functions of y only, and the fluid velocity $\vec{v} \equiv v(y)\hat{e}_y$ being a function of y only and directed in the y-direction. These variables are also taken to be time independent since only a steady-state analysis is to be attempted. Similarly, the electric field will be taken to be of the form

$$\vec{E} = E(y)\hat{e}\, e^{i(\omega_L t - k_L z)}\, e^{-\frac{\alpha}{2} z} + \text{c.c.} \qquad (223)$$

where $\hat{e}$ is a polarization unit vector, ω_L and k_L are the frequency and wave number of the laser radiation, and the factor

$$e^{-\frac{\alpha}{2} z}$$

included to allow for damping consistent with the damping term in the wave equation, (25a). Substituting (223) into (25a), an equation for E(y) is obtained:

$$\frac{d^2E}{dy^2} = \left(k_L^2 - \frac{\omega_L^2}{c^2}\varepsilon\right) E \tag{224}$$

where, by (25b),

$$\varepsilon = \varepsilon_L + \varepsilon_2 \overline{E^2} \tag{225}$$

and $\overline{E^2}$ is easily computed from (223):

$$\overline{E^2} = \frac{1}{2} E^2(y)\, e^{-\alpha z} \tag{226}$$

To further describe ε as a function of ρ and T, the Clausius-Mossotti relation will be used as shown in (25c):

$$\rho\left(\frac{\partial\varepsilon}{\partial\rho}\right)_T \approx \frac{(\varepsilon-1)\ (\varepsilon+2)}{3}\ ,\ \left(\frac{\partial\varepsilon}{\partial T}\right)_\rho \approx 0 \tag{227}$$

Since, for air and many other fluids, ε is independent of T for reasonable temperatures, (227) can be integrated at once to give

$$\varepsilon = \frac{(\varepsilon_0+2)\rho_0 + 2(\varepsilon_0-1)\rho}{(\varepsilon_0+2)\rho_0 - (\varepsilon_0-1)\rho} \tag{228}$$

where $\varepsilon_0 \equiv [\varepsilon_L + \varepsilon_2\overline{E^2}]_{y=0}$ and ρ_0 are the values of ε and ρ evaluated at $y = 0$. This relation, also, will be called the Clausius-Mossotti relation.

Now, if ρ can be found as a function of y, then (228) and (224) can be used to compute E(y) and the ray methods of geometrical optics can be used to describe the deflection of the beam. From the wave equation, one obtains the following relation between the gradient of ε and the radius of curvature R_c of the laser beam

$$\frac{1}{R_c} \approx \nabla_\perp n = \nabla_\perp \sqrt{\varepsilon} \tag{229}$$

where $\nabla_\perp n$ is the transverse component of the gradient of the index of refraction. The deflection of the laser beam, therefore, can be described by the relation

$$\frac{d\psi}{dz} \approx \nabla_\perp \sqrt{\varepsilon} \tag{230}$$

where ψ is the scattering or deflection angle shown in Figure [18].

In order, then, to compute ρ, the Navier -Stokes and heat transfer (conservation of energy) equations (26a) - (27b) must be solved along with the fluid continuity equation (28) and the equation of state of the fluid (29). Specializing these equations to the present situation, one gets:

NAVIER-STOKES

$$\rho v \frac{dv}{dy} = - \frac{dP}{dy} + (2\eta+\eta') \frac{d^2v}{dy^2} + \frac{(\varepsilon-1)(\varepsilon+2)}{3} \left[\frac{1}{2} \frac{d\overline{E^2}}{dy} + \frac{\varepsilon-1}{3} \frac{\overline{E^2}}{\rho} \frac{d\rho}{dy}\right] \tag{231}$$

HEAT TRANSFER

$$v \frac{dT}{dy} - \frac{\gamma-1}{\rho\beta} v \frac{d\rho}{dy} = \frac{2\eta+\eta'}{\rho C_v} \left(\frac{dv}{dy}\right)^2 + \frac{\kappa}{\rho C_v} \frac{d^2T}{dy^2} + \frac{\alpha c\sqrt{\varepsilon}}{\rho C_v} E^2$$
$$+ \frac{1}{\rho C_v} \left[\left(\frac{\partial \kappa}{\partial \rho}\right)_T \frac{d\rho}{dy} + \left(\frac{\partial \kappa}{\partial T}\right)_\rho \frac{dT}{dy}\right] \frac{dT}{dy} \tag{232}$$

FLUID CONTINUITY

$$\rho v = \rho_0 v_0 = \text{constant} \tag{233}$$

EQUATION OF STATE, IDEAL GAS

$$P = R\rho T \tag{234}$$

where ρ_0 and v_0 are the density and wind velocity at $y = 0$ and R is the gas

constant in units of ergs per gram per degree. To obtain (231), the Clausius-Mossotti relation was used and the dependence on gravity was dropped. For transverse winds, the force of gravity would act in the x-direction and would destroy the simplicity of the present model. For "winds" caused by rising columns of air over heated surfaces, however, gravity could act in the y-direction and would cause no essential complication in the present model. For simplicity, the gravity term will simply be dropped in the analysis given here.

Before proceeding, several additional simplifications will be made in (231) and (232). The terms involving the viscosity coefficients, $(2\eta+\eta')$, are very small and will be dropped. Furthermore, the terms involving derivatives of the thermal conductivity κ are small and will also be dropped. The continuity equation, (233), and the gas law, (234), can be used to eliminate P and v from (231) and (232). Thus, the density and temperature are described by the two equations:

$$\frac{(\rho_o v_o)^2}{\rho^2}\frac{d\rho}{dy} = R\frac{d(\rho T)}{dy} - \frac{(\varepsilon-1)(\varepsilon+2)}{3}\left[\frac{1}{2}\frac{d\overline{E^2}}{dy} + \frac{\varepsilon-1}{3}\frac{\overline{E^2}}{\rho}\frac{d\rho}{dy}\right] \tag{235}$$

and

$$v_o\frac{dT}{dy} - (\gamma-1)\,v_o\frac{T}{\rho}\frac{d\rho}{dy} = \frac{\kappa}{\rho_o C_v}\frac{d^2T}{dy^2} + \frac{\alpha c\sqrt{\varepsilon}\,\overline{E^2}}{\rho_o C_v} \tag{236}$$

where, in order to obtain (236), the relation

$$\beta \equiv -\frac{1}{\rho}\left(\frac{\partial\rho}{\partial T}\right)_P = \frac{1}{T} \tag{237}$$

following from (234), was used.

Inspecting (236) for the characteristic times for thermal changes,

one observes two characteristic times: τ_C, the thermal conductivity time, and τ_F, the flow transit time through the beam cross section. These times are conveniently taken to be:

$$\tau_C = \frac{C_v a^2 \rho_o}{\kappa} \tag{238}$$

and

$$\tau_F = \frac{a}{v_o} \tag{239}$$

For convenience, these time scales will be compared to the much shorter sound transit time:

$$\tau_s = \frac{a}{v_s} = \frac{a}{\sqrt{\gamma R T_o}} \tag{240}$$

where v_s is the isentropic velocity of sound at temperature T_o. It will also be convenient to introduce the following dimensionless parameters:

$$w \equiv \frac{y}{a} \tag{241}$$

$$\theta \equiv \frac{T}{T_o} = \text{temperature relative to temperature at } y = 0 \tag{242}$$

$$g \equiv \frac{\rho}{\rho_o} = \text{density relative to density at } y = 0 \tag{243}$$

$$f \equiv 1-g \equiv \frac{\rho_o - \rho}{\rho_o} = \text{relative density decrement} \tag{244}$$

Using this notation, (235) and (236) can be written in the form:

$$\frac{1}{\tau_F^2}\frac{d(\frac{1}{g})}{dw} + \frac{1}{\gamma\tau_s^2}\frac{d(g\theta)}{dw} = \frac{(\varepsilon-1)(\varepsilon+2)}{3\rho_o a^2}\left[\frac{1}{2}\frac{d\overline{E^2}}{dw} + \frac{\varepsilon-1}{3}\frac{\overline{E^2}}{g}\frac{dg}{dw}\right] \tag{245}$$

and

$$\frac{1}{\tau_F}\frac{d\theta}{dw} - \frac{(\gamma-1)}{\tau_F}\frac{\theta}{g}\frac{dg}{dw} = \frac{1}{\tau_c}\frac{d^2\theta}{dw^2} + \frac{\alpha c\sqrt{\epsilon}}{c_v\rho_o T_o}\,\overline{E^2} \tag{246}$$

Now, the general strategy will be to solve (245), (246) and (224) by iteration, but only one iteration will be made. A simple shape will be presumed for E(y) and then (245) and (246) will be solved for θ and g. Then, in principle, one could solve (224) for a new E(y) and continue. However, the first iteration for θ and g allows evaluation of $\nabla\epsilon$, so that (230) can be integrated to produce an estimate of the beam deflection. The initial shape presumed[†] for E(y) is

$$E(y) = \begin{cases} E_o = \text{constant, for } 0 \le y \le a \\ 0 \quad \text{otherwise} \end{cases} \tag{247}$$

Then, inside the region $0 \le y \le a$; i.e., $0 \le w \le 1$, the derivative of $\overline{E^2}$ with respect to w is zero in (245). In both (245) and (246), the replacement

$$\overline{E^2} = \frac{1}{2}E_o^2\, e^{-\alpha z} = \frac{\tilde{I}_L}{\sqrt{\epsilon_o}\,c} \equiv \frac{I_L\, e^{-\alpha z}}{\sqrt{\epsilon}_o c} \tag{248}$$

can be made, where I_L is the power per unit area in the incident laser beam. For convenience, now, the following additional time scale is introduced.

$$\tau_A \equiv \frac{C_v\rho_o T_o}{\alpha c\sqrt{\epsilon}\,\overline{E^2}} \equiv \frac{C_v\rho_o T_o}{\alpha\tilde{I}_L} \equiv \frac{C_v\rho_o T_o}{\alpha I_L e^{-\alpha z}} \tag{249}$$

The time, τ_A, is characteristic of the rate of absorption of heat in the fluid.

[†]Such a flat profile will minimize the thermal blooming because none of the rays will cross in the first iteration. Subsequent iterations would produce crossing rays which would keep the iteration procedure from converging. Crossing rays are, of course, not allowed by the wave equation.

Now, (245) can be integrated in the following way

$$\frac{1}{\tau_F^2}\left(\frac{1}{g}-1\right)+\frac{1}{\gamma\tau_s^2}(g\theta-1)=\frac{\tilde{I}_L}{3\sqrt{\epsilon_o}\,c\rho_o a^2}\int_o^w \frac{(\epsilon-1)(\epsilon+2)}{3g}(\epsilon-1)\frac{dg}{dw}\,dw=$$

$$=\frac{\tilde{I}_L}{3\sqrt{\epsilon_o}\,c\rho_o a^2}\int_o^w \frac{d\epsilon}{dg}(\epsilon-1)\frac{dg}{dw}\,dw=$$

$$=\frac{\tilde{I}_L}{6\sqrt{\epsilon_o}\,c\rho_o a^2}\int_o^w \frac{d(\epsilon-1)^2}{dg}\frac{dg}{dw}\,dw=$$

$$=\frac{\tilde{I}_L}{6\sqrt{\epsilon_o}\,c\rho_o a^2}\left[(\epsilon-1)^2\right]_1^g \qquad (250)$$

From (228), however, one gets

$$(\epsilon-1)^2=\left(\frac{3B_o g}{1-B_o g}\right)^2\approx\left[3B_o g(1+B_o g)\right]^2\approx 9B_o^2\left(g^2+2B_o g^3\right) \qquad (251)$$

where

$$B_o\equiv\frac{\epsilon-1}{\epsilon+2}\approx \text{very small for air} \qquad (252)$$

Combining (250) and (251) and solving for θ produces

$$\theta=\frac{1}{g}-\gamma\left(\frac{\tau_s}{\tau_F}\right)^2\left(\frac{1-g}{g^2}\right)-\gamma\left(\frac{\tau_s}{\tau_D}\right)^2\left[\left(\frac{1-g^2}{g}\right)+2B_o\left(\frac{1-g^3}{g}\right)\right] \qquad (253)$$

where τ_D is still another characteristic time:

$$\tau_D^2\equiv\frac{2\sqrt{\epsilon_o}\,c\rho_o a^2}{3B_o^2\,\tilde{P}_L} \qquad (254)$$

This quantity, τ_D, characterizes the direct interaction of the electromagnetic field with the fluid and arises from the electromagnetic stress term in the Navier-Stokes equation.

Equation (253) gives the temperature as a function of the density and will be useful in integrating (246). If (253) is used to express the ratio $\frac{\theta}{g}$ as a function of g, then a first integral of (246) can be obtained immediately. Then (253) can be used to eliminate θ in this first integral and a first order differential equation for g results. Continuation along this line is largely superfluous, however, and leads to implicit transcendental expressions connecting ρ and w. It is useful, and far simpler, to agree to study the situation for the case in which the density change is small from y = 0 to y = a.

For the case that $g \approx 1$, the relative density decrement, f, defined in (244), is very small and it is useful to write equations (253) and (246) in terms of f and work to first order in the density decrement. Thus (253) becomes

$$\theta \approx 1 + Qf \tag{255}$$

where

$$Q \equiv 1-\gamma \left(\frac{\tau_s}{\tau_F}\right)^2 - 2\gamma \left(\frac{\tau_s}{\tau_D}\right)^2 (1+3B_o) \, . \tag{255}$$

Then, using

$$\frac{\theta}{g} \approx \frac{1+Qf}{1-f} \approx 1 + (Q+1)\, f, \tag{257}$$

equation (246) can be integrated immediately:

$$\frac{Q}{\tau_c}\frac{df}{dw} - \frac{Q + (\gamma-1)}{\tau_F} f = -\frac{w}{\tau_A} + A_1 \tag{258}$$

where A_1 is a constant of integration. Integrating again and taking the boundary conditions $f(0) = 0$ and $\rho(1) = \rho_1$, where ρ_1 is the density of the fluid at y = a, produces

$$f = \left[\frac{\rho_o - \rho_1}{\rho_o} - \frac{\tau_F}{\gamma\tau_A(1-\sigma)}\right] \frac{e^{\lambda W} - 1}{e^{\lambda} - 1} + \frac{\tau_F W}{\gamma\tau_A(1-\sigma)} \qquad (259)$$

where

$$\sigma \equiv \left(\frac{\tau_s}{\tau_F}\right)^2 + 2\left(\frac{\tau_s}{\tau_D}\right)^2 (1+3B_o) \qquad (260)$$

and

$$\lambda \equiv \gamma \frac{\tau_c}{\tau_F} \frac{1-\sigma}{1-\gamma\sigma} \qquad (261)$$

Then, combining (251) and (259) the square root of the permittivity is approximately given by:

$$\sqrt{\varepsilon} \simeq 1 + \frac{3}{2} B_o \left(1+2B_o\right) \left[\frac{1+B_o}{1+2B_o} - f\right] \qquad (262)$$

and

$$\nabla_\perp \sqrt{\varepsilon} = \frac{d\sqrt{\varepsilon}}{df} \frac{df}{dw} \frac{dw}{dy} =$$

$$= \frac{3B_o(1+2B_o)}{2\gamma a(1-\sigma)} \left(\frac{\tau_F}{\tau_A}\right) \left\{1 - \frac{\lambda e^{\lambda W}}{e^{\lambda}-1} \left[1 - \left(\frac{\tau_A}{\tau_F}\right)\gamma(1-\sigma) \frac{\rho_o - \rho_1}{\rho_o}\right]\right\} \qquad (263)$$

Since this derivation has proceeded under the assumption that the density decrement, f, is small, the first order term involving $\frac{\rho_o - \rho_1}{\rho_o}$ is small compared to 1 and will be dropped as will terms of order B_o when compared to 1. It is convenient now to introduce the notation:

$$\frac{\tau_F}{\gamma\tau_A} = \tilde{\boldsymbol{\rho}} \frac{\tau_F}{\gamma\tau_c} \equiv \boldsymbol{\rho} e^{-\alpha z} \frac{\tau_F}{\gamma\tau_c} \qquad (264)$$

where the dimensionless power $\boldsymbol{\rho}$ is given by

$$\boldsymbol{\rho} \equiv \frac{a^2 \alpha I_L}{\kappa T_o} \qquad \text{and} \qquad \tilde{\boldsymbol{\rho}} \equiv \boldsymbol{\rho} e^{-\alpha z} \qquad (265)$$

The deflection of the laser beam can now be given in the form

$$\frac{d\psi}{dz} \approx \frac{(\epsilon_o - 1)\tilde{\mathcal{P}}}{2a\,(1-\gamma\sigma)} \left[\frac{1}{\lambda} - \frac{e^{\lambda \frac{y}{a}}}{e^{\lambda} - 1} \right] \tag{266}$$

In order to analyze this expression for the curvature of the laser beam, it is convenient to rewrite σ in the form

$$\sigma = \left(\frac{v_o}{v_s} \right)^2 + \frac{3\tilde{I}_L}{\sqrt{\epsilon_o}\,\rho_o\,c\,v_s^2} \tag{267}$$

For propagation through air at 10°C, the two terms on the right hand side of (267) are both of order 10^{-3} when $v_o \approx 5$ (km/hr) and $I_L = 1$ (MW/cm^2), so σ and $\gamma\sigma$ can be considered small compared to 1 for velocities less than 50 (km/hr) and powers less than 100 (MW/cm^2). From equations (261), (238), and (239), one has

$$\lambda = \left(\frac{1-\sigma}{1-\gamma\sigma} \right) \frac{\gamma \tau_c}{\tau_F} = \left(\frac{1-\sigma}{1-\gamma\sigma} \right) \frac{\gamma C_v \rho_o}{\kappa}\, a v_o \tag{268}$$

so that for wide beams or fast winds, the conduction time is very long, compared to the flow time and λ will be very large compared to 1. Under these conditions, the ratio of exponentials in (266) tends to be smaller than $\frac{1}{\lambda}$, so that most of the rays bend into the wind. For large enough y, however, the ratio of exponentials is greater than $\frac{1}{\lambda}$, so that some of the rays have negative curvature. Thus the downwind edge of the beam bends in the direction of the wind. Therefore, pure beam curving with no thermal blooming will never occur.

Physically, this is easy to understand. The hottest place and, hence, the minimum of the index of refraction, must lie inside the beam region. On the two sides of this minimum, the rays will bend in opposite directions. The

faster the wind, the larger λ will be and, hence, the larger y must be before the curvature changes sign. In other words, the wind can blow the hottest spot away from the center of the beam, but it can not blow the hottest spot entirely out of the beam. The position of the minimum of the index of refraction is easily obtained by determining the value of y for which the right hand side of (266) vanishes:

$$\frac{y_o}{a} = 1 - \frac{\log \lambda}{\lambda} + \frac{\log (1-e^{-\lambda})}{\lambda} \tag{269a}$$

$$\approx 1 - \frac{\log \lambda}{\lambda} \quad \text{for large } \lambda \tag{269b}$$

$$\approx \frac{1}{2} + \frac{\lambda}{24} \quad \text{for small } \lambda \tag{269c}$$

In particular, for very small λ the minimum is at the center of the beam, whereas, for large λ, the minimum is very near the downwind edge of the beam.

As the wind velocity goes to zero, equation (266) reduces to

$$\left.\frac{d\psi}{dz}\right)_{v_o=0} = \frac{(\varepsilon_o-1)\,\tilde{\rho}}{2a\,(1-\gamma\sigma)} \left[\frac{1}{2} - \frac{y}{a}\right] \tag{270}$$

which is symmetrical about the center of the beam as would be expected for pure thermal blooming. The rays at the edge of the beam have the maximum curvature

$$\xi_B = \max_y \left|\frac{d\psi}{dz}\right|_{v_o=0} = \frac{1}{2}\left[\frac{(\varepsilon_o-1)\,\tilde{\rho}}{2a\,(1-\gamma\sigma)}\right] . \tag{271}$$

In terms of this maximum curvature for pure thermal blooming, (266) can be written in the form

$$\frac{d\psi}{dz} \equiv \xi = 2\left[\frac{1}{\lambda} - \frac{e^{\lambda \frac{y}{a}}}{e^{\lambda}-1}\right] \xi_B \tag{272}$$

Clearly ξ is a monotonic function of y, giving the largest positive curvature

at y = 0:

$$\xi_{max} = 2\left[\frac{1}{\lambda} - \frac{1}{e^{\lambda}-1}\right]\xi_B \tag{273a}$$

$$\approx (1 - \frac{\lambda}{6})\ \xi_B \quad \text{for small } \lambda \tag{273b}$$

$$\approx \frac{2}{\lambda}\ \xi_B \quad \text{for large } \lambda \tag{273c}$$

As may be seen from (273a), ξ_{max} decreases monotonically with the wind velocity and is less than ξ_B if there is any wind at all. Thus, the wind blows the blooming rays back into the beam on the upwind side of the beam.

The minimum curvature; that is, the largest negative curvature, occurs at y = a:

$$\xi_{min} = -\ 2\left[\frac{e^{\lambda}}{e^{\lambda}-1} - \frac{1}{\lambda}\right]\xi_B \tag{274a}$$

$$\approx -\ (1 + \frac{\lambda}{6})\ \xi_B \quad \text{for small } \lambda \tag{274b}$$

$$\approx -2\ (1 - \frac{1}{\lambda})\ \xi_B \quad \text{for large } \lambda \tag{274c}$$

Thus, it is clear that $\left|\xi_{min}\right|$ increases monotonically with the wind velocity and is greater than ξ_B if there is any wind at all. The effect of the wind on the downwind side of the beam is to blow the blooming rays farther out of the beam.

Comparing (273) and (274), one finds that

$$\xi_{max} - \xi_{min} = \xi_{max} + \left|\xi_{min}\right| = 2\xi_B \tag{275}$$

regardless of the wind velocity. Thus the wind has no effect on the size of the spread of curvatures created by the thermal blooming. For v = 0, this spread is from ξ_B to $-\xi_B$, whereas for extremely fast winds, the spread is

essentially from 0 to $-2\xi_B$. Thus, the curvature spread can not be decreased by a wind, but it can be translated by, at most, half of its extent. There is, however, a very dramatic shift in the fractions of the power being scattered into the various curvatures. This arises because, for large λ, the distribution shown in (272) is very flat as a function of $(\frac{y}{a})$ for $y < y_0$. For $\lambda = 100$, for example,

$$0.01 \geq \frac{\xi}{2\xi_B} \geq 0 \quad \text{for} \quad 0 \leq \frac{y}{a} \leq \frac{y_0}{a} = 0.96.$$

Then, for $y > y_0$, the curvature becomes negative and falls rapidly to

$$\frac{\xi}{2\xi_B} = \frac{1}{100} - 1 = -0.99$$

at $y = a$. The net effect, therefore, is that about 96% of the power goes off with curvature $\xi \approx \xi_B/50$ and the remaining 4% blooms strongly out of the beam. For a non-uniform beam profile, the conclusions are qualitatively the same, but the distribution is no longer monotonic as in (272), so that some of the rays will cross.

One of many ways to exhibit the nature of the scattering distribution given in (272) is to show the scattering cross section for scattering of power into the various curvatures. Thus, one can define the cross section

$$\sigma(\xi)d\xi \equiv ap(\xi)d\xi = \frac{\text{laser energy flux scattered into range } d\xi}{\text{laser energy flux density}}$$

$$= \left|\left(\frac{d\xi}{dy}\right)^{-1}\right| d\xi = \frac{a\,d\xi}{2\xi_B - \lambda\xi} \,. \tag{276}$$

The quantity $p(\xi)$ is the fraction of the laser power scattered into curvature ξ. The distribution $p(\xi)$ is normalized to unity:

$$\int_{\xi_{min}}^{\xi_{max}} p(\xi)d\xi = \int_{\xi_{min}}^{\xi_{max}} \frac{d\xi}{2\xi_B - \lambda\xi} = \frac{1}{\lambda} \log \frac{2\xi_B - \lambda\xi_{min}}{2\xi_B - \lambda\xi_{max}} = \frac{1}{\lambda} \log e^{\lambda} = 1 \qquad (277)$$

where ξ_{min} and ξ_{max} are given in (273a) and (274a). The fraction of the power being scattered into negative curvatures is

$$\int_{\xi_{min}}^{0} p(\xi)d\xi = \frac{1}{\lambda} \log \left(1 + \frac{\lambda|\xi_{min}|}{2\xi_B}\right) = 1 - \frac{1}{\lambda} \log \frac{e^{\lambda}-1}{\lambda}$$

$$\approx \frac{\log \lambda}{\lambda} \text{ for large } \lambda \qquad (278)$$

The distribution $p(\xi)$ is sketched in Figure [20] for small wind speeds. The extreme values of the monotonic distribution are given by by

$$\xi_B \; p(\xi_{max}) = \frac{e^{\lambda}-1}{2\lambda}$$

and (279)

$$\xi_B \; p(\xi_{min}) = \frac{1 - e^{-\lambda}}{2\lambda} .$$

As shown in the figure, the distribution is sharply enhanced at ξ_{max}, even for $\lambda = 3$. Because of this sharp peaking of $p(\xi)$ for even very slow wind speeds, the thermal lens-wind prism effect may be pictured as in Figure [21]. At each point in the beam path the beam is essentially passing through a wind prism with a small strongly defocusing thermal lens perched on the downwind vertex of the prism. As λ increases, the half-angle of the prism decreases rapidly and the blooming lens increases its defocusing power, but shrinks rapidly in size so that only an infinitesimal portion of the downwind edge of the beam is affected. As the wind velocity increases, both the curving and the blooming effects decrease as indicated in equations (273c) and (278).

At $v_o = 10 \frac{km}{hr} = 278 \frac{cm}{sec}$, for example, with a = 1 cm and $I_L = 1 \frac{kW}{cm^2}$, one has, from (268):

$$\lambda \approx 1400\, a^2 \frac{v_o}{10 \frac{km}{hr}} \approx 1400$$

so that at a given point in the beam, about 0.5% of the beam is affected by the thermal lens. The dimensionless power shown in (265) is

$$\mathcal{P} \approx 0.043\, a^2 \approx 0.043$$

where the values: $\alpha \approx 3 \times 10^{-6}$ cm^{-1}, $\kappa \approx 2.5 \times 10^3$ ergs/(deg sec cm), and $T_o \approx 283°K = 10°C$ have been used. The blocming edge curvature is then given by (271):

$$\xi_B \approx \frac{\varepsilon_o^{-1}}{4a} (0.043\, a^2) \approx \frac{5.65 \times 10^{-4}}{4} (0.043\, a) = 6.04 \times 10^{-6}\, a \approx$$

$$\approx 6.04 \times 10^{-6}$$

so that, from (273c),

$$\xi_{max} \approx (8.64 \times 10^{-9})\, a \frac{10 \frac{km}{hr}}{v_o} \approx 8.64 \times 10^{-9}\ .$$

Thus, after the beam has propagated 1 km, it will have an inclination of the order of 9×10^{-4} radians $\approx$ 0.05 deg. For comparison, without the wind the pure thermal blooming would have produced a 70° divergence of the beam! The ratio of ψ_{max} to ψ_B is

$$\frac{8.64 \times 10^{-9}}{6.04 \times 10^{-6}} = 1.43 \times 10^{-3}$$

so that the wind can play a significant role in holding the beam together. The fraction of the power lost from this beam in 1 km is roughly

$$\frac{P_o - P(z)}{P_o} \approx (1 - e^{-\alpha z}) + \frac{1}{\lambda} \log \frac{\xi_B z^2}{a}$$

$$\approx (1 - e^{-0.3}) + \frac{1}{1400} \log [6.04 \times 10^4] \approx 0.258 + 0.008$$

so that the major loss of power arises from the damping factor $e^{-\alpha z}$ in the presence of the 10 $\frac{km}{hr}$ wind.

It is possible to compare the predictions of this section with experiment, using the nice results of Smith and Gebhardt.[17] The beam of a 20 watt cw CO_2 laser operating in the fundamental TEM_{oo} mode was passed through an enclosed, recirculating wind tunnel with a 100 cm optical path length and a variable wind speed from 0 to 500 cm/sec. The absorption of the air was increased more than a thousandfold and was controlled by the addition of varying amounts of freon-12 (CCl_2F_2). A vertical optical path, transverse to the wind direction, was used to minimize the gravitational convection effects. The $\frac{1}{e}$ beam diameter was 0.4 cm at the tunnel entrance window and, in the absence of thermal distortion, the $\frac{1}{e}$ diameter was 0.6 at the scanning detector which was located 20 cm from the wind tunnel axis window. Of course, the experiment was performed with a cylindrical beam, but one might expect to get semiquantitative agreement from the present slab beam model, particularly if one concentrates on the shift of the beam peak into the wind.

To consider the predictions of the slab beam model for the experiment of Smith and Gebhardt, one can use equation (272). A ray initially at height y will have the trajectory Y(y,z), where

$$\frac{dY}{dz} = -\tan\psi \approx -\psi. \tag{280}$$

Differentiating again and using (272), one gets

$$\frac{d^2Y}{dz^2} \approx \frac{d\psi}{dz} \approx \begin{cases} -f(y)\, e^{-\alpha z} & \text{for } z < L \\ 0 & \text{for } z > L \end{cases} \tag{281}$$

where L is the tunnel length (100 cm) and

$$f(y) \equiv 2\xi_B \left[\frac{1}{\lambda} - \frac{e^{\lambda \frac{y}{a}}}{e^{\lambda}-1}\right]. \tag{282}$$

Integrating (281), one has

$$\frac{dY}{dz} = -\frac{f(y)}{\alpha} \cdot \begin{cases} (1 - e^{-\alpha z}) \text{ for } z < L \\ (1 - e^{-\alpha L}) \text{ for } z > L \end{cases} \tag{283}$$

Another integration produces:

$$Y(y,z) = y - \frac{f(y)}{\alpha^2}\left[(1 + \alpha L)\, e^{-\alpha L} - 1 + (1 - e^{-\alpha L})\, \alpha z\right] \text{ for } z > L \tag{284}$$

In particular, for $z = \frac{6}{5} L = 100$ cm + 20 cm for $L = 100$ cm, the height of the ray at the detector will be

$$\frac{Y_{Det}}{a} \equiv \frac{Y(y, \frac{6}{5} L)}{a} = \frac{y}{a} - \frac{2\xi_B \alpha L}{\alpha^2 a}\, g(\alpha L) \left[\frac{1}{\lambda} - \frac{e^{\lambda \frac{y}{a}}}{e^{\lambda}-1}\right] \tag{285}$$

where

$$g(\alpha L) \equiv \left[1 + \left(\frac{1}{5} - \frac{1}{\alpha L}\right)\left(1 - e^{-\alpha L}\right)\right].$$

The corresponding intensity at $z = \frac{6}{5} L$ is

$$I(Y, \tfrac{6}{5} L) \approx \frac{I_0\, e^{-\alpha L}}{\left(\frac{\partial Y}{\partial y}\right)_{z = \frac{6}{5} L}} = \frac{I_0\, e^{-\alpha L}}{1 + \frac{2\xi_B \alpha L}{\alpha^2 a}\, g(\alpha L) \left[\frac{\lambda\, e^{\lambda \frac{y}{a}}}{e^{\lambda} - 1}\right]} \tag{286}$$

The peak in this intensity distribution occurs for $y = 0$ and its location is determined from (285) to be

$$\frac{Y_p}{a} = -\frac{2\xi_B \alpha L}{\alpha^2 a}\, g(\alpha L) \left[\frac{1}{\lambda} - \frac{1}{e^{\lambda}-1}\right] \tag{287}$$

This relation is conveniently put in the form

$$G(\alpha L)\,\frac{Y_p}{a} = -\,\frac{2\xi_B \alpha L}{\alpha^2 a}\left[1 - \frac{4}{5}\left(1 - \frac{1}{e}\right)\right]\left[\frac{1}{\lambda} - \frac{1}{e^{\lambda}-1}\right] \tag{288}$$

where

$$G(\alpha L) = \frac{g(1)}{g(\alpha L)} = \frac{1 + \left(\frac{1}{5} - 1\right)\left(1 - e^{-1}\right)}{1 + \left(\frac{1}{5} - \frac{1}{\alpha L}\right)\left(1 - e^{-\alpha L}\right)} \tag{289}$$

In order to compare the shift of the peak with the results of Smith and Gebhardt it will be necessary to put numbers into (288). The numerical values for the various parameters, appropriate for $T_0 = 10°C$ are shown in Part II of this report. The width, a, of the slab beam will be taken to be 0.4 cm, the $\frac{1}{e}$ diameter of the experimental beam. The 20 watt beam used would have a "uniform" transverse linear density of 20 watt/0.4 cm so that I_L will be taken to be 50 watts/cm^2. Then, in cgs units, one has

$$\lambda = \left(\frac{\gamma C_v \rho_0}{\kappa}\right) a v_0 = (0.806)\, v_0 \simeq \sqrt{65}\, v_0$$

$$\mathcal{P} = \frac{a^2 \alpha I_L}{\kappa T_0} = 1.146\ \alpha L$$

$$\xi_B = \left[4.02 \times 10^{-4}\right] \alpha L$$

$$\frac{2\xi_B \alpha L}{\alpha^2 a} = 20.12$$

Thus, for the experiment under consideration, (288) can be written

$$-G(\alpha L)\,\frac{Y_p}{a} = (9.95)\left[\frac{1}{\sqrt{65}\, v_0} - \frac{1}{e^{\sqrt{65}\, v_0} - 1}\right] \tag{290}$$

In Figure [22] the function $G(\alpha L)$ is plotted versus (αL) and, also,

$- G(\alpha L)\frac{Y_p}{a}$, the RHS of (290) is plotted versus $(\frac{1}{v_o})$. Data given by Smith and Gebhardt for $\alpha L = 0.14$, 0.53, and 1.0 are also indicated on the figure. One notices that the data for various αL does not all lie on the same "universal" curve as suggested by (290). Thus, as expected, there is some difference in a slab beam and a cylindrical beam. The important feature to be noticed, however, is that the order of magnitude of the predicted effect is correct and the "saturation" of the prism effect encountered by Smith and Gebhardt is predicted by (290). It would certainly appear that thermal conduction effects can account for the saturation of the deflection and that the other explanations suggested by Smith and Gebhardt are, perhaps, unnecessary.

In Figure [23] the intensity distribution of the laser pulse at the detector, determined by equation (286), is shown for $v_o = 2\ \frac{cm}{sec}$, $10\ \frac{cm}{sec}$, and for v_o extremely large. One notices here the rapid transition from the uniform spreading, due to thermal blooming, to much narrower distributions, peaked on the upwind side, as the wind velocity increases. The qualitative features of these curves were, of course, already illustrated in Figure [20].

This analysis has been undertaken in order to estimate the relative importance of thermal blooming and wind curving. Certain qualitative features have been discussed and perhaps some insight has been achieved. The approximations made have been rather strong and cylindrical beams and non-uniform beam profiles have not been properly considered here. These matters are currently under study and results will be presented at a later time. The approach to steady state and the usefulness of working to first order in the density changes is also under study. There are difficulties involved in asking for steady state solutions[16] and the effect of a wind on such matters must be analyzed carefully. It does, however, appear that blooming in the

absence of a wind is a quite serious problem if one wishes the beam to retain its character over long distances. A fast wind can, apparently, help considerably to alleviate the thermal blooming.

REFERENCES

1. Landau, L.D., and Lifshitz, E.M., 1959, Fluid Mechanics (Addison-Wesley Publishing Company, Inc., New York).

2. Landau, L.D., and Lifshitz, E.M., 1960, Electrodynamics of Continuous Media (Addison-Wesley Publishing Company, Inc., New York).

3. Stokes, Sir G.G., Phil. Mag. (4) 1, 305-317 (1851).

4. Brueckner, K.A., and Jorna, S., Phys. Rev. 164, 182, 1967.

5. Wagner, W.G., and Reichert, J.D., unpublished report.

6. Eckart, C., Phys. Rev. 73, 68-79, 1948.

7. Handbook of Chemistry and Physics, Chemical Rubber Publishing Co., Cleveland, Ohio (1969).

8. Douglas, J., 1956, "On the Relation between Stability and Covergence in the Numerical Solution of Linear Parabolic and Hyperbolic Equations", J. Soc. Industrial and Appl. Math., Vol. 4, p. 20.

9. Kato, T., 1960, "Estimation of Iterated Matrices, with Application to Von Neumann Condition, Numer. Math., Vol. 2, p. 22.

10. Richtmyer, R.D., 1957, Difference Methods for Initial-Value Problems (Interscience Publishers, Inc., New York).

11. Kantorowitch, L.W., 1948, Functional Analysis and Applied Mathematics, Uspekhi Mat. Nank, U.S.S.R., Vol. 3, p. 89.

12. Lax. P.D., and Richtmyer, R.D., 1956, "Survey of the Stability of Linear Finite Difference Equations", Comm. Pure Appl. Math., Vol. 9, p. 267.

13. Lax, P.D., 1961, "On the Stability of Difference Approximations to Solutions of Hyperbolic Equations with Variable Coefficients", Comm. Pure Appl. Math., Vol. 14, p. 497.

14. Strang, W.G., 1964, "Accurate Partial Difference Methods II: Non-Linear Problems", Numer. Math., Vol. 6, p. 37.

15. Harmuth, H.F., 1957, J. Math. and Phys. 36, 269.

16. Gordon, J.P., Leite, R.C.C., Moore, R.S., Porto, S.P.S., and Whinnery, J.R., Journal of Applied Physics, Vol. 36, January 1965, pp. 3-8.

17. Smith, David C. and Gebhardt, Frederick G., Applied Physics Letters, Vol. 16, 1 April 1970, pp. 275-278.

18. Akhmanov, S.A., Krindach, D.P., Migulin, A.V., Sukhorukov, A.P., and Khokhlov, R.V., IEEE Journal of Quantum Electronics, Vol. QE-4, October 1968, pp. 568-575.

19. Ede, A.J., "Advances in Free Convection", Advances in Heat Transfer, Vol. 4, edited by James P. Hartnett and Thomas F. Irvine Jr. (Academic Press, 1967).

20. Lin, C.C., The Theory of Hydrodynamic Instability, (Cambridge University Press, 1955).

21. Stuart, J.T., "Hydrodynamic Stability", in Laminar Boundary Layers, edited by L. Rosenhead, Oxford University Press, 1963.

22. Cheng, H.K., private communication.

23. Yih, C.S., in "Symposium on the Use of Models in Geophysical Fluid Mechanics", Gov. Printing Off., Washington, D.C., 1956.

24. Yih, C.S., Fluid Mechanics, (McGraw-Hill, 1969), pp. 412-416.

25. Ostrach, Simon, "Laminar Flows with Bond Forces", in Theory of Laminar Flows, edited by F.K. Moore (Princeton University Press, 1964), p. 691.

26. Landau, L.D. and Lifshitz, E.M., Fluid Mechanics, (Pergamon Press, London, 1959) p. 122.

27. Mawardi, O.K., "Aero-thermoacoustics", in Reprints on Progress in in Physics, Vol. 19, p. 180, 1956 (Published by Physical Society, London; edited by E.C. Strickland).

28. Smith, David C., and Gebhardt, Frederick G., Applied Physics Letters, Vol. 14, pp. 52-54.

29. Hayes, J.N., "The Spatio-Temporal Behavior of a Thermally Defocusing Intense Laser Beam in a Gaseous Medium", Nuclear Physics Division, Naval Research Laboratory.

30. Proceedings of the Laser Propagation Meeting 15 and 16 October 1969, Project Report LTP-3 (Laser Technology Program) Massachusetts Institute of Technology Lincoln Laboratory, Lexington, Mass.

31. Kenemuth, J.R., Hogge, C.B. and Avizonis, P.V., Applied Physics Letters, Vol., 17, pp. 220-223.

APPENDIX A

"Computer Program for Power Threshold for Instabilities"

APPENDIX A

Computer Program for Power Threshold for Instabilities

One can show from equation (68) that the threshold power for an instability lies near $k=0.01cm^{-1}$. A search was conducted for various ν with k fixed at $0.01cm^{-1}$. The power threshold was then located at $\nu=(8.45x10^{-2})\cdot k$ and found to be $P_{th}=312ergs/sec$.

In this computation the following notations have been introduced into the computer program:

S : k

R : k_3

B(6) : Coefficient of the 5^{th} order polynomial obtained from (68).

ROOT(5) : The roots of the dispersion relation.

DET : Decrement of the power.

DCROOT : Subprogram for the calculation of the roots of a polynomial.

Following is the computer program for this computation.

```
MCHEN:PROC  OPTIONS (MAIN);
DCL (W,B(6),ROOT(6),RG16(7),F1,F2,F3,F4,F5,F6,F7,F8,F9) CPLX(16) ;
W=1.1;              VS=SQRT(1.175E9);
DCROOT: PROC (A,N,ACC,ROOT,ICHK,REGEN);
                                        /*THIS IA A SUBROUTINE FOR
THE ROOTS OF A COMPLEX POLYNOMIAL OF DEGREE LESS THAN NXY WITH 16
DECIMAL DIGITS ACCURACY IN STORAGE*/
NXY=6;
 DCL (A(6)  ,Z0,Z1,Z2,Z3,H2,H3,XL2,XL3,D2,G2,FZ0,FZ1,FZ2,ROOT)5(
BUF(4),REGEN(16)   CPLX )(6);
IF A(1)(=.0 THEN DO; PUT FILE (SYSPRINT) LIST ('LEADING COEFFICIENT IS ZE
RO IN DCROOT'); EXIT; END; IF N >= NXY | N <  1 THEN DO; PUT FILE (SYSPRINT)
     LIST ('DEGREE OF POLYNOMIAL IN DCROOT IS NOT BETWEEN 0 AND NXY');
EXIT; END;
NR=0; N=N+1; REGEN = A;
S1: Z0=-1.; Z1=1.; Z2=.0; H2=-1.; XL2=-.5; D2=.5;   DO I=N TO 1 BY -1;
IF A(I)(=.0 THEN DO; NR=NR+1; ROOT(NR)=.0; END; ELSE GO TO S7;    END;
S7:NN=I; IF NR <  2 THEN GO TO S25; ELSE IF NN=2 THEN DO; Z3=-A(2)/A(1);
NR=NR+1; ROOT(NR)=Z3; GO TO S25; END; FZ0=A(NN)-A(NN-1)+A(NN-2);
FZ1=A(NN)+A(NN-1)+A(NN-2); FZ2=A(NN); NN=NN-1;
S3: G2=FZ2*XL2+D2)-FZ1*D2**2+FZ0*XL2**2;
BUF(2)=G2+SQRT(G2**2-4.*FZ2*D2*XL2**2)FZ0*XL2-FZ1*D2+FZ2);
BUF(3)=2.*G2-BUF(2); IF ABS(BUF(3)) <= ABS(BUF(2)) THEN IF ABS(BUF(2))(
 < 1.E-10 THEN DO; XL3=1.;H3=H2;GO TO S13;END;ELSE DO;BUF(4)=BUF(2);
GO TO S10; END; ELSE BUF(4)=BUF(3);
S10: XL3=-2.*FZ2*D2/BUF(4); H3=XL3*H2;
S13: Z3=H3+Z2; IF ABS(H3/Z3) <  ACC THEN GO TO S19; ELSE FZ0=FZ1;
FZ1=FZ2;
S140: BUF(1)=1.; FZ2=A(NN+1); DO I=NN TO 1 BY -1; BUF(I)=BUF(I)*Z3;
FZ2=FZ2+BUF(I)*A(I); END; IF ABS(FZ2/FZ1) <  10. THEN GO TO S18;
ELSE XL3=XL3/2.; H3=XL3*H2; Z3=H3+Z2; GO TO S140;
S18: H2=H3; XL2=XL3; Z0=Z1; Z1=Z2; Z2=Z3; D2=1.+XL2; GO TO S3;
S19: NR=NR+1; ROOT(NR)=Z3; IF NR <  N THEN DO; DO I=2 TO NN;
A(I)=A(I-1)*ROOT(NR)+A(I); END; N=NN; GO TO S1; END; ELSE;
S25: A=REGEN; IF ICHK=0 THEN RETURN; ELSE REGEN=.0*A; REGEN(1)=1.;
REGEN(2)=-ROOT(1); DO K=2 TO N; DO J=K+1 TO 2 BY -1;  REGEN(J)=REGEN(J)-
ROOT(K)*REGEN(J-1); END; END; REGEN=A(1)*REGEN;     END DCROOT;
II=1;
S=.01;  PL =100.;  DET=100.; RET : DO KA=1 TO 10;  PL=PL +DET;
DO JA=-5 TO 0;
R=8.496E-5*S+JA*VS/27.E+10;
F1=-W*0.47*S**2;  F2=-(.175E9*S**2;  F3=W*1.5605E8*S**4;
F4=-16.E10*S*R+W*9.E8);
F5=9.E20*((R*S(**2-7.14025E-9*S**4)+W*2.7E14*R*S-2.025E7;
F6=-6.347E-(5*S**2*PL;  F7=)-W*8.607E-8+2.54E-5*S*R(*S**2*PL;
F8=)W*3.442E3*R*S-1.904E6*S**21*S**2*PL;  F9=-W*2.582E(3*S**4*PL;
B(1)=1.;  B(2)=F1+F4;  B(3)=F2+F1*F4+F5+F6;
B(4)=F1*F5+F2*F4+F3+F7;  B(5)=F2*F5+F3*F4+F8;  B(6)=F3*F5+F9;
NA=5;ICHK=0;CALL DCROOT (B,NA,1.E-10,ROOT,ICHK,RG);
PUT FILE (SYSPRINT( EDIT (PL,S,JA,R) (SKIP(3),E(11,4),F(10,2),F(10),F(20,10));
PUT FILE (SYSPRINT( DATA (ROOT);
DO JJ=1 TO 5;  IF (MAG)ROOT(JJ)( < 0. THEN DO;IF II=3 THEN DO;

PUT FILE (SYSPRINT) EDIT (PL) (F(10,4));  GO TO LA;  END;
ELSE DO;   II=II+1;  PL =PL-DET;  DET=0.1*DET;  GO TO RET;  END;  END;
ELSE;END;  END;  END;  LA : END;
```

APPENDIX B

Difference Operators

APPENDIX B

Difference Operators

For the computer solution of the laser-fluid equations described in this study, the differential equations were converted to difference equations. In order to minimize truncation errors, very accurate seven point difference formulae were used to represent the differential operators. These formulae are somewhat troublesome to construct, but a useful procedure is described below. At the end of this appendix, a few of the difference formulae used in the computer analysis are listed.

Definition: The n point interpolation polynomial (abr.NIP) of the function $f(x)$ in terms of the points $x_1, x_2, \ldots, x_n$, is denoted by $\{f(x)\}_n$ and is a polynomial of order (n-1) approximating $f(x)$ in the interval $[x_1, x_n]$. $\{f(x)\}_n$ has the property that

$$\{f(x)\}_n|_{x=x_i} = f(x_i) \quad \text{for } i=1,2, \ldots, n \tag{B1}$$

and is explicitly given by the Lagrange formula

$$\{f(x)\}_n = \sum_{j=0}^{n-1} \frac{\varphi_i(x)}{\varphi_i(x_i)} f(x_i) \tag{B2}$$

where

$$\varphi_i(x) = (x-x_1)(x-x_2) \ldots (x-x_{i-1})(x-x_{i+1}) \ldots (x-x_n) \tag{B3}$$

In other words $\varphi_i(x)$ is the product of all factors of the form $(x-x_k)$ except that the factor $(x-x_i)$ is omitted. For convenience the notations, based on (B1),

$$\{f(x)\}_n|_{x=x_i}=\{f(x_i)\}_n=f(x_i)=f_i \tag{B4}$$

will also be used.

Definition: If $\hat{L}$ is a differential operator and f(x) is a suitably differentiable function of x, the n point difference quotient (abr.NDQ) representation of $\hat{L}$, denoted by $\{\hat{L}\}_{n,x}$, is defined by the following relation:

$$\{\hat{L}\}_{n,y}f(x)=\hat{L}\{f(x)\}_n|_{x=y}=\hat{L}\{f(y)\} \tag{B5}$$

The subscript y on $\{\hat{L}\}_{n,y}$ merely indicates the point at which the expression is to be evaluated. As in the case of the NIP, the list of the n mesh points, x_k, is suppressed in the notation. For convenience the notation

$$\{\hat{L}\}_{n,x_k}=\{\hat{L}\}_{n,k} \qquad \text{where } k=1,2, \ldots ,n \tag{B6}$$

will also be used.

The NDQ's of the operators $(\frac{d}{dx})^m$ have the nice property that

$$\{f(x)\}_n=\sum_{j=0}^{n-1}\frac{(x-y)^j}{j!}\{\frac{d^j}{dx^j}\}_{n,y}f(y) \tag{B7}$$

for any x and y in the interval $[x_1,x_n]$, since the Taylor expansion of any polynomial about any point produces that same polynomial. As special cases of (B7), one has

$$f_i=f(x_i)=\sum_{j=0}^{n-1}\frac{(x_i-y)^j}{j!}\{\frac{d}{dx}\}^j_{n,y}f(y)=\sum_{j=0}^{n-1}\frac{(x_i-x_k)^j}{j!}\{\frac{d}{dx}\}^j_{n,k}f(x) \tag{B8}$$

for any i and k in the set 1,2, ... ,n.

Now, by combining (B2) and (B5) (or by inverting (B8)), one finds

$$\left\{\frac{d}{dx}\right\}^m_{n,x} f(x) = \left(\frac{d}{dx}\right)^m \{f(x)\}_n = \left(\frac{d}{dx}\right)^m \sum_{i=1}^{n} \frac{\varphi_i(x)}{\varphi_i(x_i)} f_i$$

$$= \sum_{i=1}^{n} \sum_{j_1=1}^{n,} \cdots \sum_{j_m=1}^{n,} \frac{\varphi_i(x)}{\varphi_i(x_i)} \cdot \frac{f_i}{(x-x_{j_1})\cdots(x-x_{j_m})} \qquad \text{(B9)}$$

where the prime on $\sum_{j_k=1}^{n,}$ indicates that $j_k \neq i$ and $j_k \neq j_{k'}$, for $k \neq k'$.

Now (B9) can be written in the form

$$\left\{\frac{d}{dx}\right\}_{n,x} f(x) = \sum_{i=1}^{n} A_i(x) f_i \qquad \text{where}$$

$$A_i(x) = \sum_{j_1=1}^{n,} \cdots \sum_{j_m=1}^{n,} \frac{\varphi_i(x)}{\varphi_i(x_i)} \frac{1}{(x-x_{j_1})\cdots(x-x_{j_m})} \qquad \text{(B10)}$$

Thus, if one agrees to use the NDQ as his approximation for a differential operator, then (B10) shows how to express the m^{th} derivative of $f(x)$ at the arbitrary point x in the interval $[x_1, x_n]$ in terms of the values of $f(x)$ at the prescribed mesh points x_i. Actually (B10) is somewhat more general than required for the computer program described in the paper. For the purposes of this program, only the following special case of (B10) is required:

$$\left\{\frac{d}{dx}\right\}^m_{n,k} f_k = \sum_{i=1}^{n} A_{i,k} f_i \qquad \text{where } i,k=1,2,\ldots,n \text{ and}$$

$$A_{i,k} = \sum_{j_1=1}^{n,} \cdots \sum_{j_m=1}^{n,} \frac{\varphi_i(x_k)}{\varphi_i(x_i)} \frac{1}{(x_k-x_{j_1})\cdots(x_k-x_{j_m})} \qquad \text{(B11)}$$

Formula (B10) or (B11) guarantees explicit NDQ representations of any differential operator L and shows a way to compute it. Although a great deal of computation remains, even with formula (B11), at least the work is straightforward. Clearly, the

definitions and procedure shown here are trivially generalized to cases with more than one independent variable.

In the list below, the various difference operators used in the laser-fluid computer program are given. For each independent variable the grid spacings were taken to be uniform with sizes denoted by h or k. The great variety of formulae was used in order to handle the special situations near boundaries.

A. Center Difference Scheme

$$\left\{\frac{\partial}{\partial x}\right\}_{7,4} f_i = \frac{1}{h}\left[\frac{3}{4}(f_{i+1}-f_{i-1}) - \frac{3}{20}(f_{i+2}-f_{i-2}) + \frac{1}{60}(f_{i+3}-f_{i-3})\right] \quad \text{(B12)}$$

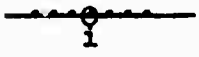

$$\left\{\frac{\partial}{\partial x}\right\}^2_{7,4} f_i = \frac{1}{h^2}\left[\frac{3}{2}(f_{i+1}+f_{i-1}) - \frac{3}{20}(f_{i+2}+f_{i-2}) + \frac{1}{90}(f_{i+3}+f_{i-3}) - \frac{49}{18}f_i\right] \quad \text{(B13)}$$

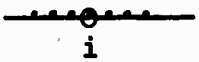

B. Off Center Difference Scheme

1.
$$\left\{\frac{\partial}{\partial x}\right\}_{7,4\pm1} f_i = \pm\frac{1}{h}\left[-\frac{7}{12}f_i + \frac{4}{3}f_{i\pm1} - \frac{2}{5}f_{i\mp1} - \tfrac{1}{2}f_{i\pm2} + \frac{1}{30}f_{i\mp2} + \frac{2}{15}f_{i\pm3} - \frac{1}{60}f_{i\pm4}\right] \quad \text{(B14)}$$

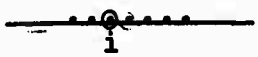

upper signs

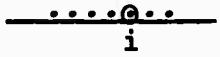

lower signs

$$\left\{\frac{\partial}{\partial x}\right\}_{7,4\mp1} f_i = \frac{1}{h^2}\left[-\frac{21}{10}f_i + \frac{13}{18}f_{i\pm1} + \frac{107}{90}f_{i\mp1} + \frac{17}{36}f_{i\pm2} - \frac{11}{180}f_{i\mp2} - \frac{3}{10}f_{i\pm3} + \frac{4}{45}f_{i\pm4} - \frac{1}{90}f_{i\pm5}\right] \quad \text{(B15)}$$

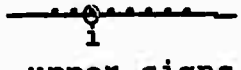

upper signs

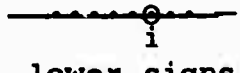

lower signs

2.

$$\left\{\frac{\partial}{\partial x}\right\}_{7,4\mp2} f_i = \pm\frac{1}{h}\left[-\frac{77}{60}f_i + \frac{5}{2}f_{i\pm1} - \frac{1}{6}f_{i\mp1} - \frac{5}{3}f_{i\pm2} + \frac{5}{6}f_{i\pm3} - \frac{1}{4}f_{i\pm4} + \frac{1}{30}f_{i\pm5}\right] \quad \text{(B16)}$$

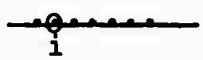

upper signs

lower signs

$$\left\{\frac{\partial}{\partial x}\right\}^2_{7,4\mp2} f_i = \frac{1}{h^2}\left[-\frac{7}{18}f_i - \frac{27}{10}f_{i\pm1} + \frac{7}{10}f_{i\mp1} + \frac{19}{4}f_{i\pm2} - \frac{67}{18}f_{i\pm3} + \frac{9}{5}f_{i\pm4} - \frac{1}{2}f_{i\pm5} + \frac{11}{180}f_{i\pm6}\right] \quad \text{(B17)}$$

upper signs

lower signs

C. Mixed Differentiation (Center)

$$\left\{\frac{\partial^2}{\partial x \partial y}\right\} f_{ij} = \frac{1}{2hk}\left[\frac{3}{2}(f_{i+1,j+1} + f_{i-1,j-1} - f_{i+1,j} - f_{i-1,j} - f_{i,j+1} - f_{i,j-1}) - \frac{3}{20}(f_{i+2,j+2} + f_{i-2,j-2} - f_{i+2,j} - f_{i-2,j} - f_{i,j+2} - f_{i,j-2}) + \frac{1}{90}(f_{i+3,j+3} + f_{i-3,j-3} - f_{i+3,j} - f_{i-3,j} - f_{i,j+3} - f_{i,j-3}) + \frac{49}{18}f_{ij}\right] \quad \text{(B18)}$$

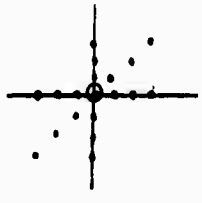

D. Mixed Differentiation (Off Center)

$$\left\{\frac{\partial^2}{\partial x \partial y}\right\} f_{ij} = -\frac{1}{2hk}\left[-\frac{21}{10}f_{ij} + \frac{13}{18}f_{i\pm1,j\mp1} + \frac{107}{90}f_{i\mp1,j\pm1} + \frac{17}{36}f_{i\pm2,j\mp2} - \frac{11}{180}f_{i\mp2,j\pm2} - \frac{3}{10}f_{i\pm3,j\mp3} + \frac{4}{45}f_{i\pm4,j\mp4} - \frac{1}{90}f_{i\pm5,j\mp5} - h^2\left(\frac{\partial}{\partial x}\right)^2 f_{ij} - k^2\left(\frac{\partial}{\partial x}\right)^2 f_{ij}\right] \quad \text{(B19)}$$

$$\left\{\frac{\partial^2}{\partial x \partial y}\right\} f_{ij} = -\frac{1}{2hk}\left[-\frac{7}{18}f_{ij} - \frac{27}{10}f_{i\pm1,j\mp1} + \frac{7}{10}f_{i\mp1,j\pm1} + \frac{19}{4}f_{i\pm2,j\mp2}\right.$$
$$- \frac{67}{18}f_{i\pm3,j\mp3} + \frac{9}{5}f_{i\pm4,j\mp4} - \frac{1}{2}f_{i\pm5,j\mp5} + \frac{11}{180}f_{i\pm6,j\mp6}$$
$$\left.-h^2\left(\frac{\partial}{\partial x}\right)^2 f_{ij} - k^2\left(\frac{\partial}{\partial y}\right)^2 f_{ij}\right] \qquad \text{(B20)}$$

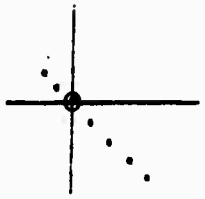

upper signs

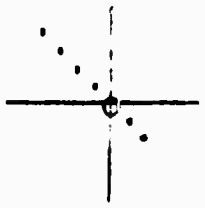

lower signs

(Additional points on the axes are to be selected for the unmixed derivatives)

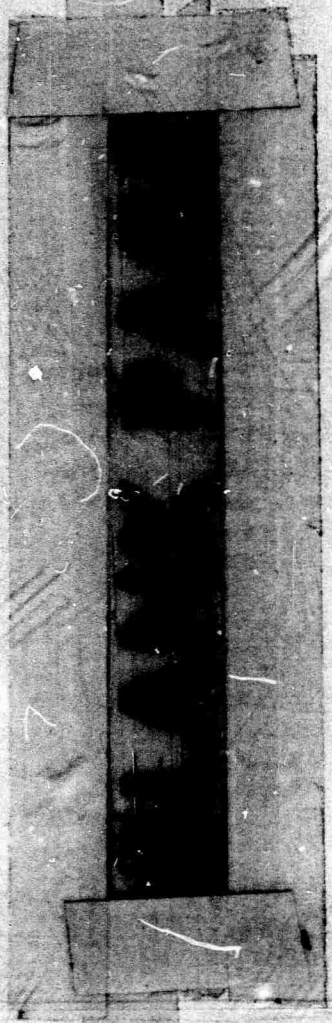

APPENDIX C

APPENDIX C

COMPUTER PROGRAM FOR THE LASER-FLUID EQUATIONS

In this appendix, the computer program for the laser-fluid system used to obtain the results discussed in Section IV is exhibited. Before programming, certain simplifications were made in Equations (174)-(186), based on the fact that α, the linear absorption coefficient, is very small in air at 10.6 μ. For $x \neq 0$, Equations (174)-(179) were reduced to:

$$\frac{\partial \rho}{\partial t} = -\left\{\rho\left[\frac{(1-x)^2}{r_o}\frac{\partial V_r}{\partial x} + \frac{(1-x)}{r_o x} V_r + \frac{\partial V_z}{\partial z}\right] + \frac{(1-x)^2}{r_o} V_r \frac{\partial \rho}{\partial x} + V_z \frac{\partial \rho}{\partial z}\right\} \tag{C1}$$

$$\begin{aligned}\frac{\partial T}{\partial t} = \frac{1}{\rho}\Bigg\{ & \frac{\kappa}{C_v}\left[\frac{(1-x)^4}{r_o^2}\frac{\partial^2 T}{\partial x^2} + \frac{(1-x)^3}{r_o^2}\left(\frac{1-2x}{x}\right)\frac{\partial T}{\partial x} + \frac{\partial^2 T}{\partial z^2}\right] + \\ & + \frac{2\eta+\eta'}{C_v}\left[\frac{(1-x)^4}{r_o^2}\left(\frac{\partial V_r}{\partial x}\right)^2 + \frac{(1-x)^2}{r_o^2 x^2} V_r^2 + \left(\frac{\partial V_z}{\partial z}\right)^2\right] + \\ & + \frac{\eta}{C_v}\left[\frac{2(1-x)^2}{r_o}\frac{\partial V_z}{\partial x}\frac{\partial V_r}{\partial z} + \frac{(1-x)^4}{r_o^2}\left(\frac{\partial V_z}{\partial x}\right)^2 + \left(\frac{\partial V_r}{\partial z}\right)^2\right] + \\ & + \frac{\eta'}{C_v}\left[\frac{(1-x)^3}{r_o^2 x} V_r \frac{\partial V_r}{\partial x} + \frac{1-x}{r_o x} V_r \frac{\partial V_z}{\partial z} + \frac{(1-x)^2}{r_o}\frac{\partial V_r}{\partial x}\frac{\partial V_z}{\partial z}\right] + \\ & + T(\gamma-1)\left[\frac{\partial \rho}{\partial t} + \frac{(1-x)^2}{r_o} V_r \frac{\partial \rho}{\partial x} + V_z \frac{\partial \rho}{\partial z}\right] + \frac{\alpha C}{2C_v}\sqrt{\epsilon}\,(E_1^2 + E_2^2)\Bigg\} \\ & - \left\{\frac{(1-x)^2}{r_o} V_r \frac{\partial T}{\partial x} + V_z \frac{\partial T}{\partial z}\right\}\end{aligned} \tag{C2}$$

$$\frac{\partial V_r}{\partial t} = \frac{1}{\rho}\left\{-\frac{R}{M}T\frac{(1-x)^2}{r_o}\frac{\partial \rho}{\partial x} + (2\eta+\eta')\left[\frac{(1-x)^4}{r_o^2}\frac{\partial^2 V_r}{\partial x^2} + \frac{(1-x)^3}{r_o^2}\cdot\right.\right.$$

$$\left.\left(\frac{1-2x}{x}\right)\frac{\partial V_r}{\partial x} - \frac{(1-x)^2}{r_o^2 x^2}V_r\right] + (\eta+\eta')\frac{(1-x)^2}{r_o}\frac{\partial^2 V_z}{\partial x \partial z} + \eta\frac{\partial^2 V_r}{\partial z^2}\Bigg\} +$$

$$+\frac{(1-x)^2}{r_o}\left\{\frac{1}{2}\left[\varepsilon'\left(E_1\frac{\partial E_1}{\partial x} + E_2\frac{\partial E_2}{\partial x}\right) + \right.\right.$$

$$\left.\left.+\frac{1}{2}\varepsilon''\left(E_1^2 + E_2^2\right)\frac{\partial \rho}{\partial x}\right] - \left(\frac{R}{M}\frac{\partial T}{\partial x} + V_r\frac{\partial V_r}{\partial x}\right)\right\} - V_z\frac{\partial V_r}{\partial z} \qquad \text{(C3)}$$

$$\frac{\partial V_z}{\partial t} = \frac{1}{\rho}\left\{-\frac{R}{M}T\frac{\partial \rho}{\partial z} + (\eta+\eta')\left[\frac{(1-x)^2}{r_o}\frac{\partial^2 V_r}{\partial x \partial z} + \frac{1-x}{r_o x}\frac{\partial V_r}{\partial z} + \frac{\partial^2 V_z}{\partial z^2}\right] + \right.$$

$$\left.+\eta\left[\frac{(1-x)^4}{r_o^2}\frac{\partial^2 V_z}{\partial x^2} + \frac{(1-x)^3}{r_o^2}\left(\frac{1-2x}{x}\right)\frac{\partial V_z}{\partial x} + \frac{\partial^2 V_z}{\partial z^2}\right]\right\}$$

$$-\left\{\frac{R}{M}\frac{\partial T}{\partial z} + \frac{(1-x)^2}{r_o}V_r\frac{\partial V_z}{\partial x} + V_z\frac{\partial V_z}{\partial z}\right\} +$$

$$+\frac{1}{2}\left[\varepsilon'\left(E_1\frac{\partial E_1}{\partial z} + E_2\frac{\partial E_2}{\partial z}\right) + \frac{1}{2}\varepsilon''\left(E_1^2 + E_2^2\right)\frac{\partial \rho}{\partial z}\right] \qquad \text{(C4)}$$

$$\frac{\partial E_1}{\partial t} = \frac{1}{\varepsilon}\left\{\frac{c^2}{2\omega_L}\left[\frac{(1-x)^4}{r_o^2}\frac{\partial^2 E_2}{\partial x^2} + \frac{(1-x)^3}{r_o^2}\frac{(1-2x)}{x}\frac{\partial E_2}{\partial x} + \frac{\partial^2 E_2}{\partial z^2} - 2K_L\frac{\partial E_1}{\partial z}\right]\right.$$

$$\left.-\left[\frac{1}{2\omega_L}\varepsilon''\left(\frac{\partial \rho}{\partial t}\right)^2 + \frac{\omega_L}{2}\left(\varepsilon_o - \varepsilon\right)\right]E_2 - \varepsilon'\frac{\partial \rho}{\partial t}E_1\right\} \qquad \text{(C5)}$$

$$\frac{\partial E_2}{\partial t} = \frac{1}{\varepsilon}\left\{-\frac{c^2}{2\omega_L}\left[\frac{(1-x)^4}{r_o^2}\frac{\partial^2 E_1}{\partial x^2} + \frac{(1-x)^3}{r_o^2}\left(\frac{1-2x}{x}\right)\frac{\partial E_1}{\partial x} + \frac{\partial^2 E_1}{\partial z^2} + 2K_L\frac{\partial E_2}{\partial z}\right] + \right.$$

$$\left. + \left[\frac{1}{2\omega_L}\varepsilon''\left(\frac{\partial \rho}{\partial t}\right)^2 + \frac{\omega_L}{2}(\varepsilon_o - \varepsilon)\right]E_1 - \varepsilon'\frac{\partial \rho}{\partial t}E_2\right\} \qquad (C6)$$

For x = 0, equations (181) - (186) become:

$$\frac{\partial \rho}{\partial t} = -\left[\rho\left(\frac{2}{r_o}\frac{\partial V_r}{\partial x} + \frac{\partial V_z}{\partial z}\right) + V_z\frac{\partial \rho}{\partial z}\right] \qquad (C7)$$

$$\frac{\partial T}{\partial t} = \frac{1}{\rho}\left\{\frac{\kappa}{C_v}\left(\frac{2}{r_o^2}\frac{\partial^2 T}{\partial x^2} + \frac{\partial^2 T}{\partial z^2}\right) + \frac{2\eta+\eta'}{C_v}\left[\frac{2}{r_o^2}\left(\frac{\partial V_r}{\partial x}\right)^2 + \left(\frac{\partial V_z}{\partial z}\right)^2\right] + \right.$$

$$+ \frac{2\eta'}{C_v}\left[\left(\frac{\partial V_r}{\partial x}\right)^2\frac{1}{r_o^2} + \frac{2}{r_o^2}\frac{\partial V_r}{\partial x}\frac{\partial V_z}{\partial z}\right] + T(\gamma-1)\left[\frac{\partial \rho}{\partial t} + V_z\frac{\partial \rho}{\partial z}\right] +$$

$$\left. + \frac{\alpha c}{2C_v}\sqrt{\varepsilon}\,(E_1^2 + E_2^2)\right\} - V_z\frac{\partial T}{\partial z} \qquad (C8)$$

$$\frac{\partial V_r}{\partial t} = 0 \qquad (C9)$$

$$\frac{\partial V_z}{\partial t} = \frac{1}{\rho}\left\{-\frac{R}{M}T\frac{\partial \rho}{\partial z} + (2\eta+\eta')\frac{\partial^2 V_z}{\partial z^2} + \eta\left(\frac{2}{r_o^2}\frac{\partial^2 V_z}{\partial x^2}\right)\right\} - \left\{\frac{R}{M}\frac{\partial T}{\partial z} + V_z\frac{\partial V_z}{\partial z}\right\} +$$

$$+ \frac{1}{2}\left[\varepsilon'\left(E_1\frac{\partial E_1}{\partial z} + E_2\frac{\partial E_2}{\partial z}\right) + \frac{\varepsilon''}{2}(E_1^2 + E_2^2)\frac{\partial \rho}{\partial z}\right] \qquad (C10)$$

$$\frac{\partial E_1}{\partial t} = \frac{1}{\varepsilon}\left\{\frac{c^2}{\omega_L}\left(\frac{1}{r_o^2}\frac{\partial^2 E_2}{\partial x^2} + \frac{1}{2}\frac{\partial^2 E_2}{\partial z^2} - K_L\frac{\partial E_1}{\partial z}\right)\right.$$

$$\left. - \left[\frac{1}{2\omega_L}\varepsilon''\left(\frac{\partial \rho}{\partial t}\right)^2 + \frac{\omega_L}{2}(\varepsilon_o - \varepsilon)\right]E_2 - \varepsilon'\frac{\partial \rho}{\partial t}E_1\right\} \qquad (C11)$$

$$\frac{\partial E_2}{\partial t} = \frac{1}{\varepsilon}\left\{\frac{-c^2}{\omega_L}\left(\frac{1}{r_o^2}\frac{\partial^2 E_1}{\partial x^2} + \frac{1}{2}\frac{\partial^2 E_1}{\partial z^2} + K_L\frac{\partial E_2}{\partial z}\right) + \right.$$

$$\left. + \left[\frac{1}{2\omega_L}\varepsilon''\left(\frac{\partial \rho}{\partial t}\right)^2 + \frac{\omega_L}{2}(\varepsilon_o - \varepsilon)\right] E_1 - \varepsilon'\frac{\partial \rho}{\partial t} E_2\right\} \qquad (C12)$$

In this computation the following notations have been introduced into the computer program:

N : The number of steps in x (or r) to be remembered.

NN : Total number of steps in x.

M : The number of steps in .

MT : The number of steps in time.

DX :	Δx	EZ :	E_o	WP :	$3(\varepsilon_o - 1)$
DY :	Δz	KL :	K_L	WQ :	c^2/ω_L
DIT :	Δt	KM :	$2K_L$	WR :	$c^2/2\omega_L$
V1 :	x	WA :	$2\eta+\eta'$	WS :	$1/2\omega_L$
V2 :	$(1-x)/r_o$	WB :	$\eta+\eta'$	WT :	$R\rho/M$
V3 :	$(1-x)^2/r_o$	WC :	η	WU :	κ/C_v
V4 :	$(1-x)^3/r_o^2$	WD :	η'	WV :	2
V5 :	$(1-x)^4/r_o^2$	WE :	$T(\gamma-1)$	WW :	$(2\eta+\eta')/C_v$
V6 :	$1/x$	SF :	$-RT/M$	WX :	$\alpha c/2C_v$
V7 :	$1/x^2$	WG :	$1/r_o^2$	WY :	1/2
V8 :	$(1-x)/r_o x$	SH :	$2/r_o^2$	WZ :	$1/r_o$
V9 :	$(1-x)^3(1-2x)/r_o^2 x$	WI :	ρ_o	VA :	$2/r_o$
V10 :	$(1-x)^2/r_o^2 x^2$	WJ :	ε_o	VH :	η/C_v
DU :	$1/\Delta x$	WK :	$\varepsilon_o - 1$	VI :	$2\eta'/C_v$
DV	$1/(\Delta x)^2$	WL :	$\omega_L/2$	VN :	1

DW : $1/\Delta z$ WM : $(\varepsilon_0+2)\rho_0$ VO : 273

DZ : $1/(\Delta z)^2$ WN : $3(\varepsilon_0+2)(\varepsilon_0-1)$ VP : 3

DT : $1/2(\Delta x)(\Delta z)$ WO : $2\eta/r_0^2$ VE : $(\gamma-1)$

H1 : $1/[(\varepsilon_0+2)\rho_0-(\varepsilon_0-1)\rho]$ H2 : (ε_0-1) H1

H3 : ε H4 : $\frac{d\varepsilon}{d\rho}$ H5 : $\frac{\partial^2\varepsilon}{d\rho^2}$

H6 : $1/\rho$ H7 : $1/\varepsilon$

H8 : $\sqrt{\varepsilon}$ H9 : $(\varepsilon_0-\varepsilon)$

X(1,K,L): E_1 X(2,K,L): E_2 X(3,K,L): ρ

X(4,K,L): T X(5,K,L): V_r X(6,K,L): V_z

FXA,FXB,FXC: $\frac{\partial}{\partial x}$ SXA,SXB,SXC: $\frac{\partial^2}{\partial x^2}$ SZA,SZB,SZC: $\frac{\partial^2}{\partial z^2}$

FZA,FZB,FZC: $\frac{\partial}{\partial z}$ MDA,MDB,MDC: $\frac{\partial^2}{\partial x \partial z}$

Following is the computer program for this study.

```
(NOUNDERFLOW): OPTJKS: PROCEDURE OPTIONS (MAIN);
NN=23;  M=81;  MT=100;  N=16;  MTT=100;  ZNN=NN;  ZN=N;  ZMT=MT;
DCL (LY,S1(7),S2(7),S3(7),S4(7),S5(7),S6(7)) LABEL;
DCL (EZ,DN,     VE,VF,  CHG, ZIJ,ZZ,
     DX,DU,DV,DY,DW,DZ,DT,D1T,DA,DB,DC,DD,DE,DF,DG,DH,DI,DJ,DL,DM,DN,DO,DP,DQ,
DR,DP,W8,W9,W10,W11,W12,W13,W14,PWT,G1(121),
XR,DS,DT,DU,DV,DW,DX,DY,DZ,PA,PM,PC,PD,PE,PF,PG,PH,PN,
WA,WB,WC,WD,WE,WF,WG,WH,WI,WJ,WK,WL,WM,WN,WO,WP,WQ,WR,
WS,WT,WU,WV,WW,WX,WY,WZ,W1,W2,W3,W4,W5,W6,W7,VA,HA,HB,HD,HE,HF,HH,HS,H1,H2,H3,
H4,H5,H7,H8,H9,VA,VI,VH,VO,VP,V1,V2,V3,V4,V5,V6,V7,V8,V9,V10,F12,
KL,KM,X1,X2,X3,X4,X5,X6,X7,X8,X9,X10,F2,F3,F4,F5,F6,F7,F8,F9,F10,F11,A(6),B(6),
C(6),D(6),E(6),F(6),X(6,16,121),Y(6,16,121)) BINARY FLOAT (53);
DCL (FXC,SXC,FXA,SXA,FXB,SXB,MDC,MDA,MDB,FF,FF1) RETURNS (BINARY FLOAT (53));
EP=1.E3;  IJ=100; ZIJ=IJ;  CHG=1.;  IC=1;
NA=N-1;  NB=N-2;  NC=N-3;  ND=N-4;  NE=N-5;  NF=N-6;  N7=N-7; NNA=NN-1;
MA=M-1;  MB=M-2;  MC=M-3;  MD=M-4;  ME=M-5;  MF=M-6;  MG=M-7;  ZMA=MA;
DU=NNA;  DX=1./DU;   DV=DU*DU;  DY=3.6E6/ZMA;  DW=ZMA/3.6E6;  DZ=DW*DW;
DT=.5*DU*DW;  D1T=1.E-5/ZMT;  DP=1./18.;  KL=SQRT(1.+5.65E-4)*5.91E3; KM=2.*KL;
DA=.75;  DB=-.15;  DC=1./60.;  DD=1.5;  DE=1./90.;  DF=-49./18.; DG=-2.1;
DH=13./18.;  DI=107./90.;  DJ=17./36.;  DK=-1.1*DP;    DL=-.3;  DM=4./45.;
DN=-DE;  DO=-7./18.;  DP=-2.7;  DQ=.7;  XR=4.75;  DS=-67./18.;  DU=-.5;
DV=-DK;  DW=1.5*DU;          DT=1.8;  DX=4./3.;  DY=-.4;  DZ=2.*DC;
PA=1.5*DM;                PC=-77./60.;  PD=2.5;  PE=-1./6.;  PF=-5./3.;
PG=-5.*PE; PH=-.25;  PM=-DX*DX;  PN=-DY*DY;
                  WA=3.55E-4;  WB=1.775E-4;  WC=WB;  WV=2.;
VP=3.;  WD=0.;  VE=.4 ;          WI=1.25E-3;  WJ=1.+5.65E-4;  WK=5.65E-4;
            WZ=5.E-3;  WG=WZ*WZ;  WN=2.*WG;  WL=.0865E14; VF=-8.3144E7/29.012;
WM=(WJ+WV)*WI;  WN=VP*WM*WK;  WO=WC*WM;  WP=1.695E-3;  WQ=9.E6/1.773;
WR=.5*WQ;  WS=.5/1.773E14;  WT=-VF;          WU=.186*W);
WW=WA/7.143E6;  WX=9.E-3/1.428E6;  WY=.5;  VA=2.*WZ;
VH=WC/7.143E6; VI=0.;  VN=1.;  VO=283.;
W1=-DV*134.89/18.;  W2=DV*12.;  W3=-DV*7.5;  W4=DV*40./9.;  W5=-DV*1.875;
W6=DV*.48;  W7=-DV*DP;
W8=DU/(441.+180.*DX);  W9=1080.*W8;  W10=-675.*W8;  W11=400.*W8;
W12=-168.75*W8;  W13=43.2*W8;  W14=-5.*W8;  W8=-674.45*W8;              RT:
EZ=(2.E2/(1.+2.82E-4))**.5/3*EP;
DO K=1 TO N;  DO L=1 TO M;  ZK=K;  ZL=L;  DN=(ZK-VN)/DU;
X(1,K,L)=EZ*EXP(-(WV*DN/(1.-DN))**2-(.10*ZL-3.0)**2);
X(2,K,L)=0.;  X(3,K,L)=W);  X(4,K,L)=VO;  X(5,K,L)=0.;  X(6,K,L)=0.;
END;  END;
DO L=M TO 1 BY -1; PUT FILE (SYSPRINT) EDIT (L,(K,X(I,K,L) DO K=1 TO NA))
(SKIP(2),X(4),F(3),4(SK)P,5(X(5),F(2),X(2),E(14,7))));  END;
FXC:  PROC (X1,X2,X3,X4,X5,X6)  BINARY FLOAT (53);
DCL (X1,X2,X3,X4,X5,X6) BINARY FLOAT (53);
F2=DA*(X1-X2)+DB*(X3-X4)+DC*(X5-X6);  RETURN (F2);  END FXC;
SXC:  PROC (X1,X2,X3,X4,X5,X6,X7) BINARY FLOAT (53);
DCL (X1,X2,X3,X4,X5,X6,X7) BINARY FLOAT (53);
F3=DD*(X2+X3)+DB*(X4+X5)+DE*(X6+X7)+DF*X1;  RETURN (F3);  END SXC;
FXA: PROC (X1,X2,X3,X4,X5,X6,X7) BINARY FLOAT (53); DCL (X1,X2,X3,X4,X5,X6,X7)
BINARY FLOAT (53); F4=PC*X1+PD*X2+PE*X3+PF*X4+PG*X5+PH*X6+DZ*X7; RETURN (F4);
END FXA;
SXA: PROC (X1,X2,X3,X4,X5,X6,X7,X8) BINARY FLOAT (53); DCL (X1,X2,X3,X4,X5,X6,
```

```
X7,X8) BINARY FLOAT (53); F5=DO*X1+DP*X2+DQ*X3+XR*X4+DS*X5+DT*X6+DU*X7+DV*X8)
RETURN (F5); END SXA;
FXB: PROC (X1,X2,X3,X4,X5,X6,X7) BINARY FLOAT (53); DCL (X1,X2,X3,X4,X5,X6,X7)
BINARY FLOAT (53)) F6=DW*X1+DX*X2+DY*X3+DU*X4+DZ*X5+PA*X6-DC*X7; RETURN (F6))
END FXB;
SXB: PROC (X1,X2,X3,X4,X5,X6,X7,X8) BINARY FLOAT (53); DCL (X1,X2,X3,X4,X5,X6,
X7,X8) BINARY FLOAT (53); F7=DG*X1+DH*X2+DI*X3+DJ*X4+DK*X5+DL*X6+DM*X7+DN*X8;
RETURN (F7); END SXB;
MDC: PROC (X1,X2,X3,X4,X5,X6,X7,X8,X9) BINARY FLOAT (53);
DCL (X1,X2,X3,X4,X5,X6,X7,X8,X9) BINARY FLOAT (53);
F8=DF*X1+DD*)X2+X3)+DB*(X4+X5)+DE*(X6+X7)+PM*X8+PN*X9;  RETURN (F8); END MDC;
MDA: PROC (X1,X2,X3,X4,X5,X6,X7,X8,X9,X10) BINARY FLOAT (53); DCL (X1,X2,X3,X4,
X5,X6,X7,X8,X9,X10) BINARY FLOAT (53); F9=DO*X1+DP*X2+DQ*X3+XR*X4+DS*X5+DT*X6+
DU*X7+DV*X8+PM*X9+PN*X10; RETURN (F9); END MDA;
MDB: PROC (X1,X2,X3,X4,X5,X6,X7,X8,X9,X10) BINARY FLOAT )53); DCL (X1,X2,X3,X4,
X5,X6,X7,X8,X9,X10) BINARY FLOAT (53); F10=DG*X1+DH*X2+DI*X3+DJ*X4+DK*X5+DL*X6+
DM*X7+DN*X8+PM*X9+PN*X10; RETURN (F10)) END MDB;
FF: PROC (X1,X2,X3,X4,X5,X6,X7) BINARY FLOAT (53);
DCL (X1,X2,X3,X4,X5,X6,X7) BINARY FLOAT (53);
F11=W1*X1+W2*X2+W3*X3+W4*X4+W5*X5+W6*X6+W7*X7)  RETURN (F11);  END FF;
FF1: PROC (X1,X2,X3,X4,X5,X6,X7) BINARY FLOAT (53);
DCL (X1,X2,X3,X4,X5,X6,X7) BINARY FLOAT (53);
F12=W8*X1+W9*X2+W10*X3+W11*X4+W12*X5+W13*X6+W14*X7;RETURN (F12);  END FF1;
DO ID=1 TO MTT;IF ID > 1 THEN DO)
IF ID>IJ THEN DO;DIT=5.E-8;  ZZ=3.E3*(ZIJ-1.)*DW;ZT=ID-1J+1;  CHG=0.5;  END;
ELSE DO;  ZZ=0.;  ZT=ID;  END;
                                        DO K=1 TO N;  ZK=K;  DN=)ZK-VN)/DU;
DO L=1,M;  ZL=L;
X(1,K,L)=EZ*EXP(-(WV*DN/(1.-DN))**2-(.10*(ZL-30.-ZZ-3.E3*(ZT-1.)*CHG*DW))**2))
END;  END;
DO L=2 TO MA;  ZL=L;  DN=(ZN-VN)/DU;
X(1,N,L)=E7*EXP(-)WV*DN/(1.-DN))**2-(.10*(ZL-30.-ZZ-3.E3*(ZT-1.)*CHG*DW))**2))
END;  END;  ELSE)
DO L=2 TO M-1;  DO K=1 TO N-1;  ZK=K;        DO J=1 TO 6; A(J)=X(J,K,L); END;
H7=WP*A(3);  H1=VN/)WM-WK*A(3));  H2=WK*H1;  H3=VN+H7*H1;  H4=WN*H1*H1;
H5=WV*H4*H2;  H7=VN-H7/)WM+1.130E-3*A(3));
H8=H3**0.5;  H9=WK*(3.+WK)*)W1-A(3))*H1;
IF K > 3 THEN DO;
V1=(ZK-VN)/DU;  V2=)VN-V1)*WZ;  V3=V2*(VN-V1);  V4=V3*V2;  V5=V3*V3;
V6=DU/)ZK-VN);  V7=V6*V6;V8=WZ*(ZNN-ZK)/(ZK-VN); V9=V4*(V6-WV);  V10=V8*V8;
                                        )F K < NC THEN DO; KA=K+1; KB=K-1) KC=K+2;
KD=K-2;KE=K+3; KF=K-3; DO J=1 TO 6;
D(J)=FXC)X(J,KA,L),X(J,KB,L),X(J,KC,L),X)J,KD,L),X(J,KE,L),X(J,KF,L))*DU;
C(J)=SXC)A(J),X(J,KA,L),X(J,KB,L),X(J,KC,L),X(J,KD,L),X(J,KE,L),X(J,KF,L))*DV;
                                        END; )F K >  7 THEN LX=7) ELSE LX=6; END;
ELSE DO; )F K=NA THEN DO;)LX=5; DO J=1 TO 6; B(J)=-FXA)A(J),X)J,ND,L),X(J,N,L),
X(J,NC,L),X)J,ND,L),X)J,N5,L),X)J,NF,L))*DU;  C)J)=SXA)A(J),X)J,NB,L),X(J,N,L),
X(J,NC,L),X(J,ND,L),X)J,N5,L),X)J,NF,L),X(J,N7,L))*DV; END; END;  ELSE DO;
LX=4; DO J=1 TO 6; B)J)=-FXB)A)J),X)J,NC,L),X(J,NA,L),X(J,ND,L),X)J,N,L),
X(J,N5,L), X(J,NF,L))*DU;  C)J)=SXB)A)J),X(J,NC,L),X(J,NA,L),X(J,ND,L),X(J,N,L)
```

```
,          X(J,N5,L),X(J,NF,L),X(J,N7,L))*DV; END; END; END; END;  ELSE DO;
IF K=1 THEN DO; LX=L;DO J=1 TO 4,6;B(J)=0.; C(J)=FF(A(J),X(J,2,L),X(J,3,L),
X(J,4,L),X(J,5,L),X(J,6,L),X(J,7,L));END;
B(5)=FF1(A(5),X(5,2,L),          X(5,3,L),X(5,4,L),X(5,5,L),X(5,6,L),X(5,7,L));
C(5)=2.*B(5);  END;  ELSE DO;
V1=(ZK-VN)/DU;  V2=(VN-V)*WZ;  V3=V2*(VN-V1);  V4=V3*V2;  V5=V3*V3;
V6=DU/(ZK-VN);  V7=V6*V6;V8=WZ*(ZNN-ZK)/(ZK-VN); V9=V4*(V6-NV);  V10=V8*V8;
IF K=2 THEN DO; LX=2; DO J=1 TO 6;B(J)=FXA(A(J),X(J,3,L),X(J,1,L),X(J,4,L),
X(J,5,L),X(J,6,L),X(J,7,L))*DU;   C(J)=SXA(A(J),X(J,3,L),X(J,1,L),X(J,4,L),
X(J,5,L),X(J,6,L),X(J,7,L),X(J,8,L))*DV; END; END;  ELSE DO; LX=3;
DO J=1 TO 6; B(J)=FXB(A(J),X(J,4,L),X(J,2,L),X(J,5,L),X(J,1,L),X(J,6,L),
X(J,7,L))*DU;   C(J)=SXB(A(J),X(J,4,L),X(J,2,L),X(J,5,L),X(J,1,L),X(J,6,L),
X(J,7,L),X(J,8,L))*DV; END; END; END;
                                                IF L > 3 THEN DO; IF L <= MC THEN
DO; LA=L+1; LB=L-1; LC=L+2; LD=L-2; L5=L+3; LF=L-3;   DO J=1 TO 6;
D(J)=FXC(X(J,K,LA),X(J,K,LB),X(J,K,LC),X(J,K,LD),X(J,K,L5),X(J,K,LF))*DW;
   E(J)=
SXC(A(J),X(J,K,LA),X(J,K,LB),X(J,K,LC),X(J,K,LD),X(J,K,L5),X(J,K,LF))*DZ; END;
IF L >  7 THEN DO;
                    GO TO S1(LX); S1(1): LY=SA; GO TO SR; S1(2): LY=SS4; GO TO
SR;  S1(3): LY=SS5; GO TO SR;  S1(4): LY=SS7; GO TO SR; S1(5): LY=SS6;GO TO SR;
S1(6): LY=SS1; GO TO SR; S1(7): LY=SS1; SR: END; ELSE DO; GO TO S2(LX);
S2(1): LY=SA; GO TO SQ;  S2(2): LY=SS2; GO TO SQ;  S2(3): LY=SS3; GO TO SQ;
S2(4): LY=SS9; GO TO SQ;  S2(5): LY=SS8; GO TO SQ;  S2(6): LY=SS1; GO TO SQ;
S2(7): LY=SS1;  SQ: END; END; ELSE DO;  IF L=MA THEN DO;          DO J=1 TO 6;
D(J)=-FXA(A(J),X(J,K,MB),X(J,K,M),X(J,K,MC),X(J,K,MD),X(J,K,ME),X(J,K,MF))*DW;
 E(J)=SXA(A(J),X(J,K,MB),X(J,K,M),X(J,K,MC),X(J,K,MD),X(J,K,ME),X(J,K,MF),
X(J,K,MG))*DZ;
END; GO TO S3(LX);  S3(1): LY=SA; GO TO SO; S3(2): LY=SS4; GO TO SO; S3(3):
LY=SS4; GO TO SO; S3(4): LY=SS6; GO TO SO; S3(5): LY=SS6; GO TO SO; S3(6):
LY=SS4; GO TO SO; S3(7): LY=SS6;  SO: END; ELSE DO; DO J=1 TO 6;
D(J)=-FXB(A(J),X(J,K,MC), X(J,K,MA),X(J,K,MD),X(J,K,M),X(J,K,ME),X(J,K,MF))*DW;
 E(J)=SXB(A(J),X(J,K,MC), X(J,K,MA),X(J,K,MD),X(J,K,M),X(J,K,ME),X(J,K,MF),
X(J,K,MG))*DZ; END; GO TO S4(LX);  S4(1): LY=SA; GO TO SM; S4(2): LY=SS4;
GO TO SM;S4(3): LY=SS5; GO TO SM; S4(4): LY=SS7; GO TO SM;S4(5): LY=SS6; GO
TO SM; S4(6): LY=SS5; GO TO SM; S4(7): LY=SS7; SM: END; END; END;  ELSE DO;
IF L=2 THEN DO; DO J=1 TO 6;
D(J)=FXA(A(J),X(J,K,3),X(J,K,1),X(J,K,4),X(J,K,5),X(J,K,6),X(J,K,7))*DW;
E(J)=SXA(A(J),X(J,K,3),X(J,K,1),X(J,K,4),X(J,K,5),X(J,K,6),X(J,K,7),X(J,K,8))*D
Z ; END; GO TO S5(LX); S5(1): LY=SA; GO TO SK; S5(2): LY=SS2; GO TO SK; S5(3):
LY=SS2; GO TO SK; S5(4): LY=SS8; GO TO SK; S5(5): LY=SS8; GO TO SK; S5(6):
LY=SS2; GO TO SK; S5(7): LY=SS8; SK: END; ELSE DO; DO J=1 TO 6;
D(J)=FXB(A(J),X(J,K,4),X(J,K,2),X(J,K,5),X(J,K,1),X(J,K,6),X(J,K,7))*DW;
E(J)=SXB(A(J),X(J,K,4),X(J,K,2),X(J,K,5),X(J,K,1),X(J,K,6),X(J,K,7),X(J,K,8))*D
Z ; END; GO TO S6(LX);
S6(1):  LY=SA; GO TO S1; S6(2):  LY=SS2; GO TO S1;  S6(3):  LY=SS3;  GO TO S1;
S6(4): LY=SS9;  GO TO S1;  S6(5): LY=SS8;  GO TO S1;  S6(6): LY=SS3;  GO TO S1;
S6(7): LY=SS9;  S1:  END;  END;  GO TO LY;SS1: DO J=5 TO 6;
F(J)=MUC(A(J),X(J,KA,LA),X(J,KB,LB),X(J,KC,LC),X(J,KD,LD),X(J,KE,L5),X(J,KF,LF)
,C(J),E(J))*DT; END;  GO TO SB;  SS2:  DO J=5 TO 6;
```

```
F(J)=MDA(A(J),X(J,K+1,L+1),X(J,K-1,L-1),X(J,K+2,L+2),X(J,K+3,L+3),X(J,K+4,L+4),
X(J,K+5,L+5),X(J,K+6,L+6),C(J),E(J))*DT;  END;  GO TO SB;  SS3: DO J=5 TO 6;
F(J)=MDB(A(J),X(J,K+1,L+1),X(J,K-1,L-1),X(J,K+2,L+2),X(J,K-2,L-2),X(J,K+3,L+3),
X(J,K+4,L+4),X(J,K+5,L+5),C(J),E(J))*DT; END; GO TO SB; SS4: DO J=5 TO 6;
F(J)=-MDA(A(J),X(J,K+1,L-1),X(J,K-1,L+1),X(J,K+2,L-2),X(J,K+3,L-3),X(J,K+4,L-4)
,
X(J,K+5,L-5),X(J,K+6,L-6),C(J),E(J))*DT; END; GO TO SB; SS5: DO J=5 TO 6;
F(J)=-MDB(A(J),X(J,K+1,L-1),X(J,K-1,L+1),X(J,K+2,L-2),X(J,K-2,L+2),X(J,K+3,L-3)
,
X(J,K+4,L-4),X(J,K+5,L-5),C(J),E(J))*DT; END; GO TO SB; SS6: DO J=5 TO 6;
F(J)=MDA(A(J),X(J,K-1,L-1),X(J,K+1,L+1),X(J,K-2,L-2),X(J,K-3,L-3),X(J,K-4,L-4),
X(J,K-5,L-5),X(J,K-6,L-6),C(J),E(J))*DT; END; GO TO SB; SS7: DO J=5 TO 6;
F(J)=MDB(A(J),X(J,K-1,L-1),X(J,K+1,L+1),X(J,K-2,L-2),X(J,K+2,L+2),X(J,K-3,L-3),
X(J,K-4,L-4),X(J,K-5,L-5),C(J),E(J))*DT; END; GO TO SB; SS8: DO J=5 TO 6;
F(J)=-MDA(A(J),X(J,K-1,L+1),X(J,K+1,L-1),X(J,K-2,L+2),X(J,K-3,L+3),X(J,K-4,L+4)
,
X(J,K-5,L+5),X(J,K-6,L+6),C(J),E(J))*DT; END; GO TO SB; SS9: DO J=5 TO 6;
F(J)=-MDB(A(J),X(J,K-1,L+1),X(J,K+1,L-1),X(J,K-2,L+2),X(J,K+2,L-2),X(J,K+3,L+3)
,
X(J,K-4,L+4),X(J,K-5,L+5),C(J),E(J))*DT; END; GO TO SB;
SA: HA=A(6)*D(3); HB=A(1)*A(1)+A(2)*A(2); Y(3,K,L)=-(HA+A(3)*(D(6)+VA*B(5)));
HD=H5*Y(3,K,L)*Y(3,K,L); HF=H4*Y(3,K,L); HH=WS*HD+WL*H9;
WE=VE*A(4);  WF=VF*A(4);
Y(4,K,L)=(WU*(WH*C(4)+E(4))+HW*(D(6)*D(6)+WH*B(5)*B(5))+V1*(WG*D(5)*B(5)
+WH*B(5)*D(6))+WE*(Y(3,K,L)                                    *HA)+WX*H8*HB)/A(3)
-A(6)*D(4);  Y(5,K,L)=0.;
Y(6,K,L)=(WF*D(3)+WA*E(6)+WO*C(6))/A(3)-(WT*D(4)+A(6)*D(6))+WY*(H4*(A(1)*D(1)
+A(2)*D(2))+HY*H5*HB*D(3));
Y(1,K,L)=H7*(WQ*(WG*C(2)+WY*E(2)-KL*D(1))-HH*A(2)-HF*A(1));
Y(2,K,L)=H7*(-WQ*(WG*C(1)+WY*E(1)+KL*D(2))+HH*A(1)-HF*A(2));GO TO SC;
SB: HS=V3*A(5); HA=HS*B(3)+A(6)*D(3); HB=A(1)*A(1)+A(2)*A(2); HE=WY*HB*H5;
Y(3,K,L)=-(A(3)*(V3*B(5)+V8*A(5)+D(6))+HA); HF=H4*Y(3,K,L);
HD=H5*Y(3,K,L)*Y(3,K,L);  HH=WS*HD+WL*H9;
WE=VE*A(4);  WF=VF*A(4);
Y(4,K,L)=(WU*(V5*C(6)+V9*B(4)+E(4))+WW*(V5*B(5)*B(5)+V10*A(5)*A(5)+D(6)*D(6))
+VH*(WV*V3*B(6)*D(5)+V5*B(6)*B(6)+D(5)*D(5))+V1*(V8*(HS*B(5)+A(5)*D(6))
+V3*B(5)*D(6))+WE*(Y(3,K,L)+HA)+WX*H8*HB)/A(3)-(HS*B(4)+A(6)*D(4));
Y(5,K,L)=(WC*E(5)+V9*(WB*F(6)+WF*B(3))+WA*(V5*C(5)+V9*B(5)-V10*A(5))/A(3)
+V3*(WY*(H4*(A(1)*B(1)+A(2)*B(2))+HE*B(3))-(WT*B(4)+A(5)*B(5)))-A(6)*D(5);
Y(6,K,L)=(WF*D(3)+WB*(V3*F(5)+VB*D(5)+F(6))+WC*(V5*C(6)+V9*B(6)+E(6)))/A(3)
-(WT*D(4)+HS*B(6)+A(6)*D(6))+WY*(H4*(A(1)*D(1)+A(2)*D(2))+HE*D(3));
Y(1,K,L)
      =H7*(WR*(V5*C(2)+V9*B(2)+F(2)-KM*D(1))-HH*A(2)-HF*A(1));
Y(2,K,L)=H7*(-WR*(V5*C(1)+V9*B(1)+E(1)+KM*D(2))+HH*A(1)-HF*A(2));
SC: END; END; DO L=2 TO M-1; DO K=1 TO N-1; DO J=1 TO 6;
X(J,K,L)=X(J,K,L)+Y(J,K,L)*DIT; END; END; END;
     IF ID=20 THEN GO TO LS; ELSE
     IF ID=40 THEN GO TO LS; ELSE
     IF ID=60 THEN GO TO LS; ELSE
     IF ID=80 THEN GO TO LS; ELSE
```

```
     IF ID=MTT THEN GO TO LS;  ELSE GO TO RR;
LS:  DO L=M TO 1 BY -1;  DO K=1 TO NA;  YI3,K,L)=X(3,K,L)-WI;  YI4,K,L)=
XI4,K,L)-VO;  DO J=1,2,5,6;  YIJ,K,L)=X(J,K,L);  END;  END;  END;
DO J=1 TO 6;
PUT FILE (SYSPRINT) PAGE;DO L=M TO 1 BY -1;  PUT FILE (SYSPRINT)                E
DIT (ID,J,L,(K,YIJ,K,L) DO K=1 TO NA)) (SKIP(2),3(X(4),F(3)),4(SKIP,5(X(5),F(2)
,X(2),E(14,7))));  END;  END;
PUT FILE (SYSPRINT) PAGE;
G1=0.;  DO L=M TO 1 BY -1;  DO K=1 TO N;  ZK=K;  VI=(ZK-1.)*DX;
V1=V1/(VN-V1)**3;
Y(1,K,L)=X(1,K,L)*X(1,K,L)+X(2,K,L)*X(2,K,L);  YI2,K,L)=V1*YI1,K,L);  END;
DO K=1 TO N-2 BY 2;
G1(L)=G1(L)+YI2,K,L)+4.*YI2,K+1,L)+Y(2,K+2,L);  END;
G1(L)=3.141593E0/WG*G1(L)*DX;
END;  DO L=M TO 1 BY -1; PWT=0.;  DO LL=L TO M-2 BY 2;  PWT=PWT+G1(LL)
+4.*G1(LL+1)+G1(LL+2);  END;IF LL<M-2  THEN PWT=PWT+.5*( G1(M-1)+G1(M));
PWT=DY*PWT/3.;  DO K=1 TO NA; YI1,K,L)=SQRT(YI1,K,L));END;
                                                PUT FILE (SYSPRINT)             E
DIT (ID,J,L,(K,YI1,K,L) DO K=1 TO NA)) (SKIP(2),3(X(4),F(3)),4(SKIP,5(X(5),F(2)
,X(2),E(14,7))));
PUT FILE (SYSPRINT) EDIT (G1(L),PWT) (SKIP,2(X(2),E(14,7)));  END;
RR:  END;  IF IC=1  THEN DO;  IC=0; EP=3.E3;  IJ=100; ZIJ=IJ;  CHG=1.;
DIT=1.E-7;
GO TO RT;  END;   END;
```

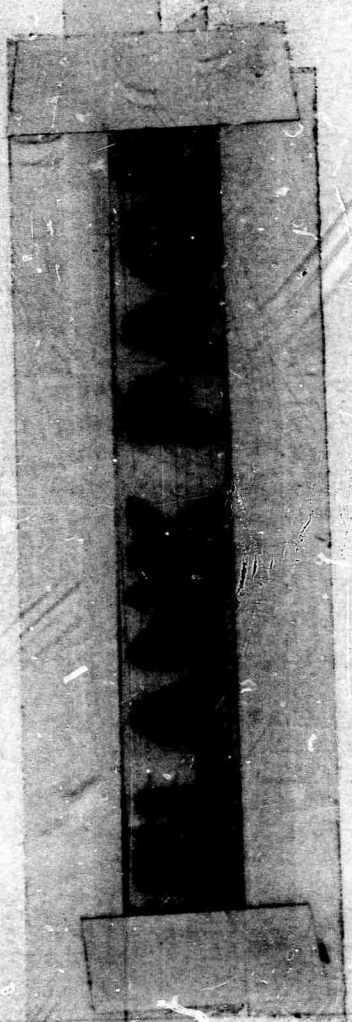

ILLUSTRATIONS

Figure 1. Fore and Aft Symmetry of the Laser Pulse.
The on-axis magnitude of the electric field, $|E|$, is shown as a function of $|z - z_c|$ at four different times. As shown in Eq. (200), $z_c \approx ct$ locates the center of the pulse. The solid curves show the leading edge of the pulse and the dotted curves depict the trailing edge. Distances along the z-axis are expressed in units of the grid size: $\Delta z = 0.45$ km. The quantity $|E|$ shown is defined in Eq. (197), so that the exponential damping factor is not included in the graphs.

Figure 2. Details of the z-profile of the Electric Field.
For detailed comparison, the z-profile of the on-axis electric field, $|E|$, is shown at several times. The unit Δz is used for distances along the z-axis. The curves have been displaced to the left and the leading edges made to coincide at height $1000\left(\frac{\text{erg}}{\text{cm}^3}\right)^{\frac{1}{2}}$ for $|E|$. The abscissa for this intersection of the curves has been labeled 42.5, the location of this point at $t = 0$.

Figure 3. Radial Profiles of the Laser Pulse.
The radial profile of $|E|$ is shown for $t = 0$ and for $t = 10^{-5}$ sec for slices taken through the on-axis maximum, z_p, in the z-profile.

Figure 4. Details of the Radial Profile of the Laser Pulse.
Details of the radial profile are shown for various times. In all four cases the radial slice through the on-axis maximum of the z-profile is exhibited.

Figure 5. Off-axis Maximum in Laser Pulse.

An off-axis maximum in the radial profile is shown at $t = 10^{-5}$ sec. The slice shown exhibits the radial profile at $z = 31$, whereas the principal peak of the pulse is on-axis at $z = 35.3$. The slice at $z = 31$ contains the greatest off-axis effect and, therefore, locates the two secondary peaks which have developed in the pulse. These secondary peaks are also indicated on Figure 9.

Figure 6. Phase of the Electric Field Amplitude.

Phase information is presented by showing $|E_1|$ as a function of z at $t = 6 \times 10^{-6}$ sec. For comparison, the dashed curve shows $|E|$. Equations (162) and (197) of the text define $|E_1|$ and $|E|$.

Figure 7. Phase of the Electric Field Amplitude.

At $t = 8 \times 10^{-6}$ sec., $|E_1|$ and $|E|$ are shown on-axis as functions of z. Two nodes have developed and E_1 is negative in the region of the power peak. The sign of E_1 in the various regions is indicated on the figure. The nodes are also shown in Figure 9.

Figure 8. Phase of the Electric Field Amplitude.

At $t = 10^{-5}$ sec., $|E_1|$ and $|E|$ are shown on-axis as functions of z. The sign of E_1 is indicated in the various regions. There are now four nodes. The nodal curves are phase fronts and are shown in detail in Figure 9.

Figure 9. Configuration of the Laser Pulse.

Various properties of the pulse are shown in the rz-plane. The location of the peak in the z-profile is shown as a function of r at $t = 0$ and at $t = 10^{-5}$ sec. The phase fronts with $E_1 = 0$ are shown at $t = 10^{-5}$ sec. The open circles locate the z-profile nodes of E_1 at $t = 8 \times 10^{-6}$ sec. The small squares locate the secondary maxima of the pulse at $t = 10^{-5}$ sec.

Figure 10. On-axis Temperature Distribution.
The on-axis temperature increment, $(T - T_o)$, is shown as a function of z at $t = 10^{-5}$ sec.

Figure 11. Radial Temperature Profile.
The radial profile of the temperature increment is shown at $t = 10^{-5}$ sec. for the slice through the maximum of the z-profile. This maximum is at z = 33 as may be seen in Figure 10.

Figure 12. Fluid Velocity Distribution, On-axis.
The z-component, v_z, of the fluid velocity is shown on-axis as a function of z at $t = 10^{-5}$ sec. A double log plot is used which omits values of v_z between 10^{-3} cm/sec and -10^{-3} cm/sec.

Figure 13. Radial Fluid Velocity Distribution.
The radial component, v_r, of the fluid velocity is shown as a function of r at $t = 10^{-5}$ sec. The slice is taken at z = 32, the location of the "center of velocity" shown in Figure 12.

Figure 14. Fluid Density Distribution, On-axis.
The on-axis fluid density decrement, $-(\rho - \rho_o)$, is shown as a function of z at $t = 10^{-5}$ sec.

Figure 15. Radial Fluid Density Distribution.
The radial density distribution is exhibited as a function of r at $t = 10^{-5}$ sec. The slice is taken at z = 32, the location of the density minimum detailed in Figure 14. A double log plot is used which omits values between $10^{-9} \frac{gm}{cm^3}$ and $-10^{-9} \frac{gm}{cm^3}$.

Figure 16. Parade of Laser and Fluid Pulses, On-axis.
On a double log plot, the various laser and fluid variables are simultaneously plotted versus z at $t = 10^{-5}$ sec so that the spatial location of the various pulses can be visualized.

Figure 17. Locations and Widths of Laser and Fluid Pulses.
The location and full $\frac{1}{e}$-widths of the various laser and fluid pulses are shown versus z. The peak to valley distance is shown for v_z. The initial and final locations of the laser power peak are also indicated.

Figure 18. Self-curving Effect of a Laser Beam in the Presence of a Wind.
The self-curving effect of a laser beam in the presence of a wind is indicated. The angle ψ, the deflection angle, increases with z. The density, permittivity, or index of refraction profile is sketched to indicate the cause of the curving.

Figure 19. Thermal Blooming of a Laser Beam.
The thermal blooming of a laser beam in the absence of wind is indicated. The angle ψ_B, the deflection angle of the outer edge of the beam, increases with z. The density, permittivity, or index of refraction profile is sketched to indicate the cause of the blooming.

Figure 20. Cross-section for Scattering into Various Curvatures.
The normalized cross-section for scattering of power into various curvatures is sketched for small wind speeds, $\lambda = 0, 1, 3$. The distribution extends from ξ_{min}/ξ_B to ξ_{max}/ξ_B for each λ. Already at $\lambda = 3$, the distribution is sharply peaked at $\xi = \xi_{max}$. All the curves must pass through the vertical axis at height 0.5 and have an asymptote at $\xi/\xi_B = 2$.

Figure 21. Effective Optical Elements for Blooming.
The effects of a wind on the beam are indicated. When $\lambda = 0$, pure thermal blooming occurs; the light rays bend as if passing through a symmetrical double concave lens at each point in the path. For $\lambda \neq 0$ the effective lens is converted into a large prism with a small defocusing lens perched on the downwind vertex of the prism.

Figure 22. Peak Displacement at Detector for Experiment of Smith and Gebhardt. For the experiment described in the text, the beam is viewed with a detector located 20cm from the end of a 100cm wind tunnel. The peak displacement into the wind, Y_p/a, is shown as a function of velocity. The notation is explained in Part VI of the text.

Figure 23. Intensity Profiles at Detector for Experiment of Smith and Gebhardt. Intensity profiles predicted by equation (290) of the text are shown at $\alpha L = 0.5$ for $v_o = 2$cm/sec and 10cm/sec. The original beam is also shown.

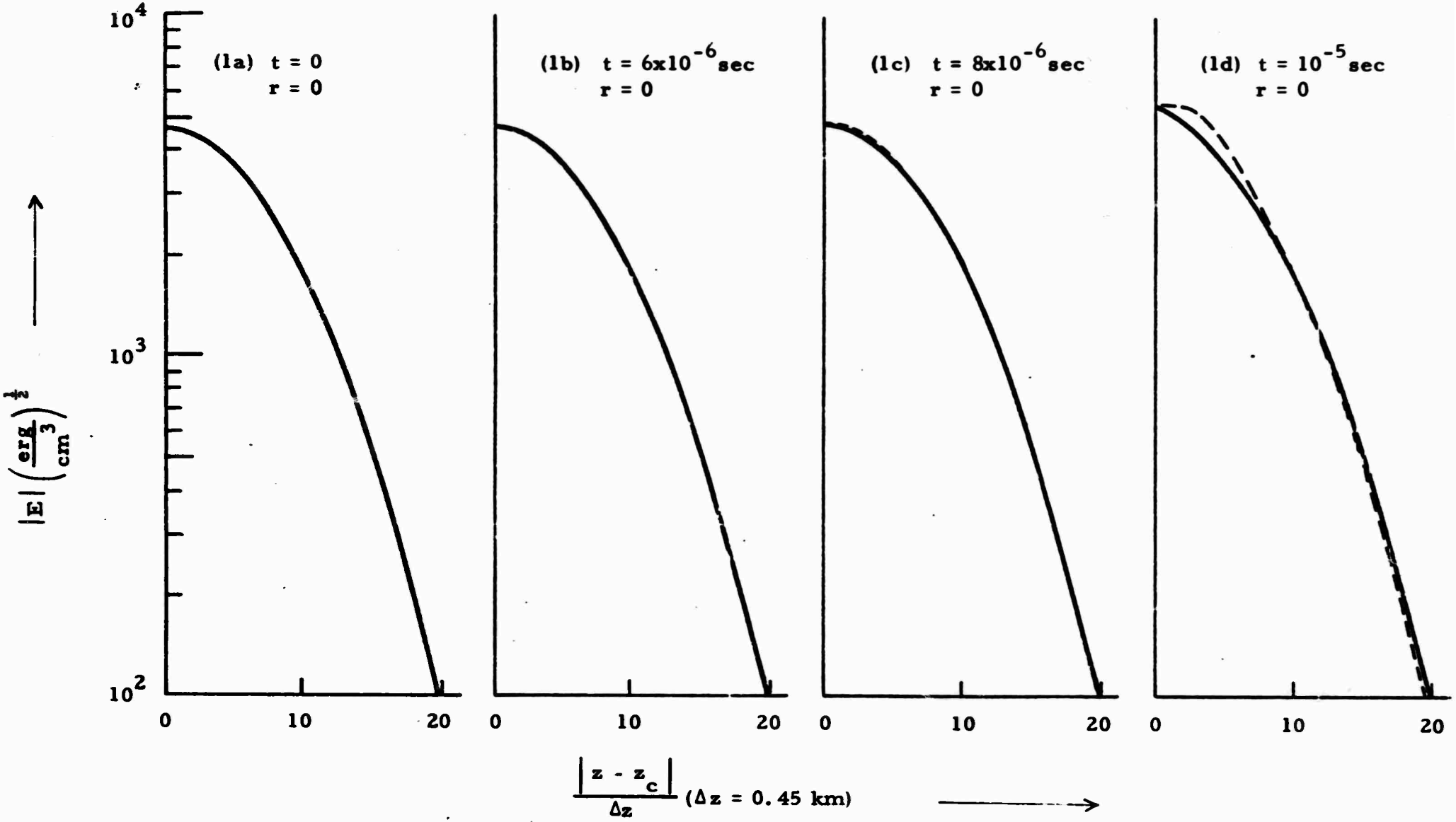

Figure 1. Fore and Aft Symmetry of the Laser Pulse
Leading edge: solid curves.
Trailing edge: dashed curves

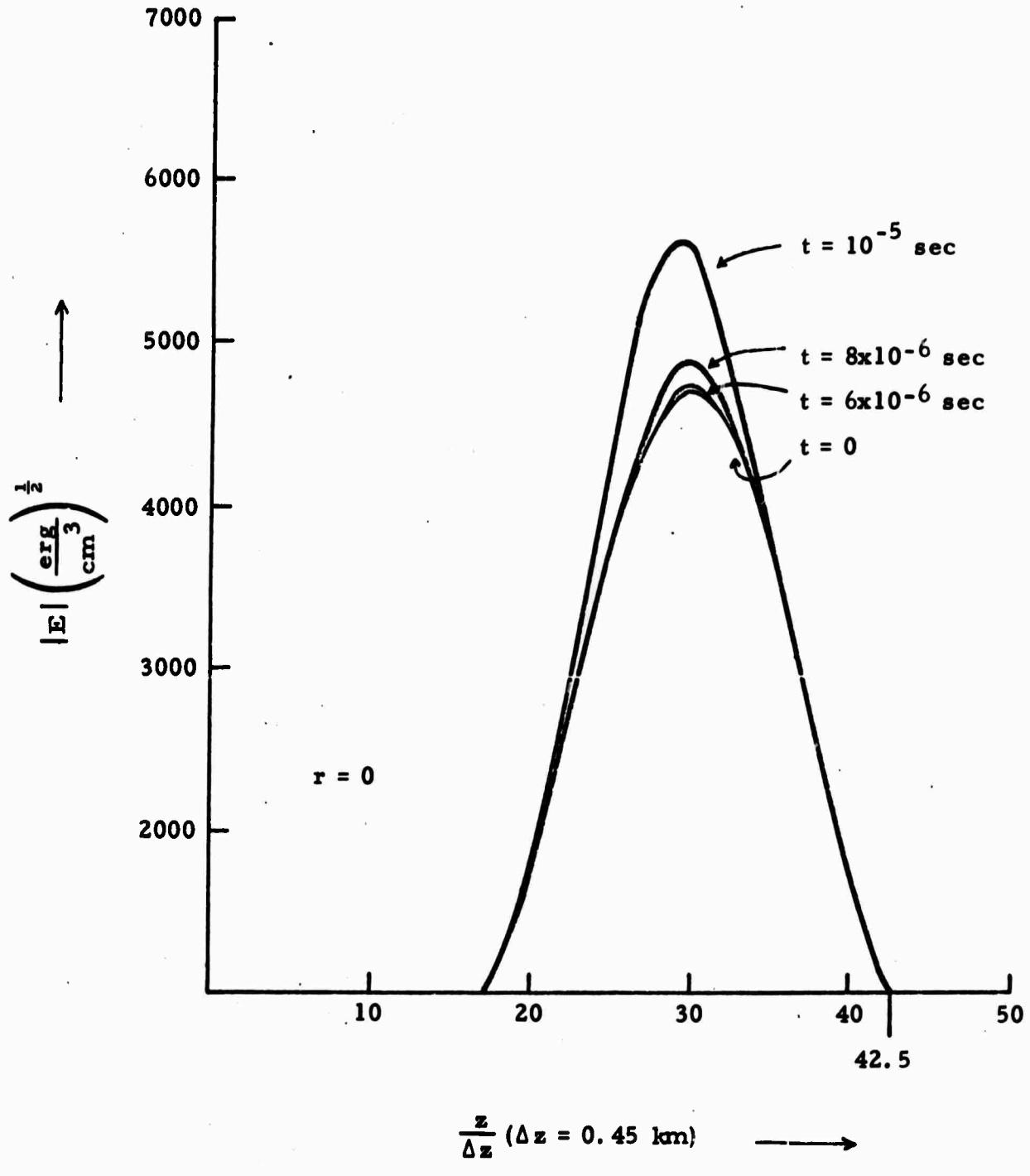

Figure 2. Details of the z-profile of the Electric Field

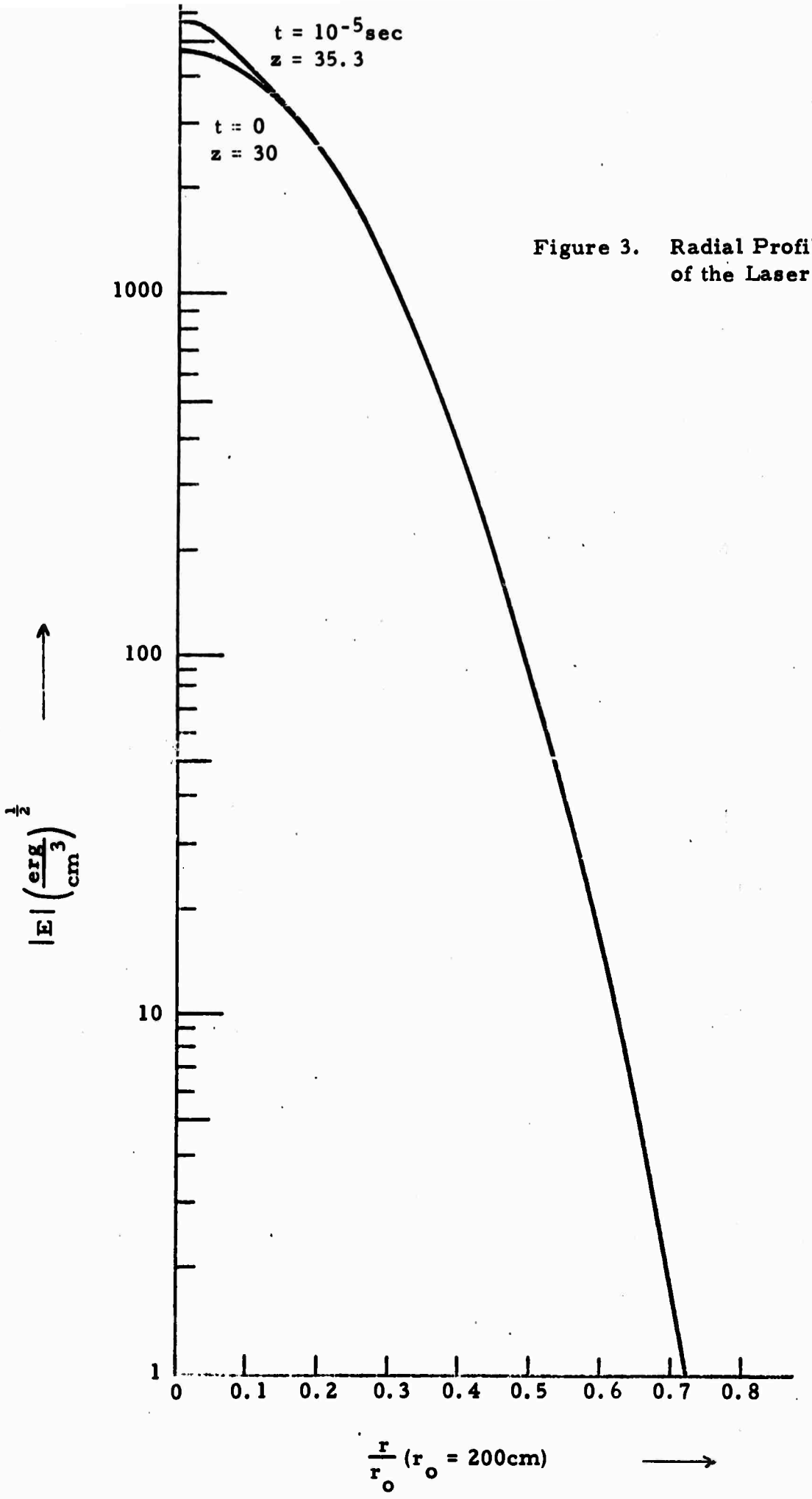

Figure 3. Radial Profiles of the Laser Pulse

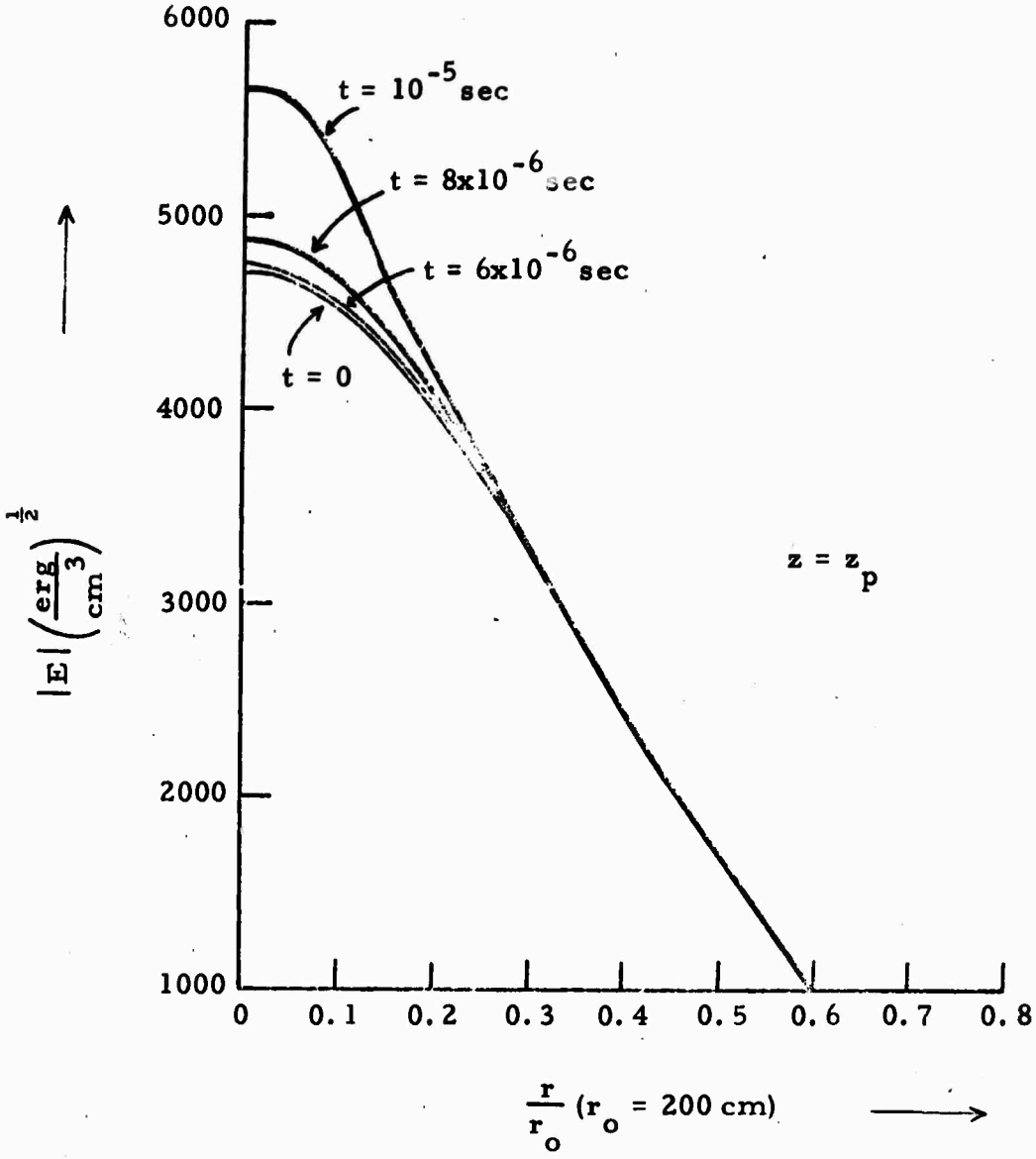

Figure 4. Details of the Radial Profile of the Laser Pulse

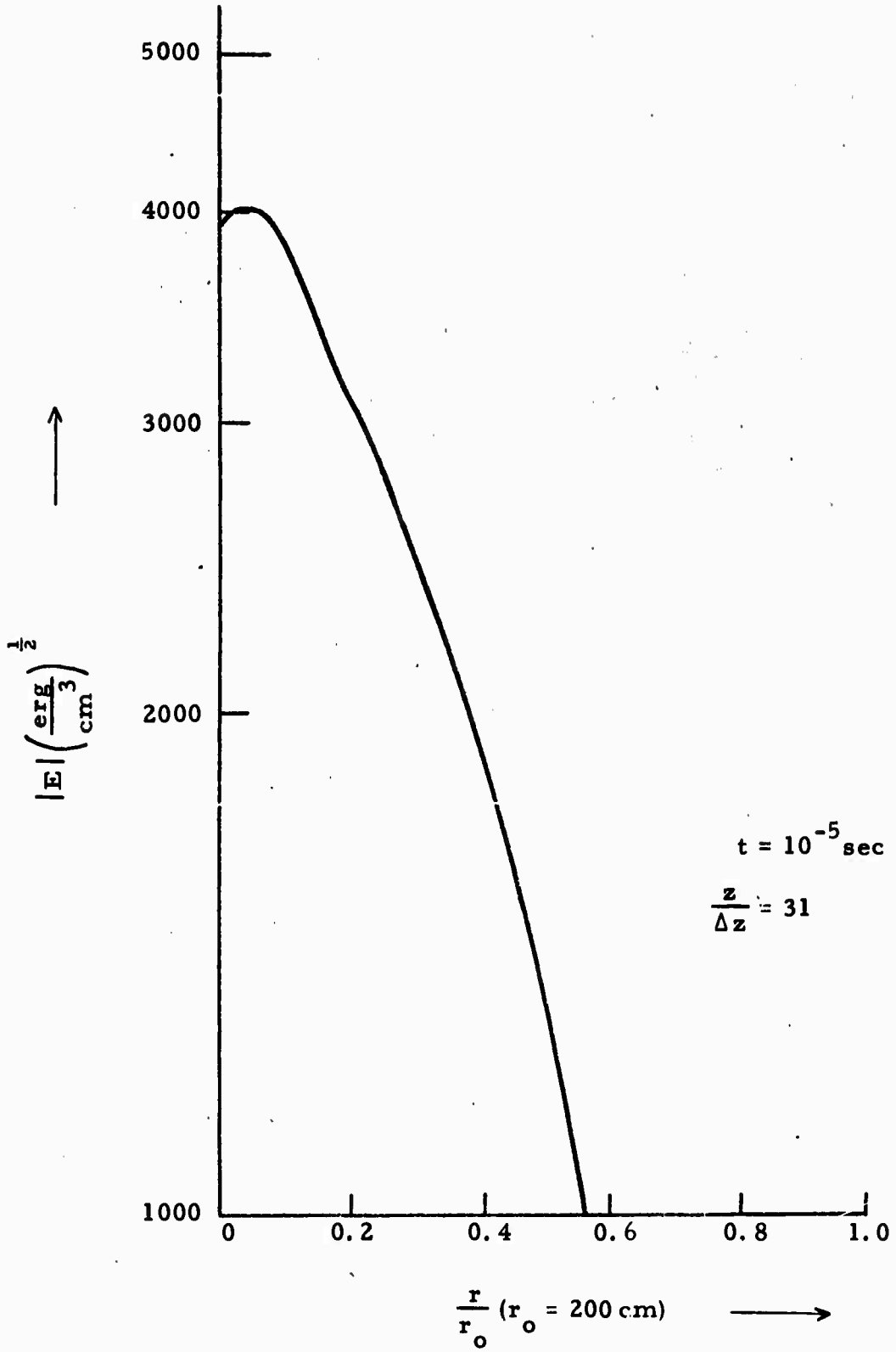

Figure 5. Off-Axis Maximum in Laser Pulse

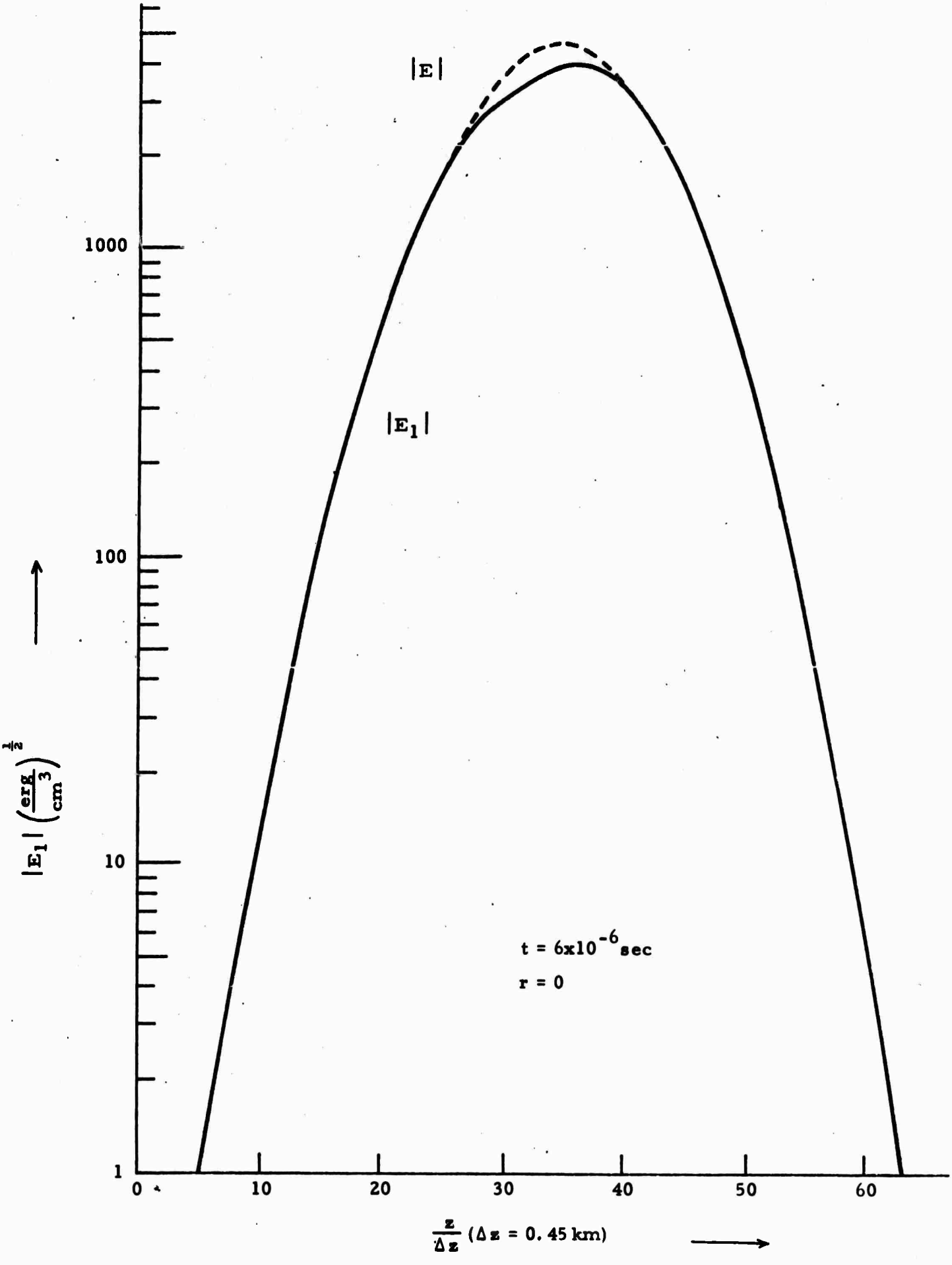

Figure 6. Phase of the Electric Field Amplitude

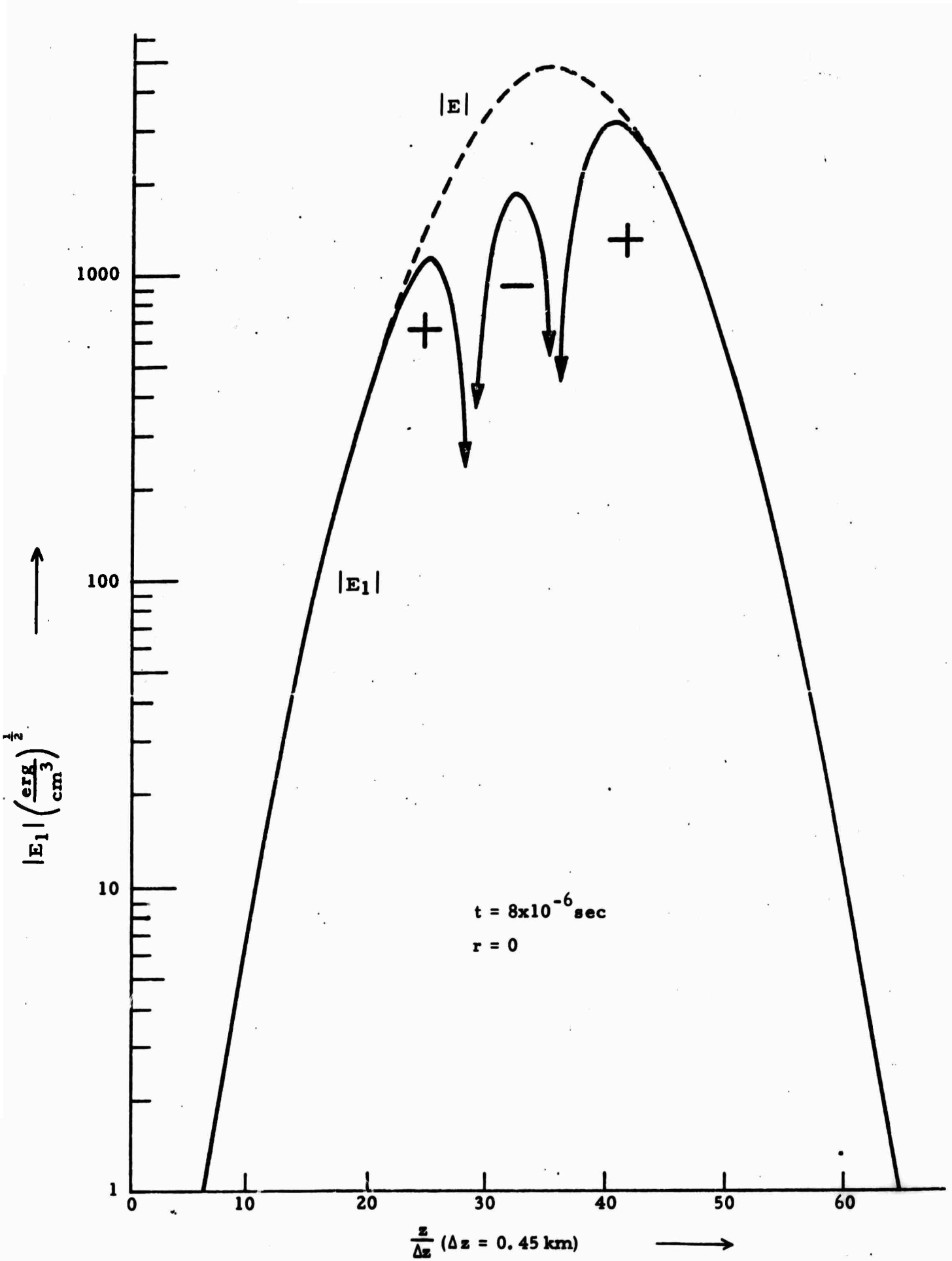

Figure 7. Phase of the Electric Field Amplitude

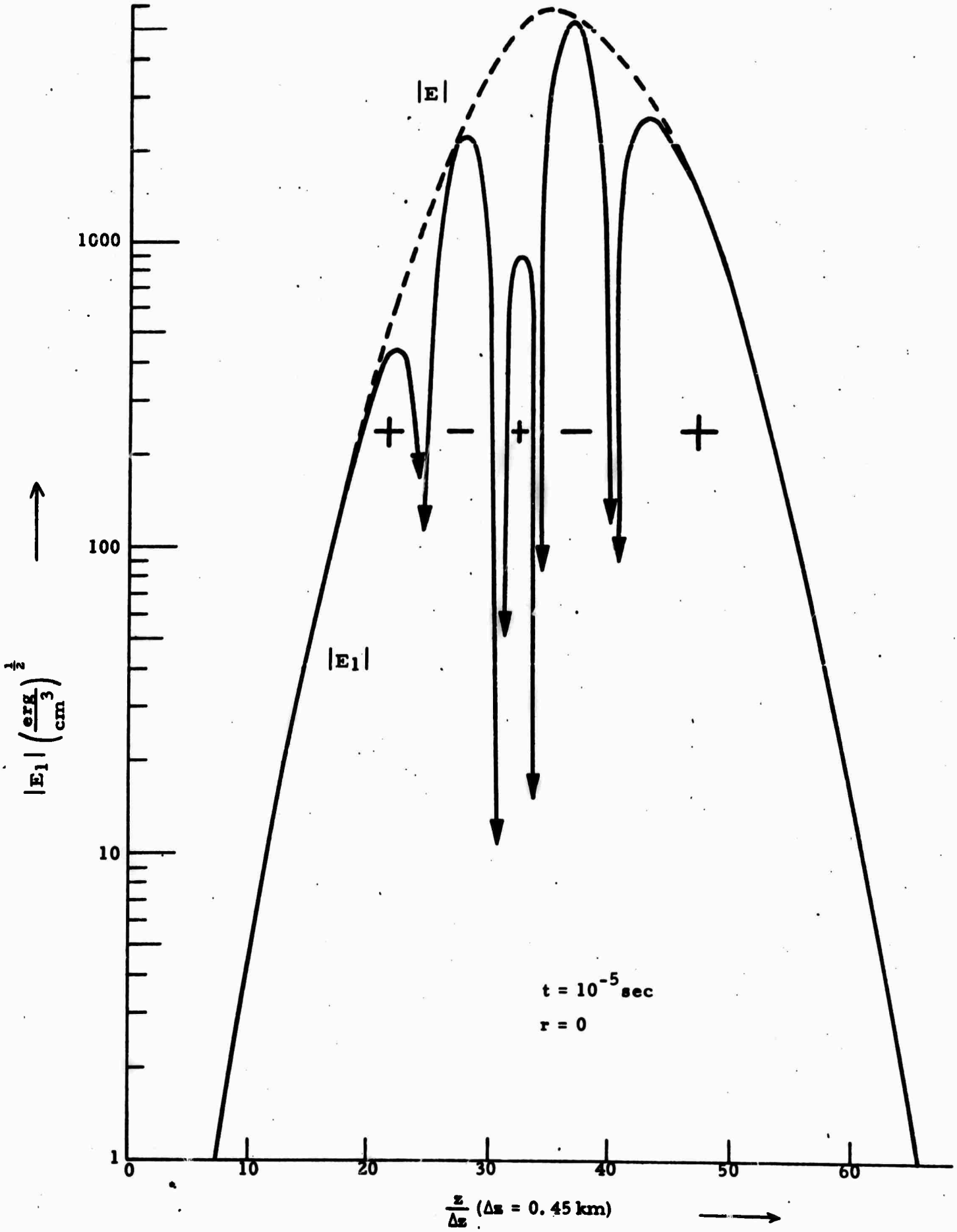

Figure 8. Phase of the Electric Field Amplitude

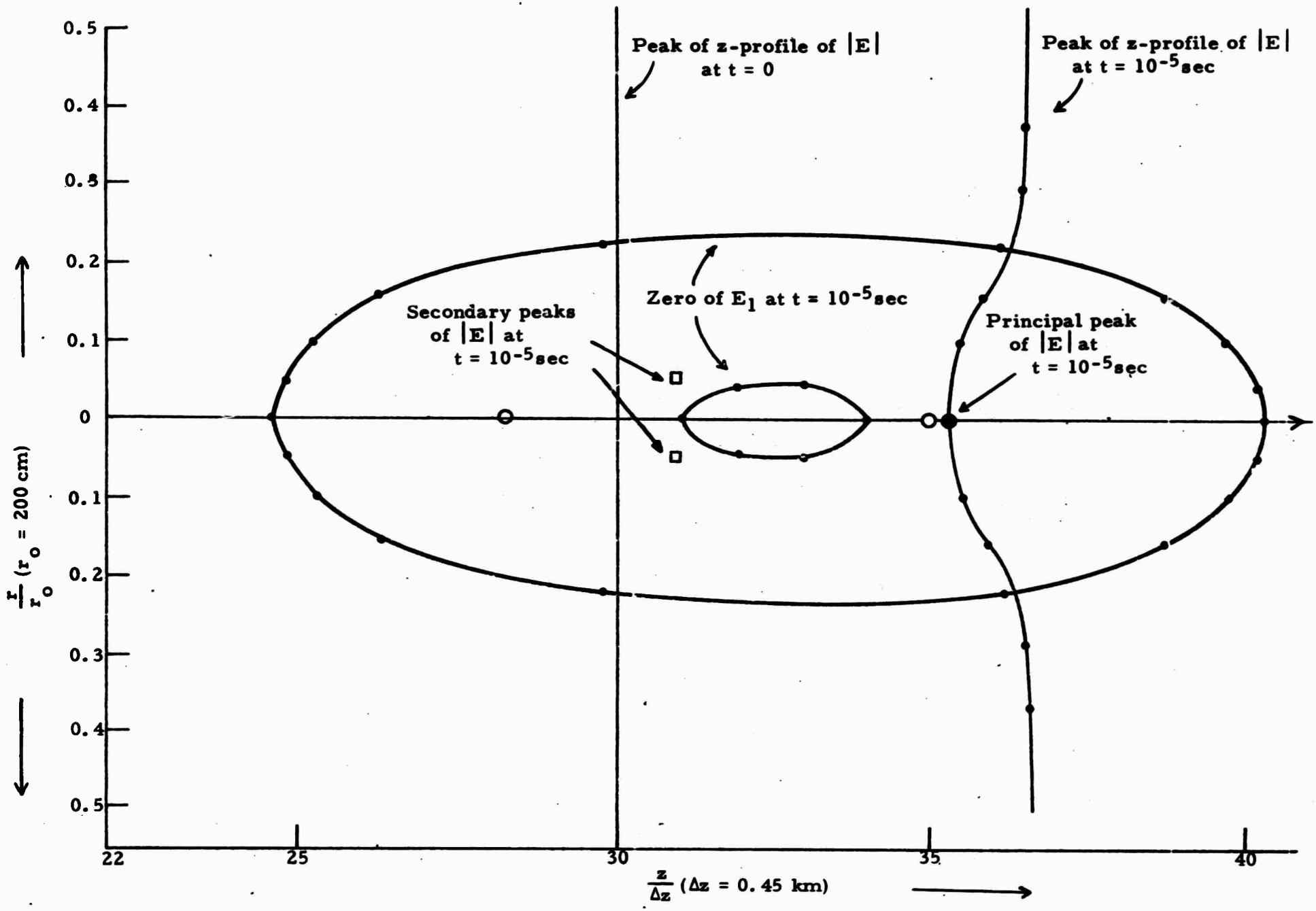

Figure 9. Configuration of the Laser Pulse

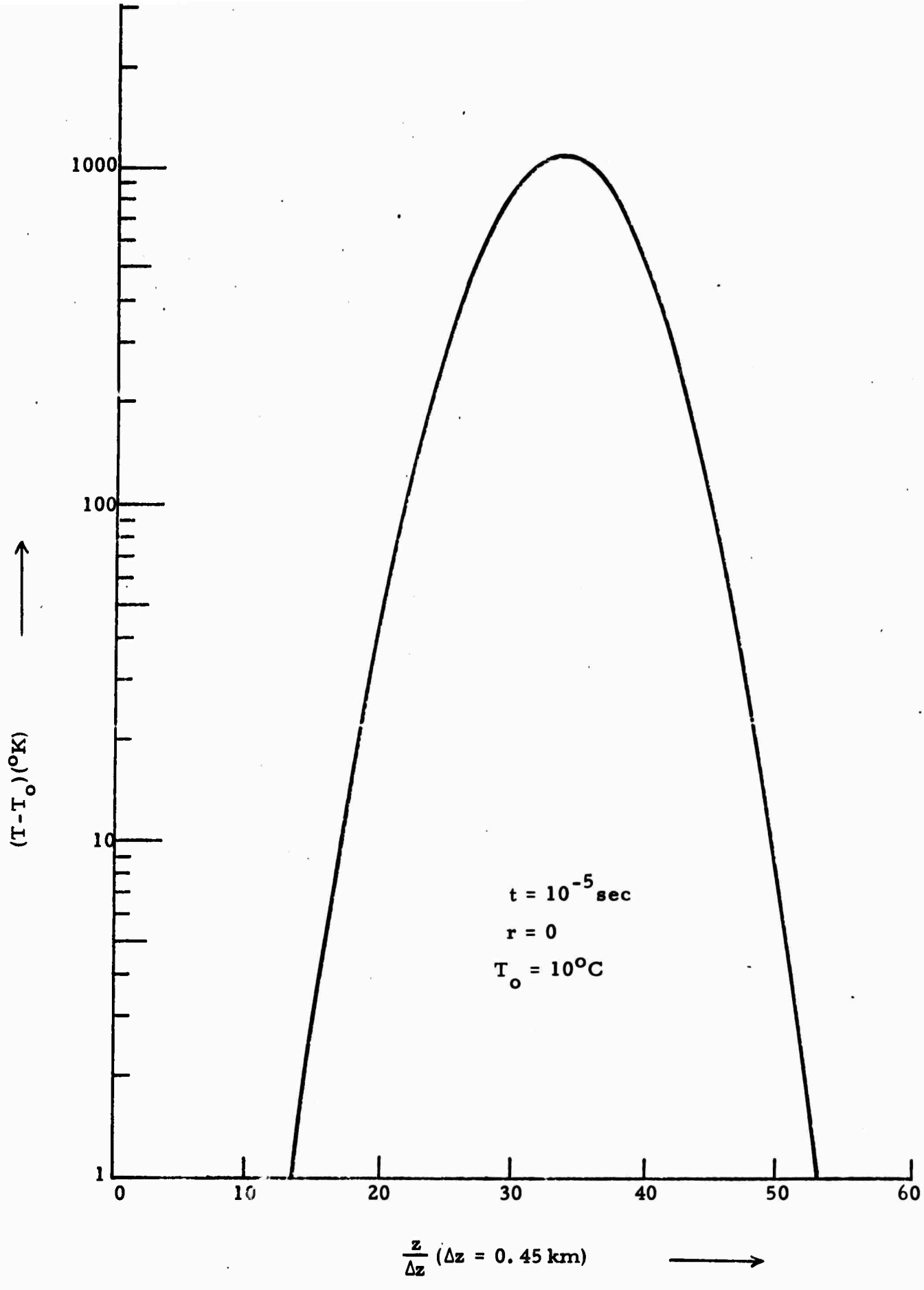

Figure 10. On-Axis Temperature Distribution

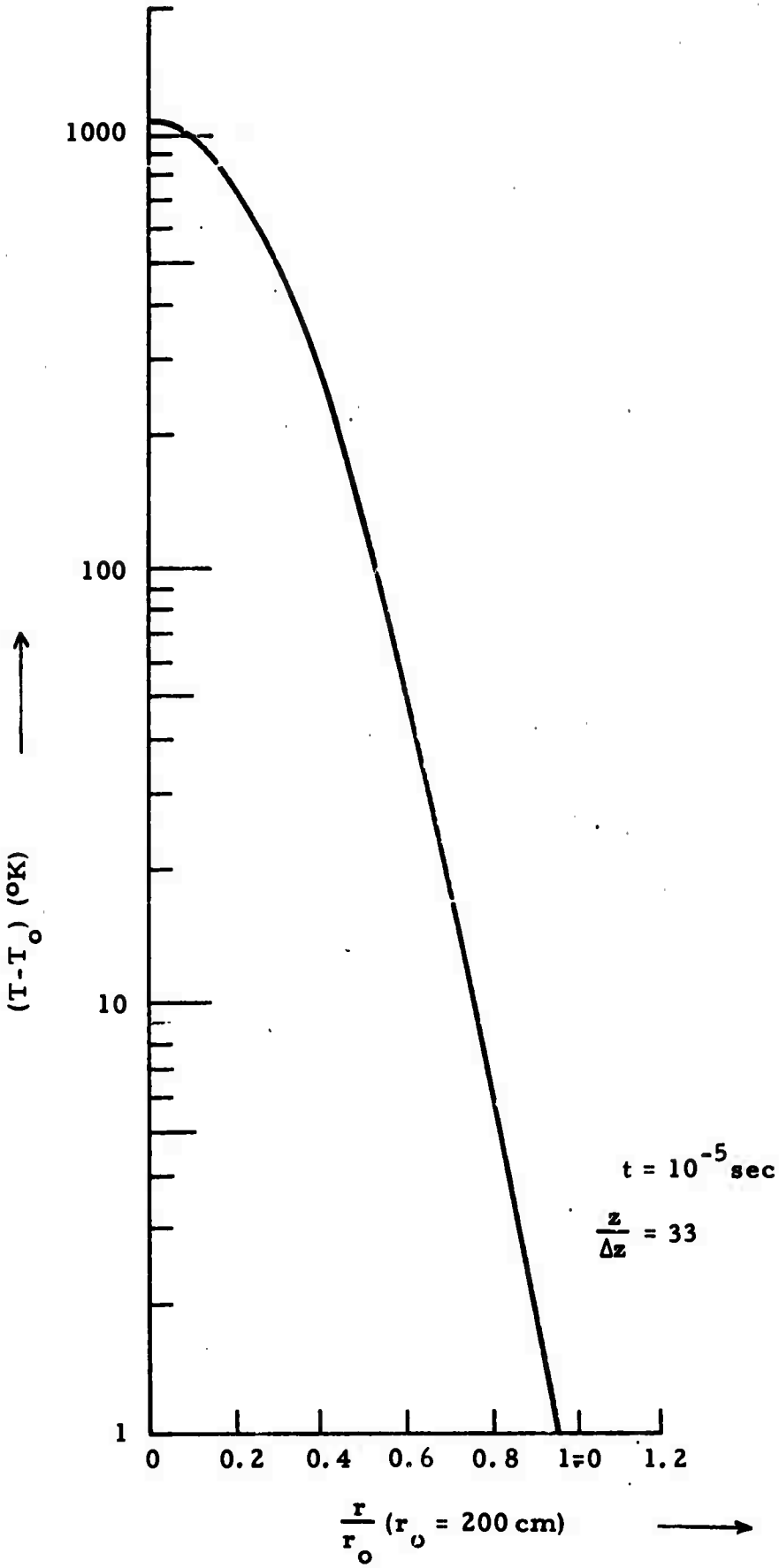

Figure 11. Radial Temperature Profile

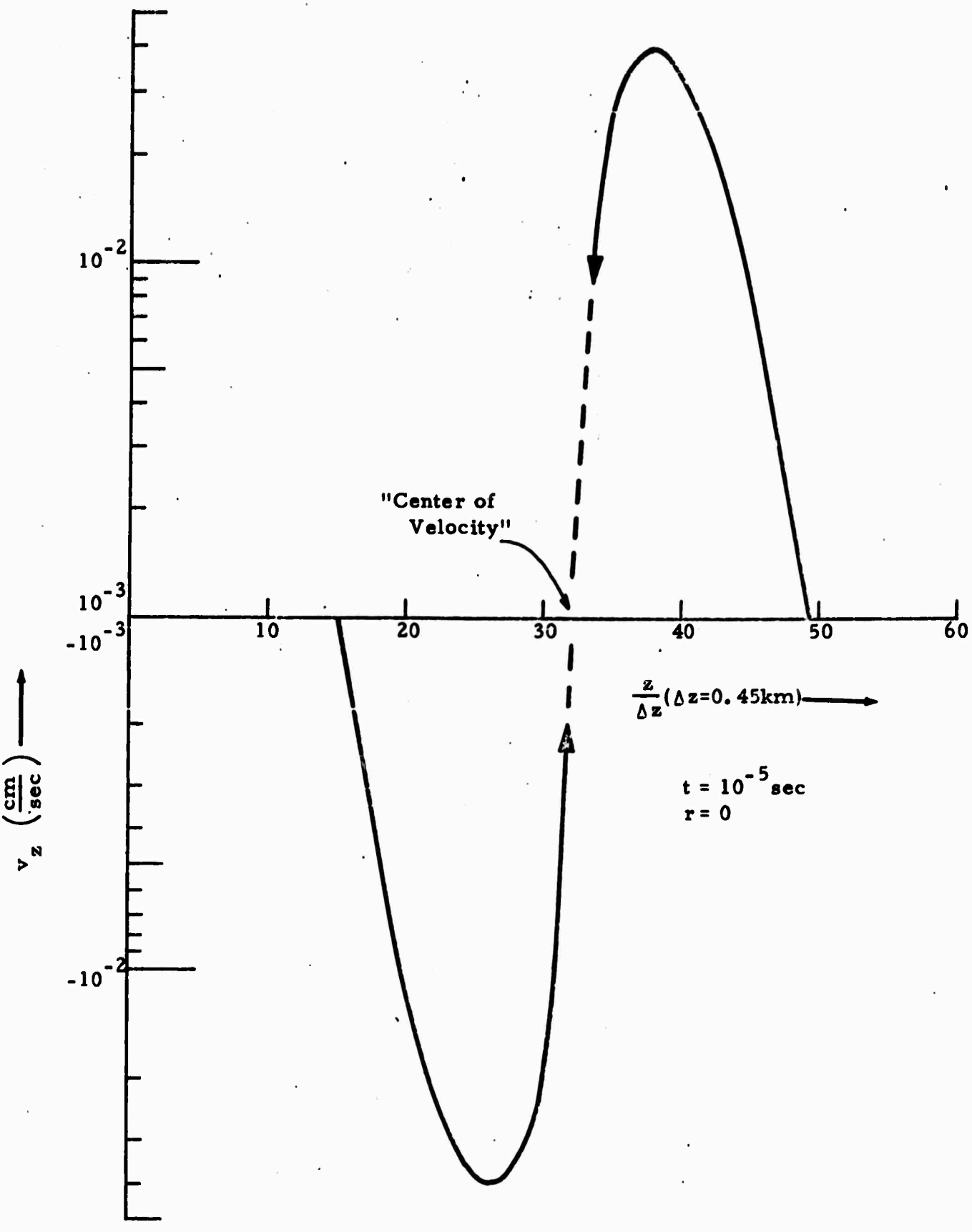

Figure 12 Fluid Velocity Distribution On-Axis

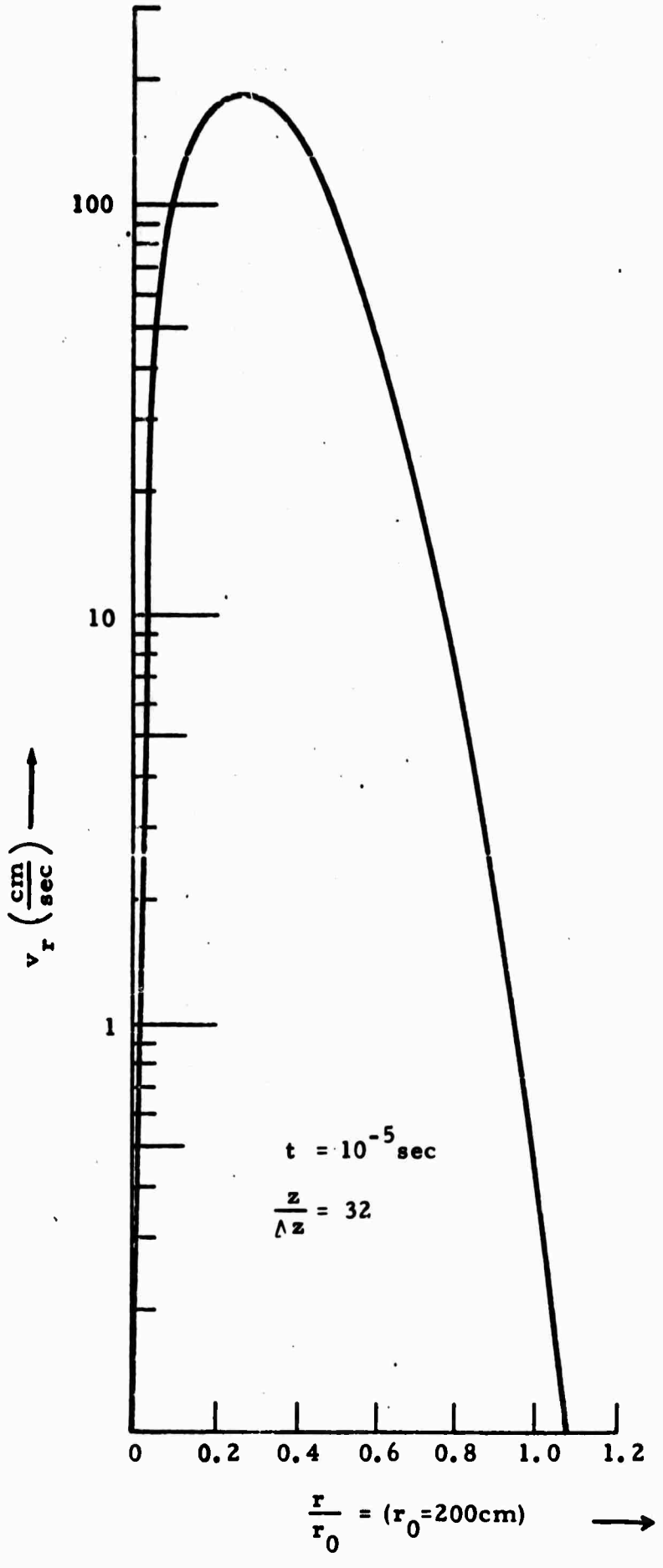

Figure 13. Radial Fluid Velocity Distribution

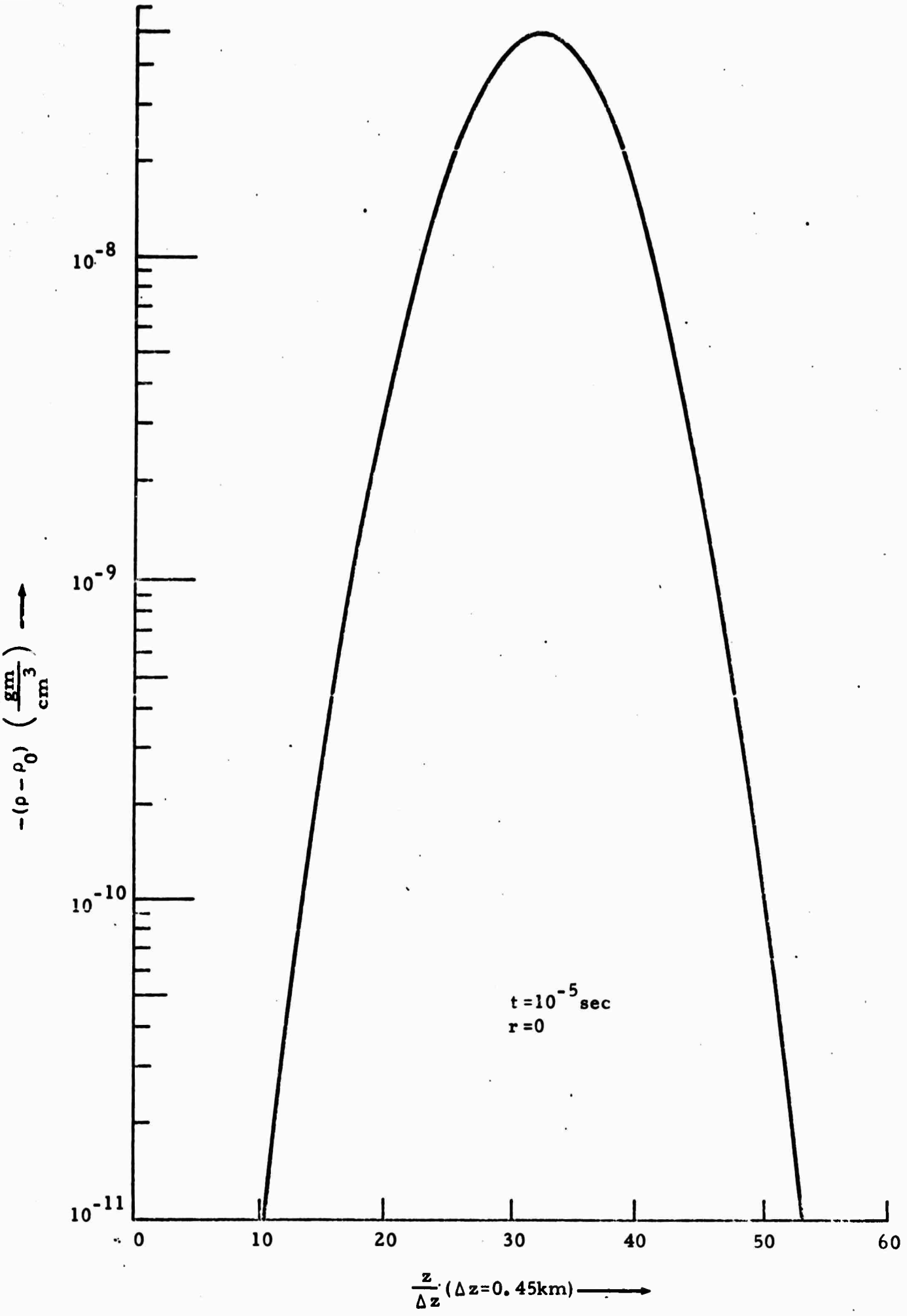

Figure 14. Fluid Density Distribution, On-Axis

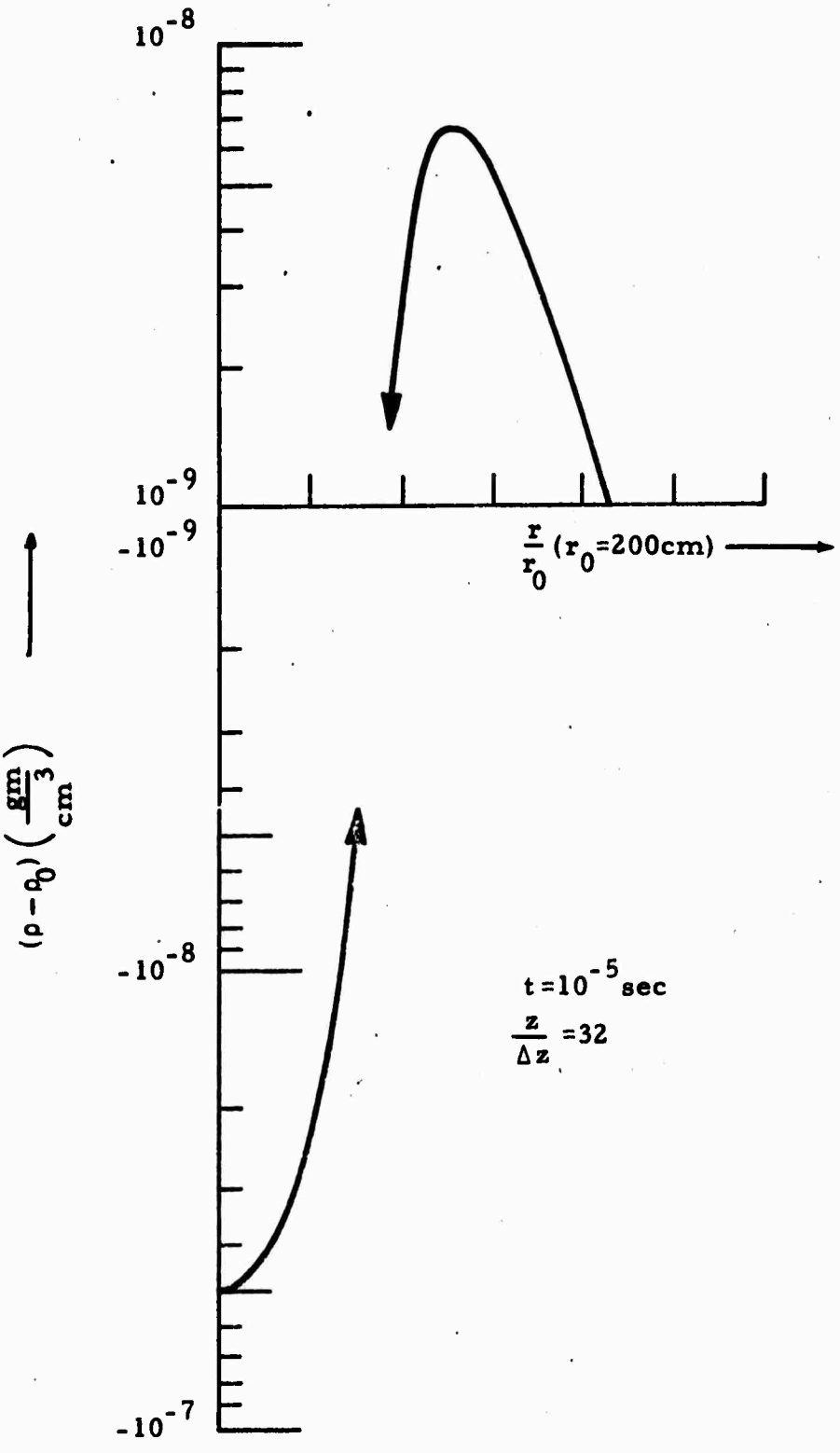

Figure 15. Radial Fluid Density Desitribution

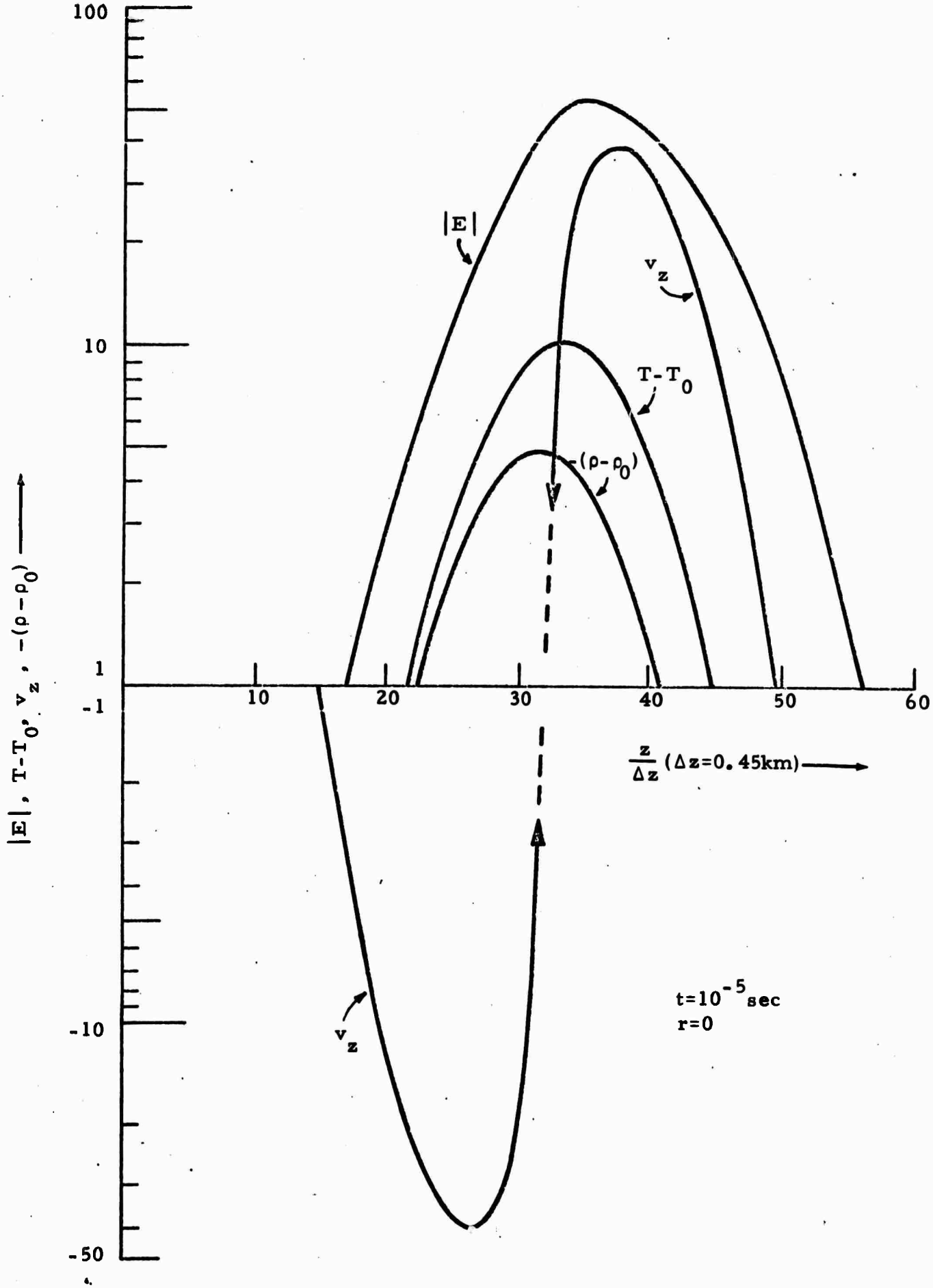

Figure 16. Parade of Laser and Fluid Pulses, On-Axis

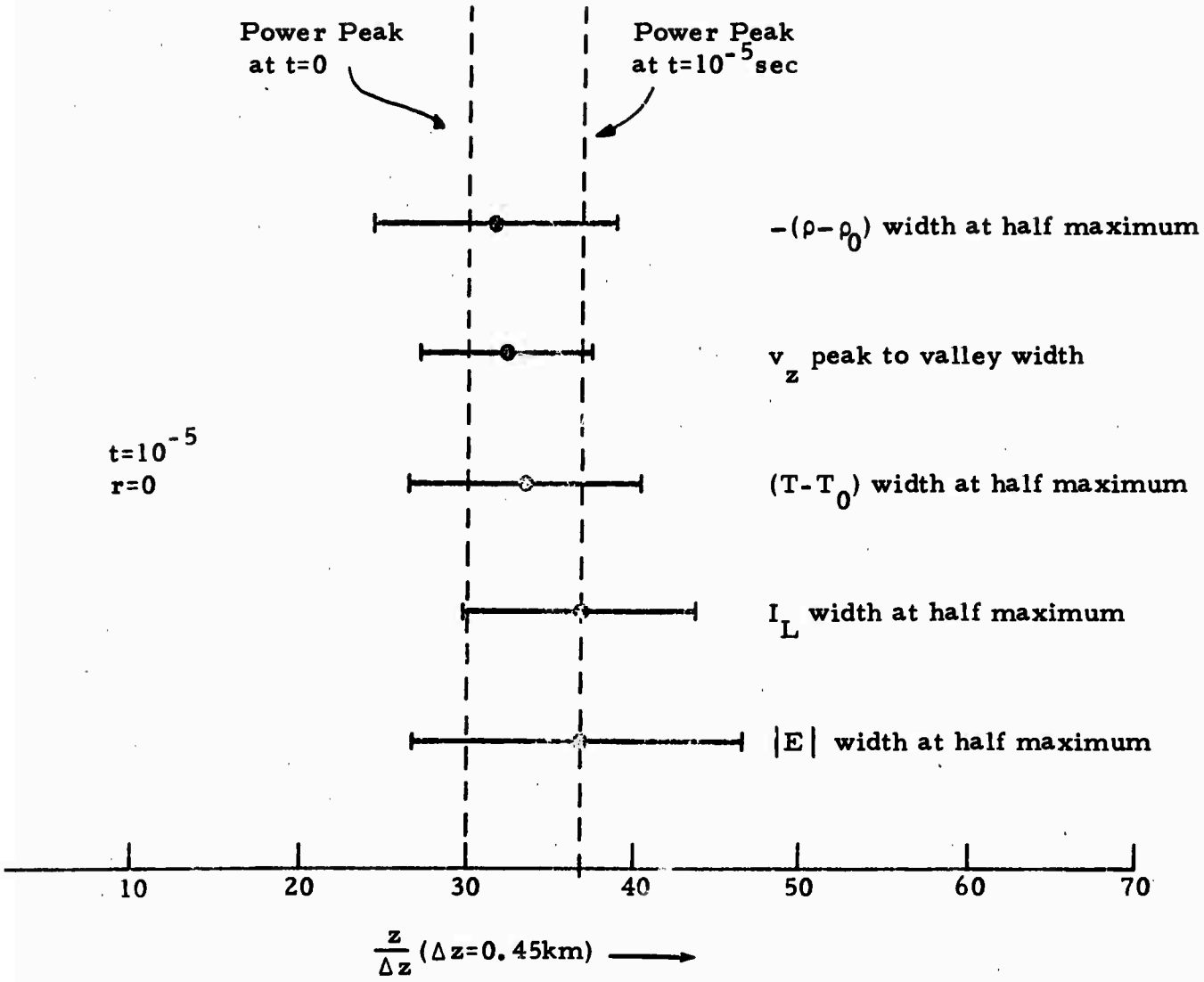

Figure 17. Locations and Widths of Laser and Fluid Pulses

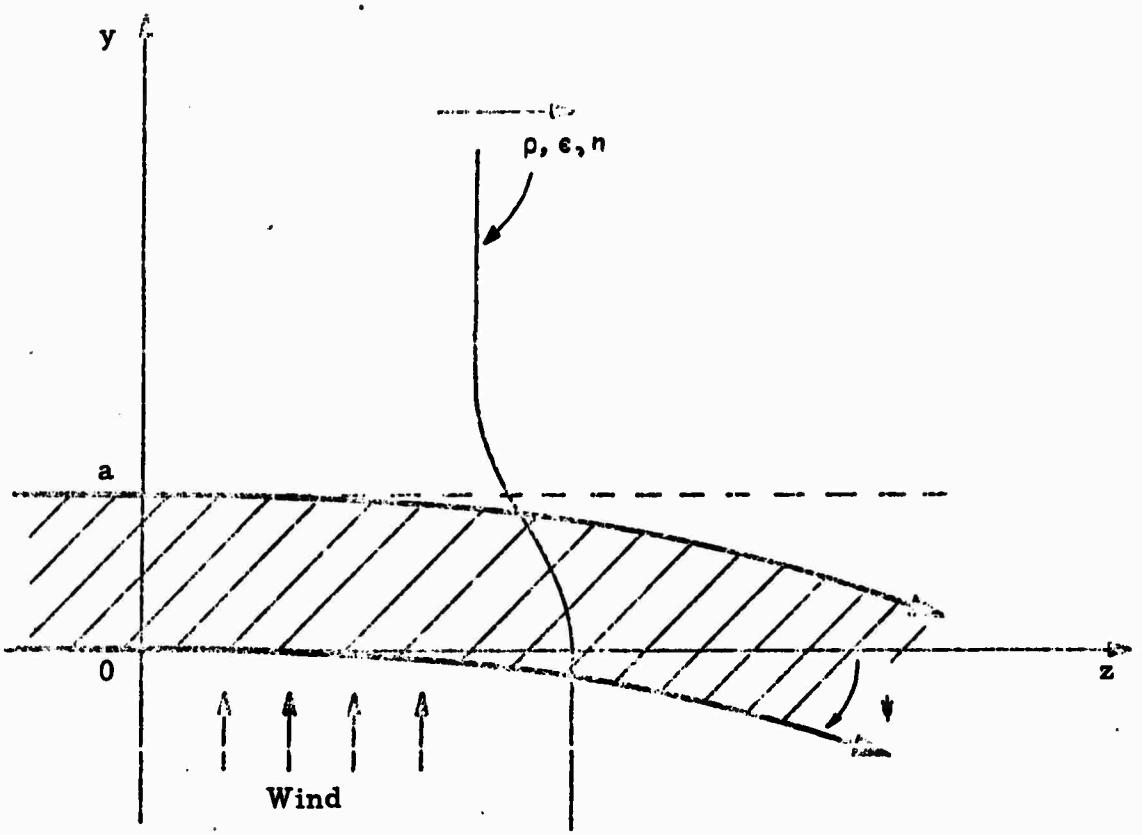

Figure 18. Self-curving Effect of a Laser Beam in the Presence of a Wind

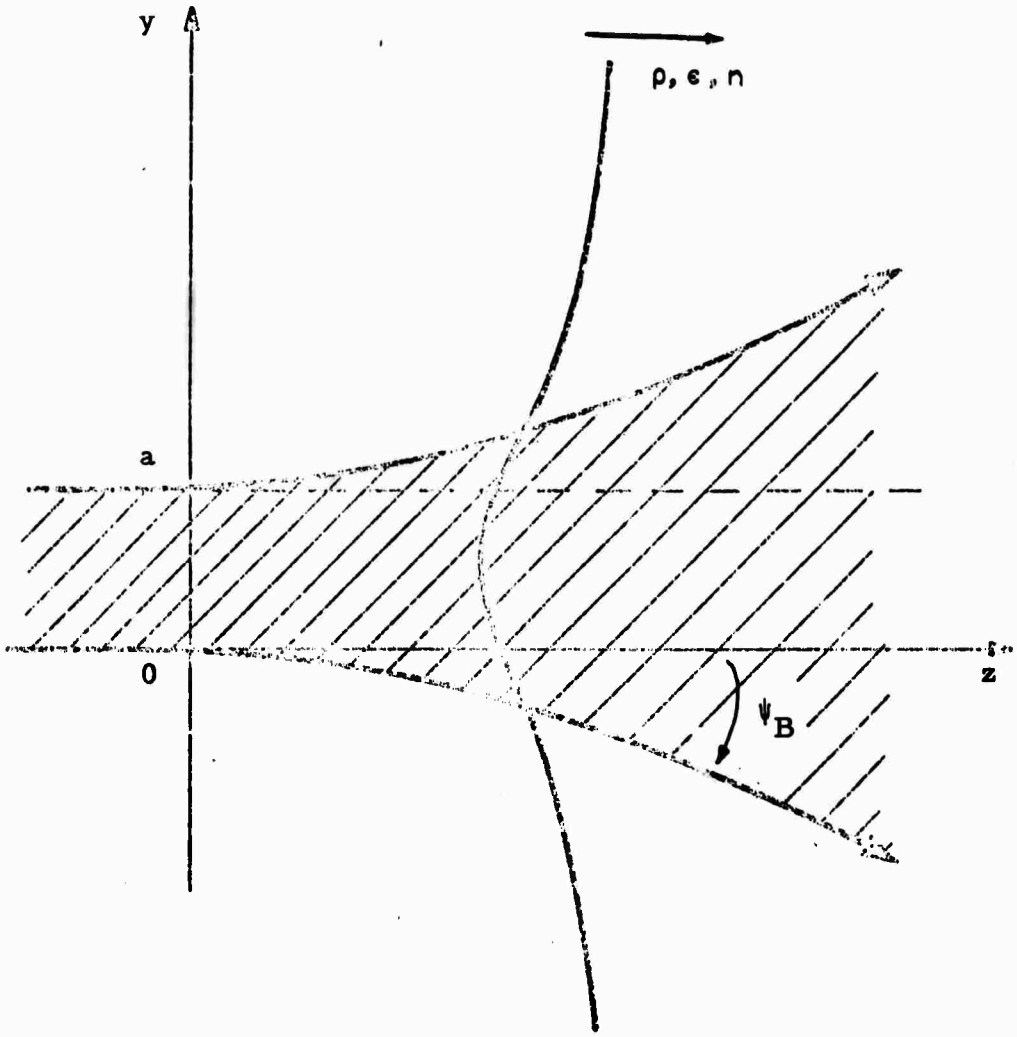

Figure 19. Thermal Blooming of a Laser Beam

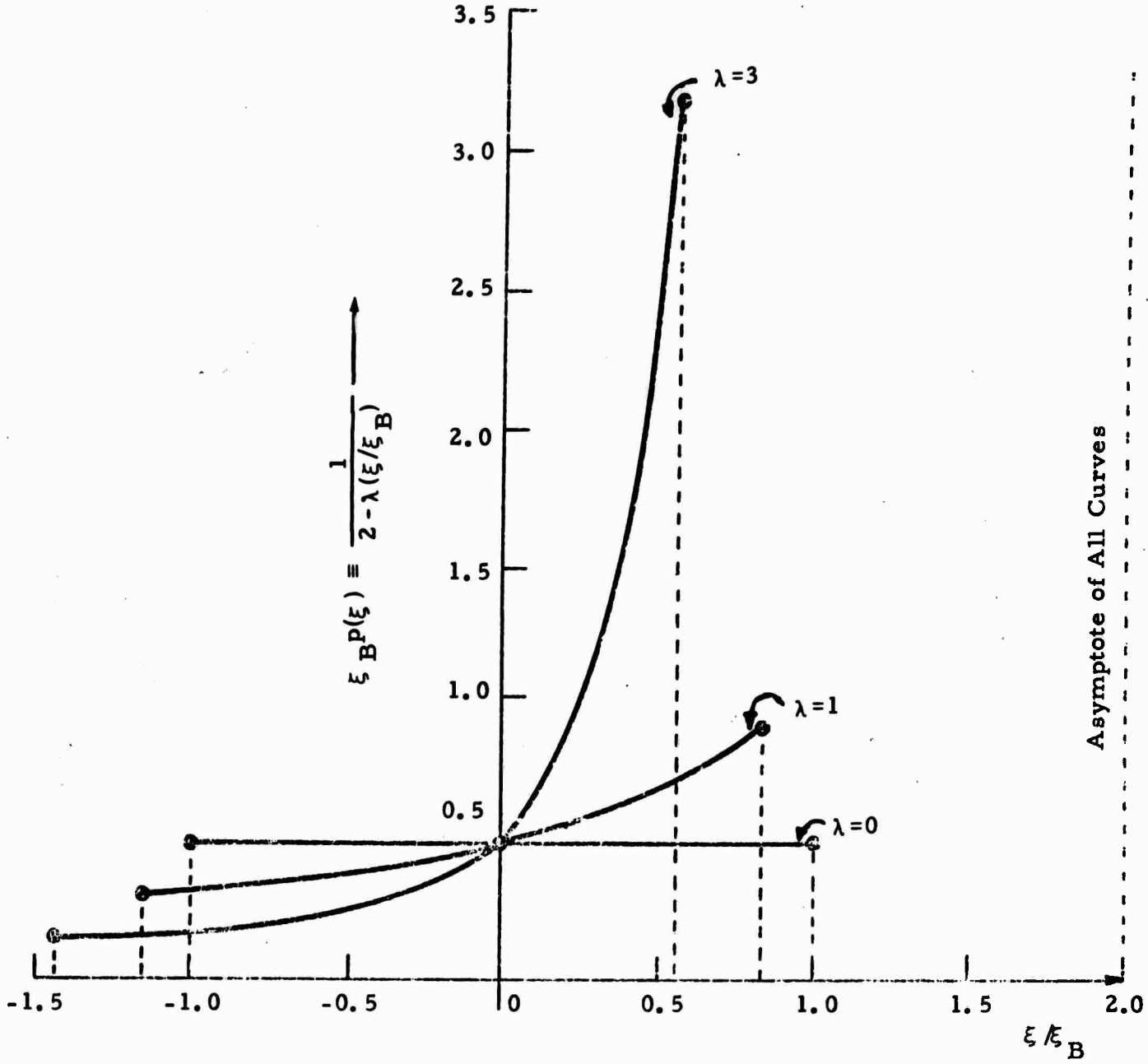

Figure 20. Cross-section for Scattering into Various Curvatures

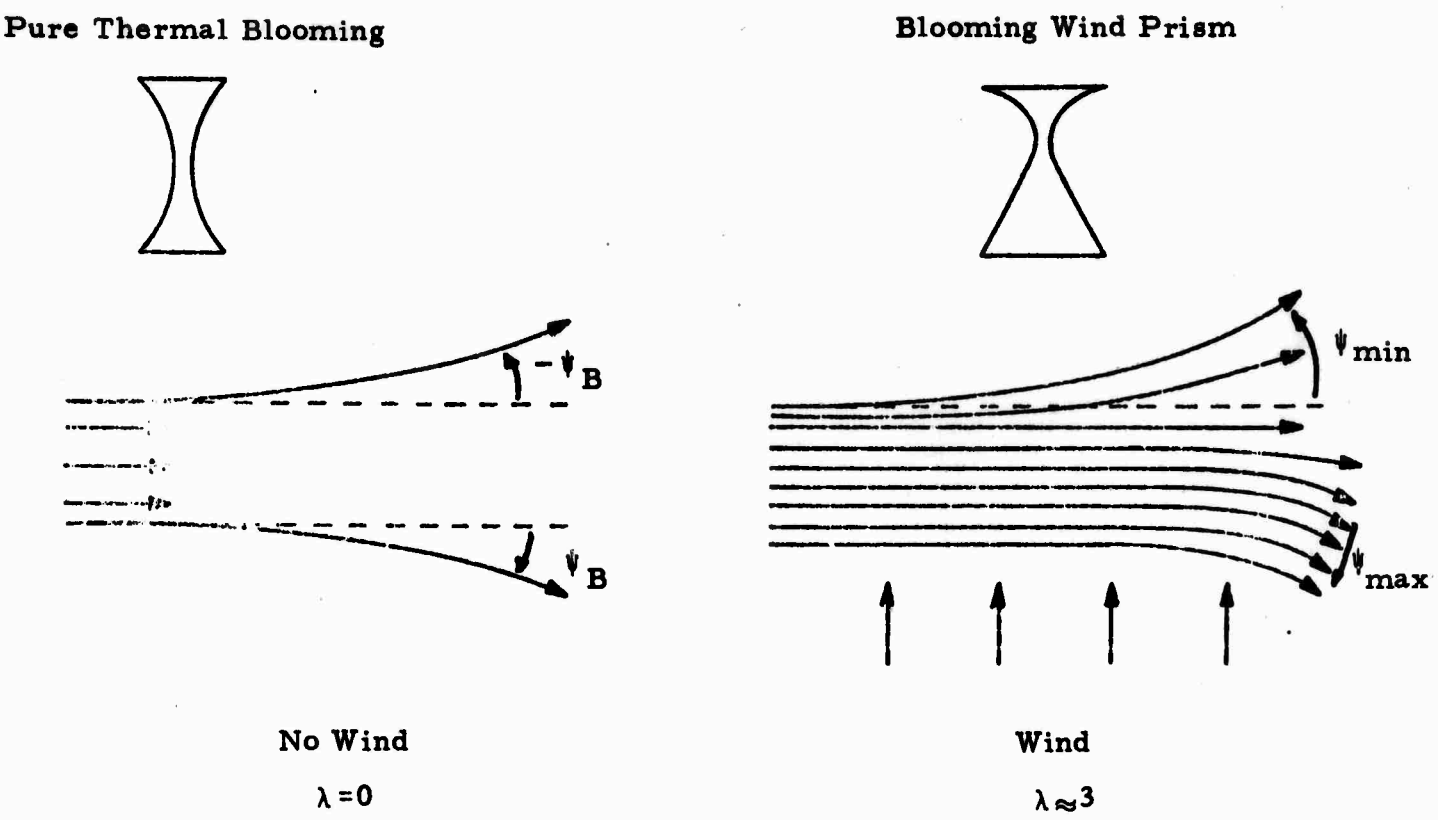

Figure 21. Effective Optical Elements for Blooming

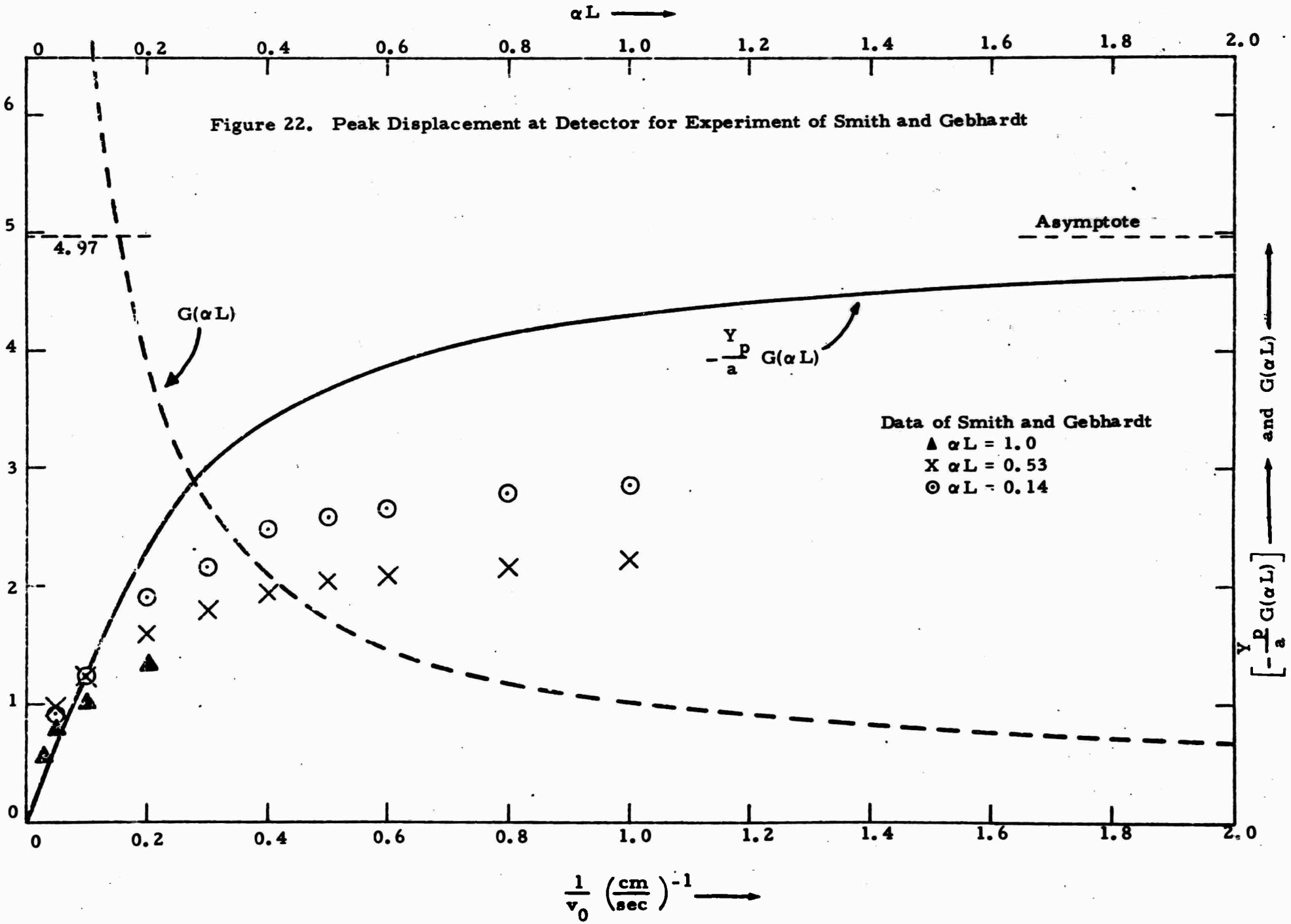

Figure 22. Peak Displacement at Detector for Experiment of Smith and Gebhardt

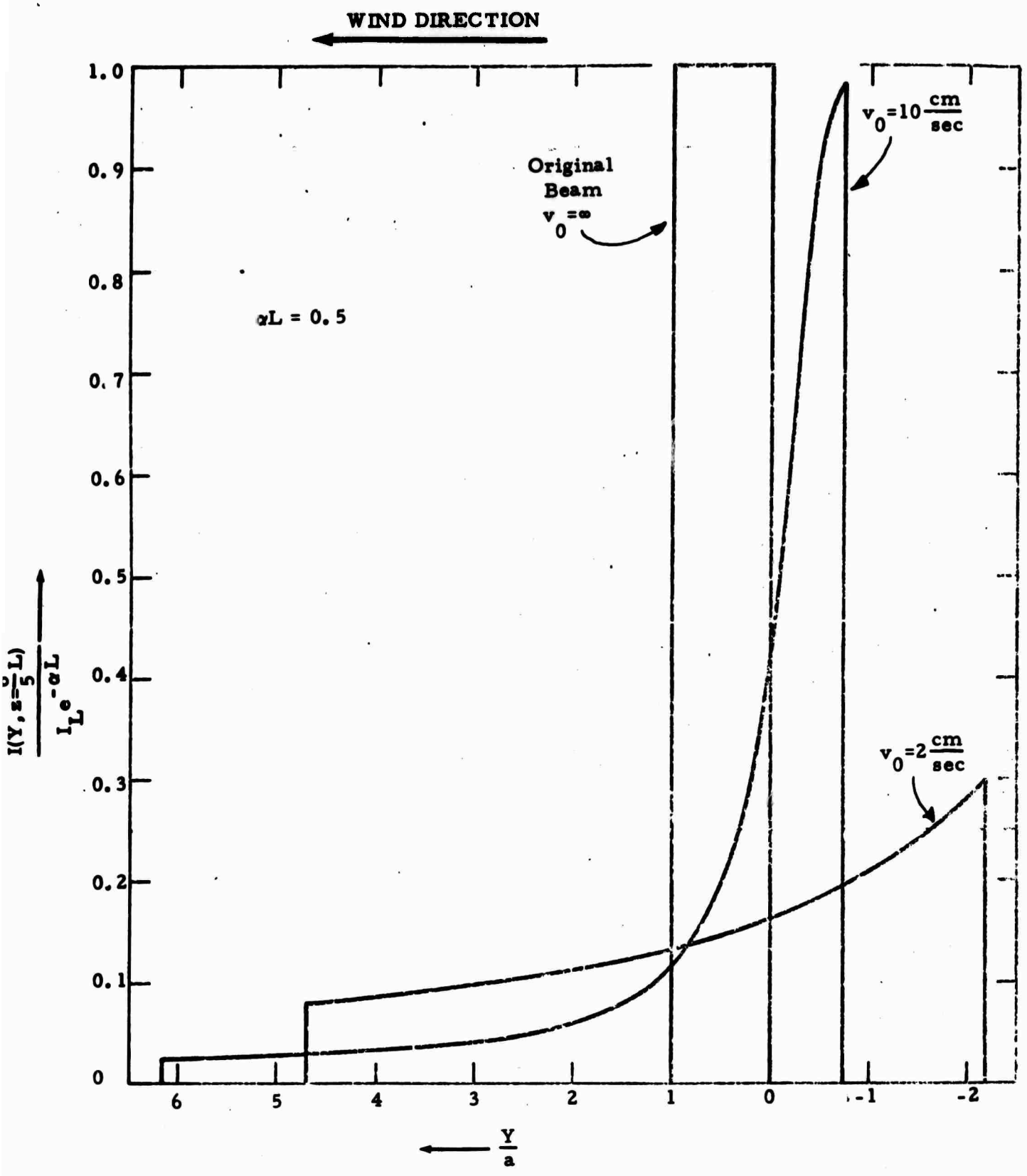

Figure 23. Intensity Profiles at Detector for Experiment of Smith and Gebhardt

UNCLASSIFIED

Security Classification

DOCUMENT CONTROL DATA - R & D

(Security classification of title, body of abstract and indexing annotation must be entered when the overall report is classified)

1. ORIGINATING ACTIVITY (Corporate author)	2a. REPORT SECURITY CLASSIFICATION
Electronic Sciences Laboratory University of Southern California Los Angeles, California 90007	UNCLASSIFIED 2b. GROUP

3. REPORT TITLE

INSTABILITIES IN LASER PROPAGATION IN FLUIDS

4. DESCRIPTIVE NOTES (Type of report and inclusive dates)

Final Report

5. AUTHOR(S) (First name, middle initial, last name)

William G. Wagner

6. REPORT DATE	7a. TOTAL NO. OF PAGES	7b. NO. OF REFS
October 1970	184	31

8a. CONTRACT OR GRANT NO.	9a. ORIGINATOR'S REPORT NUMBER(S)
N00014-67-A-0269-0006 b. PROJECT NO. c. d.	USCEE Report 400 9b. OTHER REPORT NO(S) (Any other numbers that may be assigned this report)

10. DISTRIBUTION STATEMENT

This document has been approved for public release and sale; its distribution is unlimited.

11. SUPPLEMENTARY NOTES	12. SPONSORING MILITARY ACTIVITY
	Advanced Research Projects Agency (DOD) monitored by the Office of Naval Research, Physics Branch, Wash., D. C.

13. ABSTRACT

In this work instabilities in the system of equations describing electromagnetic wave propagation and fluid dynamics are discussed. The basic equations are discussed ~~in Part~~ I, and ~~in Part II~~ the linearized stability analysis is presented along with an evaluation of the threshold for these growing waves. To follow the growth of the disturbances, computer studies were undertaken. In the course of these studies it became apparent that there was some merit to introducing a new concept to judge the value of an algorithm for computing the solutions of a system of partial differential equations. This concept was called "utility", and is discussed ~~in Part III,~~ along with several examples of its application to simpler partial differential equations. The advantage of this concept is that it is relatively easy to apply to complicated systems of partial differential equations, whereas the stability concept leads to a very complicated procedure for deciding on the value of a numerical routine. In Part IV are presented the results of a calculation of beam distortion for a very high intensity pulse propagating through air for several kilometers. Analytical arguments are advanced which suggest that the qualitative features of the distortions are correct, which lends credence to the computer output.

Speed and memory size in a computer place certain restrictions on one's ability to investigate phenomena in the laser beam problem. In the attempt to calculate distortions of the type predicted by the linearized instability analysis, cylindrical symmetry was imposed on the problem in order to facilitate the computer calculation. Had this not been necessary, or had some other independent variable been eliminated

(continued on next page)

DD FORM 1 NOV 65 1473

UNCLASSIFIED

Security Classification

14. KEY WORDS	LINK A		LINK B		LINK C	
	ROLE	WT	ROLE	WT	ROLE	WT
Electromagnetic Propagation						
High Intensity Beams						
Propagation Instabilities						
Beam-fed Turbulence						

13. Abstract (continued)

rather than the angle about the beam axis, much more pronounced evidence of beam and fluid instabilities would likely have been observed for substantially lower powers, powers that may be achievable. Arguments supporting this proposition are contained in Part V.

Part VI of this report contains an analytic discussion of beam bending and thermal blooming for a slab beam propagating through a wind. A formula is derived which provides for the transition between two regimes in which conduction and forced convection, respectively, dominate the dissipation of heat deposited in the medium from the laser beam. This formula appears to be useful for the analysis of several experiments.